The Role of L1-CNTNs in Controlling SHH-Induced Proliferation of Cerebellar Granule Neuron Progenitors

ORATAI WEERANANTANAPAN

Department of Biomedical Science

The University of Sheffield

United Kingdom

Thesis presented for the degree of Doctor of Philosophy

March 2014

This thesis is dedicated to

My Beloved Dad and Mom

Acknowledgements

First of all I would like to express my deepest gratitude to my supervisor, Dr. Andrew J.W. Furley, for giving me the great opportunity to do a PhD in his lab. Thank you for his huge patience, unwavering support, excellent mentorship and his understanding overseas students like myself. I was fortunate to have gained a place in his lab, where I learnt a lot from him, and I could not have asked for a better supervisor. Secondly, I would like to extend my appreciation to my advisors: Professor Elizabeth Smythe, Dr. Verdon Taylor and Dr. Tanya Whitfield for their useful suggestions and kind support, especially Liz, thanks for her helpful advice on Co-IP technique. I would also like to deeply thank Professor Marysia Placzek for funding and allowing me to use the Apotome microscope.

Next, I would like to acknowledge Dr. Dia Xenaki and Dr. Indira B Martin for training me on the granule cell preparation and primary culture techniques, when I first joined the lab, Dr. Puneet Dang and Dr. Basudha Basu for teaching me some useful techniques in the lab, including their helpful suggestion, Anne Marie Kimberley and William Sean Hague for supplying mice, Dr. Soheil Aghamohammadzadeh and Dr. Darren Robinson for microscopic consultation. Moreover, I would like to say a big thank you to D-floor members, who have been generous and helpful colleagues. It has been a pleasure to be among vibrant and stimulating PI's, post-docs, researchers, and post-graduate students here.

On a personal note, I would like to say "thank you" to Shantisree Rayagiri and my lovely group of Thai friends in Sheffield – Dr. Patompon Wongtrakoongate, Dr. Supatthra Narawatthana, Dr. Phakpoom Phraprasert, Dr. Natwadee Poomipark, Dr. Nisa Patikarnmonthon, Dr. Chatchawal Phansopa, Dr. Chomchon Fusinpaiboon, Dr. Rossukon Keawkao, Sujanya Boonpradit, Pornpen Panomwan, Kanidpong Banditsoawapark, Suttida Eamsamarng, Aunwaya Kaewpitak, Supakchai Ponglertsakul and Nipaporn Konthapakdee – for their assistance, support and encouragements through my PhD study.

Last, but not least, I would like to acknowledge the Royal Thai Government and Suranaree University of Technology for funding my scholarship, which allows me to pursue a PhD in Sheffield.

ขอกราบขอบคุณเตี่ยกับแม่ผู้เป็นพระในบ้านของลูก เตี่ยกับแม่อบรม สั่งสอน สนับสนุน และเป็นกำลังใจให้ลูกได้ทำในสิ่งที่อยากทำมาโดยตลอดโดยไม่เคยมีเงื่อนไข ขอบคุณก้อยที่เป็นกำลังใจและช่วยดูแลเตี่ยกับแม่เป็นอย่างดีตลอดช่วงระยะเวลาหลายปีที่เจ๊ไม่อยู่บ้าน ขอบคุณความรักจากทุกคนในครอบครัวของเรา

Table of Contents

	Page
Acknowledgement	I
Table of Contents	III
List of Figures	IX
List of Tables	XIII
List of Abbreviations	XIV
Abstract	1
Chapter 1: Introduction	
1.1 Introduction	4
1.2 Cerebellum	6
1.2.1 Cerebellar structure, functions and circuits	6
1.2.2 Cerebellar development	9
1.3 Medulloblastoma	12
1.3.1 Clinical aspect	12
1.4 Hedgehog signalling	15
1.4.1 Lipid modifications and release of HH from producing cells to target cells	15
1.4.2 Principles of HH signal transduction	16
1.4.3 Mammalian SHH signalling and primary cilia	18
1.4.4 Multiple roles of HH signalling	19
1.4.4.1 Morphogenic and mitogenic functions of HH	19
1.4.4.1.1 HH functions as a morphohen	19
- Morphogenic role of HH in *Drosophila* wing imaginal disc	20
- Morphogenic role of SHH in neural development	21
1.4.4.1.2 HH functions as a mitogen	23

	Page
- Mitogenic role of SHH in cerebellum	23
1.4.5 Modulation of SHH signalling during the development of GNPs	24
1.4.5.1 Modulation of SHH signalling by other signals and molecule	24
1.4.5.2 Modulation of SHH signalling by cell contacts	25
1.5 L1-CNTNs	26
1.5.1 L1-CNTN structures	26
1.5.2 L1-CNTNs and modulation of proliferation	27
1.5.3 Expression of L1-CNTNs and their roles in cerebellar development	28
1.5.4 L1-CNTNs and SHH signalling	28
1.5.5 Role of L1-CNTN2 in modulating the signal of other membrane receptor by endocytosis or trafficking	30
1.6 The hypothesis and aims of this study	31
1.6.1 To determine whether NRCAM, F3 or TAG-1 are located to the primary cilia of proliferating GNPs	32
1.6.2 To determine whether loss of NRCAM affects the localisation of SHH pathway components to the primary cilium	32
1.6.3 To test whether NRCAM interacts with SHH pathway protein components, specifically PTCH1 or SMO	32
1.6.4 To investigate how loss of NRCAM affects SHH signalling	32
Chapter 2: Materials and Methods	
2.1 Animals	34
2.2 Genotyping	34
2.3 Primary granule cell culture	34
2.3.1 Granule cell (GC) preparation	34

	Page
2.3.2 Granule cell purification-gradient centrifugation	35
2.3.3 Granule cell purification – pre-plating step	37
2.3.4 Granule plating step and culture	37
2.4 Testing the optimal SHH concentration that gives maximal proliferation	38
2.5 Immunolabelling	39
2.6 NRCAM antibody pre-absorption	39
2.7 Immunofluorescence microscopy and image analysis	39
2.8 Statistical methods	42
2.9 Immunoprecipitation	42
2.9.1 Extraction of plasmid DNA	42
2.9.2 Restriction enzymatic digestion	42
2.9.3 Transfection of Cos-7 cells and protein harvesting	43
2.9.4 Immunoprecipitaion	44
2.10 SDS-PAGE and immunoblotting	44
2.11 NIH3T3-GL cell culture and transfection	45
2.12 Quantitative PCR (qPCR)	46
2.12.1 RNA isolation	46
2.12.2 cDNA synthesis	47
2.12.3 Protocol optimisation	47
2.12.3.1 Primer concentration	47
2.12.3.2 Standard curve	48
2.12.3.3 Melt curve	48
2.12.4 qPCR experimental design	48
2.12.5 qPCR reaction optimisation	48
2.12.6 qPCR analysis	49
2.13 Tables of antibodies, media and reagents using in this study	50

	Page
Chapter 3: Investigation of how NRCAM is involved in the SHH pathway	
3.1 Introduction	68
3.2 Results	
3.2.1 Investigation of primary cilia in the cerebellar section	69
3.2.2 Development of a protocol to visualise primary cilia of GNPs *in vitro*	69
3.2.3 Demonstration of PTCH and SMO localisation in primary cilia of cultured GNPs in response to SHH or SAG	76
3.2.4 NRCAM, TAG-1 but not F3 are present in primary cilia of GNPs	88
3.2.5 Loss of NRCAM affects the localisation of SMO and PTCH in primary cilia	91
3.2.6 Loss of NRCAM does not affect the percentage of GNP with primary cilium whether or not SHH is added	99
3.2.7 The occupancy of NRCAM in primary cilia is not affected in addition of SHH or SAG	101
3.3 Discussion	
3.3.1 Primary cilia of GNPs	104
3.3.2 L1-CNTNs in primary cilia of GNPs	106
3.3.3 The localisation of SMO and PTCH in primary cilia	106
3.3.4 Loss of NRCAM affects the localisation of SMO and PTCH in primary cilia	108
Chapter 4: Investigation of the interaction of PTCH1 and NRCAM	
4.1 Introduction	
4.1.1 Known interactions of PTCH and SMO with other proteins	112
4.2 Results	
4.2.1 Choice of transfected cell systems	114

	Page
4.2.2 Testing PTCH and SMO antibodies by western blot	118
4.2.3 Optimisation of *Ptch1*-YFP and *Smo*-YFP transfection protocol	119
4.2.4 Evaluation of protein-protein interaction	124
4.3 Discussion	
4.3.1 NRCAM may directly interact with PTCH1 but not SMO	131
4.3.2 Differences in expression of different PTCH1 and SMO constructs	132
4.3.3 Investigation of colocalisation of PTCH1 and NRCAM in primary cilia and investigation of protein interaction	133
Chapter 5: Investigation of how loss of NRCAM affects SHH signalling	
5.1 Introduction	135
5.2 Results	
5.2.1 Quantitative investigation of mRNA expression of *Gli1* and *Ptch1*	137
5.2.1.1 qPCR protocol optimisation	137
5.2.1.1.1 Optimal primer annealing temperature	138
5.2.1.1.2 Optimal primer concentration	141
5.2.1.1.3 Standard curve and PCR efficiency	141
5.2.1.2 Quantitative analysis of the mRNA expression of *Gli1* and *Ptch1* in wild type and *Nrcam*$^{-/-}$ GNPs in response to SHH or SAG	144
5.2.2 Investigation of Gli1 fluorescent intensity in the staining of GNPs in response to SHH or SAG	155
5.2.3 Investigation of GLI1 protein in NRCAM over-expressed NIH3T3-GL cells in response to SHH or SAG	159
5.2.3.1 Choice of cell for NRCAM over-expression	159
5.2.3.2 SHH signalling is not significantly affected in *Nrcam*-HA transfected NIH3T3-GL cells	162

Page

5.3 Discussion

5.3.1 Is SHH signalling really affected by loss of NRCAM? 165

Chapter 6: General discussion

6.1 The presence of NRCAM and TAG-1 in primary cilia of GNPs 171

6.2 NRCAM and SHH pathway 174

6.3 Loss of NRCAM affects SHH signalling pathway 175

6.4 Concluding remarks and future perspectives 180

References 182

List of Figures

		Page
Chapter 1: Introduction		
Figure 1.1.	Three layers in the surface gray matter of the cerebellum.	7
Figure 1.2.	The cerebellar circuitry.	9
Figure 1.3.	The development of granule neuron in mice.	11
Figure 1.4.	Hedgehog protein production and signal transduction.	16
Figure 1.5.	SHH signalling in primary cilia.	18
Figure 1.6.	The French flag model.	20
Figure 1.7.	Signal gradient plays a role in patterning the *Drosophila* wing imaginal disc.	21
Figure 1.8.	SHH gradient in the early neural tube development.	22
Figure 1.9.	Role of SHH in cerebellar growth.	23
Figure 1.10.	L1-CNTN protein structures.	27
Figure 1.11.	Possibilities of how F3 and NRCAM function in SHH pathway.	29
Chapter 2: Materials and Methods		
Figure 2.1.	Preparation of Percoll gradients for granule cell purification.	36
Figure 2.2.	30nM SHH drove maximal proliferation of GNPs at 24 hours.	38
Figure 2.3.	The principle of the quantification of interesting protein occupancy.	41
Chapter 3: Investigation of how NRCAM is involved in SHH pathway		
Figure 3.1.	Percentage of GNP populations after GNP preparation.	70
Figure 3.2.	Comparison of visualization of primary cilia of cultured	72

		Page
	WT GNPs at 2 different time-points: 6 and 24 hours.	
Figure 3.3.	Primary cilium is present on GNP.	75
Figure 3.4.	The localisation of SMO in primary cilia is increased upon addition of SHH and SAG.	79
Figure 3.5.	The localisation of PTCH in primary cilia is decreased upon addition of SHH or SAG.	81
Figure 3.6.	No nonspecific binding in secondary antibody labelling control.	83
Figure 3.7.	Grid-Apotome visualisation of the localisation of SMO and PTCH in primary cilia of GNPs when the cells were treated with SHH or SAG.	84
Figure 3.8.	Quantification of SMO and PTCH occupancies in primary cilia of GNPs after addition of SHH or SAG.	86
Figure 3.9.	NRCAM, TAG-1 but not F3 are present in primary cilia of WT GNPs.	89
Figure 3.10.	Loss of NRCAM affects SMO localisation in primary cilia of GNPs after addition of SHH or SAG.	93
Figure 3.11.	Loss of NRCAM also affects PTCH exit from primary cilia.	96
Figure 3.12.	No significant difference in the percentages of WT and *Nrcam*$^{-/-}$ GNPs with primary cilium after addition of SHH for 4.5 hours.	100
Figure 3.13.	The occupancy of NRCAM in primary cilia is not significantly affected by addition of SHH or SAG.	102
Chapter 4: Investigation of the interaction of PTCH1 and NRCAM		
Figure 4.1.	Comparative *Nrcam*-FL over-expression in NIH3T3 and Cos-7 cells.	116
Figure 4.2.	NIH3T3 and Cos-7 cells possess primary cilia.	117
Figure 4.3.	Testing SMO and PTCH1 antibodies on NIH3T3 cell lysate.	118
Figure 4.4.	Immunoblot of SMO-YFP and PTCH1-YFP protein	120

	overexpression in NIH3T3 cells.	
Figure 4.5.	Overexpression of PTCH1-GFP and SMO-GFP in Cos-7 cells.	123
Figure 4.6.	NRCAM seems to interact with PTCH1, but not SMO.	125
Figure 4.7.	NRCAM seems to interact with PTCH1 but the non-specific interactions are also present.	127
Figure 4.8.	NRCAM may interact with PTCH1 but not SMO.	130

Chapter 5: Investigation of how loss of NRCAM affects SHH signalling

Figure 5.1.	Optimal annealing temperature.	139
Figure 5.2.	Primer dimer is not shown in the qPCR reaction that performs with optimal annealing temperature of Gli1 primer.	140
Figure 5.3.	Specificity of primers used in this study.	142
Figure 5.4.	Examples of standard curves using primers used in this study.	143
Figure 5.5.	Quantitative PCR measurement of *Gli1* transcripts after addition of SHH for 4.5 and 24 hours to WT and *Nrcam*$^{-/-}$ GNPs.	146
Figure 5.6.	Quantitative PCR measurement of *Gli1* transcripts after addition of SAG for 4.5 and 24 hours to WT and *Nrcam*$^{-/-}$ GNPs.	148
Figure 5.7.	Quantitative PCR measurement of *Ptch1* transcripts after addition of SHH for 4.5 and 24 hours to WT and *Nrcam*$^{-/-}$ GNPs.	151
Figure 5.8.	Quantitative PCR measurement of *Ptch1* transcripts after addition of SAG for 4.5 and 24 hours to WT and *Nrcam*$^{-/-}$ GNPs	153
Figure 5.9.	Mean fluorescent intensity of GLI1 in WT and *Nrcam*$^{-/-}$ GNPs treated with SHH or SAG for 4.5 hours.	157
Figure 5.10.	Verification of GLI1 expression in 2 lines of NIH3T3 cells.	160

		Page
Figure 5.11.	Verification of GLI1 expression in NIH3T3-FC and NIH3T3-GL cells.	161
Figure 5.12.	The Expression level of GLI1 in NIH3T3-GL cells after *Nrcam*-HA transfection.	163
Figure 5.13.	qPCR machine performances before and after standardization.	167
Chapter 6: General discussion		
Figure 6.1.	Proposed model of the interaction of NRCAM and PTCH1 mediates the translocation of PTCH1 in primary cilia.	180

List of Tables

		Page
Chapter 2: Materials and Methods		
Table 2.1.	List of Primers used in this study	51
Table 2.2.	List of Buffer and Reagents for GC preparation and culture	52
Table 2.3.	List of Culture Media	55
Table 2.4.	List of Buffers and Fixative used in this study	56
Table 2.5.	List of Recombinant Proteins and Small Molecules	59
Table 2.6.	List of Primary antibodies used in this study	60
Table 2.7.	List of Secondary antibodies used in this study	62
Table 2.8.	List of DNA constructs used in this study	63
Table 2.9.	Recipes for SDS-PAGE 1.5mm mini	64
Table 2.10.	List of Kits and Special Materials	65
Table 2.11.	List of optimal annealing temperature and concentration of primers used in this qPCR experiment	66
Chapter 4: Investigation of the interaction of PTCH1 and NRCAM		
Table 4.1.	*Smo*-YFP, *Ptch1*-YFP and GFP transfection efficiencies in NIH3T3 cells	119
Table 4.2.	Comparison of methods to overexpress *Smo*-YFP and *Ptch1*-YFP in NIH3T3 cells	121
Table 4.3.	Comparison of the transfection efficiencies of NIH3T3 and Cos-7 cells	122
Table 4.4.	*Smo*-GFP and *Ptch1*-GFP transfection efficiencies in Cos-7 cells	122
Chapter 5: Investigation of how loss of NRCAM affects SHH signalling		
Figure 5.1.	Summary of the efficiencies of qPCR primers used in this study	144

List of abbreviations

AICD	Amyloid β precursor protein intracellular domain
amps	Amperes
ANOVA	Analysis of variance
APP	Amyloid β precursor protein
avg	Average quantity
BG	Bergmann glial cell
BIG-1/CNTN3	Contactin 3
BIG-2/CNTN4	Contactin 4
BME	Basal medium eagle
BMP	Bone morphogenetic protein
BOC	Brother of CDO
bp	Base pair
BSA	Bovine Serum Albumin
CAMs	Cell adhesion molecules
Caspr/CNTNAP	Contactin-associated protein
cDNA	Complementary DNA
CHL1	Cell adhesion molecule L1-like
Ci	Cubitus interruptus
CMF-PBS	Calcium- and magnesium- free phosphate-buffered saline
Co-IP	Co-Immunoprecipitation
CO_2	Carbon dioxide
Cos2	Costal-2
CPEC	Choriod plexus epithelium cell
C_t	Threshold cycle
CV	Coefficient of variation
DAPI	4',6-Diamidino-2-Phenylindole, Dihydrochloride

DEPC water	Diethylpyrocarbonate-treated water
dH_2O	Distilled water
DHH	Desert Hedgehog
DISP	Dispatched
DNA	Deoxyribonucleic acid
Dpp	Decapentaplegic
DTX1	Deltex1
E	Embryonic day
ECL	Enhanced chemiluminescence
ECM	Extracellular matrix
EDTA	Ethylenediaminetetraacetic acid
EGL	External granular layer
EvC	Ellis-van Creveld Syndrome
F3/CNTN1	Contactin 1
F3/fc	Cross-linked F3 protein
FBS	Fetal bovine serum
FGF	Fibroblast growth factor
FGFR	Fibroblast growth factor receptor
FN	Fibronectin
Fu	Fused
g	Acceleration of gravity
GAPDH	Glyceraldehyde-3-phosphate dehydrogenase
GAS1	Growth arrest-specific 1
GC	Granule cell
GCM	Granule cell medium
GCM+S	Granule cell medium with serum
GFAP	Glial Fibrillary Acidic Protein
GFP	Green fluorescent protein

Gli	Glioma-associated oncogene family zinc finger
GN	Granule neuron
GNP	Granule neuron progenitor
GPI	Glycosphosphoinositol
GSK2	G-protein couple receptor kinase 2
hESC	Human embryonic stem cell
HH	Hedgehog
HH-N	N-terminal domain of Hedgehog protein
HRP	Horseradish peroxidase
iEGL	Inner external granular layer
IFT	Intraflagella transport
Ig	Immunoglobulin
IGF	Insulin growth factor
IGL	Internal granular layer
IHH	Indian Hedgehog
ILK	Integrin-linked kinase
IP	Immunoprecipitation
KIF	Kinesin family member
L1-CNTN	L1-contactin
L1/L1CAM	L1 cell adhesion molecule
LB agar	Luria-Bertani agar
LB medium	Luria-Bertani medium
LN	Laminin
MB	Medulloblastoma
MEM	Minimal essential medium
MIZ	Myc-interacting Zinc finger protein
ml	milliliter
ML	Molecular layer

mm	Millimeter
mm	Millimeter
MN	Motor neuron
N.S.	not significant
NB-2/CNTN5	Contactin 5
NB-3/CNTN6	Contactin 6
NFASC	Neurofascin
ng	Nano gram
NRCAM	Neural cell adhesion molecule
NRP	Neuropilin
oEGL	Outer external granular layer
p	p-value
P	Postnatal day
PAX6	Paired box 6
PBS	Phosphate-buffered saline
PBT	Triton-X in phosphate-buffered saline
PCL	Purkinje cell layer
PCR	Polymerase chain reaction
PDL	Poly-D-Lysine hydrobromide
PFA	Paraformaldehyde
PLA	Proximity Ligation Assay
PTCH	Patched
qPCR	Quantitative polymerase chain reaction
r	Radius
Rab	Rab GTPase
RIPA buffer	Radioimmunoprecipitation assay buffer
RNA	Ribonucleic acid
rpm	Round per minute

RPTPβ	Receptor protein tyrosine phosphatase β
RT	Reverse transcriptase
SAG	Smoothened agonist
SAGE	Serial analysis of gene expression
SDS-PAGE	Sodium dodecyl sulfate polyacrylamide gel electrophoresis
SEER	The Surveillance, Epidemiology and End Results
SEM	Standard error of mean
SEMA	Semaphorin
Sema3A	Semaphorin3A
SHH	Sonic hedgehog
SMO	Smoothened
SMOA1	Constitutive active form of Smoothened
SSTR3	Somatostatin
stdev	Standard deviation of the average
SuFu	Suppressor of fused
TAE buffer	Tris-acetate-EDTA buffer
TAG-1/CNTN2	Contactin 2
TBST	Tris Buffered Saline with Tween® 20
TIE2	Angiopoeitin receptor 2
UV	Ultraviolet
VN	Vitronectin
volts	Voltages
WHO	World Health Organisation
WT	Wild type
YFP	Yellow fluorescent protein
ZPA	Zone of polarizing activity

Abstract

Proliferation of cerebellar granule neuronal progenitors (GNPs) is known to be mediated by Sonic Hedgehog (SHH) signalling and dysfunction of this signalling is known to underlie the formation of a major subset of medulloblastomas (MBs), the most common brain tumours of children; however, the mechanism by which this proliferation is regulated is not well understood. Recent data from our lab have demonstrated that neural adhesion molecules belonging to the L1CAM-contactin (L1-CNTN) family are involved in modulating GNP proliferation and differentiation. F3/contactin, a GPI-linked member of the L1-CNTN family, is able to induce the mitotic exit and neuronal differentiation of GNPs, counteracting the normal effect of SHH *in vitro*, whereas TAG-1, another member of CNTN family, acts antagonistically to F3 activity. F3 appears to act on GNPs through binding to NRCAM, an L1 family member, and can no longer suppress SHH-induced proliferation of GNPs from *Nrcam*$^{-/-}$ mice. Therefore F3 and NRCAM appear to be important for suppressing SHH-induced proliferation in GNPs.

It is known that in vertebrates Hedgehog signalling requires a primary cilium. Signalling occurs when SHH binds to its receptor Patched (PTCH) and causes it to translocate out of the cilium, which in some way allows the seven-transmembrane protein, Smoothened (SMO) to translocate into the cilium to activate SHH signalling. Exactly how these translocations occur is not fully understood, but evidence suggests that this requires endocytosis and intracellular trafficking. Since in other contexts L1-CNTNs are known to be involved in such processes, the hypothesis of this study is that L1-CNTNs might be involved in modulating SHH signalling by trafficking of SHH pathway component proteins into or out of primary cilia of SHH-induced GNP proliferation.

Here I demonstrate the presence of NRCAM and TAG-1 in primary cilia and show that loss of NRCAM affects both PTCH and SMO ciliary localisation, most likely, therefore, implicating NRCAM in PTCH trafficking. Consistent with this, my co-immunoprecipitation studies suggest that NRCAM physically interacts with PTCH1, but not SMO. I show also that the kinetics of SHH signalling in GNPs is affected by loss of NRCAM. Taken together, my data seem to suggest that NRCAM plays a role in modulating SHH signalling by regulating

the trafficking of PTCH1 in the primary cilia of GNPs. The discovery of a role for L1-CNTNs in modulating SHH signaling in principle could lead to novel treatments for MB in the future.

Chapter 1

Introduction

1.1 Introduction

Abnormal regulation of cell proliferation resulting in many kinds of cancer raises the question of how normally the cell proliferation is controlled. It is not sufficient to simply programme a cell to undergo a certain number of divisions when an organised tissue is formed. The proliferation of cells must be coordinated between cells and environment. Cellular communication is therefore very important, particularly when a tissue or structure is being formed in the developing embryo, as it needs to expand the number of cells and organise specific cell types into particular places. Not surprisingly, therefore, it has been found that molecules mediating cell-cell interactions play a vital role in controlling cell proliferation and differentiation. Among such molecules are secreted proteins such as Fibroblast Growth Factors (FGFs) (Gallagher, 2007) and Sonic Hedgehog (SHH), which can diffuse between cells to pattern growth and differentiation over long distances (Briscoe and Therond, 2013). However, it is clear that short range, cell contact interactions are also important in coordinating morphogenesis in the nervous system (Bizzoca et al., 2003, Louvi and Artavanis-Tsakonas, 2006, Kamiguchi, 2007, Decker et al., 2004, Hirano and Takeichi, 2012, Xenaki et al., 2011). Moreover, there are clear examples that these interact with signals from diffusible patterning molecules to modulate their effect (Pons et al., 2001, Blaess et al., 2004, Zhang et al., 2013). Precisely how these two different kinds of signal interact, however, is not well understood.

In the cerebellum, SHH secreted from Purkinje cells stimulates an increase in the number of dividing cerebellar granule neuron progenitors (GNPs) (Dahmane and Ruiz i Altaba, 1999, Wallace, 1999, Wechsler-Reya and Scott, 1999) and loss of SHH leads to a failure of the granule cell layer to expand normally and a severe reduction in cerebellar size (Lewis et al., 2004). SHH is therefore an essential mitogen in the growth of the cerebellar cortex and SHH signalling is a key pathway driving proliferation of GNPs. Moreover, it is clear that modulation of SHH signalling levels can affect the size and morphogenesis of the cerebellum (Corrales et al., 2004, Corrales et al., 2006). However, how SHH levels are modulated locally in the developing cerebellum is not clear. While there is some evidence that this may be done at the transcriptional level to vary signalling between lobules (Corrales et al., 2004), how local modulation is achieved is not understood. A particular puzzle, for example, is why GNP proliferation is strongest in those cells most distant from the source of SHH, the

Purkinje cells. One suggestion is that the morphogen is shaping the tissue by integrating its signal with those arising from cell contacts and in fact there is evidence for contacts affecting SHH signals (Bizzoca et al., 2003, Pons et al., 2001, Blaess et al., 2004, Xenaki et al., 2011). Therefore the main aim of this study is to understand the mechanism by which cell contacts affect SHH signalling in the context of cerebellar development looking specifically at the interaction between adhesion molecules of L1-CNTN family and SHH signalling.

L1-CNTNs are a family of neural adhesion molecules named for their founder members L1CAM (L1; (Maness and Schachner, 2007)) and F3/contactin (CNTN; (Shimoda and Watanabe, 2009)), immunoglobulin-like glycoproteins linked to the plasma membrane by transmembrane or glycosyl phosphatidylinositol (GPI) anchors, respectively. Their expression is extensive in the nervous system, albeit not exclusively, as they also expressed in endothelial tissues (Glienke et al., 2000). In the nervous system they have been implicated in a broad range of post-mitotic processes, including cell migration, axon guidance, synaptogenesis, myelination and the generation of axon potentials (Maness and Schachner, 2007, Shimoda and Watanabe, 2009). However, recent evidence suggested that they might also be involved in controlling earlier, mitotic events (Bizzoca et al., 2003, Hu et al., 2003, Ma et al., 2008, Xenaki et al., 2011) and indeed L1-CNTNs have been implicated in a number of cancers (Katidou et al., 2008).

The work of Xenaki et al (2011) showed that F3/contactin (hereafter referred to as F3) antagonises TAG-1, also a CNTN-like molecule, to suppress SHH-induced proliferation of GNPs. F3 binds to NRCAM, an L1-like member of the family, on the GNP cell surface and SHH-induced proliferation of NRCAM knockout GNPs fails to be inhibited by F3, suggesting that NRCAM is the receptor mediating F3 inhibition. However, the mechanism underlying this inhibition is not understood.

In this thesis, I have investigated how NRCAM controls SHH-induced proliferation of GNPs. Since mis-regulation of GNP proliferation resulting from aberrant SHH signalling can result in medulloblastoma (MB), the most common malignant brain tumor in children and young adults (Behesti and Marino, 2009), this study not only sheds light on the control of GNP proliferation in normal cerebellar development, but may also be relevant to the process of MB tumorigenesis and perhaps offer a method of modulating SHH signalling by

identifying novel therapeutic targets for the treatment of MB.

1.2 Cerebellum

The cerebellum has served as an excellent model system for studying cell proliferation and differentiation in the brain, as it largely develops post-natally, it has a relatively small number of cell types and a simple basic structure (Altman and Bayer, 1997). Moreover, the anatomical organisation of cerebellar cortex is well characterised and all cell types and the neuronal circuits have been studied extensively (Hatten and Heintz, 1995, Goldowitz and Hamre, 1998). For these reasons, the cerebellum is used as a model for this study.

1.2.1 Cerebellar structure, functions and circuits

The cerebellum is located on the dorsal part of the brainstem. Its structure is composed of the deep cerebellar nuclei in a central core of white matter and a large cortical region, which contains several cell types such as Purkinje neurons, Bergmann glial cells (BG), granule neurons (GN). After the cerebellum is fully developed, there are three layers in the surface gray matter of the adult cerebellum. As shown in figure 1.1, the most superficial layer is the molecular layer (ML), which consists of the axons of granule cells, known as parallel fibers, and dendrites of Purkinje cells. The middle layer, the Purkinje cell layer (PCL), is made up of the large cell bodies of Purkinje cells and Bergmann glia. The deepest layer, the granular layer, consists primarily of the cell bodies of granule neurons, very small neurons, which are also the most numerous in the brain (Altman and Bayer, 1997).

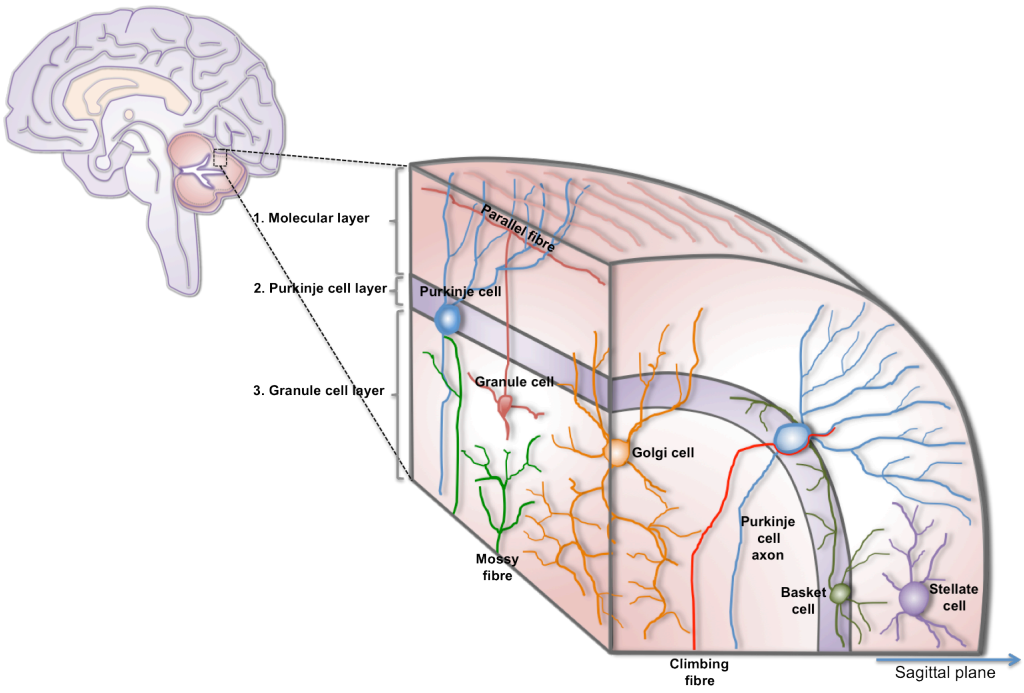

Figure 1.1. Three layers in the surface gray matter of the cerebellum. Molecular layer, Purkinje cell layer and Granule cell layer (modified from (Dale Purves, 2001).

Previously, it was thought that the major functional roles of the cerebellum are only coordination, maintenance of equilibrium and regulation of muscle tone. More recently it is evident that the cerebellum functions in motor learning processes, through which it can adapt and finely adjust motor programs in order to perform correct and precise movements via an error-driven induction of long-term depression (LTD) (Ito, 1998, Yeo and Hesslow, 1998, Ito, 2000).

The cerebellar circuitry integrates data among neurons inside and outside the cerebellum such as inferior olive, pontine nuclei (from cerebral cortex), spinal cord, vestibular system and thalamus. The functional integration of signals is mainly mediated by two types of neurons, Purkinje cells and granule neurons (Altman and Bayer, 1997). Purkinje cell axons constitute the main output projections from the cerebellum and cerebellar granule neurons control this cerebellar output by regulating Purkinje cell activity. Mice that lack cerebellar granule cells exhibit severe ataxia indicating the crucial function of these cells (Kofuji et al., 1996, Hamre and Goldowitz, 1997, Mullen et al., 1997).

As shown in Fig 1.2, axons from granule neurons ascend towards the cortical surface and then bifurcate to form T-shaped branches in the ML, forming parallel fibres. The parallel fibres relay information via synapses on the dendrites of the Purkinje neurons, as well as exciting the Golgi, stellate, and basket neurons, which here are grouped and called inhibitory interneurons. These latter also synapse on Purkinje neurons, which thus receive excitatory input from the parallel fibres and from climbing fibres from the inferior olive, and inhibitory input from the inhibitory interneurons. The granule neurons themselves receive an excitatory input from the axons extending from pontine nuclei, called mossy fibres. The deep cerebellar nuclei also receive excitatory synapse from the mossy fibres as well as the excitatory input from climbing fibres. However, they also receive inhibitory input from axons extended from Purkinje neurons. In the same time, the deep cerebellar nuclei provide an inhibitory feedback to the inferior olive. This complex interaction of inhibitory and excitatory inputs allows the cerebellum to perform its core function of LTD-mediated error correction to refine motor performance

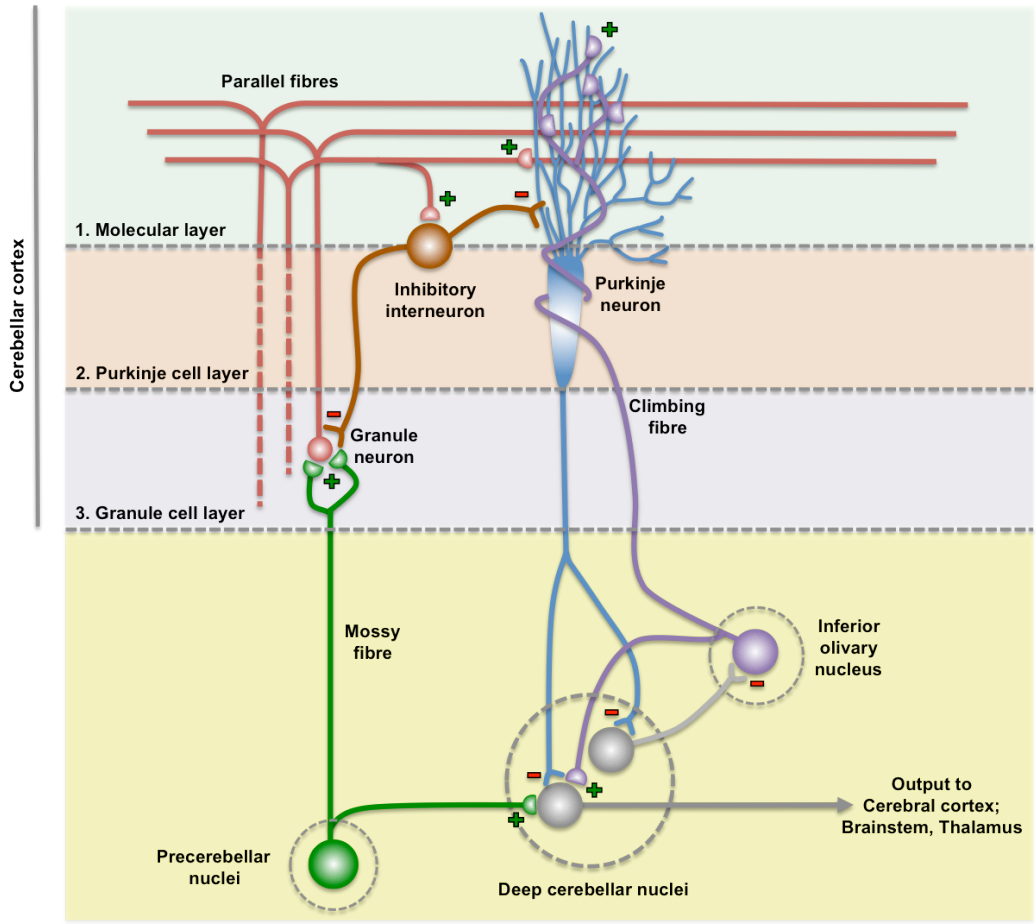

Figure 1.2. The cerebellar circuitry. Purkinje neurons, GABAergic neurons located in the Purkinje cell layer, exert an inhibitory input on the deep cerebellar nuclei, whereas the Purkinje neurons themselves receive inhibitory input from the inhibitory interneurons. However, they are stimulated by excitatory input from both climbing fibres from inferior olive and parallel fibres, bifurcated axons from the granule neurons. Although the granule neurons receive excitatory input from mossy fibres, axons from the pontine nuclei, they are also inhibited by inhibitory interneurons. The mossy fibres as well as climbing fibres send signal stimulating the deep cerebellar nuclei; at the same time, the deep cerebellar nuclei give rise axons to send the inhibitory input to the inferior olive (modified from (Ito, 2002)).

1.2.2 Cerebellar development

During cerebellar development cells arise from two different regions. The first area is the ventricular zone, from which the cells of the deep cerebellar nuclei, the Purkinje neurons, and stellate, basket and Golgi interneurons all arise. The second region is a diamond-like structure between the 4th ventricle and the

neural tube called rhombic lip, where the progenitors of cerebellar granule neurons are born. As this study focuses on the proliferation of GNPs, this introduction highlights mainly the development of GNPs in the cerebellum, which, along with the progenitors of the neurons of the lateral pontine nuclei, arise from the rostral (or cerebellar) rhombic lip (fig 1.3); cells of the medial pontine, the reticulotegmental, lateral reticular, external cuneat and inferior olive nuclei all derive from the caudal rhombic lip (Wingate, 2001).

In early development of cerebellum (from mid-gestation in the mouse), GNPs arise from the rostral rhombic lip and migrate tangentially over the dorsal surface of the rostral hindbrain (Hatten and Heintz, 1995) to form the external germinal layer (EGL). Because GNPs continue to proliferate into the early postnatal period, the thickness of EGL increases considerably. After the final mitotic division, there is also lateral tangential migration of post-mitotic granule neurons within 20-48 hours while they remain in EGL (Komuro et al., 2001, Yacubova and Komuro, 2003, Kumada et al., 2009). Then, the migratory direction of granule neurons turns to radial migration to form the internal granule layer (IGL) (figure 1.3). In this process, BG provides radial glial fibers through the ML, which direct the majority of the migrating neurons to the IGL. Meanwhile, the granule cells give rise to axons that bifurcate in the molecular layer and these T-shaped axons extend long distance to synapse on the dendrites of Purkinje cells. However, the cell bodies of granule cells continue to migrate past the PCL until they reach into the IGL.

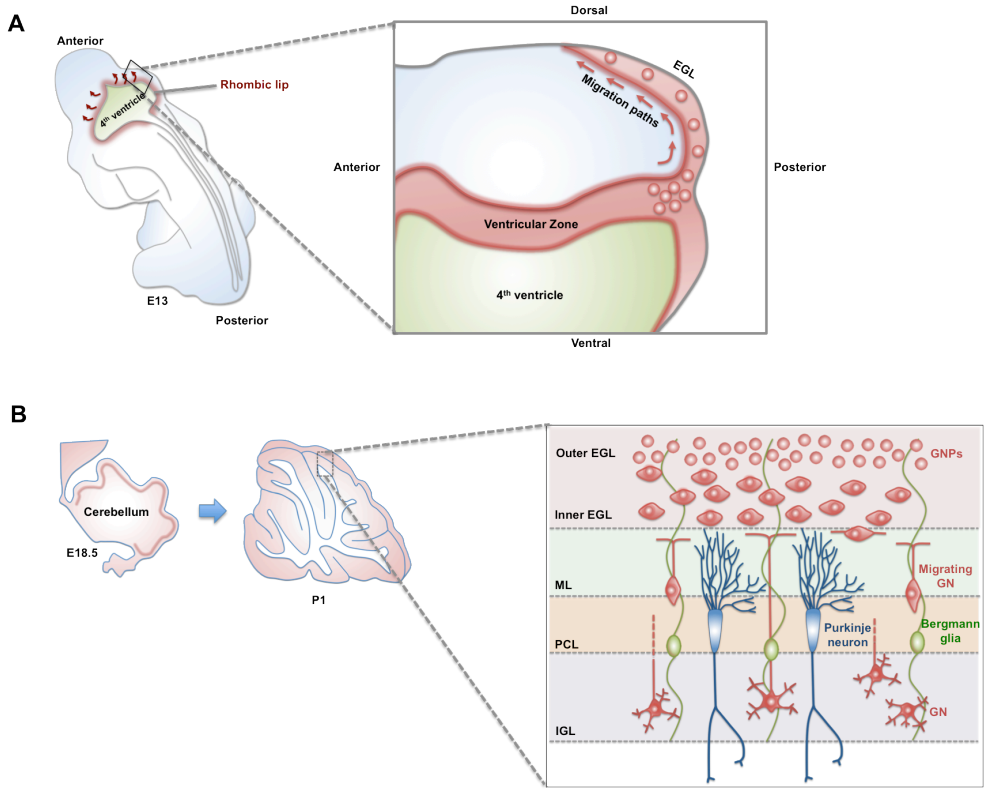

Figure 1.3. The development of granule neurons until early period in mice. **(A)** The formation of EGL from the rhombic lip. Schematic sagittal section of developing embryonic cerebellum shows the migration paths of GNPs from the rhombic lip over the surface of anlage to form the external granular layer (EGL). The GNPs then massively expand until early postnatal period. **(B)** The postnatal radial migration of post-mitotic granule neurons. After birth, the GNPs still extensively proliferate within EGL. Whenever they exit cell cycle, the appearance of their cell bodies changes from horizontal to vertical in order to migrate again along the radial fibers of Bergmann glia (BG) though molecular layer (ML) to form the internal granular layer (IGL) (modified from (Wang and Zoghbi, 2001, Marques and Fan, 2002).

A substantial amount is now known about how the proliferation and differentiation of GNPs is controlled (Behesti and Marino, 2009). Although, there are many signalling pathways known to regulate GNP production and proliferation, including FGF (Gao et al., 1991, Tao et al., 1996, Wechsler-Reya and Scott, 1999), BMPs (Alder et al., 1999, Rios et al., 2004, Machold et al., 2007), Notch (Solecki et al., 2001), IGF (Ye et al., 1996, Lin and Bulleit, 1997), WNT, (Anne et al., 2013), a key player in this process is the secreted factor Sonic hedgehog (SHH), which is made by Purkinje cells and drives the

proliferation of GNPs in the EGL (Dahmane and Ruiz i Altaba, 1999, Wallace, 1999, Wechsler-Reya and Scott, 1999, Lewis et al., 2004, Corrales et al., 2004, Corrales et al., 2006). Dysregulation of this pathway can cause the cerebellar tumor, medulloblastoma (MB), for example through mutation of the SHH receptors Patched (*Ptch1*) and Smoothened (*Smo*) (Goodrich et al., 1997, Oro et al., 1997, Xie et al., 1998). MB is the most common malignant brain tumor in children and young adults (Fan and Eberhart, 2008). Below I first briefly review the clinical classification of MB and introduce how a substantial proportion of MB involves dysfunction of the SHH pathway. Then I go on to consider in more detail the involvement of the Hedgehog (HH) signalling pathway in normal cerebellar morphogenesis and how this may relate to MB.

1.3 Medulloblastoma

Medulloblastoma (MB) is the most common pediatric malignant brain tumor (Chintagumpala et al., 2001), with origins in the cerebellum. According to the Surveillance, Epidemiology and End Results (SEER) database, MB affects 1:150,000 children (Smoll and Drummond, 2012) and this accounts for approximately 20% of all pediatric central nervous system tumors (Dhall, 2009). MB is thought to be caused by deregulation of neural cerebellar precursor cell proliferation. Since the main focus of this thesis is to investigate the mechanism of how L1-CNTNs modulate the SHH signalling, which is the key pathway of driving GNP proliferation, findings from this study may be applied to new treatments of MB to specifically regulate the SHH signalling in the future. Therefore, here I briefly introduce a clinical perspective of MB, which includes the current treatment of MB and the signaling pathways thought to contribute to MB tumorigenesis.

1.3.1 Clinical aspect

According to the 2007 WHO classification of the tumors of the central nervous system, MB are sub-classified onto 5 histologic types (Giangaspero et al., 2007): (1) classic MB which is characterised by the presence of small cells with small round nuclei, which are are arranged in layers or sheets, (2) desmoplastic/nodular MB which is defined by small mitotic cells and in which the nodules of tumour cells are surrounded by collagen rich tissue (Gilbertson,

2004). It has been shown that the desmoplastic MB is linked to the SHH signalling aberration (Pietsch et al., 1997, Wolter et al., 1997), (3) MB with extensive nodularity (MBEN), (4) anaplastic MB which the tumor cells are large and they are not differentiated and (5) large cell MB which the tumor cells are relatively high ratio of cytoplasm to nuclei.

MB is also molecularly sub-classified into four subtypes (Taylor et al., 2012, Kool et al., 2012) as follow:

(1) Subtype 1: MB with aberration of the WNT signalling pathway which accounts for 10-15% of MB (Li et al., 2013): this subtype is characterized by the gene expression signature of WNT signalling and beta-catenin nuclear staining. It is usually classified as the classic MB on the basis of histological examination.

(2) Subtype 2: MB with the aberration of SHH signalling pathway, which accounts for 25-30% of MB (Li et al., 2013): this subtype is characterised by frequent deletion of chromosome 9q, desmoplastic/nodular histology and SHH pathway gene mutations, such as *Ptch1, Smo* and *SuFu.* The tumor is thought to arise from the EGL of the cerebellum. The SHH subset normally occurs in children younger than 3 years and also in adolescents and adults.

(3) Subset 3 (Group 3): This subtype appears histologically as classic MB or large cell MB or anaplastic MB. A variety of mutations are present in this subtype, including the presence of 17q isochromosome (i17q, in which the short arm of chr 17 is lost and the long arm duplicated), which is a negative prognostic factor in the disease. Subset 3 occurs throughout childhood and also in infants.

(4) Subset 4 (Group 4): This subset shows molecularly a *CDK6* amplification and *MYCN* amplification, and it may also present with i17q. The histology of the subset 4 is classic MB, large cell MB or anaplastic MB. The subset 4 tumour is observed from infancy into childhood and adulthood.

As this study is focused on SHH signalling, which is important for the GNP proliferation during the cerebellar development, the findings from this study may be useful and implicated in the desmoplastic MB/Subtype 2. Below, I review how the SHH pathway is implicated in medulloblastic transformation and pathogenesis

It has been shown that mutation of the genes encoding the key proteins of SHH pathway (PTCH, SUFU and SMO; see below for a detailed description of the pathway) results in 25% of sporadic human MB (Zurawel et al., 2000). Moreover, a number of studies in mouse have shown that activation of the SHH pathway causes MB: the classic example is the development of MB in Patched heterozygotes (*Ptch*$^{+/-}$). PTCH is a negative regulator of the pathway (see below); although *Ptch* null (*Ptch*$^{-/-}$) mice die during embryonic stages, *Ptch*$^{+/-}$ mice are viable but develop MB from around 5 weeks after birth and approximately 30% of *Ptch*$^{+/-}$ mice developed MB within the 12-25 weeks of age (Goodrich et al., 1997). This mimics the human condition known as Gorlin (or nevoid basal cell carcinoma) syndrome, suffers of which also develop a variety of generalised overgrowth problems, MB and rhabdomyosarcoma, many of which have also been found in *Ptch*$^{+/-}$ mice and can be related to increased SHH signalling (Hahn et al 1998).

Similar to the *Ptch*$^{-/-}$ mouse, *Sufu*$^{-/-}$ mice are also early embryonic lethal around E10 due to failures of neural tube closure and heart defects. Although the MB formation is not frequent in *Sufu*$^{+/-}$ mice, it is present in 58% of *Sufu*$^{+/-}$ *p53*$^{-/-}$ mice, whereas this is not observed in *p53*$^{-/-}$ mice alone (Lee et al., 2007). Moreover, 94% of homozygous transgenic mice, which express the constitutive active form of *Smo (*SmoA1*),* shows MB formation within 2 months after birth (Hatton et al., 2008). Taken together, the studies clearly demonstrate that aberration of SHH pathway regulation contribute to MB tumorigenesis.

Similar to the other brain cancers, MB treatment commonly involves surgery, chemotherapy and radiotherapy. Although advances in the current treatment of MB can cure patients, leading to a five year overall survival about 70%-90% with standard to high risk patients (Carlotti et al., 2008), the majority of the surviving children still suffer from the long-term neurocognitive and neuroendocrine complications due to the side-effects of the therapy (Mulhern et al., 2005, Ribi et al., 2005), as well as other long term consequences, resulting from the cytotoxicity and lack of specificity of the treatment (Marino, 2005). Therefore, better understanding of aberrant signalling pathway involving in MB pathogenesis and how to regulate the signalling would provide potential pharmaceutical target treatment or new perspectives of therapeutic development of the MB in the future.

1.4 Hedgehog signalling

The hedgehog (*hh*) gene was originally discovered as a regulator of body segment polarity in *Drosophila melanogaster* (Nusslein-Volhard and Wieschaus, 1980). This gene was found later to encode a lipid-modified secreted signalling molecule, Hedgehog (HH), which plays a crucial role by acting as a local mediator in many developmental processes in vertebrates. The HH signalling pathway has been studied extensively particularly in embryogenesis (Ingham and Placzek, 2006). Abnormal regulation in the HH pathway can lead to organ malformation or even lethality and cancer such as basal cell carcinoma, MB (McMahon et al., 2003, Nieuwenhuis and Hui, 2005).

Although there is only 1 *hh* gene in *Drosophila*, there are 3 mammalian *Hh* genes encoding similar secreted proteins: Sonic Hedgehog (SHH), Indian Hedgehog (IHH) and Desert Hedgehog (DHH). DHH plays an important role in spermatogenesis (Bitgood et al., 1996), whereas IHH controls endochondral ossification (Vortkamp et al., 1996) and also regulates blood island angiogenesis (Byrd et al., 2002). Among these ligands, SHH is the most extensively studied (Gilbert, 2000) and it is involved in development of left-right axis as well as regulation of the ventral cell fate in the central nervous system. Moreover, it plays a vital role in specification of anteroposterior axis of the limb development and morphogenesis of various organs, including eye development (McMahon et al., 2003). Abnormal regulation of the level of HH signalling, including complete loss of SHH (Chiang et al., 1996) is associated with variety of defects during the development including cyclopia, defective axial patterning and limb abnormalities. Complete loss of SHH is embryonic lethal (Chiang et al., 1996).

1.4.1 Lipid modifications and release of HH from producing cells to target cells

The HH protein undergoes various processing steps before it can function. As shown in fig 1.4 (a HH secreting cell is on the left), HH is produced as a 45kDa precursor protein, followed by the post-translational modification. First, the HH precursor protein is autocatalytically cleaved, resulting in a 20kDa *N*-terminal domain (HH-N) and 25kDa *C*-terminal domain. After autocatalytic cleavage, cholesterol is added to the carboxyl end of HH-N, followed by addition of palmitate to the *N*-terminal. This mature HH is then released to the secretory pathway via Dispatched (Disp), a 12-transmembrane protein that works as a HH

transporter.

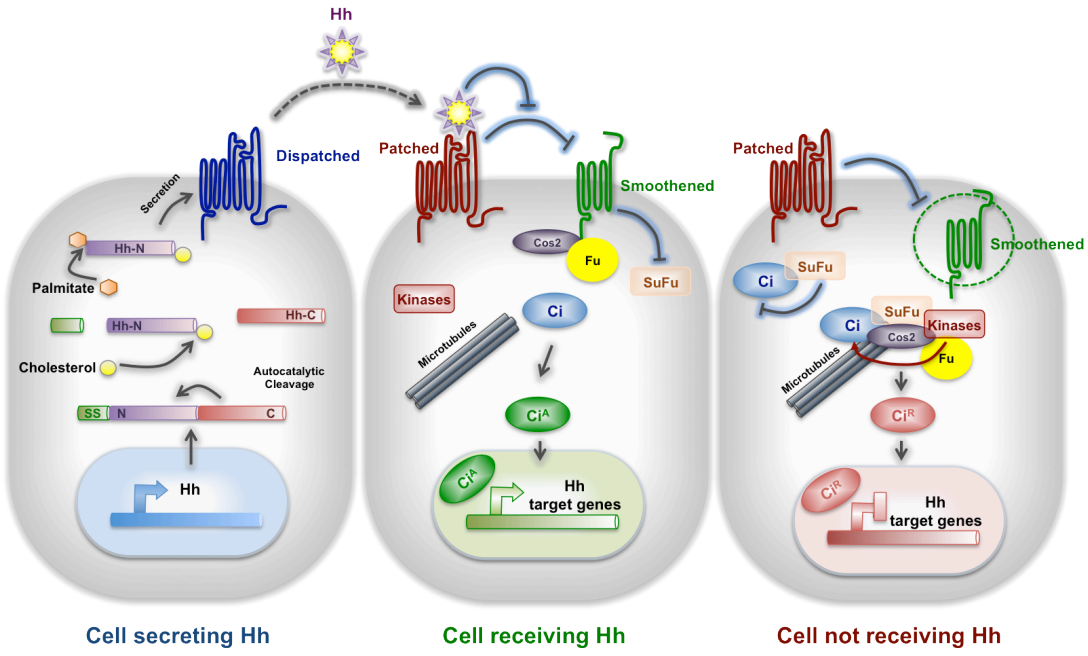

Figure 1.4. Hedgehog protein production and signal transduction. In HH-secreting cell (left), full-length HH is autocatalytically cleaved to yield an *N*-terminal fragment (HH-N), which is modified by cholesterylation. After palmitoylation, Dispatched (Disp) mediates the secretion of a mature HH-N. In *Drosophila*, when HH is released to the cell receiving HH (middle), it binds to its receptor, Patched (PTCH). This binding relieves PTCH inhibition of Smoothened (SMO), leading to the accumulation of SMO on the cell surface and the downstream pathway can be activated via CI^A, resulting in the transcription of HH target genes. In the absence of HH (right), SMO activation is blocked by PTCH, resulting in the phosphorylation of full-length CI (CI) to repressor form (CI^R), which prevents the transcription of HH target genes in the nucleus. The diagram is adapted from (Nieuwenhuis and Hui, 2005, Goetz and Anderson, 2010)

1.4.2 Principles of HH signal transduction

The HH pathway in *Drosophila* is much simpler than that in the mammals. In *Drosophila*, there is only one Patched (PTCH) protein, which is a 12-transmembrane HH receptor. In the absence of HH, PTCH represses the activation of Smoothened (SMO), a 7-transmembrane receptor (Figure 1.4, right). Although it has been shown that the subcellular localisation of SMO is

affected in HH-stimulated cells in *Drosophila* salivary gland (Zhu et al., 2003), how exactly SMO is repressed by PTCH in unstimulated cells remains unclear. A full-length zinc-finger transcription factor Cubitus interruptus (Ci), which normally forms a microtubule-associated complex with kinesin-like protein Costal-2 (Cos2), Fused (Fu) and Suppressor of fused (SuFu), is phosphorylated by multiple protein kinases, including Protein kinase A (PKA), Casein kinase I (CKI) and Glycogen synthase kinase 3β (GSK3β), resulting in a subsequent cleavage to truncated repressor form (Ci^R), which inhibits HH target genes. Cos-2 acts as a scaffold to bind Ci and the protein kinases, whereas, SuFu inhibits the nuclear translocation of the full-length Ci. The HH signalling occurs when the HH protein binds PTCH, which relieves the SMO repression (Figure 1.4, middle), allowing SMO to accumulate on the cell surface and disrupt the phosphorylation of the full-length Ci and subsequent cleavage to the repressor form, Ci^R by dissociating Cos-2/Ci/kinase complexes. Fu antagonises the inhibition of SuFu, when a high level of HH is present to convert the full-length Ci to become a transcriptional activator (Ci^A), which can activate HH target genes.

The binding of HH to PTCH results in the removal of PTCH from the cell surface by dynamin-dependent endocytosis and its accumulation in intracellular vesicles with subsequent degradation in lysosomes (Incardona et al., 2000, Martin et al., 2001). However, it has been suggested that the HH signal transduction does not require the internalisation of HH-PTCH complex (Torroja et al., 2004). Instead, the internalisation and degradation of HH-PTCH complex may be required to limit HH availability which may play a role in the formation of HH gradients (Chen and Struhl, 1996, Torroja et al., 2004),

In mammals, there are 2 HH receptors, PTCH1 and PTCH2. Although, there are three HH proteins in mammals, they bind both receptors with similar affinity (Carpenter et al., 1998). However, PTCH2 is expressed at high level in the testis and the signal is mediated by DHH (Carpenter et al., 1998). As in *Drosophila*, however, there is only one vertebrate SMO which is implicated in all HH signalling (Zhang et al., 2001, Chen et al., 2001). The Kinesin proteins, KIF7 and KIF27 are vertebrate homologue proteins of Cos-2 protein in fly (Tay et al., 2005, Katoh and Katoh, 2004), and they act as positive and negative regulators of HH signalling pathway (Endoh-Yamagami et al., 2009, Liem et al., 2009, Cheung et al., 2009, Tay et al., 2005). The Ci homologs in mammals are the GLI family transcription factors GLI1, GLI2 and GLI3. GLI1 acts as a transcriptional

activator, while GLI3 plays a repressor role. Critically, however, GLI2 can act as either transcriptional activator or repressor, which is an essential part of the signalling pathway (see below).

1.4.3 Mammalian SHH signalling and primary cilia

In the last ten years or so, it has been shown that the activity of the mammalian SHH signalling pathway requires tiny subcellular structures known as primary cilia for its function (Huangfu et al., 2003, Corbit et al., 2005, Huangfu and Anderson, 2005, Rohatgi et al., 2007, Han et al., 2008, Spassky et al., 2008) (Figure 1.5). Several essential components in the transduction of SHH signalling have been detected in the primary cilia including PTCH1, SMO and the GLIs (Corbit et al., 2005, Haycraft et al., 2005, Huangfu and Anderson, 2006).

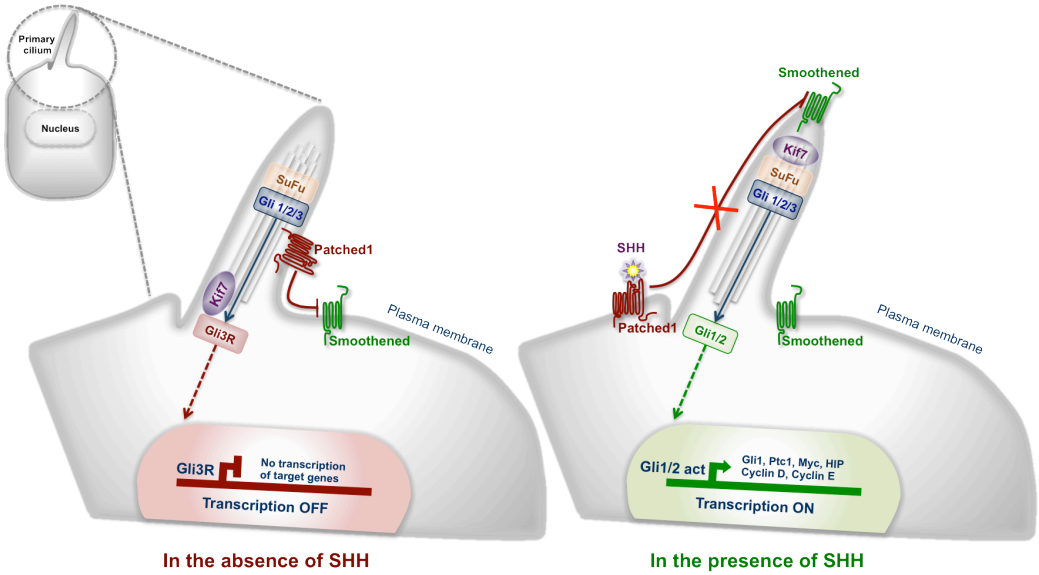

Figure 1.5. SHH signalling in primary cilia. In vertebrates, the primary cilium is required for SHH signalling. In the absence of SHH, PTCH1 localises in the primary cilium and this inhibits SMO ciliary localisation. The GLI accumulation in the cilium is blocked by the localisation of KIF7 at the base of the primary cilium, resulting in the production of the repressor form of GLI (GLI^R). In the presence of SHH, SHH binds to PTCH1 and the complex translocates out of the cilium. This allows SMO entry to the cilium. KIF7 localises at the tip of the cilium, leading to the accumulation of GLI at the cilia tip. The function of SUFU is inhibited by KIF7, which now localises at the tip of cilia. The activator form of GLIs is promoted resulting in the transcription of SHH target genes.

However, the localization of SMO to cilia normally is dependent on the presence of SHH. In its absence, PTCH1 in some way normally prevents SMO translocation, although SMO ciliary translocation can occur without PTCH removal when using SMO-agonists, such as SAG (Rohatgi et al., 2007). As SHH binds to PTCH1, translocation of PTCH1 out of primary cilia occurs (Rohatgi et al., 2007). This allows SMO localisation to primary cilia and causes the activation of the GLI family of transcription factors (Ingham, 1998). SMO stimulates the activation of GLI2 and prevents GLI3 repressor formation, resulting in SHH target gene expression (Corbit et al., 2005). Exactly how the translocation of PTCH1 and SMO is controlled, however, is not well understood.

The signalling of HH through the primary cilium appears to be important in most circumstances when HH signals in vertebrates (Goetz and Anderson, 2010), however, the way in which HH signals differs considerably according to the cellular context. Below, I will highlight the different functions of HH that relate to this study.

1.4.4 Multiple roles of HH signalling

Classically, The HH proteins functions as morphogens in regulating various developmental processes of both invertebrate and vertebrate. However, in other circumstances, it appears to act as a mitogen, driving proliferation (Ho and Scott, 2002). Moreover, it also may be involved in directing axon growth or directing cell migration (Marti and Bovolenta, 2002, Fu et al., 2004). Differences in the way it acts in some of these latter circumstances may be attributed to signalling outside of the cilium (Bijlsma et al., 2012). However, the core mechanism, involving PTCH and SMO translocations in primary cilia, seems to be acting both when SHH works as a morphogen and as a mitogen. Therefore, in this section I will focus on only the morphogenic and mitogenic functions of HH.

1.4.4.1 Morphogenic and mitogenic functions of HH

1.4.4.1.1 HH functions as a morphohen

The idea of how a signal gradient can give rise to order cell fates in a tissue was introduced in 1969 and explained in the form of the ‘French flag model’ (Wolpert, 1969, Wolpert, 1996). As shown in Fig. 1.6, the French flag colors: blue, white, red represent different cell states affected by the different

signal gradient concentrations. The secreted signal is released from the source towards the target tissue, and so generates a signalling gradient. The different concentrations of signal affect the cells locating at the different positions of the tissue by turning on the different sets of target genes. A signal that functions in this way is called a morphogen. The two characteristics of the morphogen are defined: the signal has to act in a concentration-dependent manner to stimulate different responses at different thresholds, and that signal has to propagate toward a target tissue to affect over a long range from the source of its signal (Briscoe, 2009).

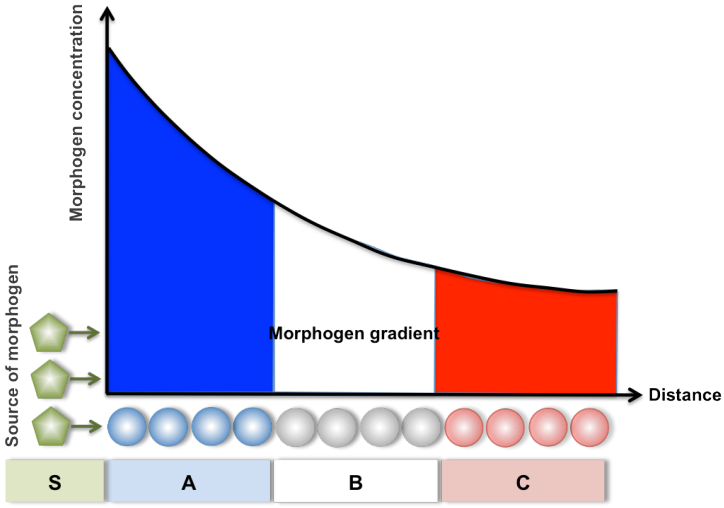

Fig. 1.6. The French flag model. The signal is released from the source (S) and propagated through the tissue, resulting in different concentrations of signal. The signal gradient affects differently on the cells locating at different distance from the source of the signal, inducing distinct cell fates (A, B, C) from specific concentration thresholds (blue, white, and red) (adapted from (Wolpert, 1969).

Below, I will review two examples of the morphogenic function of HH in invertebrates and vertebrates, which are in the wing disc of *Drosophila* and in the neural tube of vertebrates.

Morphogenic role of HH in *Drosophila* wing imaginal disc

Although, HH was first shown to act as a morphogen in the epidermis of the developing *Drosophila* embryo (Heemskerk and DiNardo, 1994), its morphogenic role is perhaps better illustrated in the patterning of the wing

imaginal disc, from which the fly wing is derived (Strigini and Cohen, 1999). In *Drosophila* wing imaginal disc, HH is produced by the cells in posterior compartment of the disc and it locally induces gene expression of the anterior compartment cells to pattern the anterior wing region adjacent compartment boundary (Fig 1.7). Moreover, HH functions distantly by inducing the expression of the BMP family morphogen, Decapentaplegic (Dpp). Dpp diffusing to both anterior and posterior compartments of imaginal disc plays a role in regulating the growth and patterning of the whole wing (Fig. 1.7). The different levels of HH expression activate different gene targets. It has been shown that *dpp* expression is activated by the low level of HH, whereas the activation of Patched (*ptch)* is stimulated by the high level of HH (Jiang and Hui, 2008). Thus, in invertebrates, HH can act as a morphogen eliciting different cellular responses according to its concentration.

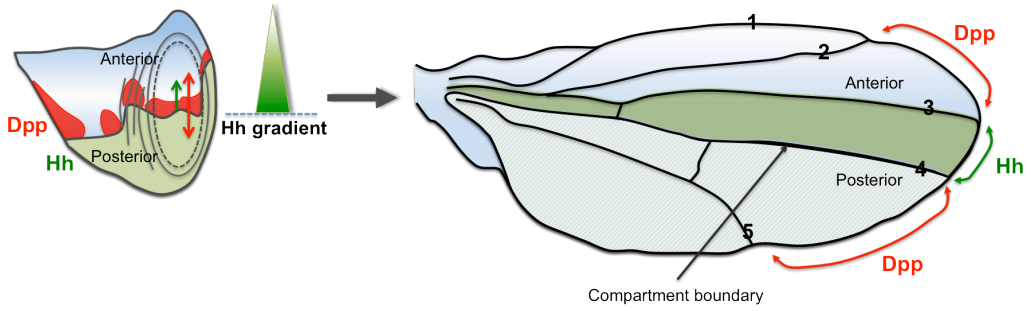

Figure 1.7. Signal gradient plays a role in patterning the *Drosophila* wing imaginal disc. The HH is secreted from the anteroposterior boundary of the *Drosophila* wing imaginal disc and stimulates Dpp (red), which spreads anteriorly and posteriorly (red arrow) to pattern the anterior and posterior compartments. The HH itself (green) spreads anteriorly (green arrow) and functions in patterning the anterior compartment (Left). Developed *Drosophila* wing shows the regions formed from the anterior (top) and posterior (bottom) compartments, and the regions affected by HH (green, between wing veins 3 and 4) and Dpp (red arrows) (Right) (adapted from (Varjosalo and Taipale, 2008).

Morphogenic role of SHH in neural development

Among those HH proteins in vertebrates, SHH has been shown to be the most broadly expressed mammalian HH signalling molecule. It plays a pivotal role in

regulating cell proliferation and differentiation in various types of tissue (Ingham and McMahon, 2001, McMahon et al., 2003). In nervous system as well as the other systems, it functions as a morphogen. SHH plays a role in patterning and cell fate specification in developing neural tube as well as in patterning of limbs. Here, I highlight only the morphogenic role of SHH signalling in neural tube development.

During ventral spinal cord patterning of vertebrate embryos, SHH is secreted from notochord and floor plate at the ventral midline of neural tube and it regulates the neuronal cell specification in a concentration-dependent manner by generating a ventral-to-dorsal gradient to indicate the cell fate of neuronal progenitors at different locations in the dorsal-ventral axis. As shown in Fig. 1.8, an increase in the concentration of SHH determines the generation of distinct neuronal subtypes; interneurons (V0-V3) and motor neuron (MN) (Ingham and McMahon, 2001). Precisely how these different cell types are induced according to the SHH concentration remains unclear, but current models suggest that a gradient of GLI activity is set up by the amount and duration of SHH signal which in turn determines when and where genes are activated (Balaskas et al., 2012).

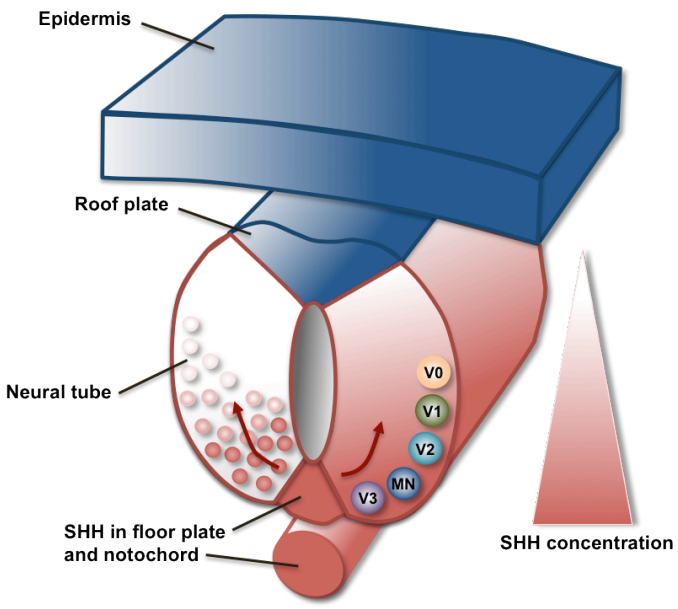

Figure 1.8. SHH gradient in the early neural tube development. SHH is expressed at the notochord and floor plate of the neural tube and spreads from ventral to dorsal, forming a SHH gradient to regulate the cell fate of neuronal subtypes; interneurons (V0-V3) and motor neuron (MN) (adapted from (Briscoe, 2009)).

1.4.4.1.2 HH functions as a mitogen

In contrast to the morphogenic role of SHH in neural development, SHH acts apparently as a mitogen in cerebellum. During cerebellar development, it is required for the proliferation of GNPs (Wechsler-Reya and Scott, 1999, Wallace, 1999, Dahmane and Ruiz i Altaba, 1999).

Mitogenic role of SHH in in cerebellum

In the cerebellum, SHH stimulates an increase in the number of dividing granule neurons (Dahmane and Ruiz i Altaba, 1999, Wallace, 1999, Wechsler-Reya and Scott, 1999) and loss of SHH in Purkinje cells leads to a failure of the granule cells layer to expand normally and a severe reduction in cerebellar size (Lewis et al., 2004). SHH is therefore an essential mitogen in growth of the cerebellar cortex.

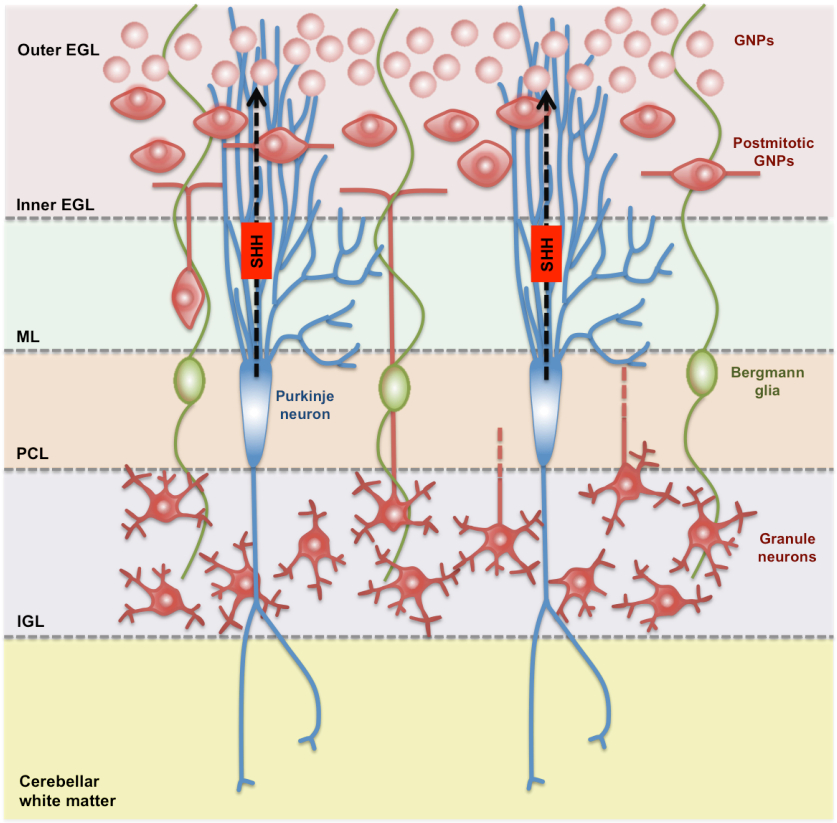

Figure 1.9. Role of SHH in cerebellar growth. Schematic representation of the mouse cerebellum in the first postnatal week, showing the position of neurons and glia in the cerebellar cortex. SHH is secreted and spreads towards the EGL, consequentially promoting the proliferation of GNPs in the EGL (modified from (Ruiz i Altaba et al., 2002).

As shown in figure 1.9, SHH is secreted in the Purkinje cell layer of cerebellum and it spreads upwards and causes proliferation of granule neurons. Interestingly, GNPs closest to where SHH presumably is secreted (ie those in the inner EGL; iEGL) proliferate less than GNPs in outer EGL (oEGL); indeed the iEGL is where GNPs become post-mitotic (Miyazawa et al., 2000). Even so, it is clear that SHH target genes are activated, even in the iEGL, where *Ptch1* expression is highest (Lewis et al., 2004), although activation of other SHH targets, notably *Gli1*, is greatest in the outer layers (Corrales et al., 2004). A key question that arises here, therefore, is how SHH activity is spatially restricted in cerebellar morphogenesis, and whether the response to SHH is solely mitogenic. One obvious possibility is that other molecules may modulate SHH signalling, either simply attenuating the mitogenic response to allow differentiation, or perhaps even qualitatively changing the signal to drive different responses in different contexts.

To investigate the response of SHH signalling, based on proliferation response, as a readout is too far from the SHH signalling. *Gli1* and *Ptch1* are normally used as readouts of the SHH response (Wechsler-Reya and Scott, 1999, Humke et al., 2010, Hillman et al., 2011). Moreover, *Nmyc* and *CyclinD1* are downstream gene targets of the SHH signal. It has been shown that *Nmyc* and *CyclinD1* are direct targets of SHH signalling (Oliver et al., 2003, Kenney et al., 2003, Martinez et al., 2013). *Nmyc* and *CyclinD1* are expressed in proliferating GNPs of the developing cerebellum and upregulation of *Nymc*, resulting in the promotion of GNP proliferation following SHH stimulation (Kenney et al., 2003).

Apparently, SHH does not play a morphogenic role to determine the cell fate specific in the cerebellum. Therefore, this raises the question of whether this is fundamentally different between morphogenic and mitogenic effects and how the signalling mechanisms are different. Although, SHH plays a distinct mitogenic role in the cerebellum, it is not known how morphogenic and mitogenic effects are related from one system to another system. One of the possible explanations is that the SHH signalling interacts with other molecules, which alters the signal from a concentration-dependent morphogen to a simple on-off mitogen.

1.4.5 Modulation of SHH signalling during the development of GNPs

1.4.5.1 Modulation of SHH signalling by other signals and molecules

Several signals have been suggested to control GNP proliferation in response to SHH. Bone Morphogenetic Protein 2 (BMP2) has been shown to turn SHH-mediated proliferative response of GNPs into the differentiation of the granule neurons. Moreover, BMP2 treated GNPs demonstrate the down-regulation of SHH pathway gene components, such as SMO, GLI1 (Rios et al., 2004).

Although it is clear that BMP signalling has a major role in antagonising SHH-induced proliferation, it is not clear that BMP is the signal that initiates cell cycle exit. Although it can induce differentiation in culture, *in vivo* phospho-Smad – the readout of BMP2/4 signalling, does not appear in granule cells until they reach the Purkinje cell layer (Rios et al., 2004), by which time they are already post-mitotic. This suggested that even though BMP signalling is playing an important role in inducing GNP differentiation, other signals are likely to be involved.

In contrast to the effect of BMP2 on the SHH-induced proliferative response of SHH signalling on GNPs, Fernandez et al. (2010) proposed that Insulin-like Growth Factor 1 and 2 (IGF1 and IGF2) modulate SHH signalling by reinforcing the effect of SHH on inducing GNP proliferation. However the complete picture of such modulation, particularly *in vivo* has not been elucidated (Fernandez et al., 2010).

1.4.5.2 Modulation of SHH signalling by cell contacts

On the other hand, it has been known for some time that cell contact influences granule cell proliferation and differentiation (Gao et al., 1991, Baptista et al., 1994). Contacts mediated by Notch interactions with Delta-like ligands appear to stimulate GNP proliferation (Solecki et al., 2001). Adhesive contacts with extracellular matrix (ECM) proteins also appear to modulate GNP proliferation. On the one hand, laminin (LN) is expressed in the meningeal layer and potentiates SHH-induced proliferation (Blaess et al., 2004). Since LN binds SHH directly, this may be one way that its activity is localised in the EGL, but this does not explain what causes cell cycle exit in the iEGL. On the other hand, vitronectin (VN) is found in the iEGL and regulates SHH activity *in vitro* by turning proliferation to differentiation (Pons et al., 2001). However, cerebellar development is not affected by VN loss (Zheng et al., 1995), and the VN receptor, integrin αvβ3, is apparently not expressed until the cells are already post-mitotic (Pons et al., 2001)

In contrast, adhesion molecules (CAMs) of the related L1 and contactin families (L1-CNTNs) are expressed throughout the EGL and have been shown to affect GNP proliferation when mis-expressed in the cerebellum (Bizzoca et al., 2003). The properties of this family are discussed in greater details as follow.

1.5 L1-CNTNs

1.5.1 L1-CNTN structures

The L1-CNTNs are members of the immunoglobulin protein superfamily, and are part of a subfamily characterised by the presence of both Ig domains and fibronectin type III (FNIII) domains. Although this family includes an array of cell surface receptors, many of which are associated with neural development - such as Deleted in Colorectal Cancer (DCC), a Netrin receptor and Roundabout (Robo), a Slit receptor - the L1-CNTNs are a clearly related sub-group defined by a similar topology that suggests they arose by gene duplication (Brummendorf and Lemmon, 2001). They are further divided into the L1-like family, whose members are type1 transmembrane proteins and the CNTN-like family, whose members are anchored to the cell surface by glycosphosphoinositol (GPI) linkages (Brummendorf and Rathjen, 1995). As shown in Fig. 1.10, the transmembrane L1 family consists of L1 cell adhesion molecule (L1/L1CAM), neuronal cell adhesion molecule (NRCAM), cell adhesion molecule L1-like (CHL1) and neurofascin (NFASC). Except for NFASC, they all contain 6 Ig and 5 FNIII domains, connecting with an intracellular domain to transduce the intracellular signalling. The intracellular domains of all four L1-like molecules are highly conserved and include binding sites for ankyrin, FERM proteins, Doublecortin and PDZ-containing proteins. In immature neurons, L1, NFASC and NRCAM also include an alternatively spliced exons which encodes a binding site for Adaptor Protein 2 (AP2), which is required for their endocytosis (Herron et al., 2009).

The GPI-linked CNTN family comprises of contactin 1 (CNTN1 or F3), contactin 2 (CNTN2 or TAG-1), contactin 3 (CNTN3 or BIG-1), contactin 4 (CNTN4 or BIG-2), contactin 5 (CNTN5 or NB-2) and contactin 6 (CNTN6 or NB-3) and they all contain 6 Ig domains and 4 FNIII domains, anchored to the cell membrane by the GPI.

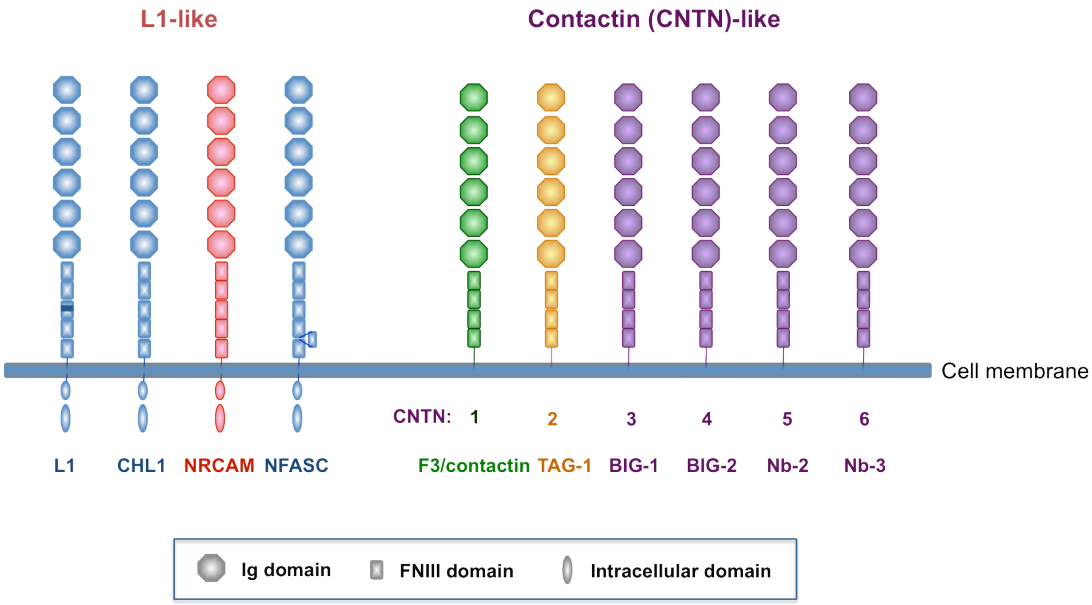

Figure 1.10. L1-CNTN protein structures. Schematic representation of the protein structures of L1-like and CNTN-like families.

Classically, L1-CNTNs play a role in broad range of processes such as cell migration, axon growth and guidance, myelination and synaptogenesis (Maness and Schachner, 2007). L1 and β1-Integrins together play a role in potentiating neuronal migration to extracellular matrix proteins (Thelen et al., 2002). In addition, it has been demonstrated that L1 as well as NRCAM functions in promoting axon guidance. The L1-deficient mice showed defective corticospinal axon guidance (Cohen et al., 1998). Similarly, NRCAM-deficient mice also showed an error of retinal axon guidance (Williams et al., 2006). Below, however, I will focus on more recent studies that implicate L1-CNTNs in the earlier stages of neuronal differentiation.

1.5.2 L1-CNTNs and modulation of proliferation

In contrast to the post-mitotic roles of L1-CNTNs mentioned above, recent evidence links them with the earlier events in neurogenesis. It has been shown that L1 is implicated in modulating cell proliferation. Substrate-coated L1 decreases the neural precursor cell proliferation in a dose-dependent manner (Dihne et al., 2003). TAG-1 binds to Amyloid β precursor protein (APP). This interaction stimulates secretase-dependent cleavage of APP and subsequently releases *C*-terminal APP intracellular domain (AICD), resulting in the

suppression of neurogenesis (Ma et al., 2008). In contrast to the role of F3 in cerebellum, which decreases neurogenesis by suppressing GNP proliferation when mis-expressed on progenitors (Bizzoca et al., 2003), F3 mis-expression in the developing cortex increases the number of proliferating ventricular zone precursors of TAGF3 transgenic mice and stimulates the proliferation of primary forebrain cells from WT mouse embryo *in vitro* (Bizzoca et al., 2012). Although the mechanisms involved in these effects remain unclear, together they suggest that L1-CNTNs do not only function in post-mitotic events but also play a role in modulating neuronal progenitor cell proliferation.

1.5.3 Expression of L1-CNTNs and their roles in cerebellar development

Loss-of-function experiments also support a role for L1-CNTNs in the cerebellum: individually, loss of NRCAM, CHL1, NFASC or L1 does not dramatically affect the size or morphology of the cerebellum, although the L1 and NRCAM single mutants show slight size reductions in specific lobules (Sakurai et al., 2001, Heyden et al., 2008, Zonta et al., 2011). However, loss of NRCAM and L1 together leads to a severe reduction of the size and defects in foliation of the cerebellum (Sakurai et al., 2001), which is not seen in the other mutant combination that have been tried (Heyden et al., 2008) and which strongly suggests that NRCAM and L1 have redundant functions in the growth of the cerebellum. Cerebellar development is also severely disrupted when F3, a ligand of both of these L1-like molecules, is lost, leading to ataxia and early postnatal death (Berglund et al., 1999). F3 is normally expressed on post-mitotic granule neurons in the iEGL and IGL (Xenaki et al., 2011); however, our group and collaborators have shown that ectopic expression of F3 on mitotic GNPs in transgenic mice leads to a transient, but substantial reduction in cerebellar size (Bizzoca et al., 2003). Although these previous studies suggested that these molecules had their effects on cerebellar development through a role in post-mitotic events, recent experiments from our laboratory suggest these L1-CNTNs may have a role in the modulation of SHH signalling, which I will review below.

1.5.4 L1-CNTNs and SHH signalling

The observation that F3 mis-expression in the cerebellum transiently inhibits cerebellar growth (Bizzoca et al., 2003) led our laboratory to test whether purified F3 protein (made soluble by fusion to human immunoglobulin fc domain: F3-fc) can inhibit SHH-induced proliferation and promote differentiation of

purified GNPs *in vitro* (Xenaki et al., 2011). Interestingly, not only was F3-fc able to inhibit SHH-induced proliferation, but also this inhibition was antagonised by the simultaneous addition of TAG-1. TAG-1 is normally expressed in the iEGL, but is present on both mitotic and post-mitotic GNPs, though not on granule neurons in the IGL. Moreover, immunolabelling revealed that F3-fc and TAG-fc bind to, and co-localise with NRCAM on granule neurons (Xenaki et al., 2011), consistent with their known abilities to bind NRCAM directly (Brummendorf and Rathjen, 1995). Furthermore, F3-fc is unable to suppress proliferation of purified GNPs of NRCAM null mice. These results indicate that F3 requires NRCAM for its function and that TAG-1 can act antagonistically to F3 activity, suggesting that F3 and TAG-1 compete for NRCAM as a receptor (Xenaki et al., 2011).

The question that arises is how F3, TAG-1 and NRCAM modulate SHH signalling. One possibility is that regulation of cell proliferation through NRCAM is completely independent of SHH signalling pathway (Fig. 1.11A). Another possibility is that NRCAM is in some way directly involved in the SHH signalling pathway (Fig. 1.11B).

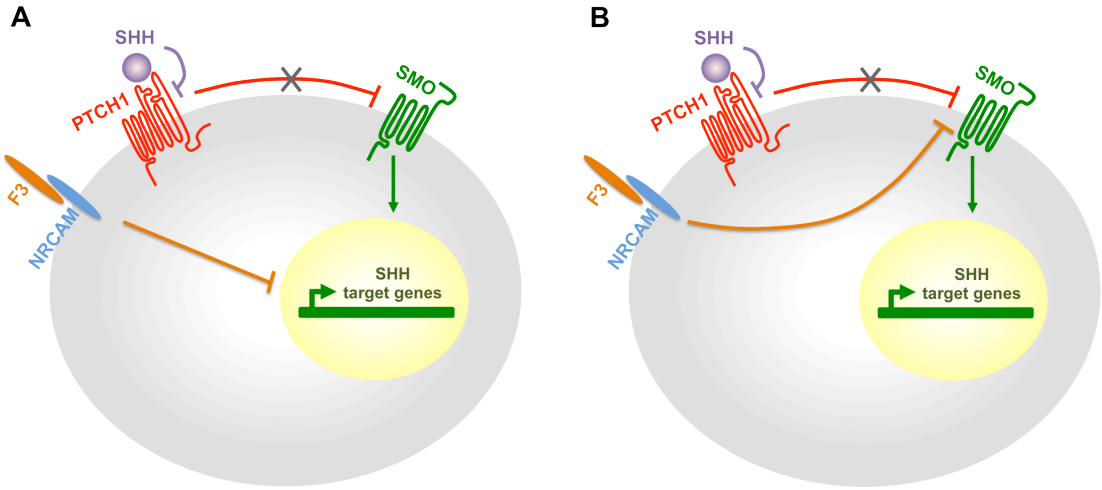

Figure 1.11 Possibilities of how F3 and NRCAM function in SHH pathway. **(A)** The first possibility: F3 and NRCAM act independently through some unknown pathway. **(B)** The second possibility: they function somewhere in SHH pathway.

To address this, our laboratory preliminarily tested whether GNPs from transgenic SmoA1 mice, expressing a constitutively activate SMO protein (Hatton et al., 2008), were responsive to F3 protein in culture. As expected,

purified SmoA1 GNPs proliferated without addition of SHH, but this proliferation was not suppressed by F3 protein (Xenaki, unpublished data). To confirm this result, Smoothened Agonist (SAG), which is a chlorobenzothiophen-containing compound that is known to bind SMO and activate SHH signalling (Chen et al., 2002), was used to stimulate WT GNPs. Our preliminary data (Xenaki, unpublished data) showed that, as expected, SAG can induce the proliferation of WT GNPs, however, F3-fc was not able to inhibit this proliferation even though it could inhibit SHH-induced proliferation in the same experiment (in agreement with previous results; (Xenaki et al., 2011)). The inability of F3-fc to inhibit either genetically (SmoA) or pharmacologically (SAG) activated SMO, strongly suggests that F3 and NRCAM may regulate the SHH signalling pathway upstream of SMO (Figure 1.11B).

1.5.5 Role of L1-CNTNs in modulating the signal of other membrane receptor by endocytosis or trafficking

These preliminary results lead to the interesting question of how exactly F3 and NRCAM might be involved in inhibiting SHH signalling in cerebellar granule neurons. As noted above, classically these molecules are regarded as adhesion molecules. However, a number of lines of evidence suggest that they have a role in the localisation of other proteins to particular parts of the membrane, either at the cell surface or intracellular. Of particular interest is their role in the formation and maintenance of the node of Ranvier (Salzer, 2003). NFASC and NRCAM, both L1-like CAMs, have been demonstrated to facilitate node formation by recruiting ankyrin G, a cytoskeletal scaffold protein, and hence sodium channels to the node (Dzhashiashvili et al., 2007). Similarly, it has been shown that TAG-1 is required to localise contactin-associated protein 2 (Caspr2; CNTNAP2) and potassium channels to the juxtaparanodal region (Poliak et al., 2003). F3 similarly associates with Caspr1 and together these are required to separate sodium channels from potassium channels by maintaining the integrity of the paranode axon-glia adhesion. Loss of either protein leads to a failure of the other to be trafficked to the cell surface and a breakdown of the paranodal complex (Boyle et al., 2001). This evidence clearly suggests that L1-CNTNs are important in organising the membrane into specific subdomains.

From studies in other contexts, it is also clear that L1-CNTNs can modulate the signalling of other membrane receptors. A study in the context of neuronal responses to axon guidance cues found that L1 is required for receptor

endocytosis during growth cone responses to Semaphorin3A (Sema3A), one of the secreted semaphorins (Castellani et al., 2004). Importantly, L1 binds directly to neuropilin1 (NRP1), which in turn is required for the endocytosis of the signalling component of the receptor, PlexinA. NRP1 is also involved VEGF receptor endocytosis and may have a general role in trafficking. NRCAM is similarly involved in responses to Sema3F, though in this case it binds to neuropilin2 (NRP2), which associates with a different subset of Plexins (Falk et al., 2005). Recently our laboratory has shown that TAG-1 is also involved in both these responses (Law et al., 2008); Law, unpublished) and, in the case of Sema3A responses, is required for the intracellular separation of L1 from NRP1 and PlexinA, which is necessary for Sema3A to elicit the full set of signalling components required for sensory neuron growth cone collapse (Dang et al., 2012).

These observations indicate that L1-CNTNs are required in a number of contexts to localise other membrane molecules to specific subcellular locations, raising the possibility that they could modulate SHH signalling by controlling the trafficking of the membrane-bound components of the pathway. The most obvious trafficking event is the translocation of SMO and/or PTCH1 into/out of the cilium. Therefore, in this study I set out to test whether NRCAM might be involved in this trafficking.

How exactly SHH signalling is regulated during GNP proliferation is key to understanding both normal development and tumorigenesis. An understanding of the role of L1-CNTNs in controlling SHH-induced proliferation in cerebellar granule neurons therefore could provide a mechanism by which to modulate SHH function in the cerebellum and possibly lead to a novel therapeutic approach for the treatment of MB in the future.

1.6 The hypothesis and aims of this study

The inability of F3-fc to suppress SHH induced proliferation of GNPs when NRCAM is missing, suggests that NRCAM is involved in regulating SHH signalling. In this thesis, the main hypothesis is that this regulation is due to the ability of NRCAM to affect the trafficking of SHH signalling pathway components in the primary cilium. The specific aims are as follows.

1.6.1 To determine whether NRCAM, F3 or TAG-1 are located to the primary cilia of proliferating GNPs

Our lab has previously shown that NRCAM is expressed on proliferating GNPs (Xenaki et al., 2011). However, it was not tested whether NRCAM is present in the primary cilium of these cells. If NRCAM is involved the trafficking of SHH pathway components to the cilium it seems likely that NRCAM or its interacting ligands, TAG-1 or F3 should be present in or around the primary cilium.

1.6.2 To determine whether loss of NRCAM affects the localisation of SHH pathway components to the primary cilium

If NRCAM is present in or around the primary cilium, it is more likely that NRCAM is involved in the ciliary translocation of the key protein components of SHH pathway, especially either PTCH1 or SMO.

1.6.3 To test whether NRCAM interacts with SHH pathway protein components, specifically PTCH1 or SMO

If NRCAM is involved in the trafficking of SHH pathway components, it is likely, though not necessary, that it is able to physically associate, directly or indirectly with these components.

1.6.4 To investigate how loss of NRCAM affects SHH signalling

Although we know that NRCAM is required to mediate the effects of F3-fc on SHH signalling (Xenaki et al., 2011), we do not know what role, if any; NRCAM is playing in SHH signalling *in vivo*. Even if the phenotype of NRCAM knockout mice (Sakurai et al., 2001) is not equivalent to that of SHH knockout mice (Chiang et al., 1996), it is still possible that NRCAM affect the level of SHH signalling, rather than being absolutely required for SHH.

Chapter 2

Materials and Methods

2.1 Animals

All mice were maintained on a C57/BL6 strain background (≥10 generation backcross). NRCAM mutant mice were a kind gift from T. Sakurai. All mice were bred and maintained at the University of Sheffield animal facility, and all experiments performed, in accordance with UK Home Office regulations. All *in vitro* GNP experiments were performed at postnatal day 5 (P5).

2.2 Genotyping

0.5-1cm of mouse-tail was collected from individual mouse and its DNA was extracted using a quick extraction protocol (Truett et al., 2000). Briefly, 100µl extraction buffer (recipe in table 2.4) was added into an eppendorf tube containing mouse-tail and boiled at 95°C at least 30 minutes. Then 100µl neutralisation buffer (recipe in table 2.4) was added followed by spinning down at 13000 rpm for 5 minutes. The supernatant was transferred to a fresh tube and PCR reaction was set up using the primers listed in table 2.1. Each PCR reaction contains 10µl 2x Bio-Red mix (BIO-25005, Bioline), 5µl extract DNA, 1µl of each primer (20µM stock concentration), and the reaction volume was made up to 20µl using dH_2O. The reaction tubes were run in a thermal cycler (Hybaid or PTC-200 Peltier Thermal Cycler, MJ research), using the programme as follows:

NRCAM: 94°C for 3 minutes, 30 cycles of 94°C for 30 seconds, 60°C for 45 seconds, 72°C for 1 minute, final extension at 72°C for 10 minutes and cooling at 4°C indefinitely.

10µl of the PCR product then was resolved on a 2% agarose gel in Tris-acetate-EDTA buffer (TAE buffer) (see recipe in table 2.4) containing 0.5µg/ml ethidium bromide. The gel was run at 85 volts for 50 minutes and visualised using a UV transilluminator (UVdoc, Uvitec).

2.3 Primary granule cell culture

2.3.1 Granule cell (GC) preparation

Primary GC culture methodology was modified from a previous report (Hatten, 1985), as described by Xenaki et al. (2011). P5 mice were sacrificed by

overdose of IsoFlu (B506, Abbott) and their cerebella were dissected out. Their meninges were carefully removed in cold calcium- and magnesium-free PBS (CMF-PBS) media under a dissecting microscope (Stemi SV6, Zeiss). Each clean cerebellum was transferred to a 15ml conical tube filled with 10ml cold CMF-PBS until all cerebella were dissected. The CMF-PBS was carefully discarded from the tube, and 1ml 1% Trypsin-DNase solution (recipe in table 2.2) was added to the cerebella which were then incubated in a 37°C water bath for 8 minutes to dissociate the cells from the remainder of brain tissue. The Trypsin-DNase solution was then replaced with 1ml DNase (recipe in table 2.2). The cells were gently dissociated by trituration with a 1ml-Gilson pipette, and then with fine and extra fine-bore fire-polished Pasteur pipettes, respectively, until cell clumps were not visible. 3ml CMF-PBS was added to the cells and which were then centrifuged at 700*g* for 5 minutes at 4°C. The supernatant was removed and the pellet was gently triturated in 1ml DNase again until a homogeneous solution was seen. A further 3ml CMF-PBS was added to the suspension, which was gently mixed and then carefully applied over a two step-percoll gradient as described (Solecki et al., 2001) for a further granule cell purification step, as follows.

2.3.2 Granule cell purification – gradient centrifugation

The cell suspension was applied over two step-percoll gradients which were prepared as follows (see Figure 2.1): First, 10ml 35% Percoll (white) was added into a conical 50ml tube. A 10ml syringe with 18G needle was placed in the bottom of the tube, then 10ml 60% Percoll (with trypan blue) was added into the syringe and left to flow by gravity under the 35% percoll. Then, the syringe was carefully removed without disturbing the clear sharp line between the 35% and 60% Percoll layers (see figure 2.1).

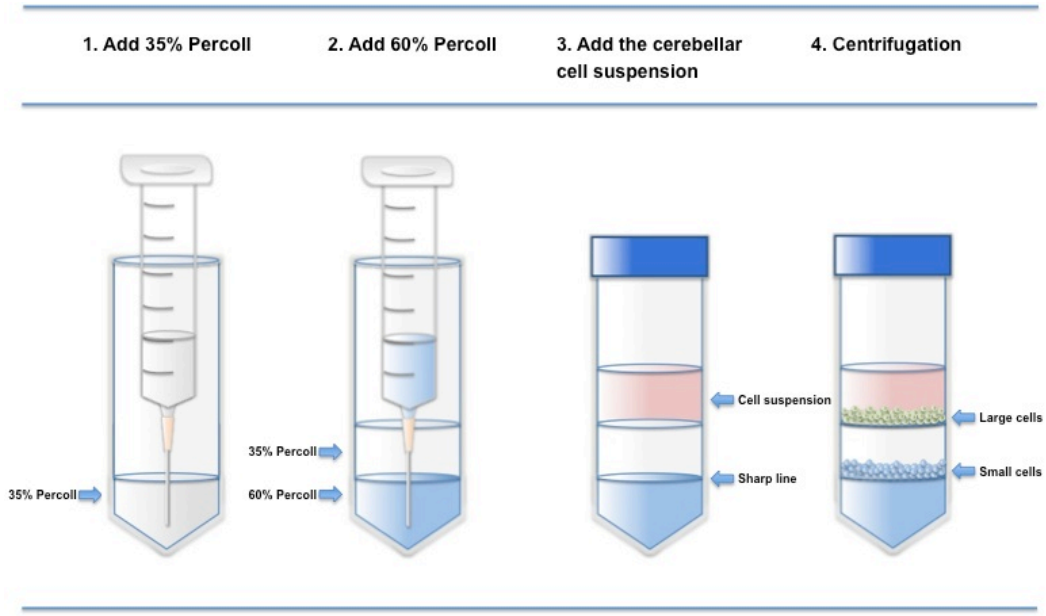

Figure 2.1. Preparation of Percoll gradients for granule cell purification. The Percoll gradients were prepared for granule cell purification by adding 10ml 35% Percoll (white solution), followed by underlaying 10ml 65% Percoll (blue solution) through a syringe. The cerebellar cell suspension was then carefully added to the top without disturbing a sharp line between the gradients. After centrifugation, the granule cells were accumulated at the interface of the gradients.

The cell suspension from the previous step was carefully applied on top of the Percoll gradient, then centrifuged at 3200 rpm (2378.96 × *g*) for 17 minutes in a swing out rotor (SX4750A swing out bucket, r_{max} = 207.8 mm) in a Beckman Coulter Allegra X-12R centrifuge and then allowed to slow to a stop with the brake off. During centrifugation, cells are selected by the different gradients according to their density, which broadly correlates with their size. The low density, large cell fraction, which contains cells such as glia cells, Purkinje cells, and interneurons, collects above the upper-phase of the gradient; whereas, high density, small cells, including cerebellar granule cells and fibroblasts, collect at the interface of the 35% and 60% Percoll solutions (Hatten et al., 1997, Lee et al., 2009). To purify the cells, the upper phase was carefully removed without disturbing the interface, where the small cells accumulated. The interface was transferred to a 50ml conical tube, containing 40ml cold CMF-PBS, and centrifuged at 700 × *g* for 5 minutes at 4°C to get rid of the Percoll, which can be toxic to the cells. The supernatant was removed and the pellet was transferred

to a new 15ml conical tube containing 15ml cold CMF-PBS, and centrifuged again at 700 × *g* for 5 minutes at 4°C.

2.3.3 Granule cell purification – pre-plating step

The pellet from the previous step was re-suspended in 1.5ml warm Granule Cell Medium with Serum (GCM+S), a pre-plating medium, (see recipe in table 2.2) on a 35mm plastic dish and incubated for 20 minutes at 37°C to get rid of fibroblasts. Then the cell suspension was transferred to a 35mm-tissue culture dish (153066, Nunclon®), which was previously coated with 0.1mg/ml Poly-D-Lysine hydrobromide (PDL; P1024-50MG, Sigma) for at least 3 hours at room temperature and washed twice with 1.5ml water before cell suspension transfer (the stock concentration was 5mg/ml, was diluted 1:50 by sterile water). To remove glia cell contamination, the cell suspension were incubated again for 2 hours at 37°C as glia cells are more likely able to adhere to the dish coated with the lower concentration of PDL than GCs (Lee et al., 2009).

2.3.4 GC plating step and culture

As serum contains glutamate causing neuronal death (Schramm et al., 1990), after the 2-hour pre-plating step, the cells were washed serum off by transferring to a new 15ml conical tube and CMF-PBS was added to 15ml total volume, then centrifuged at 1000*g* for 5 minutes. The GC cell pellet was resuspended in 1ml GC medium (GCM) (recipe in table 2.2). Then, the GC cells were plated on the circular glass 13mm diameter coverslips (631-0150, VWR), which were pre-coated with PDL the day before using the following protocol: the glass coverslips were put in a glass beaker and flamed for 2-3 minutes with shaking every 30 seconds to prevent overheating and bending. Flamed forceps were used to transfer the coverslips into each single well in a 4 well dish (176740, Nunclon®). Then, 90µl of 0.5mg/ml PDL (PDL stock concentration was 5mg/ml, which was diluted 1:10 with sterile water) was carefully transferred onto each coverslip to form a drop and incubated at 37°C overnight. The coverslips were then washed twice with 2ml sterile water directly before GC plating. The number of GCs was counted and plated at a cell density of $0.5x10^6$ cells/coverslip in 300µl GCM, and incubated at 37°C in a standard 5% CO_2 tissue culture incubator. All GC experiments were terminated at 6 hours post-plating, unless otherwise indicated. The cells were fixed either with 4% Paraformaldehyde (PFA) in 0.1M Phosphate buffer (PB buffer) (see recipe in table 2.4) or harvested for RNA collection at that time. Any treatment – for instance, SHH [Recombinant Human Sonic Hedgehog

(C24II), *N*-Terminus; 1845-SH, R&D Systems] or SAG (Smoothened Agonist; ALX-270-426, Enzo Life Sciences) (see list of drugs in table 2.5) – was added to GCs, after plating for 1.5 hours. All reagents and medium recipes for GC preparation and culture are listed in table 2.2-2.3.

2.4 Testing the optimal SHH concentration that giving maximal proliferation

Before verifying that SHH can drive SMO into primary cilia, the dose of recombinant SHH (1845-SH, R&D Systems) was typically titrated to find what concentration gives maximal proliferation of GNPs. As shown in fig 2.2, 30nM SHH drove maximal proliferation of GNPs at 24 hours treatment. As a result of this, the 30nM SHH concentration was selected to use in all further experiments.

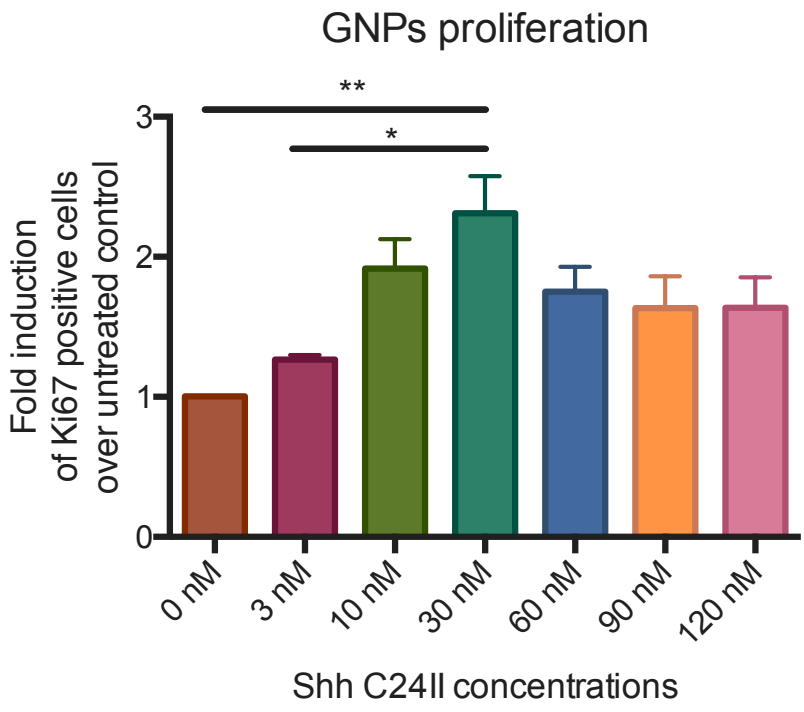

Figure 2.2. 30nM SHH drove maximal proliferation of GNPs at 24 hours. The GNPs were plated for 1.5 hours and then the various concentrations of recombinant SHH (C24II), which is from E.*coli*-derived, Cys24-Gly197 (Cys24Ile-Ile), with and N-terminal Met, were added to the cells for 24 hours. The cells were stained with anti-Ki67 antibody and the $Ki67^{+}$ cells were quantified as a percentage of proliferative GNPs.

2.5 Immunolabelling

After 6 hours in culture (4.5 hours after treatment), the GNPs growing on PDL-coated coverslips were fixed with 4% PFA for 20 minutes at room temperature, followed by 3 washes with 0.05% Triton-X in PBS (PBT) for 15 minutes each time. Primary antibodies, diluted in 3% Donkey serum in PBT, were added to the cells overnight at 4°C. Next day, the cells were washed 3 times with PBT for 15 minutes and then secondary antibodies were added to the cells for 40 minutes at room temperature. The cells were washed 3 times again with PBT for 15 minutes, then mounted with Vectashield mounting medium with DAPI (H-1200, Vector). The primary and secondary antibodies used in this study were listed in table 2.6-2.7.

2.6 NRCAM antibody pre-absorption

The NRCAM 838 antibody, which was kindly provided by Prof. Martin Grumet, USA, was pre-absorbed with head tissue from E13.5 *Nrcam*$^{-/-}$ embryos to remove non-specific reactivities: The tissue was cut into small pieces, then fixed with 4%PFA in 0.1M PB buffer on the roller overnight at 4°C. Next day, the tissue was washed 3 times with PBS for 30 minutes. The 1x NRCAM 838 antibody (see its concentration in table 2.6) was diluted with PBS to 0.4x and added to an appropriate amount of washed tissue, which was calculated so as to have 100x more protein. This mixture was put on a roller at 4°C overnight. Next day, the antibody was centrifuged twice at 13,000 rpm (Sigma centrifuges, Nr.12124) for 10 minutes to remove as much of the tissue as possible. The supernatant was collected and tested for an optimal concentration on WT and *Nrcam*$^{-/-}$ GNPs. The appropriate concentration was chosen by the maximal signal from pre-absorbed NRCAM staining on WT GNPs, while seeing no signal on *Nrcam*$^{-/-}$ GNPs. After pre-absorption, the antibody was named NRCAM 838^{-} antibody.

2.7 Immunofluorescence microscopy and image analysis

All cilia images were obtained on an Apotome (Imager.Z1 Apotome, Zeiss) microscope. Unless otherwise noted, images were taken with a 100x objective lens. The initial exposure time of each channel was chosen from optimal

exposure, and then it was kept constant between the experiments. Only the cilium clearly protruded beyond the cell body and the whole shaft of cilium was clearly in focus so that ciliary labelling was not confused with labelling in the main body of the cell. Cilia were classified as either occupied or not occupied with the relevant protein according to whether fluorescence could be seen by eye anywhere along the shaft of the cilium, including the tip in a dark room. For each condition, thirty images were analysed for each of three independent experiments. An example of how the ciliary protein occupancies were quantified is illustrated in Fig 2.3. The puncta of relevant protein at the base of primary cilium was not included for quantification for several reasons. Firstly, the protein puncta became obscure by the background; therefore, it was very difficult to distinguish them against the background. Secondly, in case of SMO, although Milenkovic et al. proposed the model of how SMO trafficks from Golgi to primary cilium (Milenkovic et al., 2009), it has been shown that SMO localisation in the cilium is essential for the activation of the pathway (Corbit et al., 2005, Wilson et al., 2009). Moreover, Yoo et al. showed that the tip-base ciliary localisation of SMO is related to the SHH pathway activation (Yoo et al., 2012).

To avoid bias during counting SMO, PTCH and NRCAM occupancy in primary cilia, blind quantifications were also done in parallel. The blind quantifications of the SMO/PTCH/NRCAM ciliary occupancy were performed by randomising data and quantitating for the protein ciliary occupancy again by a fellow PhD student at the same department who was not told which images were from untreated, SHH-treated or SAG-treated GNPs.

All image analysis of GLI1 fluorescent intensity was performed using the Volocity programme, version 6.1.1 (Improvision). Mean fluorescent intensity of GLI1 on whole cell GNPs were measured and subtracted by background nearby the cells. Twenty fields of images (1,200-1,600 cells) were analysed for each condition of three independent experiments.

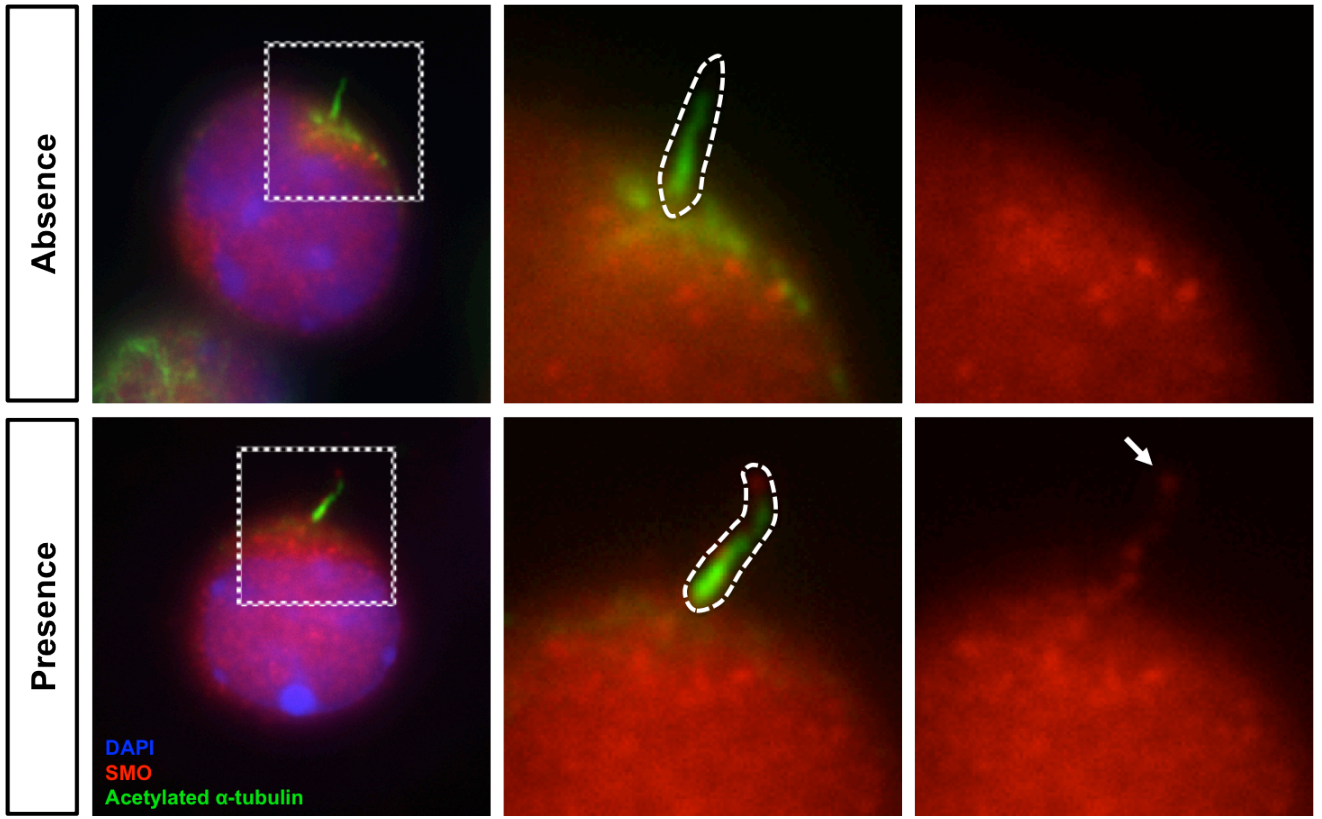

Figure 2.3. The principle of the quantification of interesting protein occupancy. Acquired images from Apotome-epifluorescent microscope were scored for protein occupancy in primary cilia by eye in a completely dark room. Only protein puncta from proximal to distal end of cilium (dashed line around the cilium) were scored as either absence (top panel) or presence (bottom panel). Arrow shows the presence of SMO along the shaft of the cilium.

2.8 Statistical methods

Compiled data sets from each experiment were analysed for statistical significance in Prism software (GraphPad Prism version 6). Unless otherwise noted, all data are graphed showing the Standard Error of the Mean (SEM) and have been tested for statistically significant differences among the control and treated samples using one-way ANOVA, followed by Bonferroni's post-test. Confidence interval was set to 95%, with a *p*-value less than 0.05 taken as statistically significant. Statistical significances are indicated as asterisks; *: $p<0.05$, **: $p<0.01$, ***: $p<0.001$ and N.S.: not significant.

2.9 Immunoprecipitation

2.9.1 Extraction of plasmid DNA

50µl of subcloning efficiency competent DH5α cells (18265-017, Invitrogen) were thawed from -80°C on ice, to which 1µl of plasmid DNA (0.1-2µg) was added (see the list of plasmid DNA constructs in table 2.8). The same amount of dH_2O was also added to the cells in another tube as a negative control, gently mixed and incubated on ice for 30 minutes. The mixture was heat-shocked at 37°C for 20 seconds, then incubated on ice for 2 minutes. To allow the cells to recover, 1ml of Luria-Bertani (LB) medium (see the recipe table 2.4), without antibiotics was added to the mixture and incubated for approximately 2 hours with occasional mixing at 37°C. 500µl of the transformation mix was spread plated on LB agar (see the recipe table 2.4) containing appropriate antibiotic (50 µg/ml ampicillin or kanamycin). The plates were incubated at 37°C overnight (12-16 hours) in a bacterial incubator. After 16 hours, 3 individual colonies were picked and used to inoculate 10ml starter cultures of LB supplemented with appropriate antibiotic, incubated at 37°C with agitation (200 rpm) overnight (12-16 hours). Next day, 5ml of each starter culture was used to extract DNA using Miniprep kit (27104, QIAGEN) according to the manufacturer's instructions. To verify the DNA construct, the DNA extracts from 3 individual colonies were tested by restriction enzymatic digestion.

2.9.2 Restriction enzymatic digestion

The digestion mix consisted of 500ng DNA construct, 2µl buffer (for the double digestion, the compatible buffer for each enzyme was checked from the

Promega-Restriction enzymes resource website), 2µl 10 × BSA, 0.5µl restriction enzyme (for double digestion, 0.5µl of each restriction enzyme was used), and dH_20 to get 20µl total volume. These materials were combined and then the appropriate enzyme was added to the reaction. The uncut reaction was also prepared by mixing only 50ng DNA and dH_20. The reactions were incubated at 37°C for at least 1 hour. To verify the molecular weight of the vector and insert, the products were resolved on an 0.8% agarose gel containing 0.5µg/ml ethidium bromide at 80 volts for 50 minutes and then visualised on UV transilluminator (UVidoc, UVitec). The clone showing the correct inserts was selected for scaling up the DNA production by adding the remaining starter culture of this clone to 250ml LB medium containing selective antibiotics, and grown in the bacteria shaker incubator at 37°C, at 240 rpm overnight (12-16 hours). Next day, the DNA was extracted from the bacterial culture using Maxiprep kit (12163, QIAGEN) following the manufacturer's instructions. The concentration of the purified DNA was measured by ND-100 spectrophotometer (NanoDrop Technologies, USA) using programme NanoDrop 1000 3.7.1, Nucleic acids, DNA-50, averaged and adjusted to 1µg/ml.

2.9.3 Transfection of Cos-7 cells and protein harvesting

Cos-7 cells were plated in a 100mm tissue culture dish at 10^6 cells/dish in 10% FBS DMEM and incubated at 37°C, 5% CO_2 for 24 hours. Next day, the cells were transfected with expression plasmids for indicated proteins (see the list of the DNA constructs in table 2.5). The medium was changed to Opti-MEM (31985, Invitrogen) without antibiotics. 15µl Lipofectamine 2000 (11668-019, Invitrogen) was added to the fresh-clean tube containing 250µl Opti-MEM per 100-mm dish and incubated for 5 minutes at room temperature. 5µg DNA was directly added to the Lipofectamine 2000/Opti-MEM complex and mixed by pipetting gently and incubated for 20 minutes at room temperature. Then the complex was carefully dispersed on cells covered with 5ml Optimem. The cells were left in the incubator for 8 hours and then the medium was changed to 10% FBS DMEM. After 24 hours, the cells were washed twice with cold-PBS and then 150µl RIPA buffer (see the recipe in table 2.4), containing Complete ULTRA tablet protease inhibitor cocktail, EDTA-free (05 892 791 001, Roche) was added to the cells. The protein was collected using a cell scraper (83.1830, Sarstedt), and the cells were broken mechanically by passing through a 25G needle ten times and incubated on ice for 30 minutes. Then, the lysate was clarified by centrifugation at 13000 × *g* for 20 minutes at 4°C. The supernatants

were collected and separated into 3 tubes; the volume of the first tube was about 3-5µl for measuring protein concentration using Bradford protein assay (500-0006, BioRad). The second tube was prepared for performing Western blot to check protein input and the third portion was for immunoprecipitation.

2.9.4 Immunoprecipitation

In a pre-clearing step, 25µl protein A/G-PLUS agarose beads (sc-2003, Santacruz) were pre-washed with 100µl IpH buffer (see the recipe in table 2.4), without protease inhibitor. Then, 2 sets of 500µg of protein extract from each sample were added to pre-washed beads — labelled as 'mock IP' (protein extract and beads) and 'IP' (protein extract, beads and antibody), respectively — and pre-cleared at 4°C on rotation for 45 minutes. The protein-bead complex was then centrifuged at 12000*g* for 20 seconds and the supernatant was taken to a fresh tube. The relevant antibodies (listed in table 2.6) were then added to the 'IP' samples and all tubes were incubated for a further 45 minutes at 4°C. Then, both samples were transferred to new tubes containing pre-washed agarose beads and immune-precipitated on a roller for 1 hour at 4°C. The beads were then pelleted and washed 5 times with 500µl IpH buffer containing protease inhibitor for 25 minutes at 4°C. The samples were spun down and the supernatants were discarded. At room temperature, 6x sample buffer (see table 2.4) was diluted to 1x strength with dH_2O and 25µl was added to each sample to elute the precipitated protein from the beads. As SMO and PTCH1 are the multipass transmembrane proteins, which are more likely to aggregate in the loading buffer when boiled at high temperature because of their hydrophobic nature, the precipitated proteins and their input samples were run directly on an SDS-PAGE gel without boiling (Steves Morin, Pers. Comm.; see also (Hillman et al., 2011)), followed by immunoblotting with appropriate antibodies (Table 2.6-2.7).

2.10 SDS-PAGE and immunoblotting

Protein samples from cell lysates and immunoprecipitations were loaded onto 7.5% resolving gel (see the recipe in table 2.9) and run at a constant current of 85 amps (BioRad PowerPAC 300, BioRad). This was followed by transferring to a Polyvinylidene fluoride (PVDF) membrane (IPVH00010, Millipore) at 85 volts, constant voltage for 90 minutes. To block the nonspecific proteins, the

membrane was incubated in 5% non-fat dry milk in 0.05% Tween-20 (P9416, Sigma) in TBS (TBST) (see the recipe in table 2.4), on a roller mixer for 2 hours at room temperature. The blocking solution was then replaced by fresh blocking solution in which an appropriate primary antibody was diluted (table 2.6), and then the membrane was incubated overnight at 4°C. Next day, the membrane was washed 3 times for 20 minutes in TBST, followed by incubation with an appropriate secondary antibody conjugated to horseradish peroxidase (HRP) (table 2.7), diluted in 5% non-fat dried milk in TBST, for 1 hour at room temperature. The membrane was again washed with TBST for 20 minutes 3 times before processing for enhanced chemiluminescence (ECL) detection according to the manufacturers directions (RPN2109, Amersham). The protein signal was captured with different exposure times on X-ray film (28906837, Amersham), and then developed in an X-ray developer (Optimax2010 X-ray film processor).

2.11 NIH3T3-GL cell culture and transfection

NIH3T3-GL cells (a gift from Dr. Frederic Charron, Montreal, Canada) were cultured in 10% FBS DMEM. To begin transfection, the cells were plated in a 60mm tissue culture dish at a density of $5.5x10^5$ cells/dish in 10%FBS DMEM and incubated at 37°C, 5% CO_2 for 24 hours. Next day, 3µg either of pIRES-neo empty vector or *Nrcam*-HA plasmid (kindly provided by Dr. Catherine Faivre-Sarrailh, France), as well as, 9µl Lipofectamine-2000 were diluted in 250µl Opti-MEM and incubated for 5 minutes at room temperature. The diluted plasmids were combined with the diluted Lipofectamine-2000 and incubated again for 20 minutes at room temperature. Meanwhile, the cells were washed twice with 10%FBS DMEM without Penicillin-Streptomycin (15140, Invitrogen) and 3ml 10%FBS DMEM without Penicillin-Streptomycin was added to each well. Then the DNA-Lipofectamine-Opti-MEM complex was added to the cells and left in the incubator for 18 hours.

Next day, the cells were serum starved with 0.5% FBS DMEM for 24 hours, and treated with 30nM SHH or 100nM SAG in 0.5% FBS DMEM for 24 hours (Karen Cholmondeley pers comm; see also (Rohatgi et al., 2007)). Then the cells were washed twice with cold-PBS, scraped and lysed in a lysis buffer (see the recipe in table 2.8), with Complete ULTRA tablet protease inhibitor cocktail, EDTA-free.

The cells were broken mechanically by passing through a 25G needle ten times and incubated on ice for 30 minutes. Then, the lysate was clarified by centrifugation at 13000*g* for 20 minutes at 4°C. The supernatants were collected and the protein concentration was measured using Bradford protein assay. The protein from each sample was supplemented with 4x SDS loading buffer (see the recipe in table 2.4), and boiled at 95°C for 10 minutes and briefly spun down. 50mg total protein from each sample was loaded to 7.5% SDS-PAGE, followed by immunoblotting and probed with appropriate antibodies (table 2.6-2.7).

2.12 Quantitative PCR (qPCR)

2.12.1 RNA isolation

RNA from the GNPs after SHH or SAG treatment was extracted by adding 500 µl TRIzol Reagent (15596-018, Invitrogen) to each well (from 4 well-dish) and passing the cell lysate several times through a pipette. The homogenised samples were incubated for 2 minutes at room temperature to allow complete dissociation of nucleoprotein complexes, and then transferred to a fresh tube. 100µl chloroform was added and mixed vigorously by shaking for 15 seconds and incubated at room temperature for 3 minutes. The samples were centrifuged at 12,000*g* for 15 minutes at 4°C. After centrifugation, to obtain RNA, the upper aqueous phase was taken to a fresh new tube (about 250µl). RNA was precipitated by adding 625µl 100% ethanol, 25µl LiCl and 1µl glycogen (901 393, *Boehringer*) and incubated at -20°C overnight. Next day, the sample was centrifuged at 12,000 × g for 30 minutes at 4°C. The precipitated RNA was seen as a gel-like pellet from which the supernatant was carefully removed. The RNA pellet was washed once with 100µl 75% ethanol, and centrifuged at 7,500 × g for 10 minutes at 4°C. The supernatant was again removed and briefly air-dried. The pellet was not left until it completely dried as this can decrease its solubility. 15µl DEPC water (see recipe in table 2.4) was added to the RNA and the solution was passed through a pipette tip several times to dissolve the RNA. Before starting cDNA synthesis, the concentration of RNA was measured by ND-100 spectrophotometer (NanoDrop Technologies, USA) using programme NanoDrop 1000 3.7.1, Nucleic acids, RNA-40. RNA purity was also taken into a consideration, as the pure RNA should have had an A_{260}/A_{280} ratio above 1.6. The RNA was stored at -80°C.

2.12.2 cDNA synthesis

500ng RNA was reverse-transcribed with QuantiTect Reverse Transcription Kit (205311, Qiagen), following the manufacturer's protocol. In addition, RT-control reactions were performed alongside using exactly the same conditions as for the experimental samples. However, the reverse transcriptase was not added to the RT-control samples to ensure that there was no genomic DNA contamination, which may affect later qPCR results. The cDNA samples were quantified by ND-100 spectrophotometer (NanoDrop Technologies, USA) using programme NanoDrop 1000 3.7.1, Nucleic acids, DNA-50, and the concentration of each sample was made to 500ng/µl. Then, 1µl cDNA from all samples was checked for the expression of *Gapdh* by semi-quantitative PCR (PTC-200 Peltier Thermal Cycler, MJ research), before performing qPCR. Only DNA, which had an A260/A280 ratio of 1.8-2.0, was allowed to continue to the next step. The cDNA samples were kept at -80°C after use. All reagents and kits for RNA isolation and cDNA synthesis were listed in table 2.10.

2.12.3 Protocol optimisation

As the accuracy of qPCR depends on proper protocol optimisation, according to manufacturer's direction (qPCR technical guide, Sigma), the guidelines to optimise to qPCR are follows; the primer concentration optimisation, experiment validation with a standard curve and investigation of melt curves. I will explain these guidelines in details below.

2.12.3.1 Primer concentration

The optimal concentrations of forward and reverse primers were determined by testing the following combinations of primer concentrations: 1000 nM, 500 nM, 250 nM, 125 nM and 62.5 nM, to determine which was the most efficient. The qPCR primers used in this study are listed in table 2.1. Each concentration was run in triplicate on an E13.5 mouse cDNA sample, which was used as a positive control. Thermal cycling was performed at an optimal temperature for each pair of primers (the optimal temperature was obtained according to the optimal temperature from gradient PCR) with iCycler iQ system. The lowest primer concentration with the combination of the lowest threshold cycle (C_t) and the highest fluorescence was chosen for subsequent experiments.

2.12.3.2 Standard curve

The optimal concentrations for each primer pair were again tested on 5 fold-dilutions of the positive control (E13.5 mouse cDNA), which are 1000ng, 100ng, 10ng, 1ng, 0.1ng DNA to investigate their efficiencies. The threshold cycle (Ct) values and the log of DNA dilutions were plotted as a standard curve and the reaction efficiency was automatically calculated by iCycler iQ Optical system software, version 3.1 (BioRad) or using the equations below:

$$\text{Amplification efficiency} = 10^{(-1/\text{slope})}$$

$$\% \text{ Efficiency} = (\text{Amplification efficiency} - 1) \times 100$$

The accepted range of %efficiency was 80-110% (Schmittgen and Livak, 2008).

2.12.3.3 Melt curve

The melt curve of each set of primers was analysed individually with a single peak to indicate that there was a single specific product. In addition, PCR products of each set of primers were also resolved on 1.2% agarose gel to check there was no primer dimer formation and non-specific product.

2.12.4 qPCR experimental design

The qPCR experimental design and methodologies used in this study were the Relative Standard Curve Method, which involves using a set of known standards relative to which unknown samples can be quantitated. The cDNA sample from WT GNP-cDNA at 4.5 hours post-treatment was set as a calibrator, a sample used as the basis for comparing results.

2.12.5 qPCR reaction optimisation

All qPCR reactions were performed with iCycler iQ system using 96 well plate (NS-96-CC/CP, Cell Projects) (see table 2.10). Each individual reaction was performed in triplicate and was made up as follows: 10µl SYBR Green JumpStart Taq Ready Mix (S4438, Sigma-Aldrich), 1µl each FW and RV primers purchased from Eurofins MWG Operons (see table 2.11 for concentrations), 2µl of 1/10 diluted cDNA, which the started concentration are 500ng/µl (=100ng), and nuclease-free water (AM9937, Ambion) to get total volume 20 µl/reaction. Standard curves of Gli1/Ptch1 and Gapdh were generated for each qPCR reaction using serial dilutions of the calibrator (WT GNP control at 4.5 hours

post-treatment cDNA sample; 1000ng, 100ng, 10ng, 1ng and 0.1ng of cDNA.). A set of primers for the gene of interest (Gli1 or Ptch1) was used alongside in the same reaction with a set of primers for a reference control (Gapdh). As the quantification was normalised to the endogenous control (Gapdh), the standard curves were performed for both the target and the endogenous reference in the same plate. The reactions were performed using the following protocol; 94°C. for 2 minutes (preincubation); 50 cycles of 94°C. for 15 seconds (denaturation), optimal annealing temperature (as indicated in table 2.11) for 1 minute and 72°C. for 1 second (amplification); 95°C. for 1 seconds, 50°C. for 1 minute (melting curve); and 40°C. for 10 minutes (cooling). The optimal temperature and primer concentration were used as listed in table 2.11.

All qPCR reactions were also run with a no reverse transcriptase (RT) control, an E13.5 positive control and a no cDNA negative control in the same plate. The melt curve from each sample was examined to verify that amplification resulted in just one product.

2.12.6 qPCR analysis

All qPCR results were analysed using iCycler iQ Optical system software. For each experimental sample, the amounts of the target genes and the endogenous housekeeping genes were each determined by their own standard curve. As each individual sample was performed the reaction for three replicates, the average quantity (avg) of each sample, the standard deviation of the average (stdev) and the coefficient of variation (CV) were calculated.

$$\%CV \quad = \quad \frac{stdev}{avg} x\ 100$$

Any outlier points giving greater than 21.8% CV was identified and removed (Bookout et al., 2006), following by recalculating the avg, stdev and CV. However, only one point per replicate can be removed.

Then the avg quantity of each sample was normalised to its respective endogenous housekeeping gene control in order to calculate a normalised target value according to the following equation. The recalculated value was used if an outlier point was removed.

$$Normalised\ target(test\ sample) = \frac{Target\ gene}{Endogenous\ control\ gene}$$

Then the normalised target values of the test samples were divided by the normalised target value of the WT control sample (a calibrator) to calculate the fold difference in target quantity between the samples and the calibrator.

$$Fold\ difference\ in\ target = \frac{Normalised\ target\ (test\ sample)}{Normalised\ target\ (calibrator\ sample)}$$

Each experimental sample was averaged from its triplicate and also repeated to 3 biological replications. A one-way ANOVA were then tested to determine significance in gene expression change between control and experimental groups.

2.13 Tables of antibodies, media and reagents using in this study

Table 2.1. List of Primers used in this study

Gene Name	Primer	Source	Gene Bank Accession No.	Primer Sequence (5′ – 3′)	Product Sizes (bp) or Amplicon (bp)	Purpose	Annealing Temperature (°C)	References
Nrcam	NRCAM	Dr. Andrew Furley, UK	-	1. Nr1 Int 3: GCTCAGGATGGTTGCGCC 2. NrMP1: CTTCCTGTGCCAGATGATCA 3. NEO F1: TGGAGAGGCTATTCGGCTATGAC 4. PAF11 B2 (NEO B5): AGCAAGGTGAGATGACAGGAGATC	NRCAM (+/+) 340 bp NEO (-/-) 260 bp	Genotyping	60	-
Gli1	mGli1	Dr. Andrew Furley, UK	NM_010296.2	FW: GCTTGGATGAAGGACCTTGTG RV: GCTGATCCAGCCTAAGGTTCTC	78 bp	qPCR	64	(Romer et al., 2004)
Ptch1	mPtch1	Dr Anne-Gaelle Borycki, UK	NM_008957.2	FW: CAACACCTGGACTCAGCACTCC RV: GCAAGGGTAAAGGTATTC TATTATCTG	150 bp	qPCR	59	Dr Anne-Gaelle Borycki, UK
Gapdh	mGapdh	Dr Anne-Gaelle Borycki, UK	NM_008084.2	FW: ACTCCACTCACGGCAAATTC RV: GACTCCACGACATACTCA GCACC	145 bp	qPCR	58-64	(Lepper et al., 2009) and Dr Anne-Gaelle Borycki, UK
Gapdh	mGapdh	Dr Anne-Gaelle Borycki, UK	NM_008084.2	FW: ACTCCACTCACGGCAAATTC RV: ACTGTGGTCATGAGCCCTTC	385 bp	Semi-quantitative PCR	59	(Lepper et al., 2009)

Table 2.2. List of Buffer and Reagents for GC preparation and culture

Reagent	CMF-PBS 500 ml	Volume	Catalogue Number	Supplier
1. CMF-PBS 500 ml	1. D-PBS (Without Ca^{2+} and $Mg^{2+)}$	500ml	14190-094	Gibco, Invitrogen
	2. 45% Glucose	2.22ml	101174Y	BDH Laboratory Supplies
	3. 7.5% Sodium Bicarbonate	0.27ml	25080	Gibco, Invitrogen
	4. Phenol Red	0.25ml	P0290	Sigma
	Mixed and kept at 4°C			
2. Trypsin-DNase100ml	1. DNase (2000u/mg)	100 mg	2139	Worthington
	2. Trypsin	1g	3703	Worthington
	3. CMF-PBS		99.4 ml	
	4. 1N NaOH	0.6 ml	102524X	BDH Laboratory Supplies
	Filtered and aliquoted 1 ml/tube and kept at 20°C			
3. DNase 200 ml	1. DNase (2000u/mg)	100 mg	2139	Worthington
	2. 30% Glucose	2.26ml	101174Y	BDH Laboratory Supplies
	3. BME, no Glutamine	197.7ml	41010	Gibco, Invitrogen
	Filtered and aliquoted 2 ml/tube and kept at 20°c			
4. 4xCMF-PBS-EDTA (for making Percoll solutions)	1. NaCl	32g	S7653-1KG	Sigma
	2. KCl	1.2g	P-9541	Sigma
	3. Glucose	8g	101174Y	BDH Laboratory

Reagent	CMF-PBS 500 ml	Volume	Catalogue Number	Supplier
				Supplies
	4. $NaH_2PO_4H_20$	2g	102454R	BDH Laboratory Supplies
	5. KH_2PO_4	1g	P-0662	BDH Laboratory Supplies
	6. 7.5% Sodium Bicarbonate	2.13ml	25080	Gibco, Invitrogen
	7. 1M EDTA, pH8 (final EDTA concentration = 2.5 mM)	10ml	-	-
	8. Sterile water		900ml	
	pH 7.35, then made up to 1L, filtered and kept at 4°C			
5. 35% Percoll (White solution)	1. 4xCMF-PBS-EDTA		25ml	
	2. Percoll	35ml	P1644-1L	Sigma
	3. Autoclaved water	40ml	-	-
	Filter sterilise			
6. 60% Percoll (Blue solution)	1. 4xCMF-PBS-EDTA		25ml	
	2. Percoll	60ml	P1644-1L	Sigma
	3. Autoclaved water	15ml	-	-
	4. Trypan Blue 0.4%	0.3ml	15250-061	Gibco, Invitrogen
	Filter sterilise			
7. GCM+S (Pre-plating	1. L-Glutamine 200mM	0.1ml	25030	Gibco, Invitrogen

Reagent	CMF-PBS 500 ml	Volume	Catalogue Number	Supplier
media)	2. Penicillin-Streptomycin	0.1ml	15140	Gibco, Invitrogen
	3. 30% Glucose	0.3ml	101174Y	BDH Laboratory Supplies
	4. Horse serum (Heat inactivated)	1ml	-	-
	5. BME, no Glutamine	8.5ml	41010	Gibco, Invitrogen
	Filter * This medium should be prepare freshly for each experiment			
8. GCM	1. L-Glutamine 200mM	0.1ml	25030	Gibco, Invitrogen
	2. Penicillin-Streptomycin	0.1ml	15140	Gibco, Invitrogen
	3. 30% Glucose	0.16ml	101174Y	BDH Laboratory Supplies
	4. N-2 supplement (100x), Liquid	0.1ml	17502-048	Gibco, Invitrogen
	5. BME, no Glutamine	9.54ml	41010	Gibco, Invitrogen
	Filter * This medium should be prepare freshly for each experiment			

Table 2.3. List of Culture Media

Reagent	Catalogue Number	Supplier
1. DMEM, high glucose, Pyruvate, no glutamine	21969-035	Gibco, Invitrogen
2. DPBS, no calcium no magnesium	14190-094	Gibco, Invitrogen
3. BME, no Glutamine	41010	Gibco, Invitrogen
4. Leibovitz's L-15	11415-049	Gibco, Invitrogen
5. Opti-MEM	31985	Gibco, Invitrogen
6. FBS-Fetal Bovine Serum	10270	Gibco, Invitrogen
7. Chicken serum	C5405	Sigma
8. 0.25% Trypsin-EDTA (1x), Phenol Red	25200-056	Gibco, Invitrogen
9. L-Glutamine 200mM solution	25030	Gibco, Invitrogen
10. Penicillin-Streptomycin	15140	Gibco, Invitrogen
11. N-2 supplement (100x), Liquid	17502-048	Gibco, Invitrogen

Table 2.4. List of Buffers and Fixative used in this study

Buffers	Formula	Amount/Volume
1. 10x Extraction buffer	1. 250mM NaOH	-
	2. 2mM EDTA	-
2. Neutralisation buffer	1. 40mM Trisma	-
	Adjust the pH to 5.5 with conc. HCl	
3. 50x TAE buffer 1 liter	1. Tris-base	242g
	2. 0.5M EDTA, pH 8.0	100ml
	3. Glacial acetic acid	57.2ml
	4. dH_2O	750ml
	Stirrer until it is completely dissolved and added up with dH_2O to bring final volume to 1000ml, stored at room temperature	
4. 4%PFA 1 liter	1. Paraformaldehyde (PFA)	40g
	2. dH_2O	500ml
	Add NaOH 2-3 drops and warm up on a hotplate with stirrer bar until it dissolves completely, then adjust the pH to 7.2	
	3. 0.2M PB buffer, pH 7.2	500ml
	Filter and make aliquots and store at -20°c	
5. 0.2M PB buffer (pH 7.2) 1 liter	1. Na_2HPO_4	21.8g
	2. NaH_2PO_4	6.4g
	3. dH_2O	900ml
	Stirrer until it is completely dissolved, then adjust the pH to 7.2 with conc. HCl, then adjust the volume to 1 liter with dH_2O	
6. 10x PBS 1 liter	1. NaCl	80g
	2. KCl	2g
	3. Na_2HPO_4	14.4g
	4. KH_2PO_4	2.4g

Buffers	Formula	Amount/Volume
	5. dH_2O	800ml
	Adjust the pH to 7.4 with conc. HCl, then adjust the volume to 1liter with dH_2O	
7. 10x TBS washing buffer (pH 7.4) 1 liter	1. Tris base	30g
	2. NaCl	80g
	3. KCl	2g
	4. dH_2O	800ml
	Adjust the pH to 7.4 with conc. HCl, then adjust the volume to 1 liter with dH_2O	
8. 4x sample buffer (for WB) 10ml	1. 0.5M Tris-HCl pH 6.8	2.5ml
	2. 20% SDS	2ml
	3. Glycerol	4ml
	4. Bromophenol Blue (1% in ethanol)	200µl
	Add 10% Mercapto-ethanol later just before using	
9. 6x sample buffer (Maniatis) for Co-IP	1. 4x Tris-Cl/SDS, pH 6.8 (take 0.5M Tris Cl, pH 6.8 10ml and add 40mg SDS)	7ml
	2. Glycerol (30% final concentration)	3.8g/3ml
	3. SDS (10% final concentration)	1g
	4. Bromophenol Blue	1.3mg
	5. Beta Mercaptoethanol (5% final concentarion)	0.5ml
	Make 0.5ml aliquots and store at -20°c	
10. 10x Leammli running buffer 1 liter	1. Tris base	30.3g
	2. Glycine	144.2g
	3. SDS	10g
	Add dH_2O to 1 liter	
11. 1x Transfer buffer	1. 1x running buffer	800ml

Buffers	Formula	Amount/Volume
	2. Methanol	200ml
12. 1x TE buffer 1 liter	1. 1M Tris-HCl, pH 7.5 (final concentration 10mM)	10ml
	2. 0.5M EDTA, pH 8 (final concentration 1mM)	2ml
	Add dH_2O to 1 liter	
13. Stripping buffer (500ml)	1. β-Mercaptoethanol (final concentration 100mM)	3.5ml
	2. SDS	10g
	3. 1.35M Tris-HCl, pH 6.7	25ml
	4. dH_2O	471.5ml
14. Lysis buffer for WB (200ml), store at 4°C	1. 1M Tris-HCl, pH 8.0 (final conc = 50mM)	10ml
	2. 0.5M EDTA (final conc = 1mM)	0.4ml
	3. NaCl (final conc = 150mM)	1.74g
	4. NaF (final conc = 50mM)	0.42g
	5. 1% Triton X-100	2ml
	6. 10% Glycerol	20ml
15. RIPA buffer for Co-IP (100ml), store at 4°c	1. 1M HEPES, pH 7.4 (final conc = 50mM)	5ml
	2. NaCl (final conc = 150mM)	0.87g
	3. 10% Glycerol	10ml
	4. 1M $MgCl_2$ (final conc = 1.5mM)	150µl
	5. 1% Triton X-100	1ml
	6. 0.5% Sodium deoxycholate (Deoxycholic acid)	0.5g
	7. dH_2O	84ml
16. IpH buffer for Co-IP (100ml)	1. 1M Tris-HCl, pH 8 (final conc = 50mM)	5ml

Buffers	Formula	Amount/Volume
	2. 400mM NaCl	2.32g
	3. 0.5M EDTA, pH 8 (final conc = 5mM)	1ml
	4. 0.1% Np40 (Nonidet-P40) (560092L, BDH)	0.1ml
	5. dH_2O	91.68ml
17. LB Broth 1 liter	1. Bacto-tryptone (T9410, Sigma)	10g
	2. Yeast extract (Y1625, Sigma)	5g
	3. NaCl	5g
	Make up to 1 liter with dH_2O and autoclave	
18. LB Agar 1 liter	1. Bacto-tryptone (T9410, Sigma)	10g
	2. Yeast extract (Y1625, Sigma)	5g
	3. NaCl	5g
	4. Agar (A5306, Sigma)	15g
	Make up to 1 liter with dH_2O and autoclave	
19. DEPC water 100ml	1. DEPC (D5758, Sigma)	0.1ml
	2. dH_2O	100ml
	Shake vigorously and incubate for 12 hours at 37°C, then autoclave for 15 minutes to remove any trace of DEPC	

Table 2.5. List of Recombinant Proteins and Small Molecules

Recombinant Proteins and Small Molecules	Catalogue Number	Supplier
1. Recombinant Human Sonic Hedgehog (C24II), N-Terminus	1845-SH	R&D Systems
2. SAG, Smoothened ligand	ALX-270-426	Enzo Life Sciences

Table 2.6. List of Primary antibodies used in this study

Primary antibody	Type	Concentration	Application and Dilution	Source
1. Anti-Acetylated α-tubulin	Mouse, monoclonal IgG2b	1.5mg/ml	IF 1:1000	Sigma (T6793)
2. Anti-γ-tubulin	Rabbit, IgG fraction of antiserum	15mg/ml	IF 1:1000	Sigma (T3559)
3. Anti-SMO	Rabbit, polyclonal antibody	-	IF 1: 1000	Prof. Kathryn Anderson's lab
3. Anti-SMO (H-300)	Rabbit, polyclonal antibody raised against amino acids 488-787 mapping at the C-terminus of Smo of human origin	0.2mg/ml	IF 1:25	Santa Cruz (sc-13943)
4. Anti-PTCH (H-267)	Rabbit, polyclonal antibody raised against amino acids 1181-1447 of patched of human origin	0.2mg/ml	IF 1:25	Santa Cruz (sc-9016)
5. Anti-NRCAM (N-18)	Goat, polyclonal antibody raised against a peptide mapping within an internal region of NRCAM of human origin	0.2mg/ml	IF 1:25	Santa Cruz (sc-18958)
6. Anti-BOC	Goat, polyclonal IgG (mouse Boc extracellular domain)	0.2mg/ml	IF 1:100, WB 1:1000	R&D systems (AF2385)
7. Anti-GAS1	Goat, polyclonal IgG	0.2mg/ml	IF 1:200, WB 1:500	R&D systems (AF2644)
8. Anti-NRCAM 838^{-}	Rabbit polyclonal	12μg/ml	IF 1:1200 (after pre-absorption)	Prof. Martin Grumet's lab

Primary antibody	Type	Concentration	Application and Dilution	Source
9. Anti-NRCAM 838	Rabbit polyclonal	38µg/ml	WB 1:1500, IP 2.5 µl	Prof. Martin Grumet's lab
10. Anti-GFP	Rabbit polyclonal serum	Not applicable	IF 1:4000, WB 1:1000	Invitrogen (A6455)
11. Anti-GFP	Chicken polyclonal IgY	10mg/ml	WB 1:500	Abcam (ab13970)
12. Anti-HA	Rat monoclonal (clone 3F10) recognized the HA peptide sequence [YPYDVPDYA]	0.1mg/ml	IF 1:1000, WB 1:1000, IP 8 µl	Roche (11 867 423 001)
13. Anti-Flag (anti-DDDDK tag antibody)	Rabbit polyclonal to DDDDK tag	1mg/ml	WB 1:4000, IP 2 µl	Abcam (ab21536)
14. Anti-TIE 2	Goat polyclonal	Not applicable	WB 1:500	Prof. Elizabeth Smythe's Lab
15. Anti-GLI1	Mouse monoclonal	Not applicable	WB 1:500, IF 1:200	Cell signaling (L42B10)
16. Anti-TUJ1	Mouse monoclonal	1mg/ml	IF 1:1000	Covance (MMS-435P100)
17. Anti-KI67	Rabbit polyclonal	Not applicable	IF 1:250	Leica (NCL-Ki67p)
18. Anti-PAX6	Mouse monoclonal	Not applicable	IF 1:50	Hybridoma Bank
19. Anti-GFAP	Rabbit polyclonal	2.9mg/ml	IF 1:1000	Dako (Z0334)
20. Anti-α-Tubulin	Mouse monoclonal	1mg/ml	WB 1:10000	Sigma (T6199)

Table 2.7. List of Secondary antibodies used in this study

Secondary antibody	Application and Concentration	Source
1. Goat Anti-Mouse IgG1-HRP	WB 1:5000	Santa Cruz (sc-2060)
2. Goat Anti-Rabbit IgG-HRP	WB 1:5000	Jackson ImmunoResearch (111-035-144)
3. Rabbit Anti-Goat IgG-HRP	WB 1:2000	Everest (EB2ND-001-HRP)
4. Donkey Anti-Chicken-HRP	WB 1:5000	Jackson ImmunoResearch (703-036-155)
5. Goat Anti-Rat-IgG-HRP	WB 1:5000	Sigma (A9037)
6. Alexa Fluor 647 Donkey Anti-Rabbit IgG	IF 1:800	Jackson ImmunoResearch (711-606-152)
7. DyLight 488 Donkey Anti-Mouse IgG	IF 1:900	Jackson ImmunoResearch (715-486-151)
8. Rhodamine Red-X-Donkey Anti-Mouse IgG	IF 1:200	Jackson ImmunoResearch (715-296-150)
9. Rhodamine Red-X-Donkey Anti-Rabbit IgG	IF 1:200	Jackson ImmunoResearch (711-296-152)
10. Rhodamine Red-X-Donkey Anti-Rat IgG	IF 1:200	Jackson ImmunoResearch (712-296-153)
11. Rhodamine Red-X-Donkey Anti-Goat IgG	IF 1:200	Jackson ImmunoResearch (705-296-147)
12. Rhodamine Red-X-Goat Anti-Mouse IgM	IF 1:200	Jackson ImmunoResearch (115-295-020)
13. Alexa Fluor 488 Goat Anti-Chicken IgG	IF 1:500	Invitrogen (A-11039)

Table 2.8. List of DNA constructs used in this study

Construct name	Vector/vector size	Insert/Site/Size	Resistance	Restriction endonuclease/ Expected band size	Source
1. *Nrcam*-FL (#272 in the lab database)	pcDNA3 (5.5 kb)	NRCAM/*Eco*RI/4 kb	Amp	*Eco*RI	Dr. Fleur Davy (University of St Andrews)
2. Rat *Nrcam*-HA	pIRES1 neo (5.3 kb)	NRCAM/EcoRI/4.04kb HA/ *Not*I-*Bst*EI/0.3kb **Note:** HA epitope was inserted by PCR 5 amino acids downstream of the signal peptide in NRCAM12 subcloned in pIRESIneo (see Falk et al., 2004)	Amp	*Cla*I and *Eco*RI/5.3, 4.04 and 0.3 kb	Dr. Catherine Faivre-Sarrailh (France)
3. *Ptch1*-GFP	pEGFP-C1	mPtc1 ORF/*Bgl*II-*Kpn*I/4305 bp	Kan	*Bgl*II and *Kpn*I/4.7 and 4.3 kb	Dr. Frederic Charron (Montreal, Canada)- Original from C.C. Hui
4. *Smo*-GFP	pEGFP-N (4.7 kb)	mSmo/*Eco*RI-SACII/2468 bp	Kan	*Eco*RI/ 4.7 and 2.468 kb	Dr. Frederic Charron (Montreal, Canada)- Original from C.C. Hui
5. Boc-FLAG	pcDNA3.1 (5.4 kb)	mBoc/*Eco*RI-*Apa*I/3 kb FLAG/259 bp **Note:** Flag-tagged at *C*-terminus	Amp	*Apa*I and *Eco*RI/ 3, 0.259 and 5.4 kb	Dr. Frederic Charron (Montreal, Canada)

Table 2.9. Recipes for SDS-PAGE 1.5mm mini

Reagents	Resolving gel					Stacking gel
	5%	6%	7.5%	10%	12.5%	
1. dH_2O	5.65ml	5.3ml	4.8ml	3.95ml	3.15ml	2.8ml
2. 30% Acrylamide/Bis solution (161-0156, BioRad)	1.65ml	2ml	2.5ml	3.35ml	4.15ml	0.85ml
3. 1.5M Tris-HCl, pH 8.8	2.5ml	2.5ml	2.5ml	2.5ml	2.5ml	-
4. 0.5M Tris-HCl, pH 6.8	-	-	-	-	-	1.25ml
5. 10% SDS (444464T, BDH)	100µl	100µl	100µl	100µl	100µl	50ml
6. 10% Ammonium Persulphate (APS) (161-0700, BioRad)*	100µl	100µl	100µl	100µl	100µl	50ml
7. TEMED (T-9281, Sigma)*	10µl	10µl	10µl	10µl	10µl	5µl

*Add APS and TEMED last when ready to pour gel.

Table 2.10. List of Kits and Special Materials

Product Name	Catalogue Number	Supplier
1. TRIzol Reagent	15596-018	Invitrogen
2. Glycogen	901 393	*Boehringer* Mannheim
3. QuantiTect Reverse Transcription Kit	205311	Qiagen
2. SYBR Green JumpStart Taq Ready Mix	S4438	Sigma-Aldrich
3. PCR Sealers Microseal 'B' Film	MSB1001	Bio-Rad
4. Non Skirted PCR 90 Well Plates	NS-96-CC/CP	Cell Projects
5. BioRad	500-0006	BioRad
6. Roche Complete protease inhibitor cocktail without EDTA	05 892 791 001	Roche
7. Lipofectamine-2000	11668-019	Invitrogen
8. DMSO	05879	Sigma
9. Quick-load 1kb DNA ladder	N0468S	New England Biolabs
10. Quick-load 100bp DNA ladder	N0467S	New England Biolabs

Table 2.11. List of optimal annealing temperature and concentration of primers used in this qPCR experiment

Gene of interest	Optimal Annealing Temperature	Primer concentrations
Gli1	64°C.	FW Gli primer: 250 nM
		RW Gli primer: 1000 nM
GAPDH		FW GAPDH primer: 500 nM
		RV GAPDH primer: 125 nM
Ptch1	59°C.	FW Ptc primer: 250 nM
		RV Ptc primer: 250 nM
GAPDH		FW GAPDH primer: 125 nM
		RV GAPDH primer: 100 nM

Chapter 3

Investigation of how NRCAM is involved in SHH pathway

3.1 Introduction

The proliferation of granule neuron progenitors (GNPs) during cerebellar development is induced by Sonic Hedgehog (SHH) signaling (Dahmane and Ruiz i Altaba, 1999, Wallace, 1999, Wechsler-Reya and Scott, 1999). Recent work from our lab has demonstrated that neural adhesion molecules belonging to L1-CNTN family are involved in SHH signalling (Xenaki et al., 2011). Soluble, cross-linked F3 protein (F3-fc) suppresses SHH-induced GNP proliferation. NRCAM, to which F3 is known to bind (Faivre-Sarrailh et al., 1999) (F3 chicken homolog, F11 (Morales et al., 1993)) is expressed in GNPs and F3-fc co-localises with it on the surface of cultured GNPs. However, F3 fails to suppress SHH-induced proliferation when NRCAM is missing. Together these data suggested that F3 suppresses SHH-induced proliferation by binding to NRCAM on the GNP cell surface. However, exactly how F3 and NRCAM impinge on the effects of SHH signalling was not clear. As the effect of F3-fc on GNP proliferation appeared to act through NRCAM, in this study we aimed to understand how NRCAM is involved in SHH signalling.

Recently, it has been shown that SHH requires a tiny cell surface protrusion called the primary cilium to mediate its signal (Michaud and Yoder, 2006, Simpson et al., 2009, Goetz and Anderson, 2010). Briefly, signalling occurs when SHH binds to PTCH and causes it to translocate out of the cilium, which in some way allows SMO to then translocate into the cilium, which activates SHH signalling (Rohatgi et al., 2007) (see greater details in the main introduction, Chapter 1, section 1.4.3). Exactly how these translocations occur is not known, but evidence suggests that this may require endocytosis and intracellular trafficking (Michaud and Yoder, 2006, Goetz and Anderson, 2010, Simpson et al., 2009). Since studies in other contexts have demonstrated that L1-CNTNs are involved in trafficking and endocytosis (Falk et al., 2005, Dang et al., 2012), our hypothesis is that NRCAM may be playing a role in the trafficking of SHH pathway components, particularly SMO or PTCH, into or out of the primary cilium of GNPs. Therefore, the main aim of this chapter is to investigate whether there is any evidence that loss of NRCAM may affect these events.

3.2 Results

3.2.1 Investigation of primary cilia in the cerebellar section

To begin to address whether NRCAM might be involved in the trafficking of SHH pathway components, we had first to be able to demonstrate whether we could visualise primary cilia on granule neuron progenitors. Although the first studies of cilia on GNPs were ultrastructure studies of the rat cerebellum using electron microscopy (Del Cerro and Snider, 1972), more recent studies have described primary cilia on mouse cerebellar sections using immunofluorescence (Spassky et al., 2008). Therefore, I began the study by attempting to verify whether primary cilia could be seen on GNPs in cryostat sections of the postnatal day 5 (P5) mouse cerebellum, as it was during this period that our previous studies had documented differences between WT and *Nrcam*$^{-/-}$ mice (Xenaki et al., 2011). P5 cerebellum was cryo-sectioned to 15μm and stained with antibody to acetylated α-tubulin, a primary cilia marker (Poole et al., 1997). However, it was very difficult to discern where the primary cilia were, because the number of GNPs and the number of axons at P5, which also stain for acetylated α-tubulin, is substantially higher than at E18.5, the time point at which previous studies were undertaken (Spassky et al., 2008). Even when I attempted to stain thinner sections at P5 (ie with fewer cells), I was still not able to clearly visualise primary cilia on the GNPs (data not shown).

3.2.2 Development of a protocol to visualise primary cilia of GNPs *in vitro*

Since I could not visualise primary cilia of GNPs on cerebellar sections, I also looked at cultured P5 GNPs, with which many of our previous observations had been made (Xenaki et al., 2011). GNPs were purified from P5 mice using our established protocol (Xenaki et al., 2011) (see Methods, section 2.3.2) and cultured for 24 hours without SHH. To establish the purity of the cultures, cells were labelled with antibodies to PAX6 [granule neuron marker; (Engelkamp et al., 1999)] and Glial Fibrillary Acidic Protein [GFAP; astrocyte marker; (Bignami et al., 1972)]. Greater than 95% of cells were PAX6+ cells (97.02±1.91%), while less than 1% (0.6±0.32%) was GFAP+ (Fig 3.1, consistent with previous results (Xenaki et al., 2011, Hatten et al., 1997).

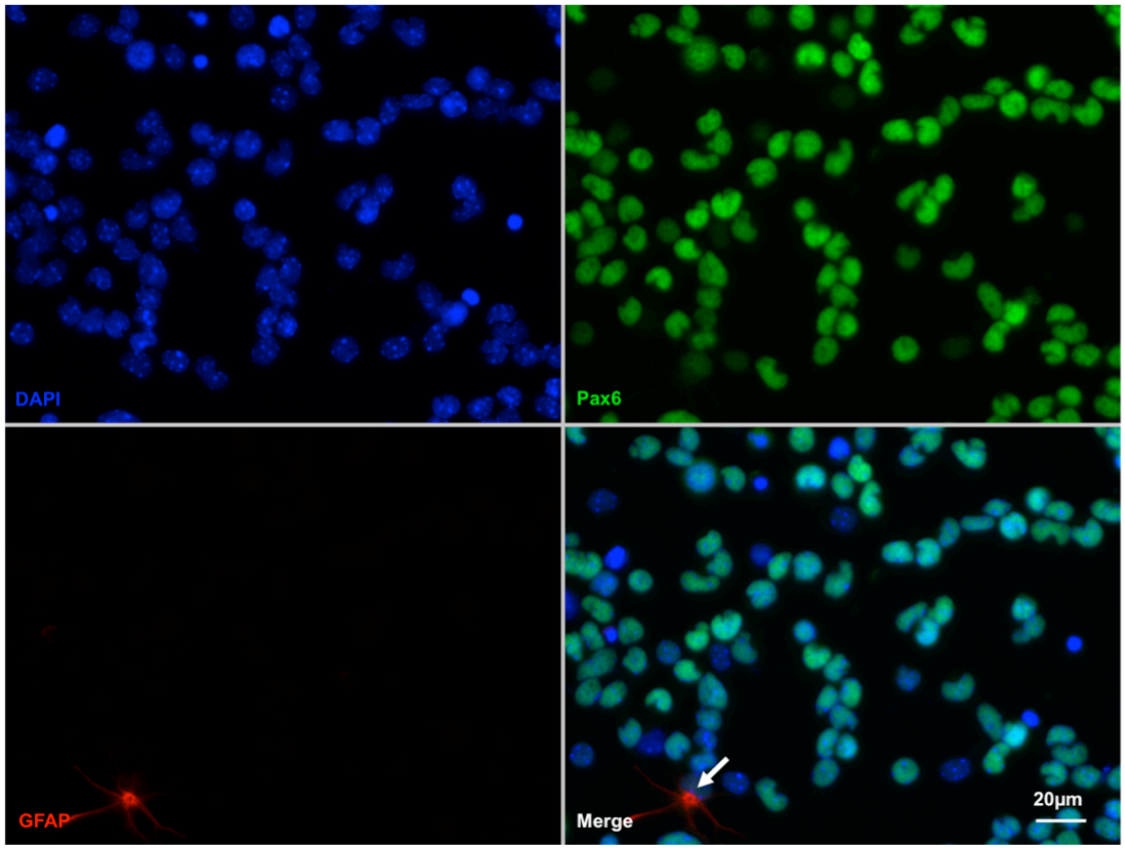

Figure 3.1. Percentage of GNP populations after GNP preparation. After GNP preparation, the cells were plated for 24 hours and fixed with 4%PFA. The cells were stained with PAX6 and GFAP and quantified percentage of GNP population. Arrow indicates the GFAP positive cell. Scale bar = 20μm.

Although our previous work had examined the downstream effects of SHH on GNP proliferation at 24 hours and 48 hours after plating (Xenaki et al., 2011), our hypothesis was that loss of NRCAM would affect the trafficking of SHH pathway components into or out of the primary cilium, most likely during the initial response to SHH addition. Since such responses, including translocation of PTCH and SMO to and from primary cilia, can be seen at least as early as 4 hours after SHH addition to NIH3T3 cells (Rohatgi et al., 2007), and since we normally add SHH to our GNP cultures soon after plating (+1.5 hours), this suggested that we should attempt to visualise primary cilia as early as possible after this. Cultures were therefore analysed 6 hours and 24 hours after plating with antibodies to acetylated α-tubulin. As shown in fig 3.2, at 6 hours a number of cells could be seen with single α-tubulin positive protrusions that appeared to be primary cilia (Fig 3.2A: a and b; arrow heads). However, more widespread labelling was apparent in other cells (Fig 3.2A: a and b; arrows), consistent with the initiation of axonal processes, and by 24 hours a complex network of axons covered the culture and obscured most cell bodies (Fig 3.2A: c and d).

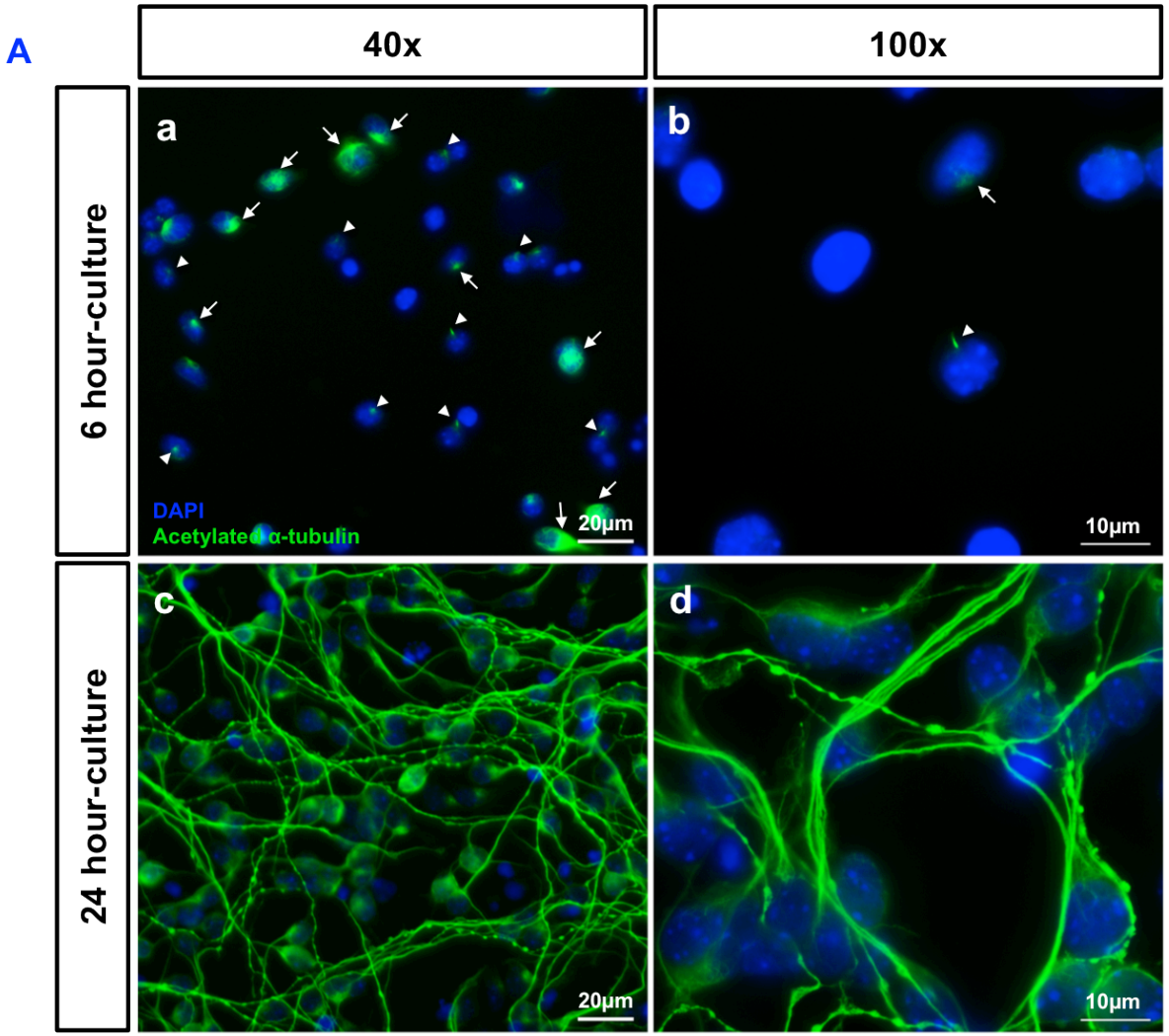
A
40x
100x
6 hour-culture
24 hour-culture
a
b
c
d
DAPI
Acetylated α-tubulin
20μm
10μm
20μm
10μm

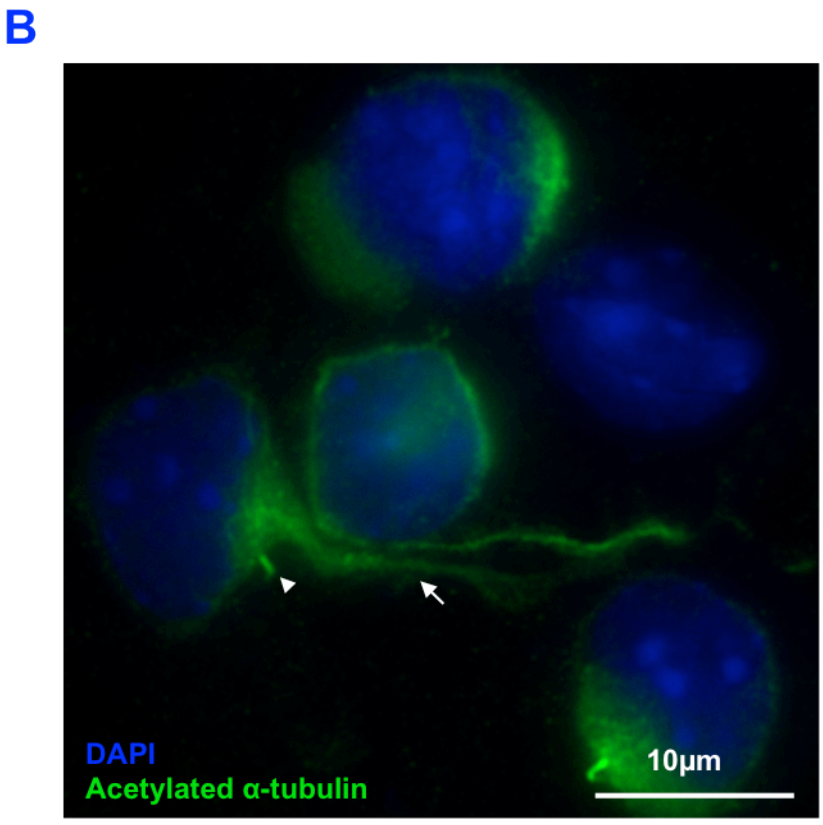

Figure 3.2. Comparison of visualization of primary cilia of cultured WT GNPs at 2 different time-points: 6 and 24 hours. (A). Primary cilia staining of WT GNPs cultured at 6 hours **(a)** at low magnification (40x). The 6 hour-cultured GNPs were stained with anti acetylated α-tubulin antibody and visualised at 40x. The primary cilium (arrow head) and the initiating axons (arrow) were shown. Scale bar = 20μm **(b)** At high magnification (100x), primary cilium (arrow head) and the initiating axons (arrow) on GNPs were more clearly shown. Scale bar = 10μm **(c)** Primary cilia staining of WT GNPs cultured at 24 hours at low magnification (40x). The 24 hour-cultured GNPs were stained with anti acetylated α-tubulin antibody and visualised at 40x. As there were many axons crossing over on 24 hour-cultured GNPs, it was hard to indicate where primary cilium was. Scale bar = 20μm **(d)** At high magnification (100x) Scale bar = 10μm **(B)** At 6 hours culture, the GNP shows primary cilium (arrowhead) and axon (arrow) on the same cell. Scale bar = 10μm

I then used antibodies to acetylated α- and γ-tubulin in combination to allow unambiguous identification of the primary cilium (acetylated α-tubulin+) overlying the basal body (γ-tubulin+) (Poole et al., 1997, Alieva and Vorobjev, 2004) on

purified GNPs *in vitro*. As shown in Fig 3.3, this allows the unambiguous identification of primary cilia, which are present on dissociated GNPs after 6 hours of culture. The percentage of primary ciliated untreated GNPs (83.41±10.67%) was not significantly different from 4.5 hours SHH treated GNPs (85.81±10.95%). Although the percentage of primary ciliated GNPs was quite high, the number of primary cilia that I could quantitate was far fewer because of the cell orientation (a typical field is shown in Fig 3.2A:a). To be able to unambiguously demonstrate whether SMO or PTCH are present in primary cilia, I selected for analysis cells in which the primary cilium clearly protruded beyond the cell body, so that ciliary labelling was not confused with labelling in the main body of the cell. At this time point, 30-35% of the cells had more extensive labelling, consistent with this indicating the initiation of axon formation (Fig. 3.2A) and 15-20% of cells have labelling suggesting they have both primary cilia and axons (Fig. 3.2B). The number of cells having axons was not obviously affected by addition of SHH for 4.5 hours (data not shown).

From these preliminary experiments, I concluded that it was considerably easier to identify primary cilia in GNPs at 6 hours than at 24 hours of culture. Although I also attempted to perform the experiment earlier than at 6 hours I found that the cells were more likely to detach from coverslips. Since 6 hours of culture is actually 4.5 hours after addition of SHH, corresponding to the point at which SMO and PTCH translocations are almost maximal in NIH3T3 cells (Rohatgi et al., 2007), this seemed a reasonable time point to use for further experiments.

After establishing that primary cilia are present in GNPs by double labelling with anti-acetylated α-tubulin and γ-tubulin antibodies (Fig 3.3), in the rest of this study, I stained only with anti-acetylated α-tubulin antibody; the intensity of labelling and the unique morphology of the primary cilium when stained with this antibody are typically sufficient for accurately differentiating the primary cilium from nascent axons (see also Fig 3.2B).

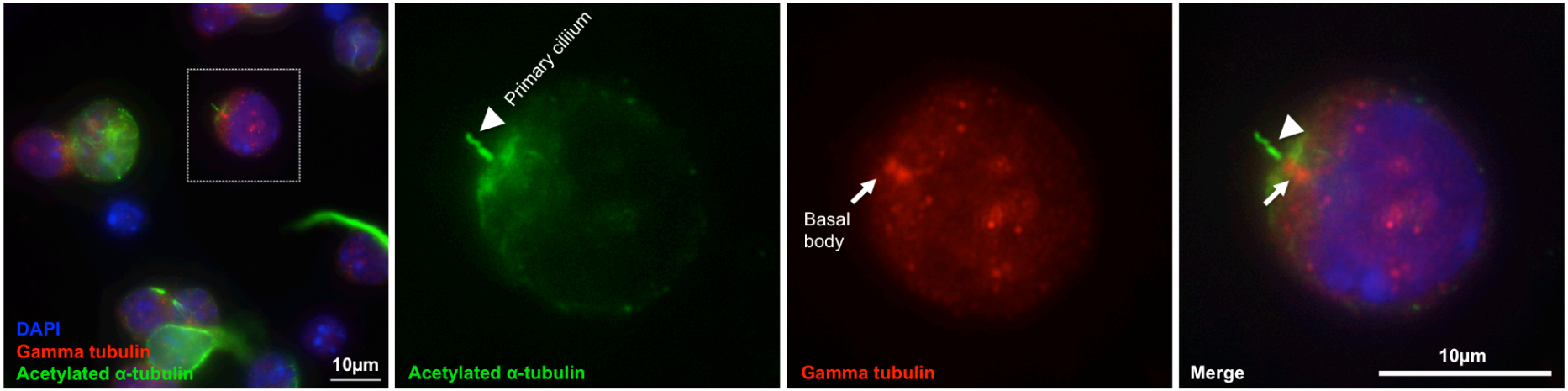

Figure 3.3. Primary cilium is present on GNP. GNPs from WT P5 mice were purified and cultured for 6 hours and immunolabelled with anti-acetylated α-tubulin (green) and anti-γ-tubulin antibodies (red). The localizations of basal body (arrow) and primary cilia (arrow head) on GNP were shown. Scale bar = 10 μm

3.2.3 Demonstration of PTCH and SMO localisation in primary cilia of cultured GNPs in response to SHH or SAG

Recently, the stimulation of PTCH and SMO translocations in primary cilia by SHH signalling has mostly been demonstrated in cultured fibroblasts (Rohatgi et al., 2007, Milenkovic et al., 2009). To determine if this can also be seen in cultured GNPs, double labelling with acetylated α-tubulin and anti-SMO (a gift from Prof. Kathryn Anderson) or anti-PTCH (Santacruz) antibodies were performed. The SMO agonist, SAG (Chen et al., 2002) was used as a positive control, since both SMO and PTCH are known to be found in primary cilium after SAG treatment in other cell types (Rohatgi et al., 2007, Milenkovic et al., 2009). The images were visualised using a Zeiss Apotome epifluorescence microscope.

Under control conditions, labelling in both cases (anti-SMO and anti-PTCH) could be seen throughout the cell, consistent with the fact that the cells were permeabilised. Some of this labelling could be attributed to non-specific labelling by the secondary antibody, but brighter labelling was evident with primary antibodies in vesicle-like structures in both cases. However, differences were seen between labelling with the two antibodies in and around the primary cilium: in the absence of SHH or SAG, while SMO labelling was strongly evident in vesicle-like structures around the base of the cilium (arrow heads in Fig 3.4), it was never seen overlapping acetylated α-tubulin labelling in the cilial protrusions. This changed significantly when either SHH or SAG was added. SMO immunoreactivity now became obvious along the primary cilium as puncta. In the SAG-activated condition, SMO was present along the shaft and the tip of the cilium in 80–90% of cilia. This was less obvious in the cilium of SHH-activated GNPs, but was still present in 45%–50% of the cases. This is consistent with quantitative fluorescent imaging in SHH- activated NIH3T3 cells, which demonstrated that there are different SMO distribution patterns in primary cilia and that SMO accumulating at the tip of the cilium is correlated with SHH transcription activation (Yoo et al., 2012).

By contrast, puncta of PTCH labelling were frequently seen along the length of the cilium, including at the cilial tip (Fig 3.5; arrow), in untreated GNPs. This cilial labelling was never seen with secondary antibody alone (Fig 3.6). This labelling changed significantly upon addition of SHH, with PTCH disappearing from the cilium of a significant proportion of the cells. By contrast, and in agreement with

the observations of others (Rohatgi et al. 2007; Milenkovic et al., 2009), the PTCH distribution did not change upon SAG treatment.

Presentation of the images of fluorescently labelled proteins in primary cilia is very challenging, even though when the data were collected in the dark microscope room, the results were obvious. For this reason, I tried to image this in a different way to verify if I got similar results. GNPs were immunolabelled with anti-SMO and anti-PTCH and fluorescence was visualised using the 'grid projection' (or 'structured illumination') function of the Apotome microscope (Gustafsson, 2000). This gave similar results for both SMO and PTCH (compare Figs 3.4 and 3.5, with Fig 3.7). Unfortunately, although in some cases the grid image was clearer, in many cases grid lines appear in the images. Therefore, only the epifluorescent images were used for quantitation. For illustration however, either epifluorescent or grid visualisation is used in the subsequent experiments, depending on which image made the results clearer.

Although I could not control for the specificity of the antibodies in the strictest sense (we did not have GNPs lacking either PTCH or SMO) several lines of argument suggest that the changes in anti-PTCH and anti-SMO labelling that we see in the primary cilia reflect changes in the distribution of the PTCH and SMO proteins. First, these changes were not seen with secondary antibodies alone. Second, both antibodies are rabbit polyclonals, yet the changes seen in cilia labelling are specific to each antibody under each condition. Third, in the case of SMO, similar changes were seen with two different sources of antibodies (Fig 3.4 and 3.7A). The GNPs were labelled with anti-SMO antibody, which was kindly provided by Prof. Kathryn Anderson, USA (Fig. 3.4) and this experiment was repeated with anti-SMO antibody (sc-13943, Santa Cruz) (Fig. 3.7A), and still showed that the localisation of SMO in primary cilia is increased in addition to SHH and SAG. Finally, the changes seen are similar to those seen in NIH3T3 cells in response to SHH and SAG (Rohatgi et al., 2007).

For the quantification of these effects, I decided to quantitate the percentage 'occupancy' of the cilia by the relevant protein (see the principle of how to quantify the SMO and PTCH ciliary occupancy in Methods, section 2.7) rather than measure fluorescence intensity of the labelling in the cilium. The reason for this was that measurements of fluorescence intensity are difficult in such a tiny structure (average diameter is 0.5-0.9 μm and average length is 2-3 μm) and

particularly complicated when the staining is punctate rather than smoothly distributed along the cilium.

After SHH treatment, the percentage of primary cilia containing SMO labelling increases (Fig 3.4 and 3.7A; see Fig.3.8A for quantification), whereas, that of cilia containing PTCH is decreased when compared with control (Fig. 3.5 and 3.7B; see Fig.3.8B for quantification). However, both SMO and PTCH are found in the primary cilia after addition of SAG (Fig. 3.4, 3.7A for SMO and Fig. 3.5, 3.7B), which is consistent with previous reports (Milenkovic et al., 2009, Rohatgi et al., 2007)

In summary, I have shown for the first time that PTCH and SMO proteins can be visualised in the primary cilia of cultured GNPs and that their behavior in response to SHH and SAG is similar to that seen in NIH3T3 cells (Rohatgi et al., 2007).

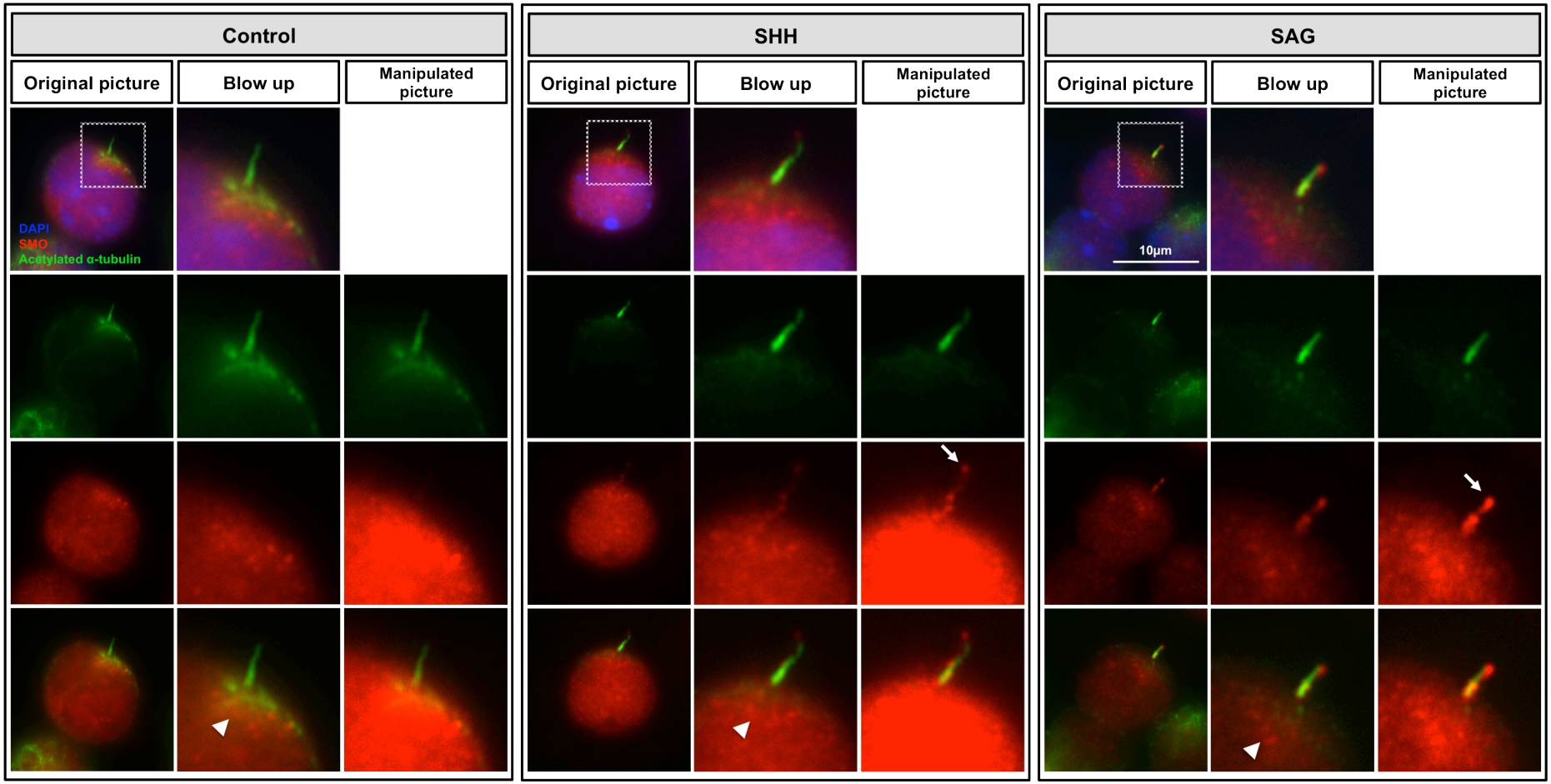
Control
Original picture
Blow up
Manipulated picture
DAPI
SMO
Acetylated α-tubulin
SHH
Original picture
Blow up
Manipulated picture
SAG
Original picture
Blow up
Manipulated picture
10μm

Figure 3.4. The localisation of SMO in primary cilia is increased upon addition of SHH and SAG. Immunofluorescence of 6 hour-cultured GNPs (4.5 hours SHH or SAG treatment) from P5 WT mice stained with anti-acetylated α-tubulin (green), anti-SMO (kindly provided by Prof. Kathryn Anderson) (red) antibodies and nuclei (blue) with DAPI staining. Arrows show the presence of SMO in primary cilia in SHH and SAG conditions and arrowheads show the accumulation of SMO vesicle-like structure around the base of the primary cilia. To clearly see if SMO is present in primary cilium, insets were made to show the area marked around the primary cilium and the fluorescent intensities were manipulated to the same extent. The fluorescent intensity of primary cilia labelling was decreased for 25% and the fluorescent intensity of SMO labelling was enhanced for 100%. Scale bar = 10μm

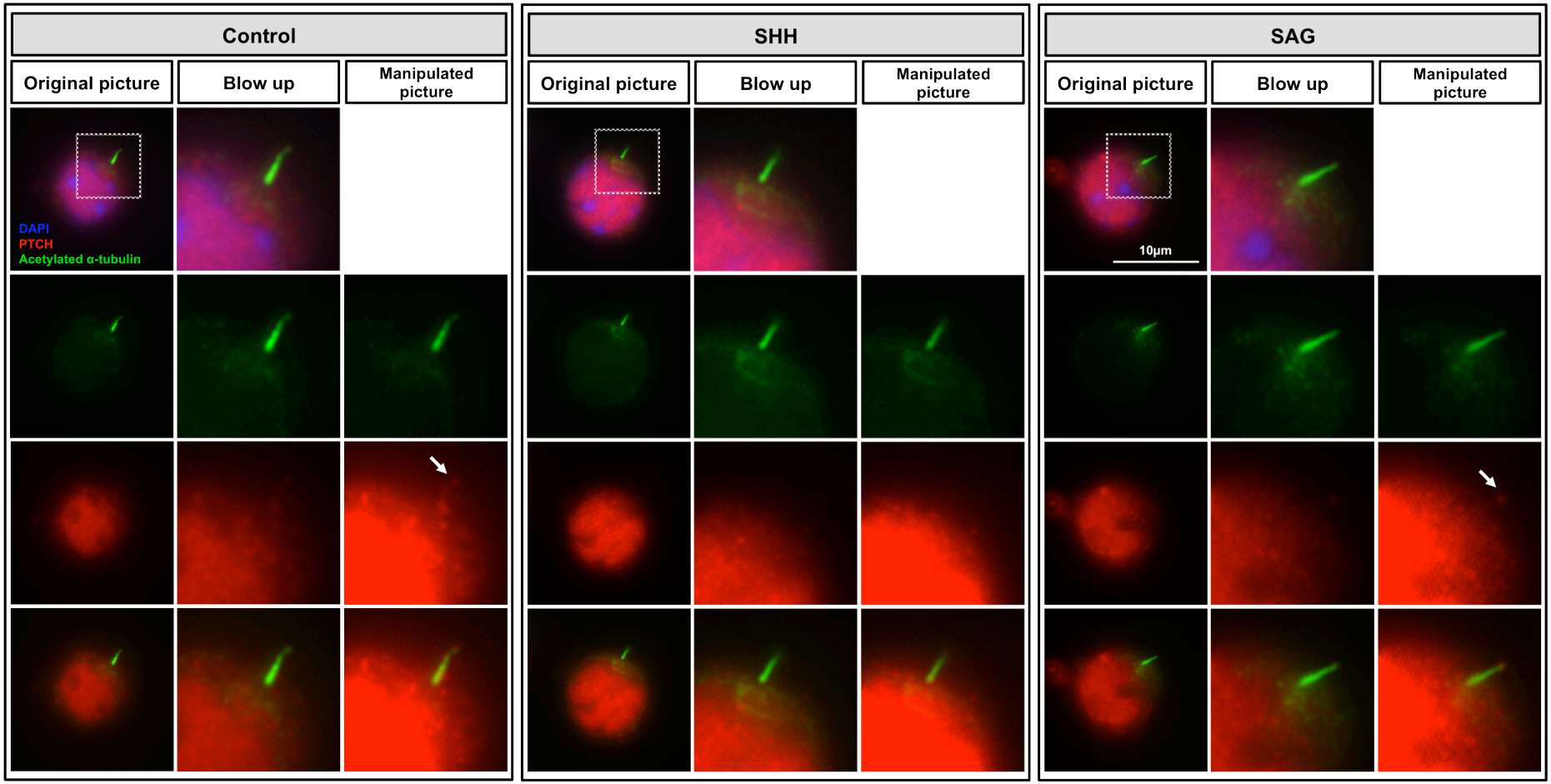
Control
Original picture
Blow up
Manipulated picture
DAPI
PTCH
Acetylated α-tubulin
SHH
Original picture
Blow up
Manipulated picture
SAG
Original picture
Blow up
Manipulated picture
10μm

Figure 3.5. The localisation of PTCH in primary cilia is decreased upon addition of SHH or SAG. Immunofluorescence of 6 hour-cultured GNPs (4.5 hours SHH or SAG treatment) from P5 WT mice stained with anti-acetylated α tubulin (green), anti-PTCH (red) antibodies and nuclei (blue) with DAPI staining. Arrows show the presence of PTCH in primary cilia in control and SAG conditions. To clearly see if PTCH is present in primary cilium, insets were made to show the area marked around the primary cilium and the brightness and contrast were enhanced to the same extent. The fluorescent intensity of primary cilia labelling was decreased for 25% and the fluorescent intensity of PTCH labelling was enhanced for 100%. Scale bar = 10μm

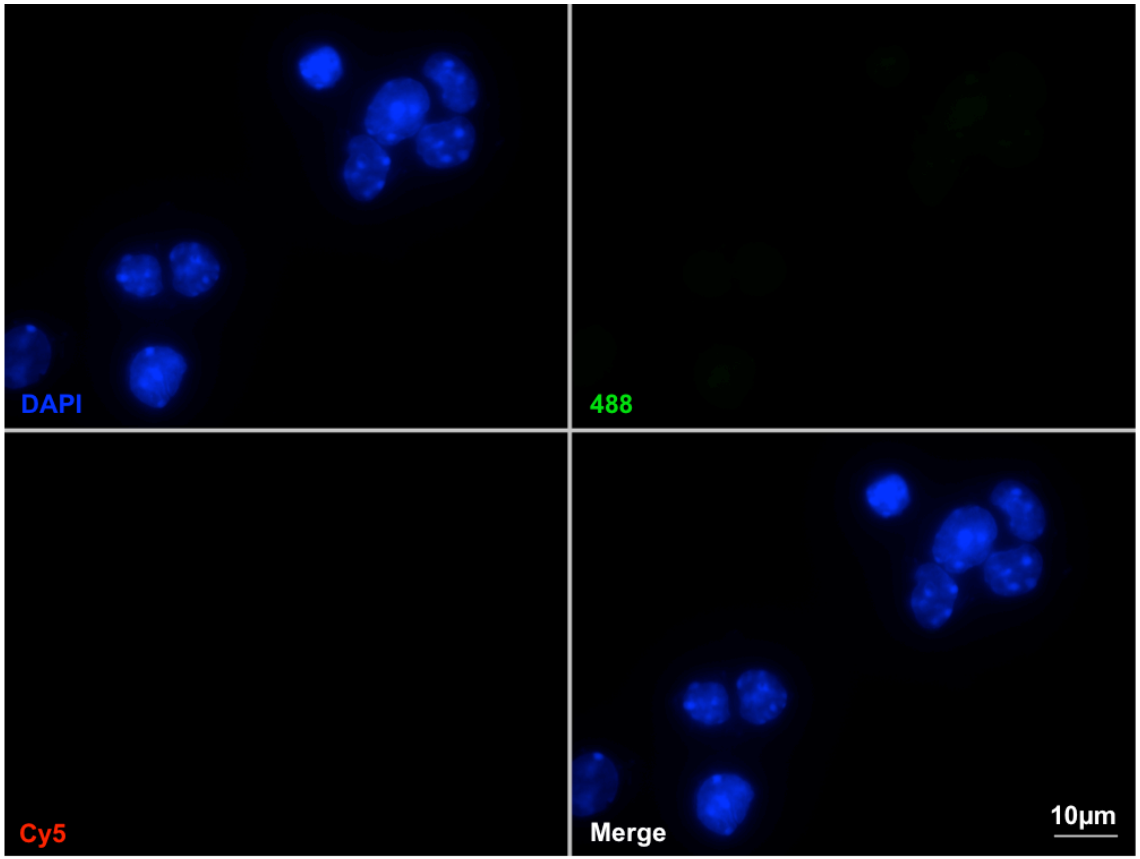

Fig. 3.6. No nonspecific binding in secondary antibody labelling control. Without adding primary antibody, the secondary antibody control was performed in parallel with every experiment. With the same exposure when imaging the GNPs using Apotome, nonspecific binding of secondary antibody was not able to be detected. Scale bar = 10μm

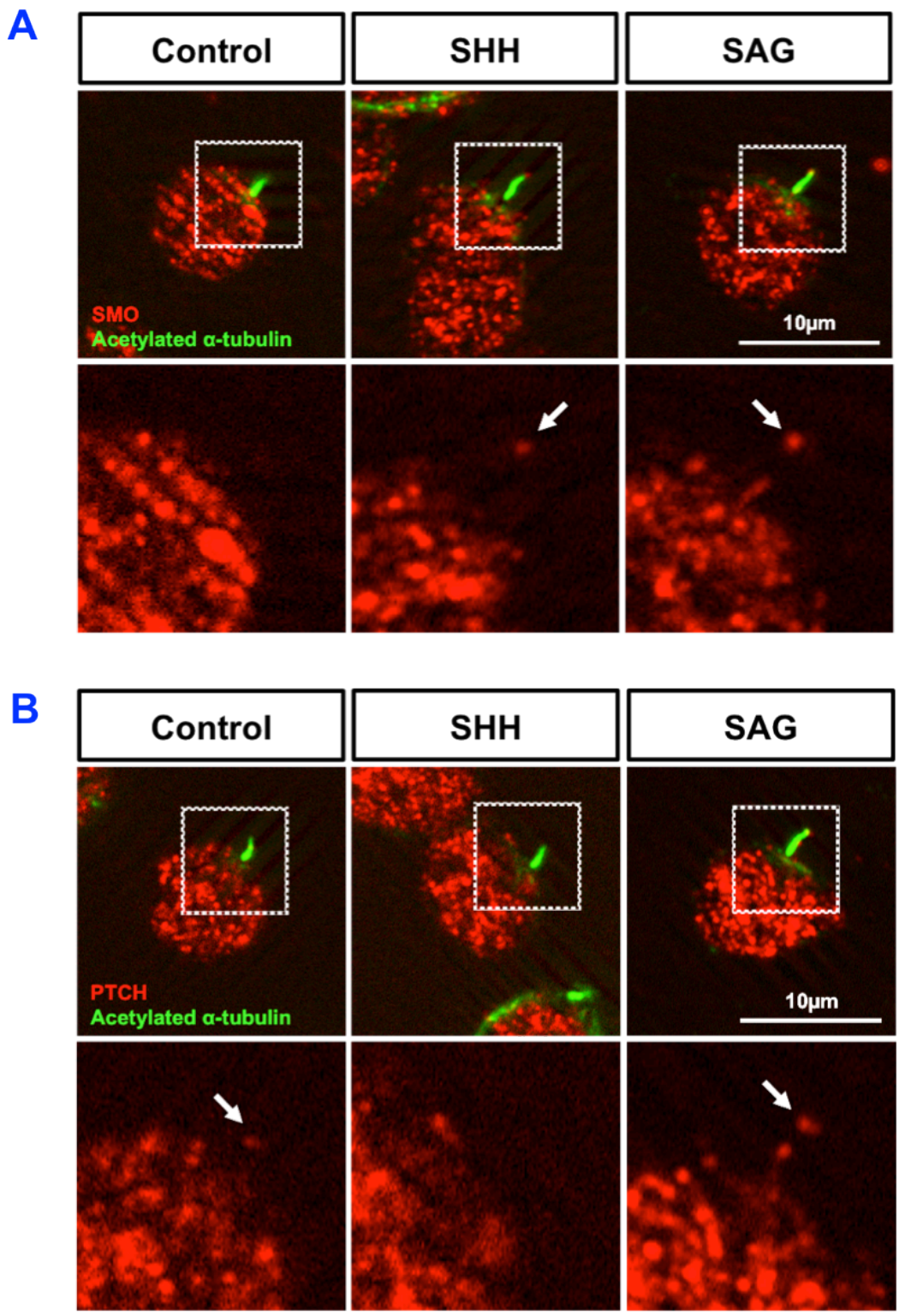
A
Control
SHH
SAG
SMO
Acetylated α-tubulin
10μm
B
Control
SHH
SAG
PTCH
Acetylated α-tubulin
10μm

Fig. 3.7. Grid-Apotome visualisation of the localisation of SMO and PTCH in primary cilia of GNPs when the cells were treated with SHH or SAG. (A) The experiments were performed similar to Fig 3.4; however, the images were taken with the grid-apotome. Briefly, immunofluorescence of 6 hour-cultured GNPs from P5 WT mice stained with anti-acetylated α tubulin (green), anti-SMO (red) antibodies (SantaCruz) and nuclei (blue) with DAPI staining. Arrows show the presence of SMO in primary cilia in control and SAG conditions. To clearly see if SMO is present in primary cilium, insets were made to show the area marked around the primary cilium and the brightness and contrast were enhanced to the same extent. Scale bar = 10μm (**B)** The experiments were performed similar to Fig 3.5; however, the images were taken with the grid-apotome. Briefly, immunofluorescence of 6 hour-cultured GNPs from P5 WT mice stained with anti-acetylated α tubulin (green), anti-PTCH (red) antibodies (Santa Cruz) and nuclei (blue) with DAPI staining. Arrows show the presence of PTCH in primary cilia in control and SAG conditions. To clearly see if PTCH is present in primary cilium, insets were made to show the area marked around the primary cilium and the brightness and contrast were enhanced to the same extent. Scale bar = 10μm

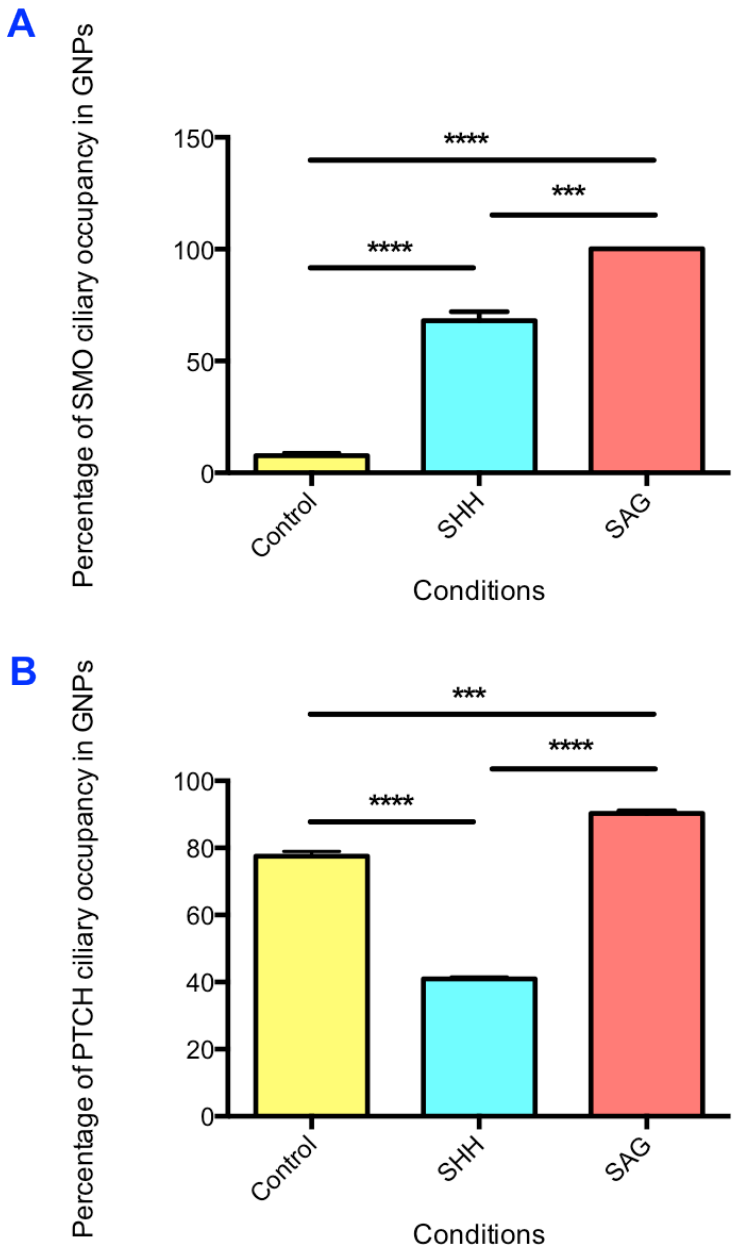
A
Percentage of SMO ciliary occupancy in GNPs
150
100
50
0
****
***
****
Control
SHH
SAG
Conditions
B
Percentage of PTCH ciliary occupancy in GNPs
100
80
60
40
20
0
***
****
****
Control
SHH
SAG
Conditions

Fig. 3.8. Quantification of SMO and PTCH occupancies in primary cilia of GNPs after addition of SHH or SAG. (A) Acquired images of 4.5 hours SHH and SAG stimulated GNPs after labelling with anti-acetylated α tubulin, anti-SMO antibodies and nuclei with DAPI were quantified the SMO ciliary occupancy. After addition of SHH or SAG to GNPs, the percentage of SMO occupancy in primary cilia is increased in SHH and SAG conditions when compare with control. Thirty GNPs were quantified the occupancy of SMO in primary cilium, from each 3 independent experiments. The data are graphed showing the Standard Error of the Mean (SEM) and tested for statistically significant differences among the control and treated samples using one-way ANOVA, followed by Bonferroni's post-test. The bar graphs show Mean±SEM. Confidence interval was set to 95%, with a *p*-value less than 0.05 taken as statistically significant. Statistical significances are indicated as asterisks; *: $p<0.05$, **: $p<0.01$, ***: $p<0.001$, ****: $p<0.0001$ and N.S.: not significant. **(B)** Acquired images of 4.5 hours SHH and SAG stimulated GNPs after labelling with anti-acetylated α tubulin, anti-PTCH antibodies and nuclei with DAPI were quantified the PTCH ciliary occupancy. After addition of 30nM SHH for 4.5 hours, the percentage of PTCH occupancy in primary cilia is decreased, however, this occupancy is not affected by addition of SAG when compare with control. Thirty GNPs were quantified the occupancy of PTCH in primary cilium, from each 3 independent experiments. The data are graphed showing the Standard Error of the Mean (SEM) and tested for statistically significant differences among the control and treated samples using one-way ANOVA, followed by Bonferroni's post-test. The bar graphs show Mean±SEM. Confidence interval was set to 95%, with a *p*-value less than 0.05 taken as statistically significant. Statistical significances are indicated as asterisks; *: $p<0.05$, **: $p<0.01$, ***: $p<0.001$, ****: $p<0.0001$ and N.S.: not significant.

3.2.4 NRCAM, TAG-1 but not F3 are present in primary cilia of GNPs

Our hypothesis is that NRCAM is involved in the trafficking of SHH pathway components, particularly PTCH or SMO, into or out of the cilium. If this is the case, we might expect that NRCAM should be present, either in the primary cilium or somewhere around base of primary cilia, where it is thought that PTCH and SMO can be found in trafficking vesicles (Pazour and Bloodgood, 2008, Martin et al., 2001, Petralia et al., 2012)

To investigate the localisation of NRCAM in primary cilia of GNPs, double-labeling with acetylated α-tubulin and NRCAM antibodies was performed on 6 hour-cultured GNPs. Anti-TAG-1 and anti-F3 labelling was also included: anti-TAG-1 as a positive control, because the majority of GNPs should express it (Xenaki et al., 2011), and anti-F3 as a matched negative control which should not be present; like anti-NRCAM, anti-F3 is a rabbit polyclonal (see Methods).

As shown in Fig. 3.9A, anti-NRCAM immunoreactivity is clearly present in primary cilia as well as in the body of the cell. I was able to see similar TAG-1 labelling, including labelling in the cilium. Perhaps surprisingly, anti-F3 immunoreactivity was also seen on vesicle-like structures within the body of the cell, notably around the base of the primary cilium, however, reactivity of anti-F3 in the primary cilia was not seen.

Because both antibodies are rabbit polyclonals, the lack of F3 labelling in primary cilium strongly suggests that the anti-NRCAM immunoreactivity in the cilium is due to the presence of NRCAM. However, given that NRCAM shares 35-40% identity with its sister molecules, L1, CHL1 and NFASC (Holm et al., 1996), I was concerned that there may be cross-reactivity. To test this, I labelled GNPs from *Nrcam*$^{-/-}$ mice with the anti-NRCAM antibody (838). Although the labelling was significantly weaker than on WT GNPs (compare with Fig 3.9A), some signal could still be detected (Fig 3.9B:a). I therefore performed an antibody pre-absorption on tissues from E13.5 *Nrcam*$^{-/-}$ embryos (see protocol in Materials and Methods, section 2.6). The resulting antibody, designated '838^{-}', was then titrated until no signal could be detected on *Nrcam*$^{-/-}$ GNPs (Fig. 3.9B:b). At these concentrations, this pre-absorbed antibody still gave a strong signal on WT GNPs (for example, Fig 3.13A) and was then used for all subsequent GNP labelling in this study.

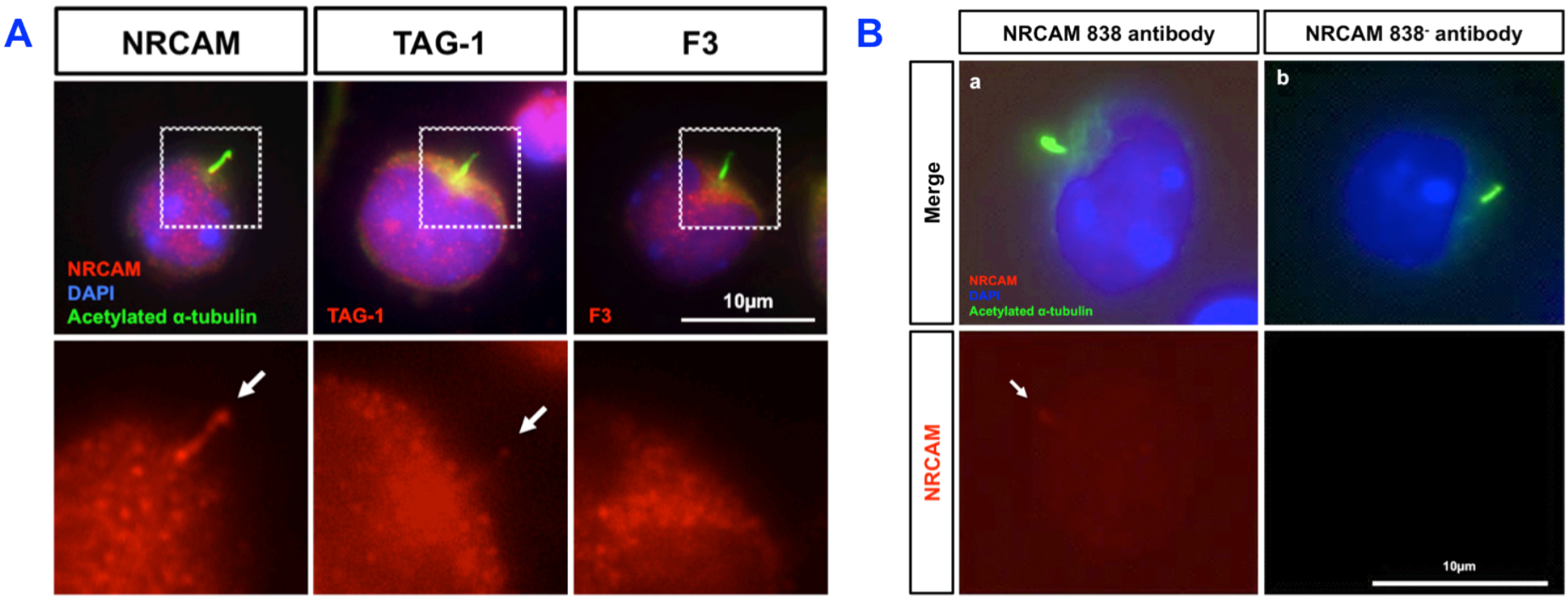
A
NRCAM
TAG-1
F3
NRCAM
DAPI
Acetylated α-tubulin
TAG-1
F3
10μm
B
NRCAM 838 antibody
NRCAM 838- antibody
Merge
NRCAM
a
b
NRCAM
DAPI
Acetylated α-tubulin
10μm

Figure 3.9. NRCAM, TAG-1 but not F3 are present in primary cilia of WT GNPs. **(A)** Immunofluorescence from 6 hour-cultured GNPs from P5 WT mice, which were purified and cultured for 6 hours and immunolabelled with anti-acetylated α-tubulin (green) and anti-NRCAM 838, TAG-1 or F3 antibodies (red). To clearly see if NRCAM, TAG-1 or F3 is present in primary cilium, insets were made to show the area marked around the primary cilium and the brightness and contrast were enhanced to the same extent. Arrows show the presence of NRCAM and TAG-1 in primary cilia. (**B)** Testing NRCAM 838 and NRCAM 838^{-} antibodies on *Nrcam*$^{-/-}$ GNPs. **(a)** Before NRCAM 838 antibody pre-absorption. GNPs from P5 *Nrcam*$^{-/-}$ mice were purified and cultured for 6 hours and immunolabelled with anti-acetylated α-tubulin (green) and anti-NRCAM 838 antibodies (red). The NRCAM 838 antibody staining shows signal on *Nrcam*$^{-/-}$ GNPs (arrow). **(b)** After NRCAM 838 antibody pre-absorption, which was named as NRCAM 838^{-} antibody. NRCAM signal is not detected on *Nrcam*$^{-/-}$ GNPs. Scale bar = 10 μm

3.2.5 Loss of NRCAM affects the localisation of SMO and PTCH in primary cilia

The results above clearly indicate that NRCAM is present in the primary cilia of 6 hour-cultured GNPs. Therefore, NRCAM is in the right place at the right time to be involved in the translocations of SMO and PTCH to or from the primary cilium. Therefore, I started testing the main hypothesis by investigating whether loss of NRCAM affects these translocations. To achieve this, immunolabelling with anti-SMO or anti- PTCH was performed with acetylated α-tubulin antibodies after SHH or SAG treatment of WT or *Nrcam*$^{-/-}$ GNPs.

Loss of NRCAM did not significantly affect the number of cilia found on cultured GNPs at 6 hours (83.41±10.67% in untreated WT GNPs and 87.72±9.24% in untreated *Nrcam*$^{-/-}$ GNPs), nor was the proportion of cilia that were scored positive for SMO immunofluorescence changed under basal (untreated) conditions (Fig. 3.10B). However, in the presence of SHH, SMO localisation in primary cilia was significantly reduced in *Nrcam*$^{-/-}$ GNPs when compared with WT GNPs (Fig. 3.10B, $p<0.0001$, one-way ANOVA, followed by Bonferroni's post-test). Interestingly, however, SAG induction of SMO translocation to primary cilia is unaffected by loss of NRCAM (Fig. 3.10B).

These results suggested that NRCAM plays a role in localising SMO to primary cilia after SHH treatment. However, I considered the alternative possibility that SMO fails to enter the primary cilium in *Nrcam*$^{-/-}$ GNPs because NRCAM is required for PTCH to leave the primary cilium. To verify this, I tested whether loss of NRCAM affects the translocation of PTCH out of primary cilia in response to SHH. If NRCAM is required for PTCH removal, PTCH should remain in primary cilia whether or not SHH is added to *Nrcam*$^{-/-}$ GNPs. Similar to SMO, the proportion of primary cilia containing PTCH protein under control conditions was unaffected by NRCAM loss (77.5±1.44% in untreated WT GNPs and 78.63±4.64% in untreated *Nrcam*$^{-/-}$ GNPs). However, addition of SHH to *Nrcam*$^{-/-}$ GNPs had no affect on occupancy (87.55±1.41%), whereas this was reduced to ~45% in WT GNPs (40.97±0.56%), suggesting that PTCH is not able to leave primary cilia when NRCAM was missing (Fig. 3.11).

We also attempted to investigate if loss of NRCAM alters the overall levels SMO and PTCH protein expressions of GNPs by performing western blot, unfortunately however our antibodies did not work properly. However, the SMO

and PTCH ciliary occupancies in SAG-activated WT and *Nrcam*$^{-/-}$ GNPs were not significantly different between WT and *Nrcam*$^{-/-}$ GNPs, and the general level of immunofluorescence in the cells appeared similar, suggesting that loss of NRCAM does not obviously affect the pools of SMO and PTCH in the cells.

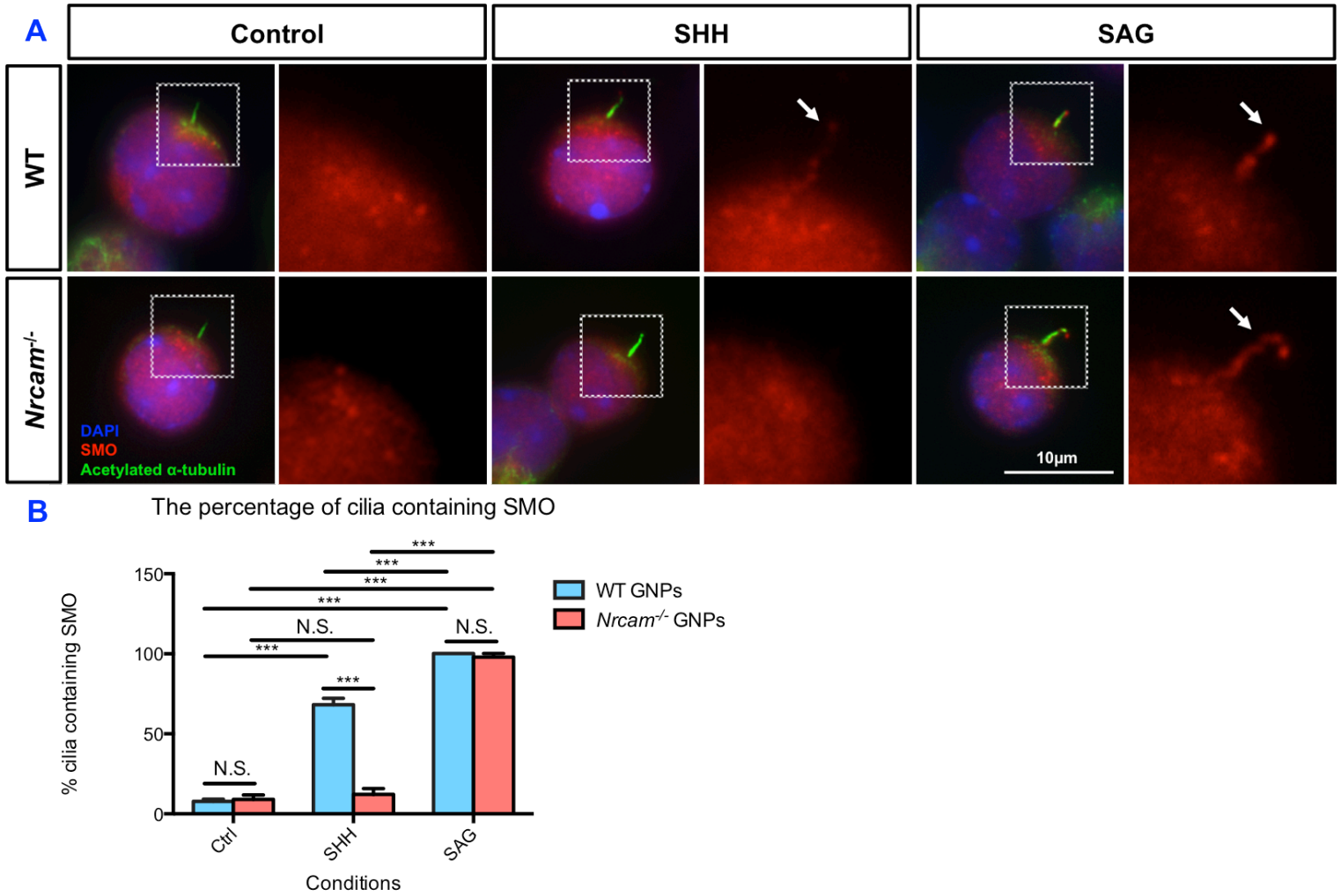
A
Control
SHH
SAG
WT
Nrcam-/-
DAPI
SMO
Acetylated α-tubulin
10μm
B
The percentage of cilia containing SMO
% cilia containing SMO
150
100
50
0
N.S.
N.S.
N.S.
***
***
***
***
***
***
Ctrl
SHH
SAG
Conditions
WT GNPs
Nrcam-/- GNPs

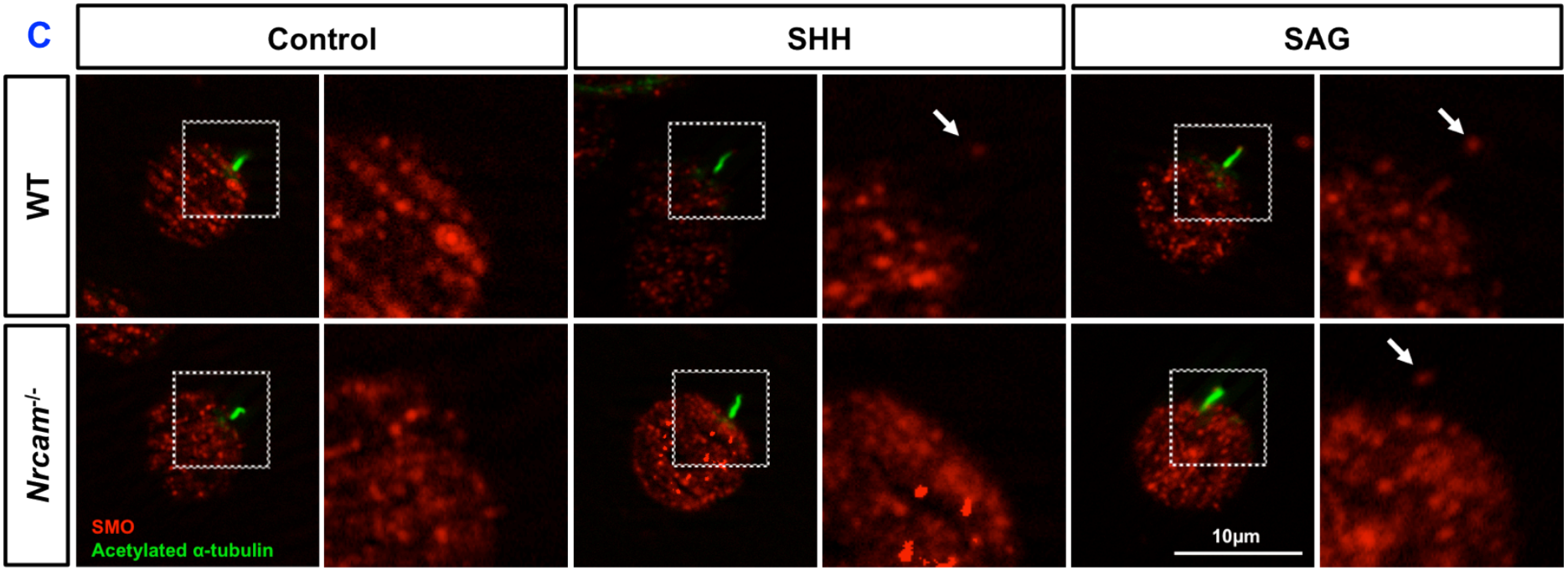
C
Control
SHH
SAG
WT
Nrcam-/-
SMO
Acetylated α-tubulin
10μm

Figure 3.10. Loss of NRCAM affects SMO localisation in primary cilia of GNPs after addition of SHH or SAG. (A) Immunostaining of cultured GNPs of P5 mice with anti-acetylated α-tubulin (green) and anti-SMO antibodies (kindly provided from Prof. Kathryn Anderson) (red) compared between wild type and *Nrcam*$^{-/-}$ GNPs in control, SHH and SAG (100nM) conditions. To clearly see if SMO is present in primary cilium, insets were made to show the area marked around the primary cilium and the brightness and contrast were enhanced to the same extent. Arrows show SMO inside primary cilia. In *Nrcam*$^{-/-}$ GNPs, SMO localization in primary cilia is not affected by addition of SHH; however, SAG can still increase SMO localisation in primary cilia. Scale bar = 10μm **(B)** Quantification of 30 fields in each condition (3n) shows the percentage of primary cilia containing SMO protein (3 independent experiments). The data are graphed showing the Standard Error of the Mean (SEM) and tested for statistically significant differences among the control and treated samples using one-way ANOVA, followed by Bonferroni's post-test. The bar graphs show Mean±SEM. Confidence interval was set to 95%, with a *p*-value less than 0.05 taken as statistically significant. Statistical significances are indicated as asterisks; *: $p<0.05$, **: $p<0.01$, ***: $p<0.001$, ****: $p<0.0001$ and N.S.: not significant. **(C)** The experiments were performed similar to (A) but GNPs were stained with anti-SMO antibody from Santacruz and the images were taken with the grid-apotome

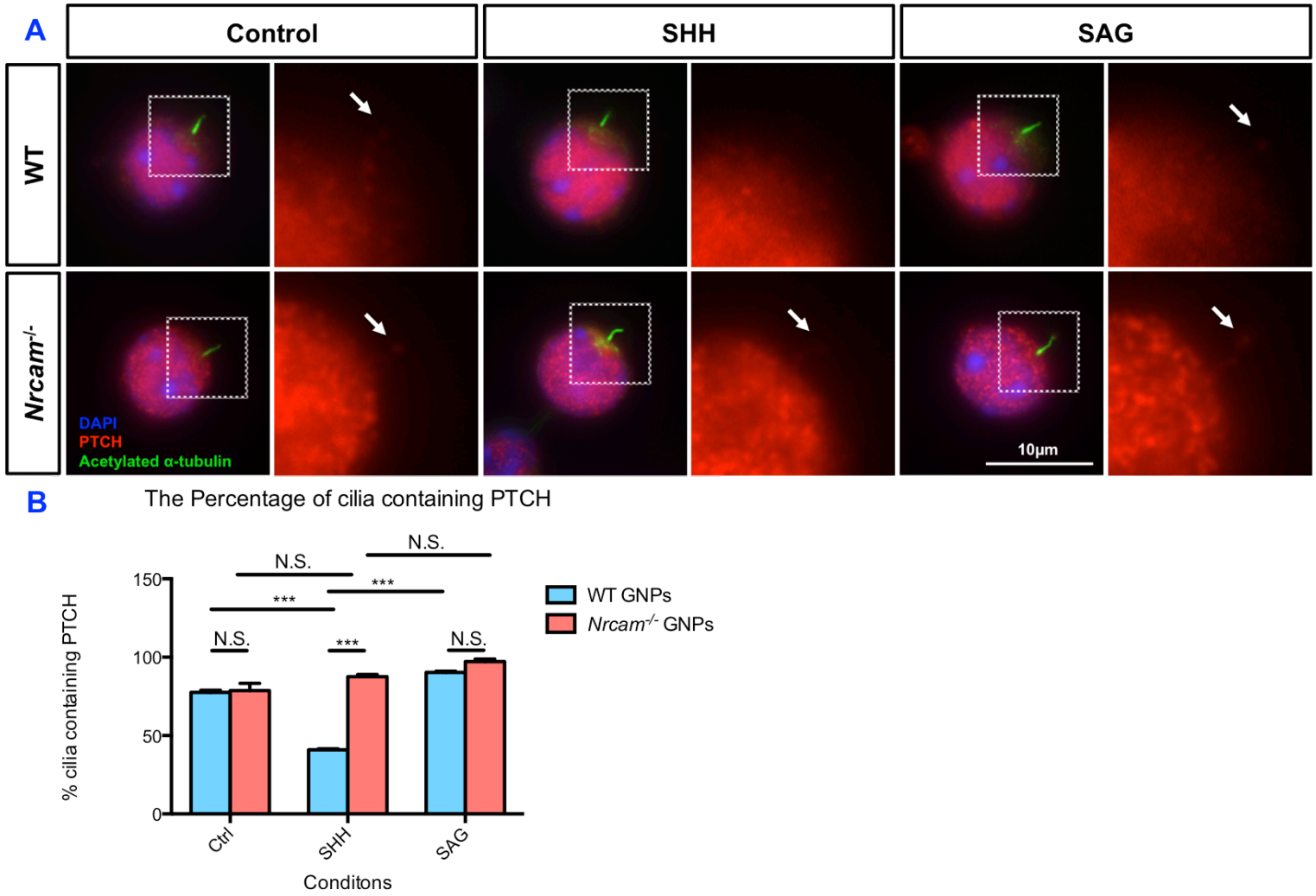
A
Control
SHH
SAG
WT
Nrcam-/-
DAPI
PTCH
Acetylated α-tubulin
10μm
B
The Percentage of cilia containing PTCH
% cilia containing PTCH
150
100
50
0
N.S.
N.S.
N.S.
***
***
***
Ctrl
SHH
SAG
Conditons
WT GNPs
Nrcam-/- GNPs

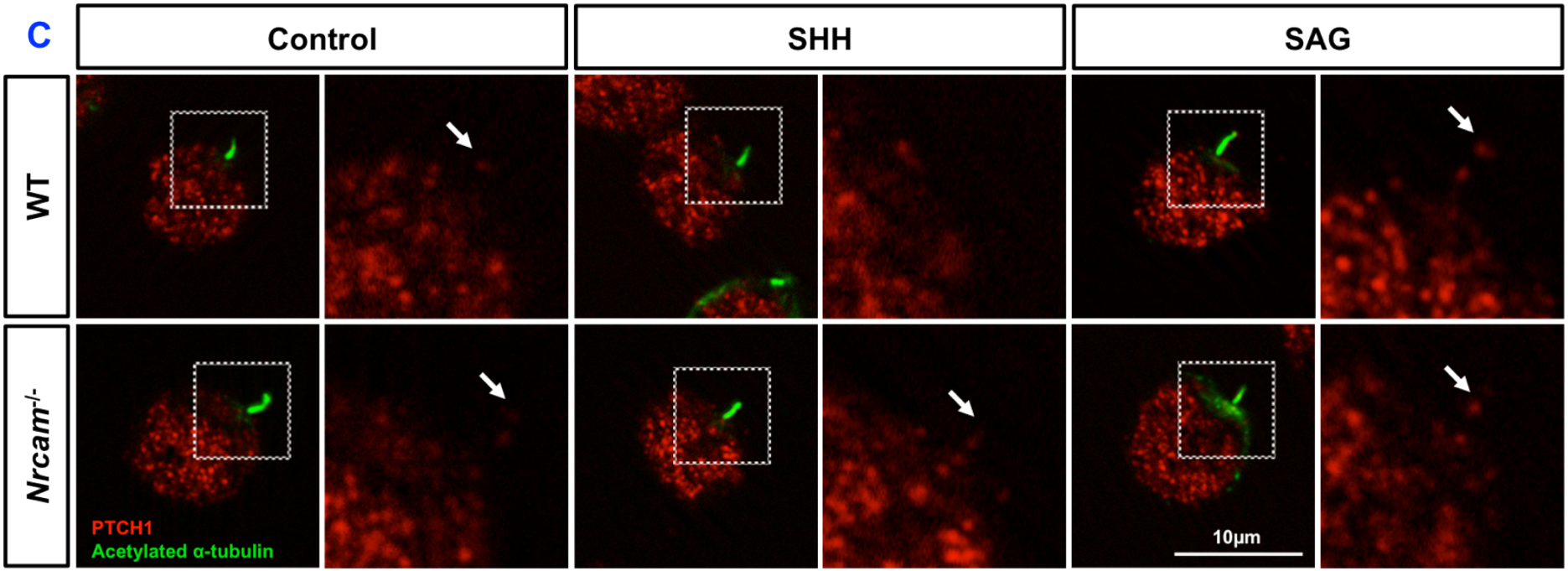
C
Control
SHH
SAG
WT
Nrcam-/-
PTCH1
Acetylated α-tubulin
10μm

Figure 3.11. Loss of NRCAM also affects PTCH exit from primary cilia. **(A)** Immunostaining in cultured GNPs of P5 mice with anti-acetylated α-tubulin (green) and anti-PTCH antibodies (red) compared between wild type and *Nrcam*$^{-/-}$ GNPs in control (no additions), SHH and SAG (100nM) conditions. To clearly see if PTCH is present in primary cilium, insets were made to show the area marked around the primary cilium and the brightness and contrast were enhanced to the same extent. Arrows show PTC inside primary cilia. In *Nrcam*$^{-/-}$ GNPs, PTCH localization in primary cilia is not changed in addition of SHH as well as in addition of SAG. Scale bar = 10μm **(B)** Quantification of 30 fields in each condition (3n) shows the percentage of primary cilia containing PTCH protein (3 independent experiments). The data are graphed showing the Standard Error of the Mean (SEM) and tested for statistically significant differences among the control and treated samples using one-way ANOVA, followed by Bonferroni's post-test. The bar graphs show Mean±SEM. Confidence interval was set to 95%, with a *p*-value less than 0.05 taken as statistically significant. Statistical significances are indicated as asterisks; *: $p<0.05$, **: $p<0.01$, ***: $p<0.001$, ****: $p<0.0001$ and N.S.: not significant. **(C)** The experiments were performed similar to (A); however, the images were taken with the grid-apotome.

3.2.6 Loss of NRCAM does not affect the percentage of GNP with primary cilium whether or not SHH is added

The results above seem to suggest that the ability of PTCH and SMO to translocate in primary cilia in response to SHH is affected by loss of NRCAM. However it is possible that the number of primary cilia may have changed which might affect the results. If loss of NRCAM affects the percentage of primary cilia of GNPs, this might affect the way we interpret data. I therefore compared the percentage of ciliated cells between WT and *Nrcam*$^{-/-}$ GNPs. Cultured WT and *Nrcam*$^{-/-}$ GNPs were treated with SHH, fixed and stained with acetylated α-tubulin antibody and quantitated for the percentage of primary cilia with and without addition of SHH. As shown in Fig. 3.12, the percentage of primary cilia of WT and *Nrcam*$^{-/-}$ GNPs were not significantly different in either condition.

Therefore, I came to the conclusion that loss of NRCAM does not affect the number of primary cilia of GNPs, however, it does affect the ability of PTCH and SMO to translocate within primary cilia in response to SHH at 4.5 hours.

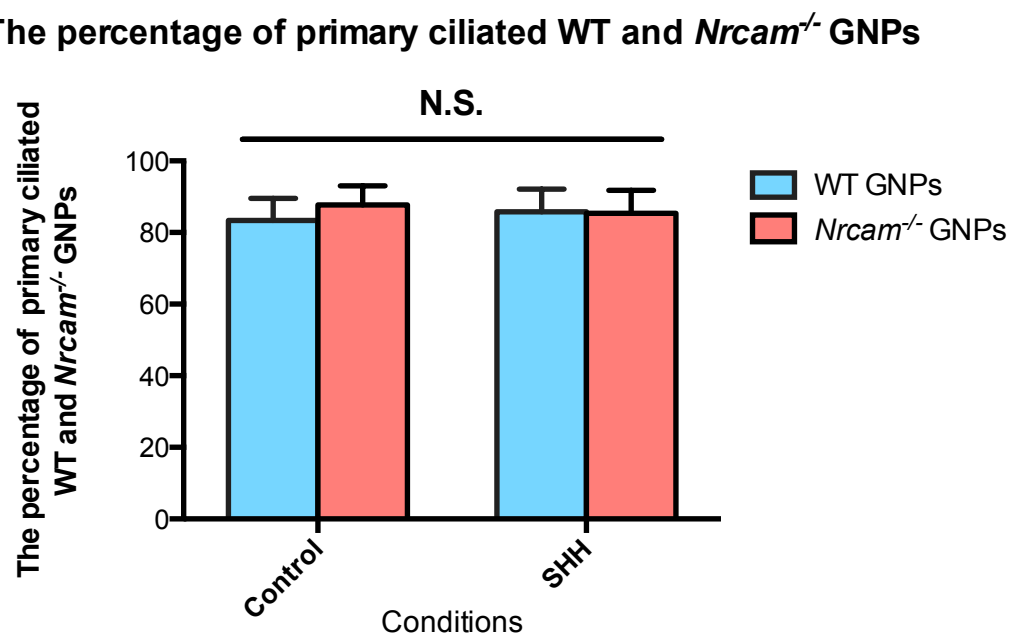

Figure 3.12. No significant difference in the percentage of WT and *Nrcam*$^{-/-}$ GNPs with primary cilium after addition of SHH for 4.5 hours. The P5 WT and *Nrcam*$^{-/-}$ GNPs were cultured and treated with SHH for 4.5 hours. Then the cells were fixed with 4% PFA and immunolabelled with anti-acetylated α-tubulin antibody to the primary cilium. 20 image fields from 3 independent experiments were quantified for the percentage of GNPs with primary cilium. There were no significant differences between the percentages of WT and *Nrcam*$^{-/-}$ GNPs with primary cilium with or without addition of SHH. The data are graphed showing the Standard Error of the Mean (SEM) and tested for statistically significant differences among the control and treated samples using one-way ANOVA, followed by Bonferroni's post-test. The bar graphs show Mean±SEM. Confidence interval was set to 95%, with a *p*-value less than 0.05 taken as statistically significant. Statistical significances are indicated as asterisks; *: $p<0.05$, **: $p<0.01$, ***: $p<0.001$ and N.S.: not significant.

3.2.7 The occupancy of NRCAM in primary cilia is not affected in addition of SHH or SAG

The results above showed that NRCAM is present in the primary cilium and that the loss of NRCAM affects the translocations of SMO and PTCH in primary cilia after SHH treatment. Therefore we speculated that if NRCAM is involved in trafficking of either PTCH removal or SMO entry to primary cilia of GNPs, NRCAM might itself be translocated in response to SHH treatment. However, as shown in fig. 3.13, the occupancy of NRCAM in primary cilia is not significantly changed by addition of SHH or SAG (p>0.9999, one-way ANOVA, followed by Bonferroni's post-test), at least not at 4.5 hours post-treatment.

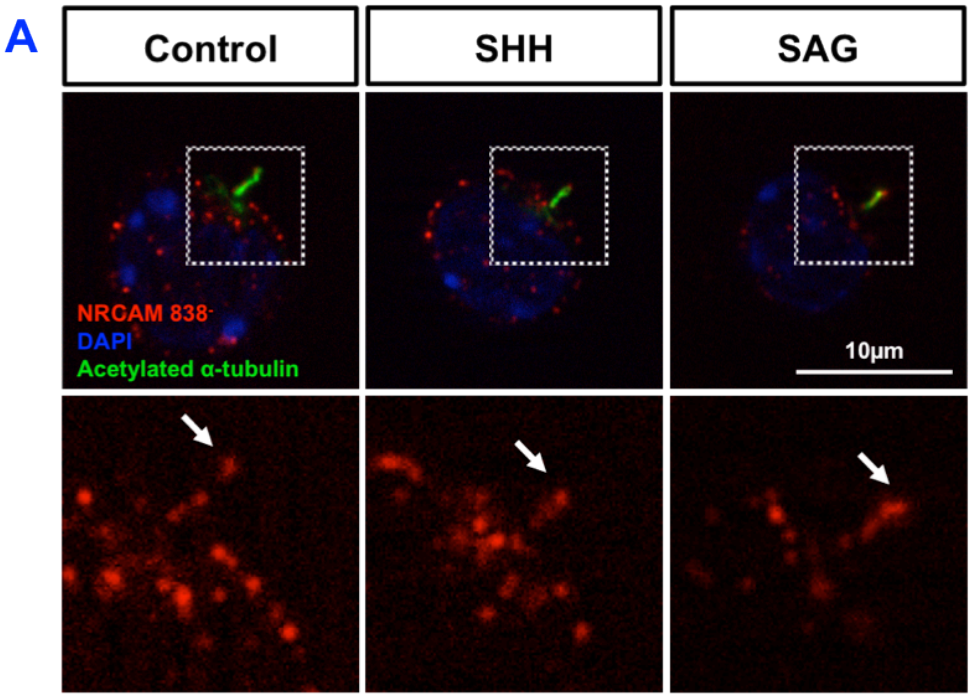
A
Control
SHH
SAG
NRCAM 838
DAPI
Acetylated α-tubulin
10μm

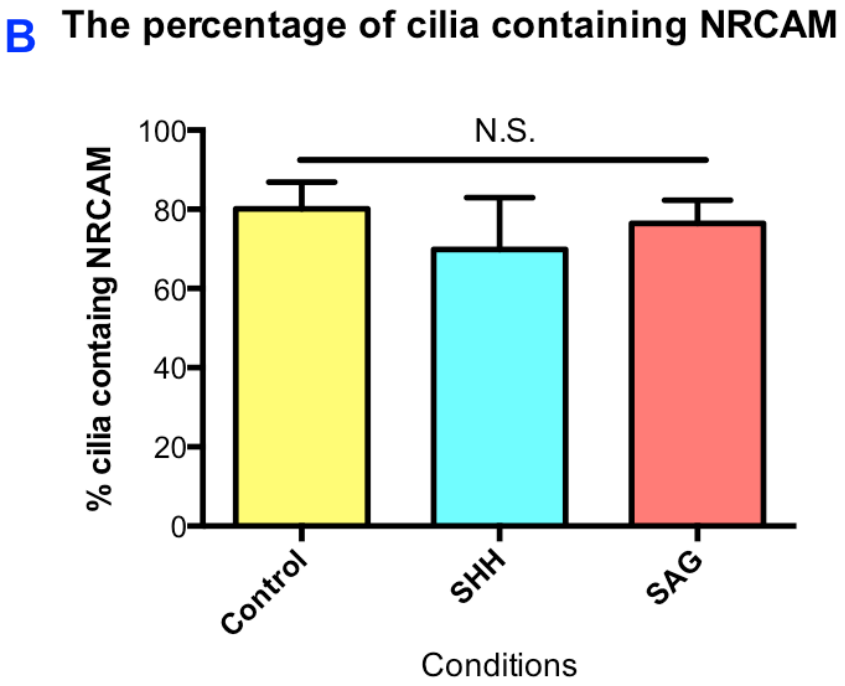
B
The percentage of cilia containing NRCAM
N.S.
% cilia containg NRCAM
100
80
60
40
20
0
Control
SHH
SAG
Conditions

Figure 3.13. The occupancy of NRCAM in primary cilia is not significantly affected by addition of SHH or SAG. (A) Immunofluorescence of cultured GNPs from P5 WT mice which were cultured and treated with SHH or SAG for 4.5 hours and immunolabelled with anti-acetylated α-tubulin (green), anti-NRCAM 838^{-} (red) antibodies and nuclei (blue) with DAPI staining. To clearly see if NRCAM is present in primary cilium, insets were made to show the area marked around the primary cilium and the brightness and contrast were enhanced to the same extent. Arrows show the presence of NRCAM in primary cilia. Scale bar = 10μm (**B)** After addition of 30nM of SHH or 100NM SAG to GNPs for 4.5 hours, the percentage of NRCAM occupancy in primary cilia is not significantly changed when compare with control. 30 GNPs were quantified the occupancy of SMO in primary cilium, from each 3 independent experiments. The data are graphed showing the Standard Error of the Mean (SEM) and tested for statistically significant differences among the control and treated samples using one-way ANOVA, followed by Bonferroni's post-test. The bar graphs show Mean±SEM. Confidence interval was set to 95%, with a *p*-value less than 0.05 taken as statistically significant. Statistical significances are indicated as asterisks; *: $p<0.05$, **: $p<0.01$, ***: $p<0.001$ and N.S.: not significant.

3.3 Discussion

Primary cilia are required for the SHH signalling in vertebrate, a key pathway controlling cell proliferation and differentiation (Michaud and Yoder, 2006, Simpson et al., 2009, Goetz and Anderson, 2010). PTCH, which is a receptor for SHH localises in primary cilium in the absence of SHH. When SHH binds PTCH, the complex leaves primary cilium and this allows SMO to translocate to the cilium and activate downstream signalling events (Rohatgi et al., 2007, Corbit et al., 2005). However, the mechanism that regulates PTCH and SMO translocation in primary cilia is not clearly understood. Since F3 can suppress SHH-induced proliferation of GNPs via binding to NRCAM (Xenaki et al., 2011), and given that we know from studies in other contexts that L1-CNTNs play a role in trafficking and endocytosis (Falk et al., 2005, Dang et al., 2012), we hypothesised that NRCAM might be involved in trafficking of either PTCH or SMO in primary cilium. In this chapter, we established for the first time that NRCAM is present in primary cilia and that loss of NRCAM affects the localisation of PTCH and SMO in primary cilia of GNPs after addition of SHH for 4.5 hours. This suggests that NRCAM might play a role in either PTCH or SMO trafficking in the primary cilia of GNPs.

3.3.1 Primary cilia of GNPs

Primary cilia of GNPs from cerebellar sections

Previous studies have demonstrated the presence of primary cilia on GNPs in cerebellar sections from rodents (Spassky et al., 2008). I initially started my study by trying to verify this using anti-acetylated α-tubulin antibody on sections of P5 mouse cerebellum. However, as anti-acetylated α-tubulin antibody also labels axons, I had difficulty to identify where exactly primary cilia are, whereas Spassky et al. were able to do this (Spassky et al., 2008). Although Spassky et al. also used anti-acetylated α-tubulin antibody, their study was conducted at E18.5, at which stage the number of axons is considerably reduced compared to P5. Other studies have been able to identify primary cilia at later stages by using antibodies against adenylate cyclase type III, which labels cilia more specifically (Chizhikov et al., 2007). Therefore, if I were to repeat these studies, I might attempt to try other primary cilia makers such as anti- Arl13b, anti-Sstr3, anti-adenylyl cyclase III antibodies, which are also shown that they are able to use as primary cilia markers (Berbari et al., 2007, Cantagrel et al., 2008, Chizhikov et al., 2007).

Primary cilia of cultured GNPs

Despite the importance of the primary cilium to GNP development (Spassky et al., 2008), it mostly has been described in cerebellar sections and only once on acutely dissociated GNPs (Cantagrel et al., 2008). So for the first time we have established that cilia can be visualised on cultured GNPs. Interestingly, about 20% of the GNPs in our cultures appeared not to have cilia (Fig 3.12). This could be for a number of reasons: the first reason may be simply the practical limits of my method of visualisation: since GNPs are quite spherical in culture, cilia can be hidden behind the body of the cell quite easily and therefore easily missed. However, it is also possible that some cells do not have cilia because they are in a specific stage of the cell cycle: primary cilia start decreasing in length in G2 phase and are disrupted when the cells go into M phase of the cell cycle (Plotnikova et al., 2009). Consistent with this possibility, we know that our cultured GNPs are a heterogeneous cell population: At 6 hours, we know that ~98% of the GNP population expresses the cell cycle marker $Ki67^{+}$ (Xenaki et al., 2011). Although we did not measure the proportion of cells in G2 and M phase, previous studies of P10 rat cerebellum suggest that this may be as much as 14% of cells (Bodenant et al., 1997) Therefore, it is possible that I was not able to see the primary cilia of some cells because they were in G2/M or M-phase of the cell cycle.

This study also provides the first evidence demonstrating that changes in SMO and PTCH localisation can be analysed in primary cilia of cultured GNPs in response to SHH and SAG and this is consistent with the previous study which was demonstrated in NIH3T3 cells (Rohatgi et al., 2007, Milenkovic et al., 2009). Apart from NIH3T3 and mouse embryonic fibroblasts (MEFs) cells, which are widely used for studying SMO and PTCH activity in primary cilia (Rohatgi et al., 2007, Milenkovic et al., 2009, Tukachinsky et al., 2010), as far as I am aware, the only other such study shows that undifferentiated human embryonic stem cell (hESC) lines possess primary cilia and the SMO and PTCH ciliary localisations are changed in response to SAG (Kiprilov et al., 2008). My study is therefore the first evidence of SMO and PTCH translocations in primary cells. This study then not only provides an alternative cell type to dissect SHH pathway but also verifies the relevance of the studies on cell lines to primary cells.

3.3.2 L1-CNTNs in primary cilia

NRCAM and TAG-1 are present in primary cilia

In this chapter I showed the presence of NRCAM and TAG-1 in primary cilium, which, as far as we are aware, is the first time that members of the L1 and contactin families have been shown to be present in cilia. Interestingly, a C. elegans L1 homolog, LAD-2 does appear in an online database of cilia-associated genes (http://www.sfu.ca/~leroux/ciliome_database.htm), but the significance of its inclusion in the original study, which used a functional genomics approach to identifying ciliary proteins, is unclear (Blacque et al., 2005). Indeed, some aspects of an L1-linked human neurological syndrome (CRASH/SPG1) bear some resemblance to ciliopathies (hydrocephalus, mental retardation;(Yamasaki et al., 1997)), but to date no link with cilia has been described.

We also showed that NRCAM is present in the right place and at the right time and this raises the possibility that NRCAM could play a role in either PTCH or SMO trafficking in primary cilium. If this is the case, we speculated that the change of NRCAM occupancy in primary cilia should positively correlate with the occupancy of PTCH or SMO in primary cilia in response to SHH. However, the percentages of cilia containing NRCAM were not altered after the treatment of either SHH or SAG for 4.5 hours. The first possible explanation of this result could be that NRCAM might not be involved with either PTCH or SMO trafficking event in primary cilia, whereas, the second possibility is that NRCAM could be recycled while trafficking PTCH or SMO in primary cilia and this clearly need to be further investigated. A study in the context of neuronal responses to axon guidance cues found that L1, another member of L1-CNTN family, is required for receptor endocytosis during growth cone responses to Semaphorin3A (SEMA3A), one of the secreted Semaphorins (Castellani et al., 2004). Indeed, NRCAM has also been shown to be associated with Neuropilin2 (NRP2) and to mediate its endocytosis and SEMA3B signalling (Falk et al., 2005).

3.3.3 The localisation of SMO and PTCH in primary cilia

Interestingly, we found that there was 7.75±1.28% SMO occupancy in primary cilia of WT GNPs even in the absence of SHH. This is consistent with the results of Yoo et al. who saw that 10%-20% of NIH3T3 cells accumulated SMO in their cilia without addition of SHH (Yoo et al., 2012). It is possible that SMO is

capable of trafficking to the cilium to maintain a low level of SMO so that upon SHH binding to PTCH, SHH signalling is fired immediately. It is also possible, of course, that the small percentage of cells I see with SMO in their cilia reflect the remnant of cells that were already receiving SHH signal at the time that the cerebellum was being dissected.

In this chapter, we also found SMO and PTCH localisations in the primary cilia of SAG-stimulated GNPs. This indicates that it is not necessary for PTCH to leave the primary cilium for SMO to enter. The result is consistent with the study in NIH3T3 cells (Rohatgi et al., 2007), however, it contradicts to study in hESc lines, which showed that SMO moves in and PTCH moves out when the cells expose to SAG (Kiprilov et al., 2008). Interestingly, the difference between these studies is that Kiprilov monitored PTCH from 1 – 4 hours after SAG treatment, whereas Rohatgi only looked at 4 hours and 24 hours and found much higher levels of PTCH in the cilium at the latter time point, suggesting that perhaps an initial removal of PTCH from the cilium of NIH3T3 cells was missed because it was followed by a subsequent replenishment at later time points.

Unexpectedly, we could see whole GNP cell labelling with SMO and PTCH (Fig 3.4 and 3.5, respectively), which were different from the study in NIH3T3 cells (Rohatgi et al., 2007). Although the cells were permeablised before immunolabelling in both studies, it would be interesting to investigate whether the labelling I see in the GNP cell body is surface labelling or internal labelling. In the case of SMO, a possible explanation of why we found SMO whole cell labelling would be that there are 2 pools of SMO, surface membrane and endosomal pools. It is not clear yet how SMO transport to primary cilia but Milenkovic et al. proposed a model of how SHH-induced SMO transport to the primary cilium (Milenkovic et al., 2009). The first way is a direct trafficking from Golgi to ciliary base. The second way is transport to the cell surface followed by lateral transport to the cilium and the last way is surface localisation followed by internalisation to recycling pathway. Therefore it would be possible that all of these dynamic events are happening all the time, resulting in the SMO labelling shows all over the whole cells. The result of seeing SMO and PTCH labelling all over the cells is also consistent with the immunofluorescent study in P2 rat hippocampal neurons that showed that PTCH and SMO were positive in soma and tips of neuronal cell processes (Petralia et al., 2011).

Interestingly, the vesicle-like structures of SMO were also found accumulated at the base of cilium (Fig 3.4, arrow heads). Although it is not clear how SMO and PTCH traffick to the cilium, immune-gold labelling of PTCH and SMO in immature rat cerebellum showed that they were present either within or near endosomes (Petralia et al., 2012).

3.3.4 Loss of NRCAM affects the localisation of SMO and PTCH in primary cilia

Having revealed the presence of NRCAM in primary cilia of GNPs, I then asked the question whether its presence was important. I showed that loss of NRCAM did not affect the percentage of GNPs with primary cilia, nor did it affect the localisation of SMO or PTCH in control conditions (Fig 3.10, 3.11). However, NRCAM loss did affect the translocation of SMO into cilia that normally occurs in response to SHH (Rohatgi et al., 2007, Milenkovic et al., 2009). In principle, this could be a direct effect on SMO translocation or it could be due to an effect of NRCAM loss on other components of the SHH pathway. We speculated that NRCAM somehow controls the translocation of PTCH out of primary cilia rather than SMO entry into primary cilia. Consistent with this, loss of NRCAM also affected the ability of PTCH to translocate out of the cilium as well as the ability of SMO to localise in the cilium after SHH treatment. Rohatgi et al. showed in NIH3T3 cells that the localisation of PTCH in primary cilia inhibits SMO entry to the primary cilia (Rohatgi et al., 2007). It seems likely; therefore, that the reason loss of NRCAM also affects SMO is because it is a consequence of the failure of PTCH to leave the primary cilia. Consistent with this idea, I found that SAG-induced translocation of SMO into the cilium is not affected by loss of NRCAM. SAG, which binds directly to SMO (Chen et al., 2002), is known to affect SMO translocation irrespective of whether PTCH leaves the cilium (Rohatgi et al., 2007). This is also consistent with previous observations in the lab that F3-fc is unable to suppress the proliferation induced by SAG, or the constitutive proliferation seen in GNPs expressing a constitutively active SMO (SMOA) (Xenaki, unpublished data). Together, all of these observations suggest that NRCAM is acting upstream of SMO affecting PTCH rather than SMO trafficking in primary cilia of GNPs.

However, clearly there could be other possibilities that directly or indirectly affect the localisation of PTCH and SMO. For example, we can not clearly rule out that NRCAM affects the trafficking of SMO into an intracellular sub-compartment,

which may be required before PTCH is able to leave the primary cilium. Indeed, recent studies suggest that SMO activation may be a multi-step process involving the localisation of SMO to different ciliary-subregions (Wilson et al., 2009). Therefore, the second possibility is that NRCAM affects SMO entry or both PTCH removal and SMO entry into primary cilia.

The next possibility is that NRCAM affects other SHH pathway components such as BOC, GAS1. It has been shown that BOC and GAS1 each are required for SHH to form a complex with PTCH (Izzi et al., 2011). We therefore speculated that NRCAM might be required for either BOC or GAS1 trafficking and this indirectly has an effect on the trafficking of PTCH out of primary cilia. However, when I tested this, I did not see that loss of NRCAM alters the localisation of neither BOC nor GAS1 in primary cilia (data not shown).

In fact, the other protein components that have been demonstrated to be involved in SHH signalling are Neurophilins (NRPs). They act as positive regulators of SHH signalling (Hillman et al., 2011). Moreover, Falk et al. showed that NRCAM interacts with NRP2 on the same membrane to act as a co-receptor for SEMA3B (Falk et al., 2005). Taken together, this suggests NRPs are possibly involved in SHH signalling via NRCAM. In fact, *Nrcam*$^{-/-}$ GNPs still proliferate in response to SHH (Xenaki et al., 2011). This is currently being investigated in our lab.

Despite these alternatives, the most obvious way that NRCAM could affect the translocations of SMO and PTCH would be through a direct interaction. Since this had not been tested before, this became the focus of the work described in the next chapter.

The other question that arises is why, if PTCH and SMO translocations are disrupted in *Nrcam*$^{-/-}$ GNPs, this does not apparently dramatically disrupt SHH signalling in *Nrcam*$^{-/-}$ mice, which are viable as homozygotes and show only minor cerebellar defects (Sakurai et al., 2001). This may be because L1 has a redundant function with NRCAM (Sakurai et al., 2001). In fact L1 has also been implicated in controlling the proliferation of normal cells (Sakurai et al., 2001, Dihne et al., 2003) and tumor cells (Agic et al., 2010, Arlt et al., 2006). However, Xenaki et al. showed that F3, which is known to bind NRCAM to suppress SHH-induced proliferation of GNPs, was not colocalised with L1 when NRCAM is missing and L1 is not normally expressed on proliferating GNPs (Xenaki et al.,

2011). Even so, *Nrcam*$^{-/-}$ GNPs apparently still proliferate in response to SHH, although this was not directly compared to the response of WT cells (Xenaki et al., 2011). However, because proliferation is measured 24 hours or longer after SHH treatment, it is possible that there are subtle changes to the kinetics of SHH signalling. To address this more directly, in Chapter 5 I look at effects on immediate early responses to SHH.

Chapter 4

Investigation of the interaction of PTCH1 and NRCAM

4.1 Introduction

The results from the previous chapter seems to suggest that NRCAM is required for the removal of PTCH from the primary cilium of granule neuron progenitors 4.5 hours after SHH treatment. Our hypothesis is that this is because NRCAM is required for the trafficking of one or more components of the SHH signalling pathway into or out of the cilium. This could be a direct or an indirect effect on PTCH and/or SMO. The simplest explanation of our data would be that NRCAM interacts directly with PTCH and is required for its trafficking out of the cilium. However, I am not be able to rule out that NRCAM affects the trafficking of SMO into an intracellular sub-compartment, which may be required before PTCH is able to leave the cilium. Indeed, recent studies suggest that SMO activation may be a multi-step process involving the localisation of SMO to different ciliary sub-regions (Wilson et al., 2009). Thus, formally NRCAM might affect either PTCH or SMO. Moreover, this may be a direct or an indirect effect, for instance, NRCAM could be required for the trafficking of accessory molecules such as BOC or GAS1 to the primary cilium, or indeed NRCAM may be required more generally for the trafficking of vesicles to or from the cilium. To put this into context, below I briefly review what is known of the trafficking of PTCH and SMO and their interactions with other proteins.

4.1.1 Known interactions of PTCH and SMO with other proteins

Upon SHH pathway activation, SHH binds PTCH and the complex translocate out of the primary cilium, followed by internalisation to the cytoplasm (Rohatgi et al., 2007, Incardona et al., 2000, Incardona et al., 2002). However, it has not been clearly shown how PTCH moves out from the cilium and whether there are other proteins physically interacting or facilitating its translocation. PTCH1 is known to associate individually with three accessory proteins - growth arrest-specific 1 (GAS1), CAM-related/down-regulated by oncogenes (CDO), and brother of CDO (BOC) - that appear to act as co-receptors with PTCH1 to facilitate HH binding and to be necessary for SHH activity (Izzi et al., 2011). Although ciliary localisation of these proteins has not been demonstrated, this raises the formal possibility that NRCAM could play a role in their trafficking and thus indirectly affect the ability of PTCH to leave the cilium.

By contrast, rather more proteins have been found to interact with SMO and regulate SHH signalling pathway, β-Arrestins, multifunctional adaptors that mediate the desensitisation and internalisation of seven-transmembrane protein

receptors (Shenoy et al., 2009), interact with SMO that has been phosphorylated by G-protein-coupled receptor kinase 2 (GSK2), which facilitates SMO endocytosis (Chen et al., 2004). β-Arrestins also appear to be required for the localisation of SMO to the primary cilium apparently by forming multimeric complex with the kinesin motor protein, KIF3A (Kovacs et al., 2008). β-Arrestins and SMO also appear to be closely associated with Integrin-linked kinase (ILK), an essential effector of β1 integrin signalling, and ILK-depleted intermedullary collecting duct cells (IMCD3) and 10T1/2 cells had an effect on SMO ciliary translocation when the cells were activated by either SHH or SAG (Barakat et al., 2013). Myc-interacting Zinc finger protein 1 (MIZ1), a member of the POZ domian/zinc finger transcription factor family, has been also found to co-precipitate with SMO and GLI2 and positively regulates SHH signalling by playing a role in GLI2 nuclear translocation (Lu et al., 2013). In addition, the study in chondrocytes has been demonstrated that EVC and EVC2, genes which responsible for the recessive skeletal dysplasia Ellis-van Creveld Syndrome (EvC), regulate IHH activity by interacting with SMO but not regulating SMO translocation. Instead EVC/EVC2 appear to control SuFu/GLI3 dissociation and GLI3 translocation in primary cilium of chondrocytes (Caparros-Martin et al., 2013).

Although, the data above seems to suggest that several proteins have been associated with SMO, only β-Arrestins have been shown to be directly involved in SMO ciliary trafficking. Since β-Arrestins have been shown to be involved in the trafficking of several seven transmembrane receptors (Shenoy et al., 2009), and there are several seven transmembrane proteins localising in primary cilia such as Somatostatiin (SSTR3) (Handel et al., 1999), Serotonin receptor (Brailov et al., 2000), Angiotensin II receptor (Woost et al., 2006), it is possible that additional proteins may be required to specify the ciliary localisation of SMO. To date, however, there is no evidence to suggest that cell adhesion molecules are involved in SMO ciliary localisation. Given the results from previous chapter, in this chapter, I therefore investigate whether NRCAM is involved in SHH signalling through direct interactions with SHH pathway components.

4.2 Results

4.2.1 Choice of transfected cell systems

Our objective was to test whether there are direct interactions of NRCAM with SHH signalling components. In principle, we would have liked to look for these interactions in primary GNPs by performing immunoprecipitaion, however there are a number of limitations to achieving this: the main limitation was that the amount of protein obtained from cultured purified GNPs was very low even when I combined collected protein from several wells. Consistent with this, we had difficulty detecting an anti-PTCH immunoreactive band in P5 GNP lysates on a western blot, even though a 140kD band (the predicted size) was detected in embryonic brain lysates (not shown).

In order to perform immunoprecipitation using A/G-PLUS agarose beads (sc-2003, Santacruz), 500µg of lysate protein is required, according to the manufacturers directions. However, the amount of protein from cultured purified GNPs that I obtained was only 10-20µg/cerebellum. Moreover, it was not clear where the interactions were likely to occur or how abundant they would be. If NRCAM is involved in removing PTCH from the cilium, for example, perhaps only those NRCAM and PTCH proteins present in the cilium would be associated. Given that there is only one cilium per cell and its volume represents ≤0.2% of the total cell volume, the amounts of associated protein may be very small. We therefore began by looking for interactions in transfected cells, where the amounts of protein that can be produced are considerably higher and constructs with epitope tags were available.

I decided to use heterologous expression cell line as a protein expression system for studying these protein-protein interactions. First, I started by finding the cell lines of choice for transient protein expression. Two key criteria of selecting expression cell line were considered. The first criterion was that the cells should have high level of protein expression so that the protein interaction, testing by Co-Immunoprecipitation (Co-IP), can be detected easily. To also investigate the protein colocalisation by immunofluorescence particularly in primary cilia of that cell line, the second criterion was that the cells should possess primary cilia. I therefore began to test those criteria. Typically, Cos-7 cells (Gluzman, 1981) or HEK-293 cells (Graham et al., 1977) were used for heterologous DNA expression based on SV40-based vectors. However, more recent studies of the SHH pathway have utilised NIH3T3 cells, derived from

mouse fibroblasts, as these cells respond to SHH and are capable of forming primary cilia when serum starved (Rohatgi et al., 2007, Milenkovic et al., 2009). As NIH3T3, kindly provided by Dr. Verdon Taylor, and Cos-7 cells were both available in the lab, I began by using these cells to compare the levels of *Nrcam*-full length (*Nrcam*-FL) produced. Importantly, as shown in fig 4.1, neither cell line expresses endogenous NRCAM at detectable levels (lane 2 and 4). When the Cos-7 cells (lane 5) were transfected by *Nrcam*-FL, they were able to be over-expressed larger amount of NRCAM than NIH3T3 cells (lane 3) were after *Nrcam*-FL transfection. The full-length NRCAM expression was also present in NRCAM transfected NIH3T3 (lane 3) and Cos-7 cells (lane 5), which normally hardly detected unless the cells were transfected with *Nrcam* (Sakurai et al., 1997). Moreover, I also performed immunolabelling to visualise primary cilia in both cell types so that I can investigate later whether NRCAM co-localises either endogenous PTCH or SMO in their primary cilia. As shown in fig 4.2A and B, the primary cilia were hardly seen on either cell types; however, the NIH3T3 cells have relatively more percentage of primary cilia than Cos-7 cells (Fig 4.2C). Given the widespread use of NIH3T3 cells to investigate SHH pathway in recent studies (Rohatgi et al., 2007, Milenkovic et al., 2009, Hillman et al., 2011), I therefore decided to choose NIH3T3 cells to perform further experiments.

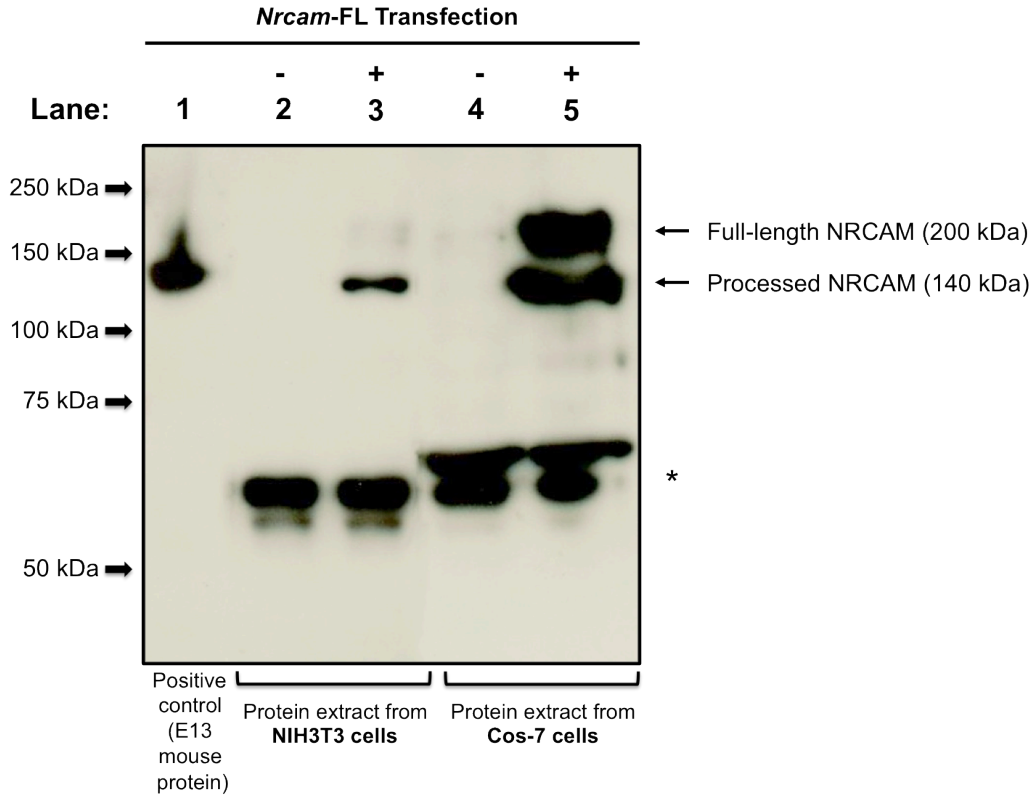

Figure 4.1. Comparative *Nrcam*-FL over-expression in NIH3T3 and Cos-7 cells. Immunoblot with antibody to NRCAM was used to investigate the amount of NRCAM over-expression protein in NIH3T3 cells, kindly provided by Dr. Verdon Taylor, and Cos-7 cells. The expression of NRCAM from the lysate of NIH3T3 cells, which were not transfected or transfected by *Nrcam*-FL, were shown in lane 2 and 3, respectively. The expression of *Nrcam* from the lysate of Cos-7 cells, which were not transfected or transfected by *Nrcam*-FL, were shown in lane 4 and 5, respectively. The E13 mouse brain lysate (lane 1) was also loaded to serve as a positive control. The NRCAM antibody also detected nonspecific (*) bands, which were present in every condition except the E13 mouse brain lysate (lane 1).

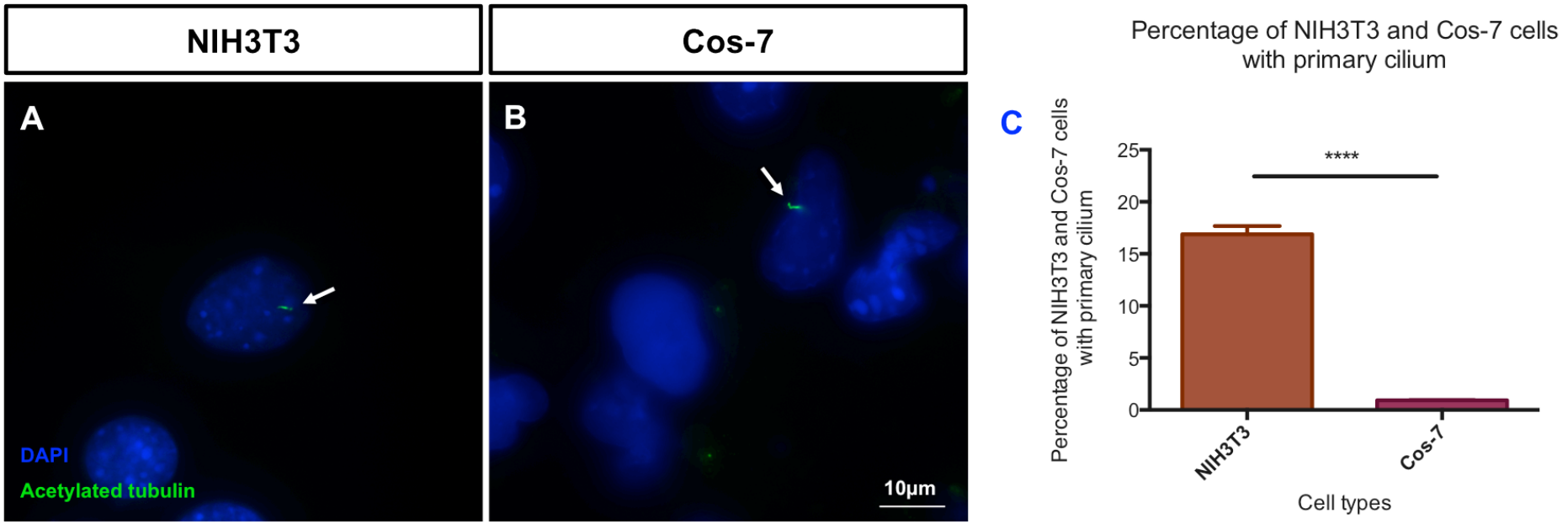

Figure 4. 2. NIH3T3 and Cos-7 cells possess primary cilia. NIH3T3 cells and Cos-7 cells were serum starved for 24 hours after plated for 24 hours. Then the cells were fixed with 4% PFA, immunolabelled by anti-acetylated α-tubulin antibody (green) and their nuclei (blue) were detected by DAPI staining. Scale bar = 10 μm **(A)** Primary ciliated NIH3T3 cell (arrow). **(B)** Primary ciliated Cos-7 cell (arrow). **(C)** Comparison of the percentage of primary ciliated NIH3T3 and Cos-7 cells. 20 image fields from 3 independent experiments were quantified the percentage of cells with primary cilium. The data are graphed showing the Standard Error of the Mean (SEM) and tested for statistically significant differences among the control and treated samples using one-way ANOVA, followed by Bonferroni's post-test. The bar graph shows Mean±SEM. Confidence interval was set to 95%, with a *p*-value less than 0.05 taken as statistically significant. Statistical significances are indicated as asterisks; *: $p<0.05$, **: $p<0.01$, ***: $p<0.001$, ****: $p<0.0001$ and N.S.: not significant.

4.2.2 Testing PTCH and SMO antibodies by western blot

The ability of our SMO and PTCH antibodies to label mouse proteins in lysates of NIH3T3 cells has not been tested. In addition, since NIH3T3 cells have been reported to express endogenous PTCH and SMO (Rohatgi et al., 2007), I first assessed whether it was feasible to look for SMO and PTCH expressions in NIH3T3 cells so that the interactions between the endogenous proteins and heterologously expressed NRCAM can be investigated later. I therefore performed western blots on such lysates. As shown in Fig 4.3, I was able to detect the expression of SMO (lane 1) but not PTCH (lane 2).

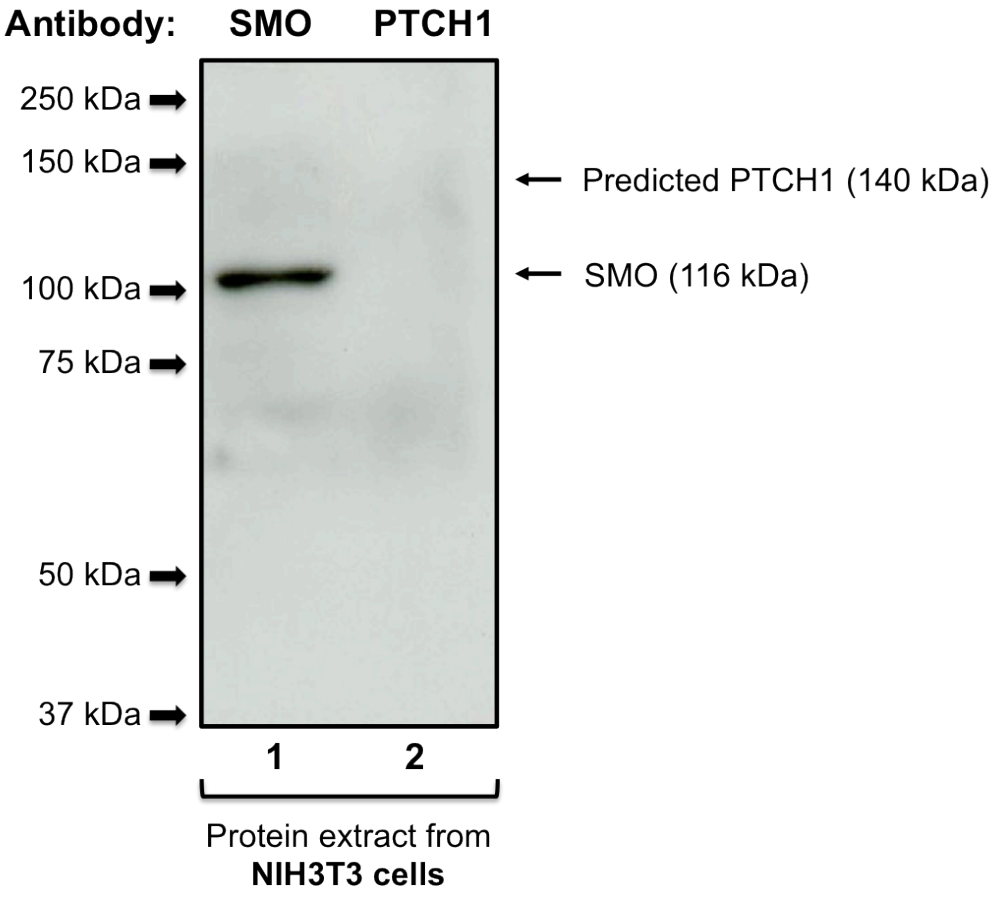

Figure 4.3. Testing SMO and PTCH1 antibodies on NIH3T3 cell lysate. Immunoblot with antibodies to SMO and PTCH1 were used to investigate the endogenous SMO and PTCH1 proteins, respectively, in NIH3T3 cells, kindly provided by Dr. Verdon Taylor. The SMO expression can be detected by the SMO antibody (lane 1), whereas, the PTCH1 expression can not be detected by the PTCH1 antibody (lane 2).

4.2.3 Optimisation of *Ptch1*-YFP and *Smo*-YFP transfection protocol

Given how poorly the PTCH antibody detected endogenous protein in NIH3T3 cell lysates; we decided to investigate the protein interaction from overexpressed PTCH, SMO and NRCAM. *Ptch1* and *Smo* expression constructs were obtained from Prof. Matthew P. Scott's laboratory. I performed single transfections of either *Ptch1*-YFP or *Smo*-YFP into NIH3T3 cells using Lipofectamine 2000 (11668-019, Invitrogen) as a transfection reagent. The transfection efficiencies of both plasmids were also evaluated by immunocytochemistry. The SMO and PTCH1 transfection efficiencies were very low compared to GFP transfected control (table 4.1), which I confirmed using anti-GFP antibody by western blot (anti-GFP is known also to detect YFP; (Veening et al., 2004). As shown in Fig 4.4, GFP transfected protein, which was used as a positive control, was shown on the blot (lane 3), however, the bands of SMO-YFP (lane 1) and PTCH1-YFP (lane 2) transfected proteins could not be detected.

Table 4.1. *Smo*-YFP, *Ptch1*-YFP and GFP transfection efficiencies in NIH3T3 cells

Transfection Efficiencies of NIH3T3 cells	Mean	SEM
1. %SMO-YFP transfected cells	7.53	1.35
2. %PTCH1-YFP transfected cells	1.03	0.42
3. %GFP transfected cells	61.07	7.22

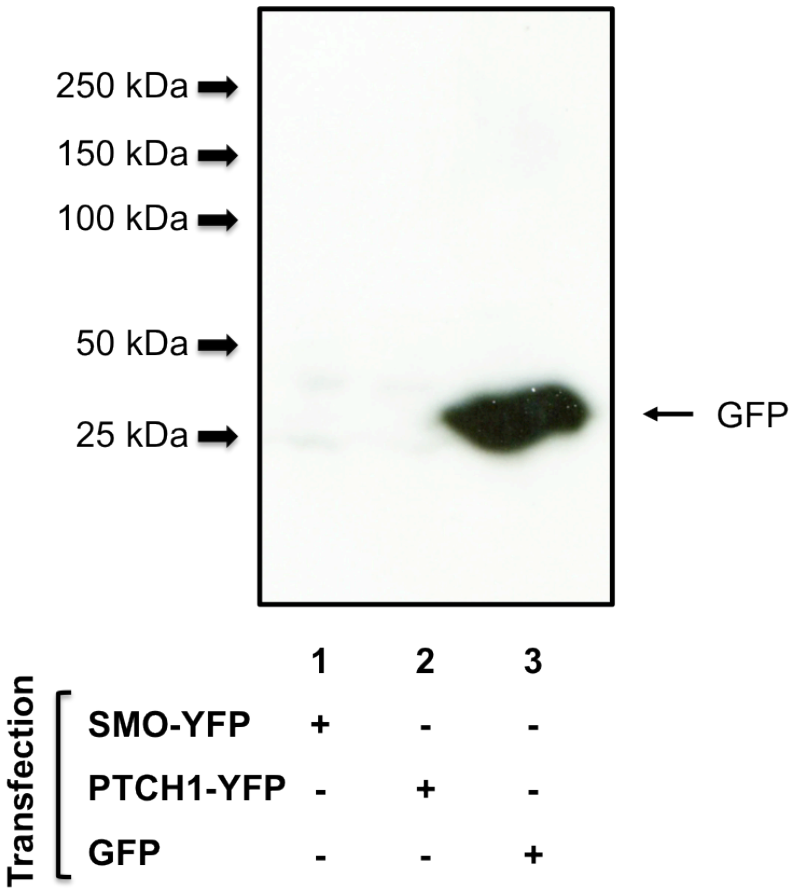

Figure 4.4. Immunoblot of SMO-YFP and PTCH1-YFP protein over-expression in NIH3T3 cells. The *Smo*-YFP, *Ptch1*-YFP and GFP (positive control) constructs were transfected to NIH3T3 cells and their proteins were extracted after transfection for 24 hours. Immunoblot was performed and probed with antibody against GFP. The GFP expression (lane 3) was detected, whereas, SMO-YFP (lane 1) and PTCH1-YFP (lane 2) expressions were hardly seen.

For these reasons, I began to optimize the transfection protocol by varying the DNA and Lipofectamine- 2000 ratio, however, the transfection efficiencies were not improved. I also attempted to use other transfection reagents such as Fugene HD (Promega), TransFectin (Bio-Rad), TransIT-2020 (Mirus) and also tried a different method by performing NIH3T3 cell electroporation using Microporator MP-100. As shown in table 4.2, the transfection efficiencies were not much different from that using Lipofectamine 2000.

Table 4.2. Comparison of methods to overexpress *Smo*-YFP and *Ptch1*-YFP in NIH3T3 cells

Efficiencies in NIH3T3 cells	**Methods**				
	Transfection (Transfection reagents)				Electroporation
	Lipofectamine 2000	Fugene HD	TransFectin	TransIT-2020	
1. %SMO-YFP positive cells	7.53±1.35	5.25±1.56	6.72±2.1	6.68±3.46	3.01±0.4
2. %PTCH1-YFP positive cells	1.03±0.42	1.53±0.8	0.85±0.23	1.29±0.85	0.23±0.1

Therefore, I turned to transfect *Ptch1*-YFP or *Smo*-YFP in Cos-7 cells using Lipofectamine 2000 as the transfection reagent. As shown in table 4.3, the transfection efficiencies were slightly more in Cos-7 cells than that in NIH3T3 cells.

I then started optimising the transfection protocol again, as I had done with NIH3T3 cells. Despite these efforts, the transfection efficiencies were only slightly increased and the levels of PTCH1 and SMO proteins seemed unlikely to be sufficient for performing Co-IP as the bands of PTCH1 and SMO were invisible on the western blot.

Table 4.3. Comparison of the transfection efficiencies of NIH3T3 and Cos-7 cells

Transfection Efficiencies	NIH3T3 cells	Cos-7 cells
1. %SMO-YFP transfected cells	7.53±1.35	9.23±3.18
2. %PTCH1-YFP transfected cells	1.03±0.42	3.56±1.30

Table 4.4. *Smo*-GFP and *Ptch1*-GFP transfection efficiencies in Cos-7 cells

Transfection Efficiencies of Cos-7 cells	Mean	SEM
1. %SMO-GFP transfected cells	46.81	12.6
2. %PTCH1-GFP transfected cells	34.02	9.53

As a result, I decided to change plasmids to *Ptch1*-GFP and *Smo*-GFP (kindly provided by Frederic Charron, with permission from Prof. Chi-chung Hui), as I know that these plasmids have been shown to work in Cos-7 cells (Izzi et al., 2011). As shown in table 4.4, the PTCH1-GFP and SMO-GFP transfection efficiencies were dramatically increased when compare to the transfection efficiencies of the previous constructs (*Smo*-YFP and *Ptch1*-YFP) (see table 4.1). The PTCH1-GFP and SMO-GFP expression levels were also evaluated by western blot using anti-GFP antibodies. The anti-GFP immunoreactive bands corresponding to the predicted molecular weights of PTCH1-GFP and SMO-GFP were seen (fig 4.5). As expected, the transfected NRCAM expression was not detected by the anti-GFP antibody under either condition.

Although, we finally sorted out that Cos-7 cells were appropriately to use as a transfected cell system, actually their numbers of primary cilia were very low (Fig 4.2C). Therefore the experiments that follow address interactions in whole cell lysates rather than in cilia.

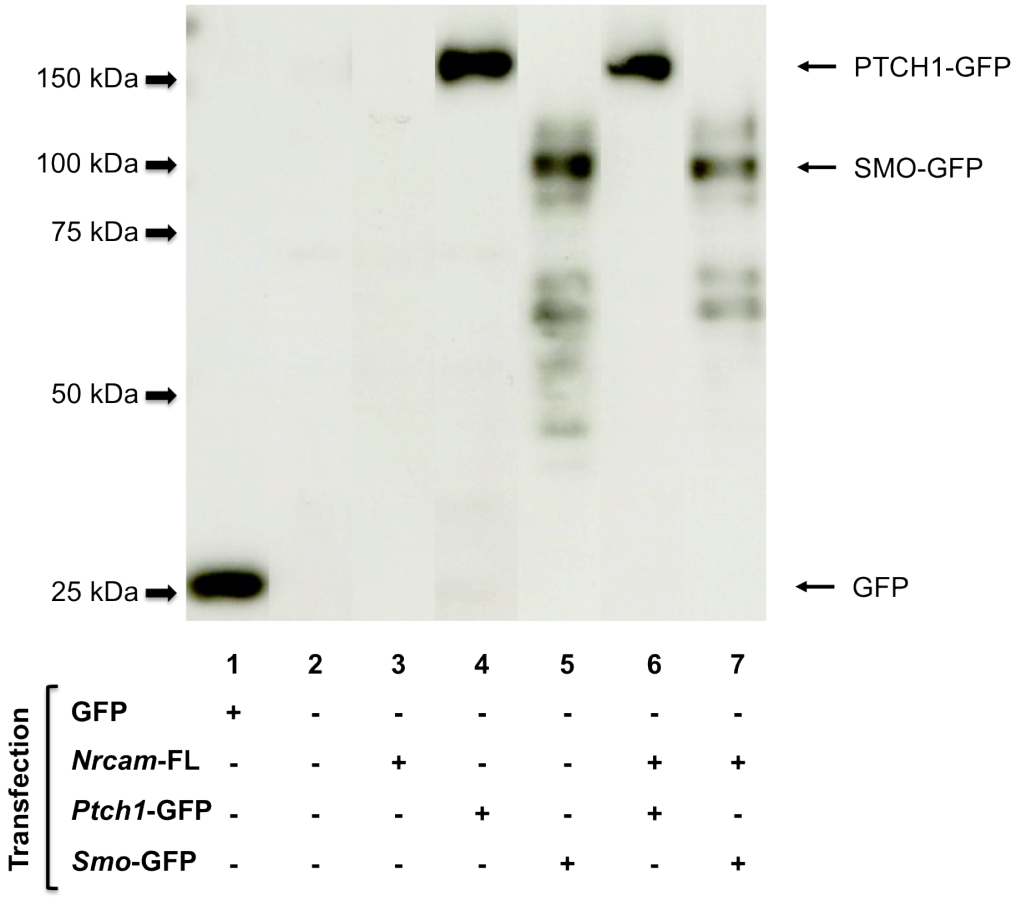

Figure 4.5. Overexpression of PTCH1-GFP and SMO-GFP in Cos-7 cells. Immunoblot with antibody to GFP was used to assess the amount of PTCH1-GFP and SMO-GFP transfected protein extracts from Cos-7 cells. The GFP (positive control; lane 1), PTCH1-GFP (lane 4, 6) and SMO-GFP (lane 5, 7) expressions were obviously shown. Note that because the aim of this experiment was to also test protein co-precipitation in the co-transfected cells, the *Nrcam*-FL transfection (lane 3) was included to determine whether *Nrcam* transfection at the same time affects the level of co-expression in the cells (lane 6, 7).

4.2.4 Evaluation of protein-protein interaction

Having achieved detectable expression of the SMO and PTCH fusion proteins, I started investigating the interaction of NRCAM and PTCH1-GFP, NRCAM and SMO-GFP by Co-IP. First, I immunoprecipitated NRCAM and looked for co-precipitation of the SMO and PTCH1 fusion proteins with anti-GFP antibody. As shown in Fig.4.6A, NRCAM seems to interact with PTCH1 (Lane 1, Fig. 4.6A) but not SMO (Lane 2, Fig. 4.6A). However, I did not have any control showing whether antibody specifically works. I therefore performed Co-IP again using the protein extracts from SMO-GFP transfected (Lane 1, Fig. 4.6B) and PTCH1-GFP transfected (Lane 3, Fig. 4.6B) Cos-7 cells as controls, immunoprecipitated with anti-NRCAM antibody. Again, I can see the band (Lane 4, Fig. 4.6B), suggesting that NRCAM may interact with PTCH1 but not SMO (Lane 2, Fig. 4.6B). However, a band was also present when NRCAM was not co-transfected (Lane 3, Fig. 4.6B), suggesting that non-specific interaction was occurring.

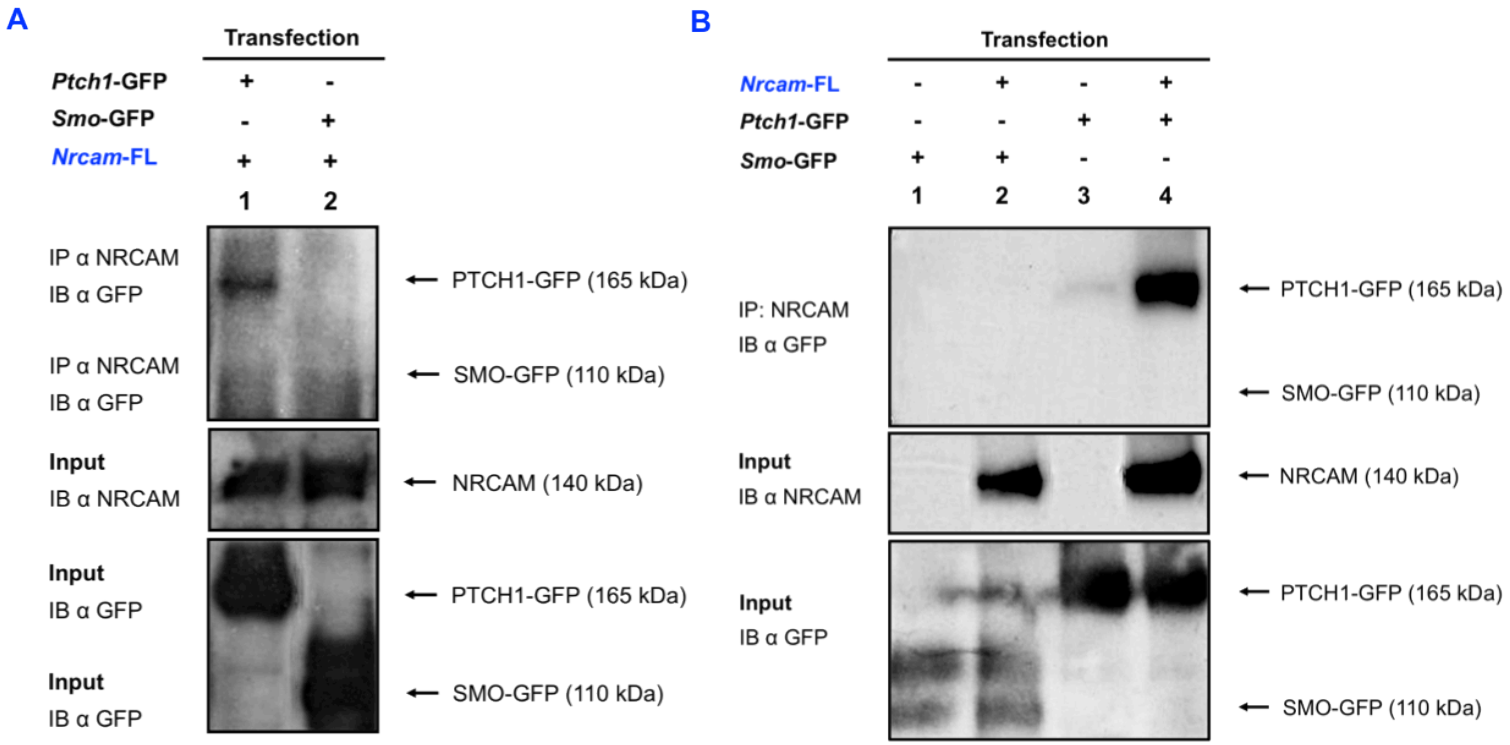

Figure 4.6. NRCAM seems to interact with PTCH1, but not SMO. Cos-7 cells were transfected with the indicated constructs and **(A)** lysates were immuno-precipitated (IP) with anti-NRCAM antibody and immunoblotted (IB) with anti-GFP antibody. **(B)** The experiment was performed as (A), however, the controls, the protein lysates from single *Smo*-GFP (lane 1) and *Ptch1*-GFP (lane 3) transfected Cos-7 cells, were included to demonstrate how specificity of Co-IP protocol was.

To begin to dissect the source of the non-specific interactions, I began to test the different components of the assay. To test whether this could reside in the polyclonal anti-NRCAM antibodies, I substituted a hemagglutinin (HA)-tagged construct (*Nrcam*-HA), kindly provided by Dr. Catherine Faivre-Sarrailh (France), in place of NRCAM-FL and repeated the experiments (Fig. 4.7A). In addition, I included as a positive control, FLAG-tagged BOC (*Boc*-FLAG), kindly provided by Dr. Frederic Charron (Canada), because PTCH1 and BOC have been shown to interact specifically (Izzi et al., 2011). To test the specificity of any interaction further, I asked whether a similar membrane protein, which like NRCAM also contains Ig domains, shows an interaction with PTCH1. Therefore, I used Fibroblast Growth Factor Receptor 3 (FGFR3), a single pass-membrane protein (Keegan et al., 1991), kindly provided by Prof. Marysia Plazek (United Kingdom) as a putative negative control. I performed co-transfection of *Ptch1*-GFP and *Boc*-FLAG, *Ptch1*-GFP and Fgfr3 construct, which contains HA-tag (*Fgfr3*-HA) as well as *Nrcam*-HA, in Cos-7 cells and co-immunoprecipitated as above. As shown in Fig 4.6C, although GFP-reactive bands were apparent in the IPs of PTCH1-GFP and NRCAM-HA transfections (Lane 4, Fig. 4.7A), similar, though weaker bands were also present in the antibody control (Lane 3, Fig. 4.7A) and the negative control (FGFR3) lanes (Lane 6, Fig. 4.7A), again suggesting non-specific interactions.

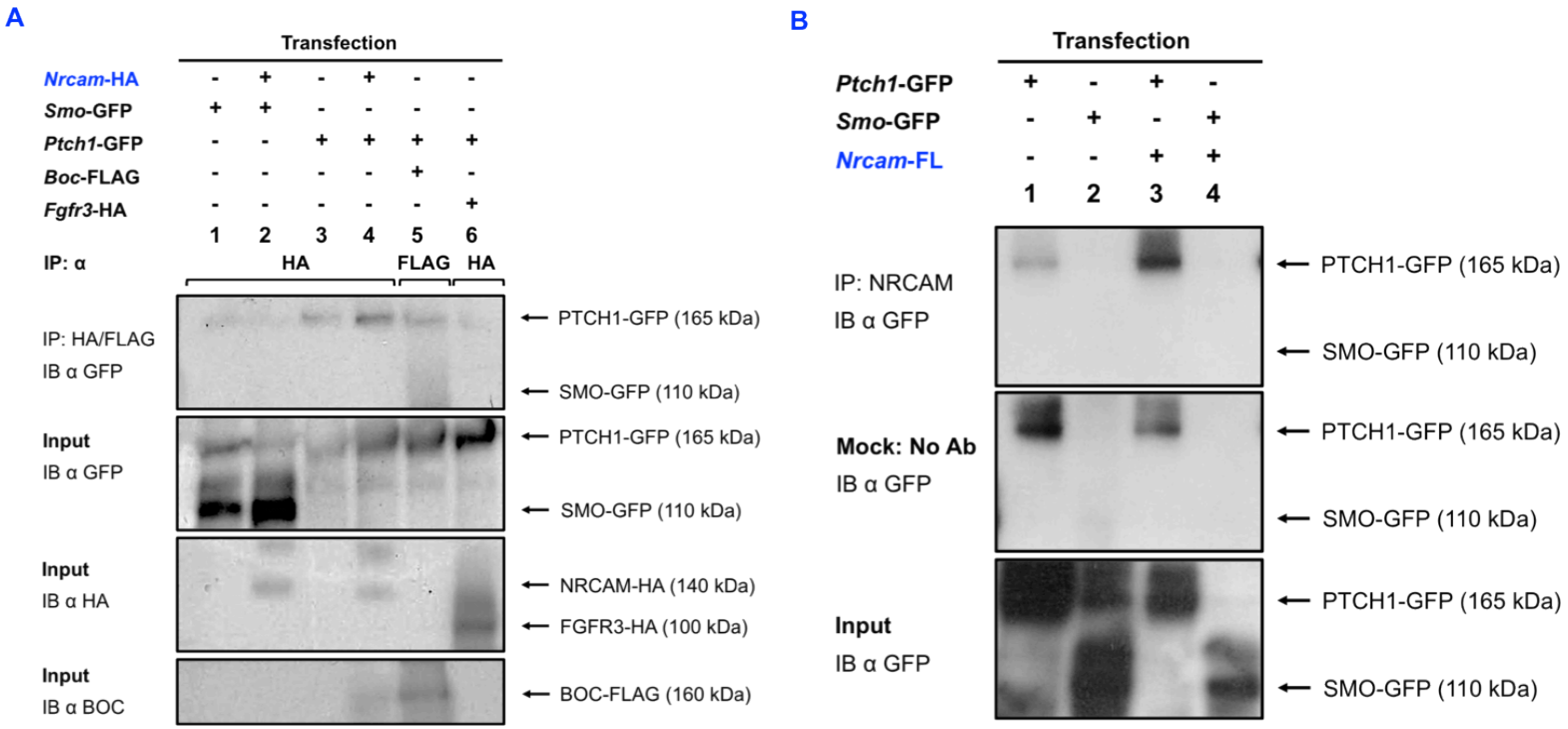

Figure 4.7. NRCAM seems to interact with PTCH1 but the non-specific interactions are also present. Cos-7 cells were transfected with the indicated constructs and **(A)** lysates were IP with an anti-HA/FLAG antibodies as indicates and IB with anti-GFP. The interaction of PTCH1-GFP and BOC-FLAG was used as a positive control (Izzi et al., 2011), whereas, the lysate from the co-transfection of PTCH1-GFP and FGFR3-HA was used as a negative control. **(B)** To investigate the cause of non-specific interaction, the mock experiment (no antibody adding in IP step) was also performed in parallel. The lysates were IP with anti-NRCAM antibody followed by IB with anti-GFP antibody.

Since these bands were present whenever *Ptch1*-GFP was transfected, I considered whether this protein could be directly interacting with components of the immunoprecipitation other than the primary antibody (anti-HA or anti-NRCAM). I therefore tested whether these bands appeared in the absence of anti-HA or anti-NRCAM antibodies. As shown in Fig 4.7B, in mock condition (no antibody), the lysate from PTCH1-GFP showed the non-specific interactions (lane 1 and 3), whereas, that from SMO-GFP (lane 2 and 4) did not. This demonstrated that PTCH1-GFP does indeed interact directly with the ProteinA/G beads under my standard conditions.

Therefore, I started optimizing the Co-IP protocol to get rid of this background interaction as much as possible and to see if there is the real PTCH1 and NRCAM interaction. I added a pre-clearing step before performing Co-IP as incubation of protein lysate with A/G-PLUS agarose beads first can remove the possibility of non-specific binding in the later stage of the IP. I also adjusted the recipes of RIPA buffer, which was used for extracting protein, and wash buffer called lpH buffer (see the final recipes in table 2.3). For example, NaCl concentration was increased in lpH buffer as this helps to reduce ionic and electrostatic interaction. Sodium deoxycholate, which is ionic detergent that is useful for disrupting and dissociating interactions, was added to RIPA buffer. In addition, the time for the washing step was increased, whereas, I decreased incubation time of proteins, beads and antibodies (see the full final Co-IP protocol in chapter 2, section 2.8.4).

After including all these changes, the background band from the antibody-only control was removed (Lane 4, Fig. 4.8A), whereas anti-GFP-reactive bands from the NRCAM-HA with PTCH1-GFP co-IP (Lane 5, Fig. 4.8A) and also from the positive control (Lane 6, Fig. 4.8A) were still detected, suggesting that PTCH1 can indeed be seen to co-precipiate with NRCAM.

Of some concern, is that a weak anti-GFP reactive band was detected in a co-IP of the Angiopoeitin receptor 2 (TIE2), a single-transmembrane protein containing Ig domains (Partanen and Dumont, 1999), kindly provided by Prof. Elizabeth Smythe (United Kingdom), with PTCH1-GFP, which was included as a negative control (Lane 7, Fig. 4.8A). This leaves some doubt as to the specificity of the NRCAM and PTCH1 interaction detected.

Importantly, however, under these more stringent conditions, SMO-GFP was not seen to co-precipitate with NRCAM (lane 2 and 3 Fig 4.8A), making it unlikely that NRCAM regulates SMO through direct interactions between the proteins. To confirm this result, the protein lysates were precipitated again but in an

inversed order. NRCAM appeared to be co-precipitated with PTCH1-GFP (lane 3, Fig 4.8B), as well as BOC-FLAG and PTCH1-GFP (lane 4, Fig 4.8B). Again, NRCAM and SMO co-precipitation was not seen. Therefore these results suggested that NRCAM might interact with PTCH1 but not SMO.

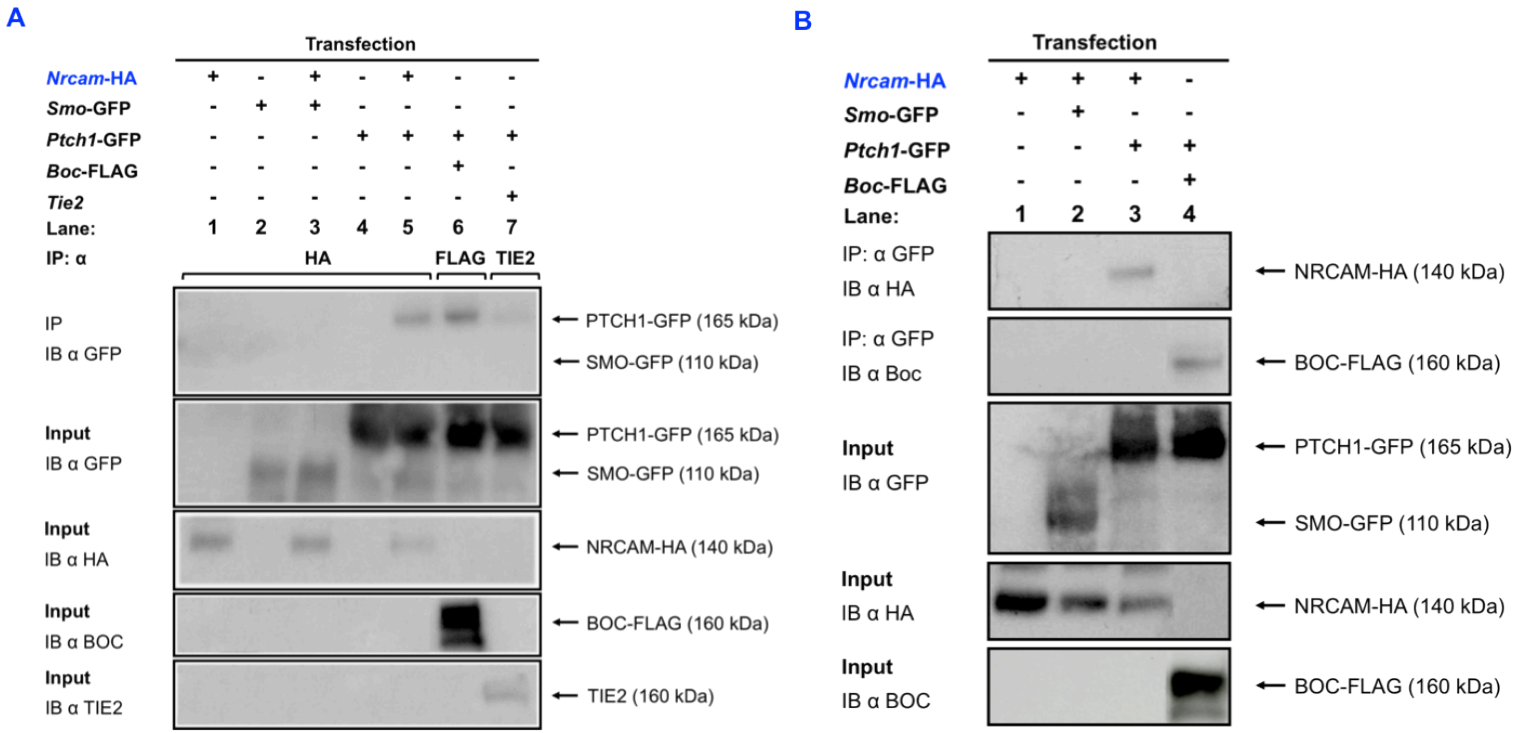

Figure 4.8. NRCAM may interact with PTCH1 but not SMO. Cos-7 cells were transfected with the indicated constructs. **(A)** After optimising the Co-IP protocol to eliminate non-specific interaction, the lysates were IP with an anti-HA/FLAG/TIE2 antibodies and IB with anti-GFP. The co-transfection of *Ptch1*-GFP and *Tie2* was also used as a negative control. After Co-IP protocol optimisation, the band suggesting that PTCH1 may or may not interact with NRCAM whereas SMO does not was shown. The experiments were repeated 3 times (3 biological replications). **(B)** To confirm the result above, the lysates were also IP with anti-GFP and IB with anti-HA antibody. The interaction of PTCH1 and BOC was again used as a positive control.

4.3 Discussion

I showed in the previous chapter that NRCAM can be visualised in the primary cilium of GNP and its loss affects SMO and PTCH ciliary localisation. Although, we were not able to distinguish whether NRCAM plays a role PTCH leaving the cilium or SMO entering the primary cilium in the previous chapter, Co-IP results from this chapter seem to suggest that NRCAM may physically associate with PTCH1 but not SMO.

4.3.1 NRCAM may directly interact with PTCH1 but not SMO

The clear result from the experiments in this chapter, is that NRCAM does not interact with SMO under any of the conditions that were tried (Fig. 4.6, 4.7, 4.8), suggesting that it is highly unlikely that there is an interaction between NRCAM and SMO. However, although after optimisation of my Co-IP conditions I was able to see some evidence of an interaction of PTCH1 with NRCAM (Fig. 4.6, 4.7, 4.8), this data must be treated with caution, because the proteins that we included as putative negative controls, TIE-2 and FGFR3, also co-precipitated PTCH1. As far as we are aware, nothing has previously been reported to suggest that interactions might exist between the SHH pathway and these proteins, although there is some evidence showing that FGFR2 is involved in SHH pathway (Mukhopadhyay et al., 2013). Nonetheless, these apparent interactions inevitably give us some concern that non-physiological kinetics may result from over-expression of proteins in the Cos-7 cell system.

Nonetheless, the interactions with TIE-2 and FGFR3 appear weaker than that with NRCAM, which, by contrast, appears to be at least as strong as the interaction of PTCH1 with BOC, which has been verified independently (Izzi et al., 2011). Moreover, I was able to demonstrate the NRCAM-PTCH1 interaction in 'both directions', i.e. anti-GFP (PTCH1-GFP) precipitated NRCAM as well as anti-NRCAM (or anti-HA for the NRCAM-HA experiments) was able to precipitate PTCH1. Finally, it seems unlikely that the interaction is due simply to the hydrophobicity of PTCH1 because NRCAM clearly does not interact with SMO, which also a multi-transmembrane receptor. Therefore, I tentatively conclude that NRCAM may interact with PTCH1.

Importantly, of course, even without the above caveats, co-immunoprecipitation would not be definitive evidence of a direct binding between NRCAM and PTCH1. Co-immunoprecipitation may happen due to indirect binding through associated in the same protein complex, or even because two proteins are

present in the same intracellular vesicles. In fact it was originally argued that PTCH and SMO bound together on the basis that they could be co-immunoprecipitated from co-transfected HEK-293 cells (Carpenter et al., 1998) and also Cos-1 cells (Murone et al., 1999). Evidence of direct binding requires a demonstration of binding between the purified proteins which, given the size and hydrophobicity of PTCH, may require substantial genetic or proteolytic subfractionation of the protein to prove. Nonetheless, corroborative evidence could be obtained, for instance, if PTCH1 and NRCAM could be demonstrated to be present in the same intracellular vesicles of GNPs, by immunostaining or perhaps by Proximity Ligation Assay (Soderberg et al., 2006), which our lab is now determining.

Clearly the possible interaction of NRCAM and PTCH1 is consistent with the main hypothesis of this thesis, which is NRCAM might play a role in trafficking SHH components in primary cilia. If, however, the co-localisation studies noted above do not demonstrate evidence of NRCAM association with PTCH1 within cells, it remains possible that NRCAM may indirectly be involved in trafficking of the other molecules required for SHH pathway activation, for example BOC and GAS1 (Izzi et al., 2011).

4.3.2 Differences in expression of different PTCH1 and SMO constructs

Although, finally the problem of expression PTCH1 and SMO protein in the transfected cells were solved, I still wonder what factors causing different plasmids gave different transfection efficiencies. In spite of the fact that the *Smo*-YFP and *Ptch1*-YFP constructs were already used in published papers (Rohatgi et al., 2007, Milenkovic et al., 2009), the results in this chapter still show low transfection efficiencies for both of them. This could be due to several reasons, first; the methods used a different. The method that Rohatgi et al. and Milenkovic et al. used was retroviral infection, whereas, we attempted to used transfection reagents or electroporation. In addition, although the cells used were similar which is NIH3T3 cells, they are still different, as our NIH3T3 cells were discovered later that they were not respond well to either SHH or SAG (see Chapter 5). Therefore, these could be the reasons why we were not able to use both *Smo*-YFP and *Ptch1*-YFP to perform the experiment.

4.3.3 Investigation of colocalisation of PTCH1 and NRCAM in primary cilia and investigation of protein interaction

In this chapter, I was not able to visualise the colocalisation of PTCH1 and NRCAM in the cilia of Cos-7 cells, as the percentage of primary ciliated cells was very low. Although I know that NIH3T3 cells have a higher percentage of ciliated cells, I did not perform SMO-GFP and PTCH1-GFP transfection in the cells. In the next chapter, the NIH3T3 cells that we initially attempted to use at the beginning of this chapter are revealed not to respond well to SHH and SAG (see chapter 5). For this reason, as a part of the future work, the investigation of PTCH1 and NRCAM colocalisation could be studied in GNPs or in NIH3T3-GL cells, kindly provided by Dr. Fredderic Charron (Canada). In addition, I recently attempted to co-transfect *Ptch1*-GFP and *Nrcam*-HA into the NIH3T3-GL cells and the preliminary results showed high percentage of co-transfected cells and a high percentage of cells with primary cilia in this cell type (data not shown). Unfortunately, I have not had time to complete this study to look at co-localisation.

To conclude from the previous chapter to this chapter, we have shown that NRCAM is present in primary cilium of GNP and loss of NRCAM affects the ciliary localisation of PTCH and SMO. We initially hypothesised that NRCAM is required for PTCH trafficking out of primary cilia rather than SMO entry to the cilium as we think that the inability of SMO ciliary trafficking could be due to the consequence of PTCH ciliary localisation. In this chapter, we discovered that NRCAM might interact with PTCH1 but not SMO, which is consistent with the hypothesis that we have made in the previous chapter. However, at the very least I would need to demonstrate colocalisation of the proteins in cells, perhaps using the PLA assay, to confirm the validity of this result.

Chapter 5

Investigation of how loss of NRCAM affects SHH signalling

5.1 Introduction

A variety of studies support the idea that the SHH signal transduction pathway plays a key role in GNP proliferation and patterning of the cerebellum (Dahmane and Ruiz i Altaba, 1999, Wallace, 1999, Wechsler-Reya and Scott, 1999, Lewis et al., 2004, Corrales et al., 2006). Although SHH null mutants (*Shh*^{n}) are early embryonic lethal (Chiang et al., 1996), Lewis et al, 2004 and Corrales et al, 2006 used a LoxP-flanked conditional mutant of the gene (*Shh*^{c}) to provide evidence that SHH signalling is required not only for GNP expansion, but that the level of signalling regulates the complexity of cerebellar foliation (Lewis et al., 2004, Corrales et al., 2006). Lewis et al used *Shh*^{c}*/Shh*^{n}*, Pax2-Cre* mutant mice, in which the promoter of *Pax2* drives Cre recombinase expression from as early as E8 leading to loss of SHH in almost all cells of the EGL and Purkinje Cell Layer (PCL). In these mice, cerebellar fissures failed to develop and the EGL was decreased in thickness at E18.5 and, by P5, the number of lobes was severely reduced and a visible EGL was absent, although some TAG-1+ granule neurons are present (Lewis et al., 2004). Similarly, reduction of SHH signalling level by removal of both GLI1 and GLI2, or of SMO, also diminished cerebellar foliation (Corrales et al., 2006).

Previous work from our lab, and the evidence presented in the previous two chapters, suggests that L1-CNTNs are able to modulate the SHH signalling pathway. F3/contactin suppresses SHH-induced proliferation of GNPs *in vitro* and the cerebellum of TAG-F3 mice is reduced in size during the early postnatal period (Bizzoca et al., 2003, Xenaki et al., 2011). F3 appears to act by binding to NRCAM to suppress SHH-induced proliferation of GNPs (Xenaki et al., 2011). Moreover, we found that NRCAM is present in the primary cilium of GNPs and loss of NRCAM suppresses the translocation of SMO to this structure after 4.5 hour-SHH treatment of GNPs (Chapter 3). In addition, we are able to co-immunoprecipitate NRCAM with PTCH1 in transfected Cos-7 cells (Chapter 4).

Although, all of these evidences suggest that NRCAM plays a role in SHH signalling pathway, it is clear that loss of NRCAM is not equivalent to loss of SHH. Complete loss of SHH leads to early embryonic lethality due to multiple defects such as incorrect brain, heart, lung and skeleton developments. Particularly for the nervous system defect, a decrease in the size of the brain and the spinal cord was obvious in E9.5 SHH mutant embryos, when compared with their normal littermates and an abnormal of cephalic flexure was present

(Chiang et al., 1996). Moreover, at E11.5, progressively severe abnormalities were demonstrated in hindbrain, midbrain and forebrain and bilateral eye structures were absent.

By contrast, *Nrcam* knockout mice are viable and fertile, and show only a slight reduction of cerebellar size with no dramatic effect on other systems (Sakurai et al., 2001). In agreement with this, Moré et al. also reported no major abnormalities in independently created NRCAM-deficient mice, except cataract formation and a mild motor defect (More et al., 2001). Thus, NRCAM is unlikely to be playing a general role in SHH signalling, although it is striking that some of its expression mirrors that of SHH, notably along the midline (Lustig et al., 2001). Even in the cerebellum, GNPs lacking NRCAM still show some proliferative response to SHH *in vitro* (Xenaki et al., 2011). This may be explained by NRCAM being redundant with L1 in this function (Sakurai et al., 2001); loss of NRCAM and L1 leads to a dramatic reduction in cerebellar size and complexity. However, even the double knockout mutant (*Nr/L1*) phenotype (Sakurai et al., 2001) is not as severe as the total loss of SHH shown by Shh^{c}/Shh^{n}*, Pax2-Cre* mutant mice (Lewis et al., 2004) or loss of *Smo* (Corrales et al., 2006), although it is similar in effect to the targeted loss of *Shh* from Purkinje cells (Lewis et al., 2004) and the loss of *Gli2*. Therefore, both these *in vivo* and our *in vitro* results suggest that NRCAM may affect the amount of SHH signalling, rather than being absolutely required for the signal generation.

To begin to address whether loss of NRCAM does indeed have a quantitative effect on SHH signalling, in this chapter I attempted to acquire a quantitative readout of SHH signalling by assaying immediate early responses in both GNPs and in NIH3T3 cells, which are known to respond to SHH (Wechsler-Reya and Scott, 1999, Dahmane and Ruiz i Altaba, 1999, Rohatgi et al., 2007, Hillman et al., 2011). Our previous studies used GNP proliferation as a readout of SHH signalling (Xenaki et al., 2011). However, cell division is considerably downstream of the initial signal and may not be a direct readout of the amount of SHH signal. Indeed, in other contexts, varying the amount of SHH signal has qualitative as well as quantitative consequences for cell proliferation and differentiation (Plaisant et al., 2011, Bermudez et al., 2013). Moreover, I also investigate the effect of loss or gain of NRCAM expression in these systems.

5.2 Results

5.2.1 Quantitative investigation of mRNA expression of *Gli1* and *Ptch1*

An immediate early response to SHH signalling is increased *Gli1* and *Ptch1* gene transcription (Wechsler-Reya and Scott, 1999). GLI1 is an activator of the pathway and induction of *Gli1* transcription forms part of a positive feedback loop (Lee et al., 1997), whereas PTCH1 is a negative regulator of SHH signalling (Stone et al., 1996, Goodrich et al., 1996). Increases in *Ptch1* and *Gli1* transcription can be seen obviously within 4 hours of SHH addition (Humke et al., 2010, Hillman et al., 2011). Since SMO translocation to primary cilia after SHH treatment occurs on a similar timescale in WT but not *Nrcam*$^{-/-}$ GNPs (Chapter 3), I set out to investigate whether loss of NRCAM also affected *Gli1* and *Ptch1* transcriptional activation using Real Time quantitative PCR (qPCR).

5.2.1.1 qPCR protocol optimisation

The principle of both qPCR and traditional PCR is similar, which is an amplification of a DNA fragment. However, the difference is that the traditional PCR measures the amount of PCR products when the amplification process is ended, whereas, the qPCR does that after each round of amplification during exponential phase. The amplification products from the qPCR are measured when they are generated using a fluorescent label. When the fluorescence is increased to the point that is first detected as statistically significant above the background, that point is called the threshold cycle or C_t value, which is an inverse correlation of the logarithm of the initial DNA copy number. The higher initial amount of DNA, the lower the C_t value as the amplification product is detected sooner. The C_t value is used to quantify the amount of DNA in the samples.

There are 2 main qPCR detection systems, which are a dye-based detection and a probe-based detection. Both of them use a fluorescent signal to quantify the amount of DNA in a sample. The dye-based detection system is based on an incorporation of a DNA binding dye to double-stranded DNA (dsDNA), which is generated during the PCR amplification, leading to the emission of the fluorescent signal. The probe-based detection is performed using sequence specific DNA-based fluorescent reporter probes, which contain a fluorescent reporter molecule, a quencher molecule and sequence-specific primers. The reporter molecule and the quencher molecule are closely located in order to allow the quencher to prevent fluorescence and they are separated when the

probe hybridises to the complementary target, resulting in the increase in fluorescent signal of the reporter.

The local availability of an iCycler iQ qPCR system (BioRad) dictated that the dye-based detection system was used in the study. SYBR green was chosen as the DNA binding dye of detection for qPCR analysis. The qPCR protocol was firstly optimised so that the qPCR conditions can be acquired to enable accurate in later actual qPCR reactions. The guidelines of optimising qPCR and the criteria to determine the optimal condition of performing qPCR are previously shown in Methods, section 2.12.3.

5.2.1.1.1 Optimal primer annealing temperature

In this chapter, I describe the use of 3 pairs of qPCR primers, called Gli1, Ptch1 and Gapdh (see primer sequences in table 2.1), to detect transcripts from the *Gli1, Ptch1 and Gapdh* genes respectively; transcription from *Gapdh* gene, which encodes glyceraldehyde-3-phosphate dehydrogenase, is included as a reference gene for the total amount of mRNA, as its transcription is considered broadly invariant from cell to cell (Radonic et al., 2004). Ptch1 and Gapdh primers were kindly provided by Dr. Anne-Gaelle Borycki and I adopted the conditions for these used routinely in her lab on the same equipment. The Gli1 primer sequences were as described by (Romer et al., 2004) and therefore optimal conditions needed to be established on our PCR equipment.

To approximately estimate the optimal annealing temperatures of Gli1 primers, I started by using gradient PCR (PTCH-200 Peltier Thermal Cycler, MJ Research). Clearly the characteristics of this machine might be different from the iCycler qPCR machine. However, the iCycler qPCR machine had a fault in its gradient qPCR function. As shown in Fig 5.1, PCR reactions of the Gli1 primer set, which was performed from E13.5 mouse cDNA (see Methods, section 2.12.3), seemed to give the least non-specific products in the temperature range 62°C-64°C. Initially, the lowest temperature in the range, 62°C, was selected in order to maximise yield of the diagnostic band. However, when the experiment was repeated using the iCycler the qPCR reaction analysis showed non-specific product (Fig 5.2A). Therefore I raised the temperature and determined that qPCR reactions of Gli1 primer set at 64°C showed the highest primer specificity (Fig 5.2B). This temperature was used throughout this study.

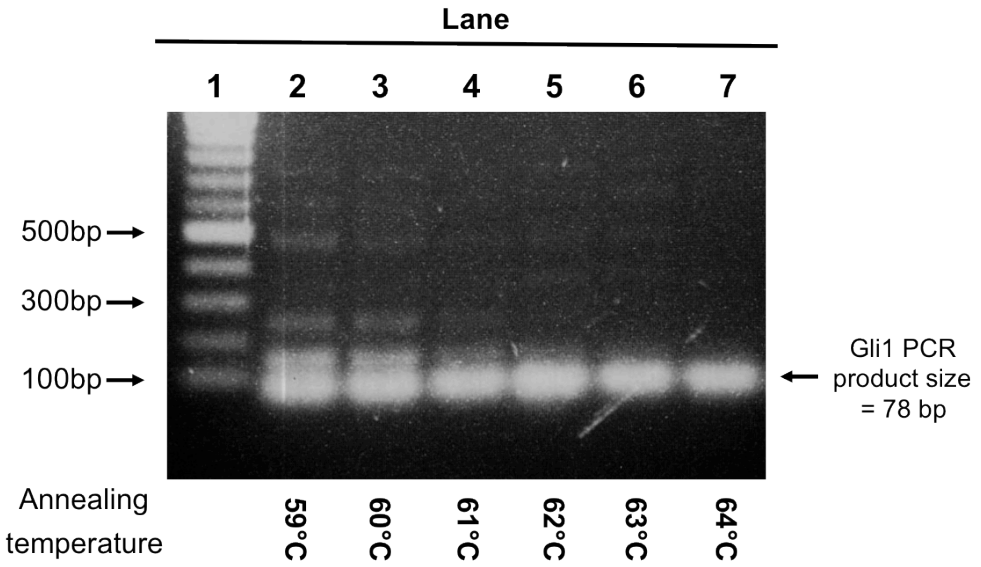

Fig 5.1. Optimal annealing temperature. Electroporesis of PCR products from E13.5 mouse cDNA using gradient PCR showed that the optimal annealing temperature of Gli1 primers used in this study is 62°C-64°C, where only the specific target products can be amplified. This range of annealing temperatures had to be tested again by performing qPCR reaction to ensure that there is no primer-dimer formation with that annealing temperature.

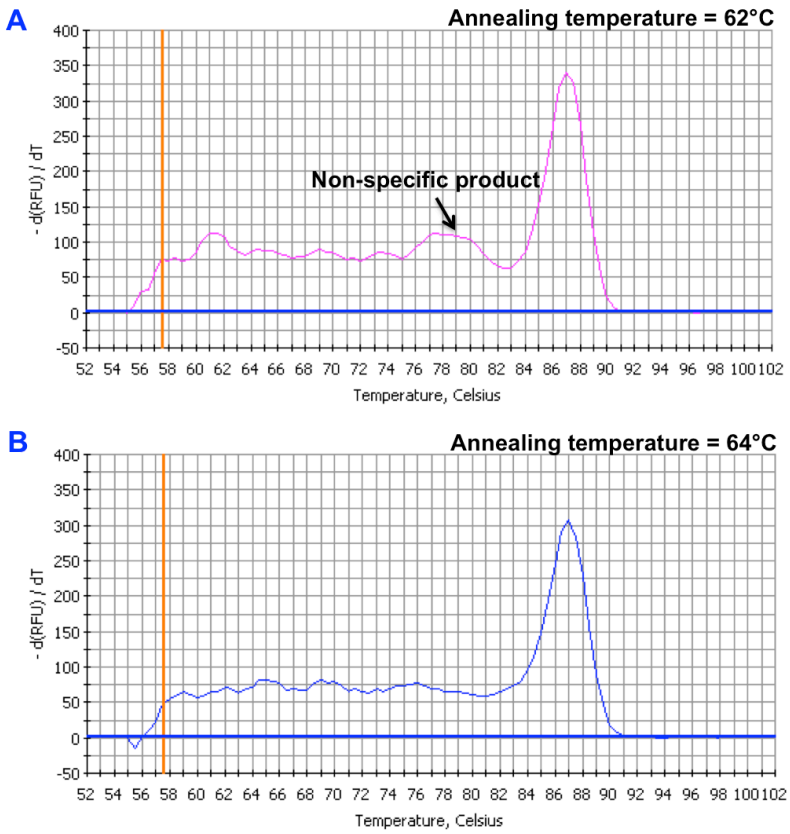

Fig 5.2. Primer dimer is not shown in the qPCR reaction that performs with optimal annealing temperature of Gli1 primer. The melt curves are plotted by temperature (°C) (X-axis) the first negative derivative of the fluorescence as a function of temperature (-dF/dT) (Y-axis) **(A)** The melt curve of Gli1 primers showed non-specific product in the reaction that perform with the 62°C annealing temperature, whereas, **(B)** when increase the annealing temperature to 64°C, the melt curve showed single peak, indicating the high primer specificity.

5.2.1.1.2 Optimal primer concentration

Performing qPCR using sub-optimal concentrations of primer reduces the rate of PCR amplification, whereas using excessive concentrations of primers will increase the amount of non-specific binding. Therefore, the optimal primer concentration for each pair of primers used in this study was determined. After varying the concentration of forward and reverse primers and running the qPCR reactions (see Methods, section 2.12.3) using the optimal annealing temperature acquired in the previous section, the primer combinations with the lowest C_t value and highest fluorescence were selected. The optimal annealing temperatures and the optimal primer concentrations of each pair of primers are shown in Table 2.11.

To ensure the primer specificity, the melt curve of each set of forward and reverse primer combination concentration was also analysed individually to ensure the production of a single peak, indicating that there was a single specific product (Fig 5.3A). In addition, PCR products for each set of primers were also run on agarose gel to confirm there were no primer-dimer formation and no obvious non-specific products (Fig 5.3B).

5.2.1.1.3 Standard curve and PCR efficiency

To validate the qPCR reaction, the PCR efficiency, which is the rate at which a PCR product is generated (see Methods, section 2.13.3), was investigated. The qPCR reactions of 5 fold-dilutions of the positive control (E13.5 mouse cDNA) were run at the optimal concentration for each pair of primers, at the respective optimal annealing temperature, to create a standard curve (see Methods, section 2.12.3). Examples of standard curve of each set of primers are shown in Fig. 5.4. The accepted range of PCR efficiency is 80-110% (Schmittgen and Livak, 2008). A summary of the selected set of primers used in this study and their average percentage of efficiencies are shown in Table 5.1.

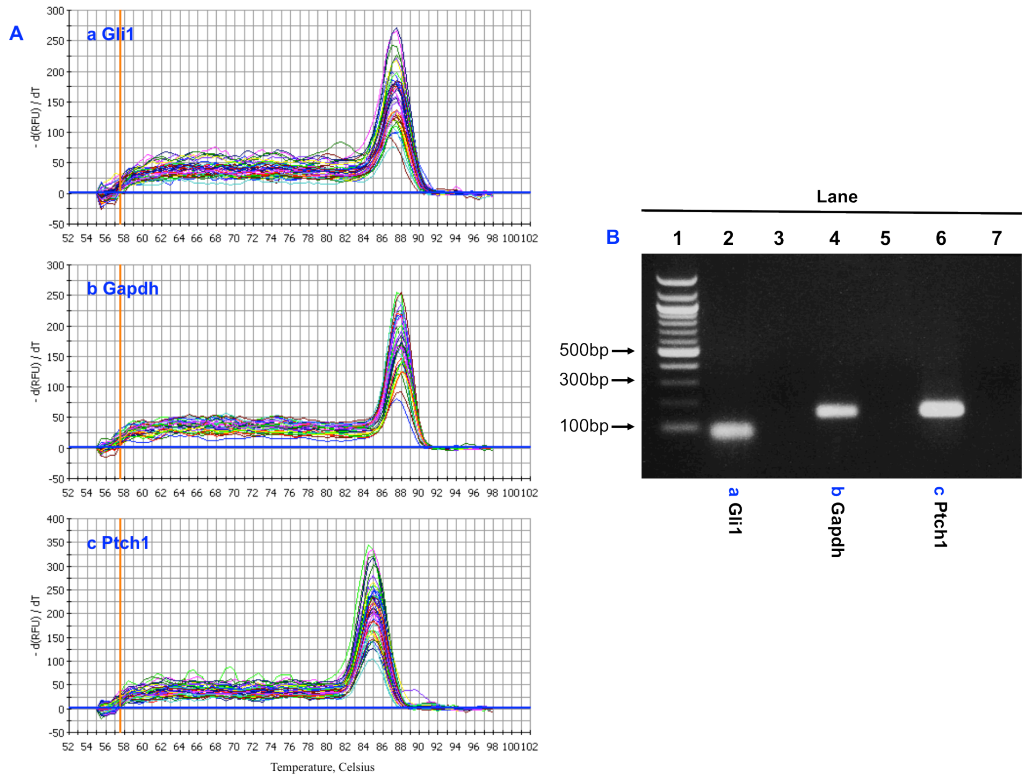

Fig 5.3. Specificity of primers used in this study. **(A)** The melt curves are plotted by temperature (°C) (X-axis) the first negative derivative of the fluorescence as a function of temperature (-dF/dT) (Y-axis). The melt curves of each pair of forward and reverse primer combination concentration showed single peak indicating specificity of primers **(a)**: Gli1, **(b)**: Gapdh, **(c)**: Ptch1 **(B)** Electroporesis of random qPCR products from (A). After performing qPCR reaction, the graphical traces were confirmed visually by resolving qPCR products on agarose gel to demonstrate that the primers used in this study were amplified only their specific target sequences. Lane 2: random qPCR product from Gli1 primer, Lane 4: Gapdh, Lane 6: Ptch1, Lane 3, 5, 7 are negative control reactions (Nuclease-free water).

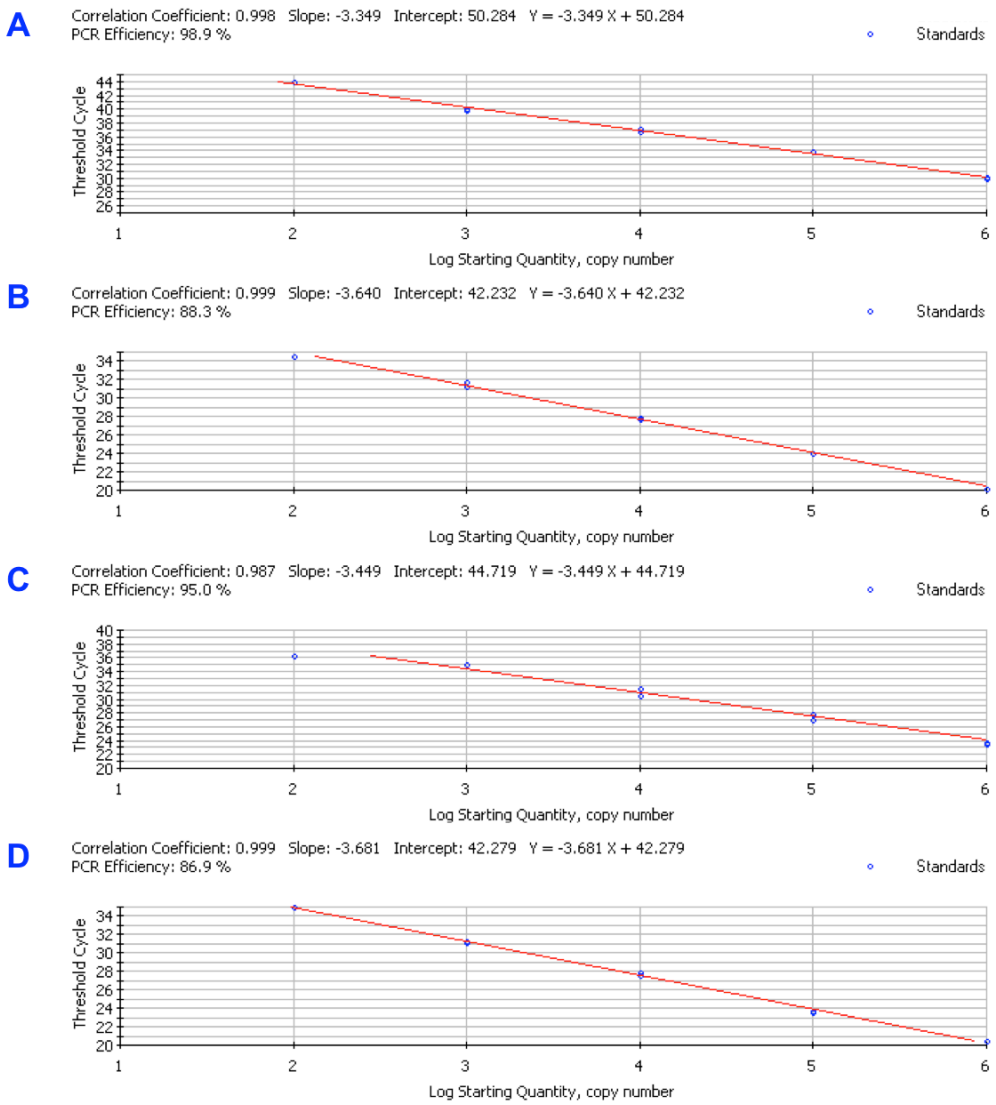

Fig 5.4. Examples of standard curves using primers used in this study. The graphs are plotted with threshold cycle (Y-axis) number versus log DNA dilution (X-axis). To determine a standard curve, the 5 fold-dilution of E13.5 mouse cDNA are set as the standard (blue dots) and the PCR amplification efficiency is calculated from the curve. **(A)** Gli1 and **(B)** Gapdh at annealing temperature 64°C, **(C)** Ptch1 and **(D)** Gapdh at annealing temperature 59°C

Table 5.1. A summary of the efficiencies of qPCR primers were used in this study

qPCR primers	Gli1	Gapdh	Ptch1	Gapdh
Optimal annealing temperature (°C)	64	64	59	59
Average percentage of efficiencies	99.46%±8.15 %	92.95%±4.65 %	95.93%±4.01 %	86.93%±7.26 %

As shown in table 5.1, the PCR efficiencies of the primer pairs of the genes of interest (*Gli1* and *Ptch1*) are different to that of the reference gene primer pair (Gapdh) under each condition; therefore, the standard curve method (see Methods, section 2.12.6) was used instead of ΔΔCt method since the ΔΔCt method can be used only when both primer sets have similar PCR efficiencies (slopes = -3.3±0.1 with R^2 = 0.99) (Bookout et al., 2006).

5.2.1.2 Quantitative analysis of the mRNA expression of *Gli1* and *Ptch1* in WT and *Nrcam*$^{-/-}$ GNPs in response to SHH or SAG

To investigate if SHH signalling is affected by loss of NRCAM, I looked at the mRNA expression of *Gli1* and *Ptch1,* transcriptional targets of SHH signal transduction, after addition of SHH to GNPs for 4.5 and 24 hours. I looked at 4.5 hours SHH addition time point because it is the same time point as used in chapter 3, where the results suggested that the localisations of PTCH and SMO in primary cilia of GNPs were affected when NRCAM is missing, and *Ptch1* and *Gli1* transcription are known to be affected as early as 4 hours after SHH treatment (Wechsler-Reya and Scott, 1999). However, since I could not be certain when NRCAM loss would have its effect, I investigated also at 24 hours, which is known to give maximal expression of *Gli1* and *Ptch1* after SHH induction (Wechsler-Reya and Scott, 1999). GNPs were therefore, as usual;

cultured 1.5 hours followed by SHH addition for 4.5 hours or for 24 hours. RNA was then extracted and reverse-transcribed to cDNA to perform qPCR. SAG was again used to treat GNPs as a positive control.

As shown in Fig 5.5, as expected, *Gli1* mRNA levels of WT GNPs were significantly increased when compared with control at 4.5 hours and 24 hours addition of SHH. Levels of *Gli1* mRNA in *Nrcam*$^{-/-}$ GNPs were also significantly higher than control after 4.5 hours of SHH treatment. However, unlike in WT cells, *Gli1* levels were not sustained after 24 hours of SHH treatment. Interestingly, 4.5 hours after addition of SHH, *Nrcam*$^{-/-}$ GNPs have significantly more *Gli1* mRNA expression than WT GNPs, whereas by 24 hours *Nrcam*$^{-/-}$ GNPs significantly have less *Gli1* mRNA expression.

By contrast, the response of *Nrcam*$^{-/-}$ GNPs to SAG, which directly activates SMO (Fig 5.6), was similar to WT. Although the response of WT cells at 4.5 hours was just sub-threshold ($p = 0.0689$), there was a clear elevation in *Gli1* mRNA levels which became highly significant by 24 hours ($p = 0.0014$). For *Nrcam*$^{-/-}$ GNPs, both time points showed a significant induction of *Gli1* mRNA levels compared to controls. However, in contrast to the response to SHH, although there appeared to be a slight elevation compared to WT at 4.5 hours, and perhaps a slightly lower response at 24 hours, these differences were not significantly different to WT at either 4.5 or 24 hours.

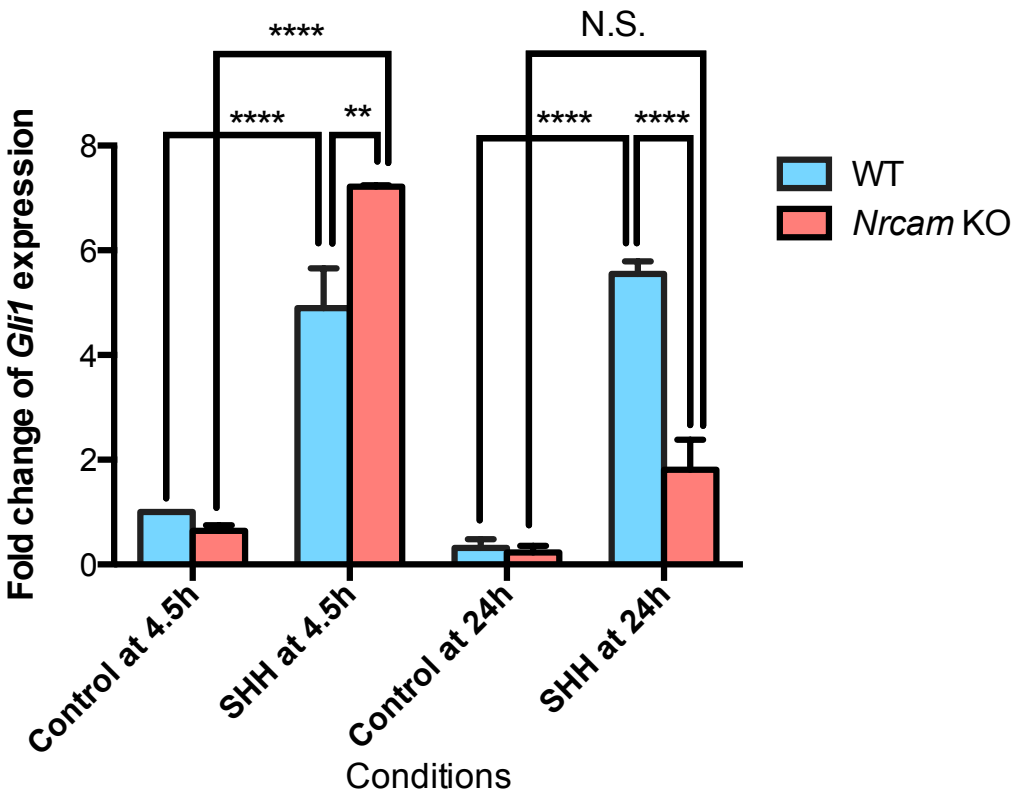

One-way analysis of variance	
F value	59.22
P value	<0.0001
P value summary	****
Are differences among means statistically significant? (P<0.05)	Yes
R square	0.9628

Bonferroni's multiple comparisons test	Significant?	Summary	Adjusted P Value
WT ctrl at 4.5h vs. WT SHH at 4.5h	**Yes**	********	**< 0.0001**
WT ctrl at 4.5h vs. WT ctrl at 24h	No	ns	> 0.9999
WT ctrl at 4.5h vs. WT SHH at 24h	Yes	****	< 0.0001
WT ctrl at 4.5h vs. Nrko ctrl at 4.5h	No	ns	> 0.9999
WT ctrl at 4.5h vs. Nrko SHH at 4.5h	Yes	****	< 0.0001
WT ctrl at 4.5h vs. Nrko ctrl at 24h	No	ns	> 0.9999
WT ctrl at 4.5h vs. Nrko SHH at 24h	No	ns	> 0.9999
WT SHH at 4.5h vs. WT ctrl at 24h	Yes	****	< 0.0001
WT SHH at 4.5h vs. WT SHH at 24h	No	ns	> 0.9999
WT SHH at 4.5h vs. Nrko ctrl at 4.5h	Yes	****	< 0.0001
WT SHH at 4.5h vs. Nrko SHH at 4.5h	**Yes**	******	**0.0086**
WT SHH at 4.5h vs. Nrko ctrl at 24h	Yes	****	< 0.0001
WT SHH at 4.5h vs. Nrko SHH at 24h	Yes	***	0.0004
WT ctrl at 24h vs. WT SHH at 24h	**Yes**	********	**< 0.0001**
WT ctrl at 24h vs. Nrko ctrl at 4.5h	No	ns	> 0.9999
WT ctrl at 24h vs. Nrko SHH at 4.5h	Yes	****	< 0.0001
WT ctrl at 24h vs. Nrko ctrl at 24h	No	ns	> 0.9999
WT ctrl at 24h vs. Nrko SHH at 24h	No	ns	0.2676
WT SHH at 24h vs. Nrko ctrl at 4.5h	Yes	****	< 0.0001
WT SHH at 24h vs. Nrko SHH at 4.5h	No	ns	0.1295
WT SHH at 24h vs. Nrko ctrl at 24h	Yes	****	< 0.0001
WT SHH at 24h vs. Nrko SHH at 24h	**Yes**	********	**< 0.0001**
Nrko ctrl at 4.5h vs. Nrko SHH at 4.5h	**Yes**	********	**< 0.0001**
Nrko ctrl at 4.5h vs. Nrko ctrl at 24h	No	ns	> 0.9999
Nrko ctrl at 4.5h vs. Nrko SHH at 24h	No	ns	0.986
Nrko SHH at 4.5h vs. Nrko ctrl at 24h	Yes	****	< 0.0001
Nrko SHH at 4.5h vs. Nrko SHH at 24h	Yes	****	< 0.0001
Nrko ctrl at 24h vs. Nrko SHH at 24h	**No**	**ns**	**0.187**

Fig 5.5. Quantitative PCR measurement of *Gli1* transcripts after addition of SHH for 4.5 and 24 hours to WT and *Nrcam*$^{-/-}$ GNPs. The WT and *Nrcam*$^{-/-}$ GNPs were cultured for 1.5 hours, then treated with SHH for 4.5 or 24 hours. The RNA was extracted and reverse-transcribed to cDNA to perform qPCR. The graph shows as the fold change of *Gli1* expression level normalised to those of *Gapdh* from each of 3 independent experiments. The data are graphed showing the Standard Error of the Mean (SEM) and tested for statistically significant differences among the control and treated samples using one-way ANOVA, followed by Bonferroni's post-test. The bar graphs show Mean±SEM. Confidence interval was set to 95%, with a *p*-value less than 0.05 taken as statistically significant. Statistical significances are indicated as asterisks; *: $p<0.05$, **: $p<0.01$, ***: $p<0.001$, ****: $p<0.0001$ and N.S.: not significant. The different data groups were analysed using 1-way ANOVA and statistic details are shown in the tables.

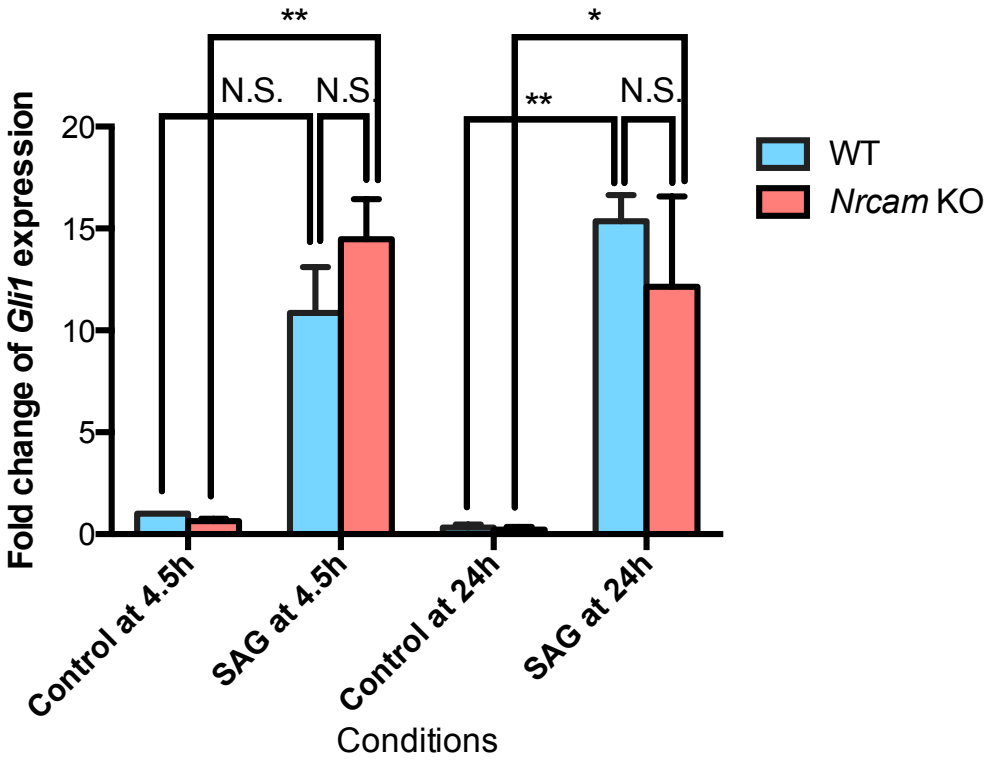

One-way analysis of variance	
F value	12.63
P value	<0.0001
P value summary	****
Are differences among means statistically significant? (P<0.05)	Yes
R square	0.8467

Bonferroni's multiple comparisons test	Significant?	Summary	Adjusted P Value
WT ctrl at 4.5h vs. WT SAG at 4.5h	**No**	**ns**	**0.0689**
WT ctrl at 4.5h vs. WT ctrl at 24h	No	ns	> 0.9999
WT ctrl at 4.5h vs. WT SAG at 24h	Yes	**	0.0023
WT ctrl at 4.5h vs. Nrko ctrl at 4.5h	No	ns	> 0.9999
WT ctrl at 4.5h vs. Nrko SAG at 4.5h	Yes	**	0.0045
WT ctrl at 4.5h vs. Nrko ctrl at 24h	No	ns	> 0.9999
WT ctrl at 4.5h vs. Nrko SAG at 24h	Yes	*	0.0257
WT SAG at 4.5h vs. WT ctrl at 24h	Yes	*	0.0408
WT SAG at 4.5h vs. WT SAG at 24h	No	ns	> 0.9999
WT SAG at 4.5h vs. Nrko ctrl at 4.5h	No	ns	0.0524
WT SAG at 4.5h vs. Nrko SAG at 4.5h	**No**	**ns**	**> 0.9999**
WT SAG at 4.5h vs. Nrko ctrl at 24h	Yes	*	0.0382
WT SAG at 4.5h vs. Nrko SAG at 24h	No	ns	> 0.9999
WT ctrl at 24h vs. WT SAG at 24h	**Yes**	****	**0.0014**
WT ctrl at 24h vs. Nrko ctrl at 4.5h	No	ns	> 0.9999
WT ctrl at 24h vs. Nrko SAG at 4.5h	Yes	**	0.0027
WT ctrl at 24h vs. Nrko ctrl at 24h	No	ns	> 0.9999
WT ctrl at 24h vs. Nrko SAG at 24h	Yes	*	0.0153
WT SAG at 24h vs. Nrko ctrl at 4.5h	Yes	**	0.0018
WT SAG at 24h vs. Nrko SAG at 4.5h	No	ns	> 0.9999
WT SAG at 24h vs. Nrko ctrl at 24h	Yes	**	0.0013
WT SAG at 24h vs. Nrko SAG at 24h	**No**	**ns**	**> 0.9999**
Nrko ctrl at 4.5h vs. Nrko SAG at 4.5h	**Yes**	****	**0.0034**
Nrko ctrl at 4.5h vs. Nrko ctrl at 24h	No	ns	> 0.9999
Nrko ctrl at 4.5h vs. Nrko SAG at 24h	Yes	*	0.0196
Nrko SAG at 4.5h vs. Nrko ctrl at 24h	Yes	**	0.0025
Nrko SAG at 4.5h vs. Nrko SAG at 24h	No	ns	> 0.9999
Nrko ctrl at 24h vs. Nrko SAG at 24h	**Yes**	****	**0.0143**

Fig 5.6. Quantitative PCR measurement of *Gli1* transcripts after addition of SAG for 4.5 and 24 hours to WT and *Nrcam*$^{-/-}$ GNPs. The WT and *Nrcam*$^{-/-}$ GNPs were cultured for 1.5 hours, and then treated with SAG for 4.5 or 24 hours. The RNA was extracted and reverse-transcribed to cDNA to perform qPCR. The graph shows as the fold change of *Gli1* expression level normalised to those of *Gapdh* from each of 3 independent experiments and then the data were treated as in Fig 5.5.

To try to find corroborative evidence that loss of NRCAM affects SHH signalling at 4.5 and 24 hours, *Ptch1* mRNA transcription levels were also evaluated. However, as shown in Fig 5.7, although there was a trend towards higher levels of *Ptch1* transcripts when SHH was added to WT GNPs for 4.5 hours, this change was not significant nor was it different in *Nrcam*$^{-/-}$ GNPs. Surprisingly, although *Ptch1* mRNA transcription levels at 24 hours were higher than at 4.5 hours, this occurred irrespective of SHH addition or *Nrcam* genotype. Similar results were obtained for *Ptch1* induction when the GNPs were treated with SAG for 4.5 or 24 hours in both WT and *Nrcam*$^{-/-}$ GNPs (Fig 5.8).

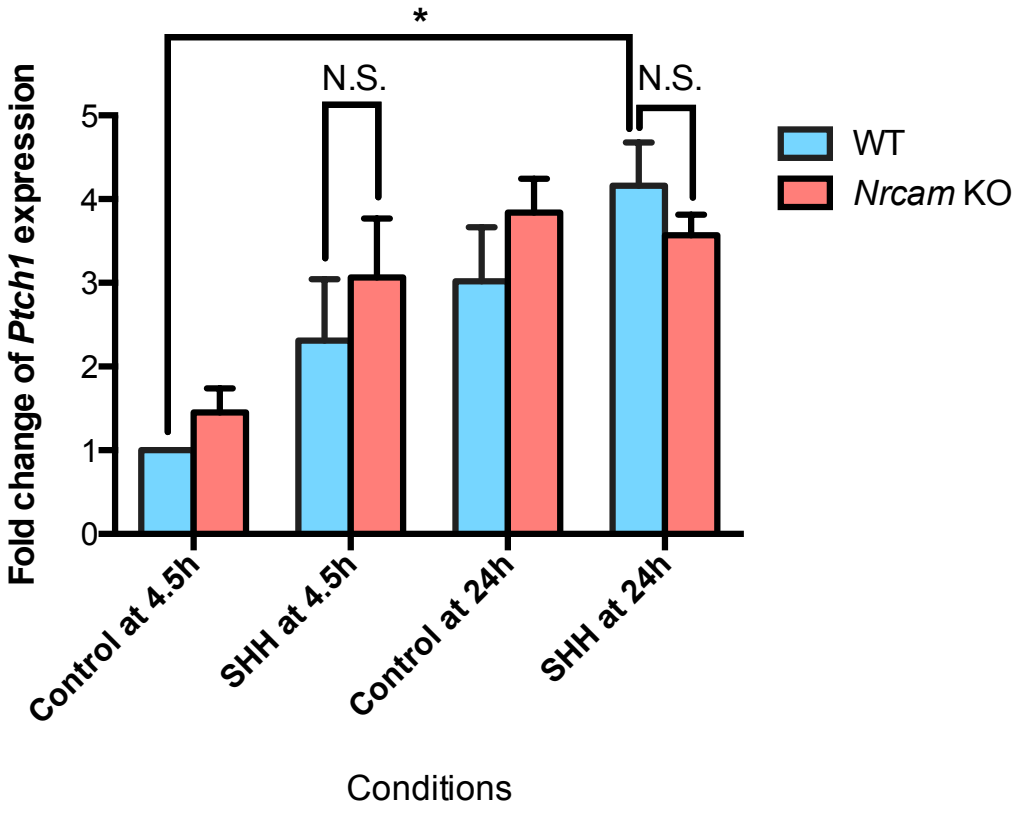

One-way analysis of variance	
F value	5.055
P value	0.0035
P value summary	**
Are differences among means statistically significant? (P<0.05)	Yes
R square	0.6886

Bonferroni's multiple comparisons test	Significant?	Summary	Adjusted P Value
WT control at 4.5h vs. WT SHH at 4.5h	**No**	**ns**	**> 0.9999**
WT control at 4.5h vs. WT control at 24h	No	ns	0.3321
WT control at 4.5h vs. WT SHH at 24h	**Yes**	*****	**0.0113**
WT control at 4.5h vs. Nrko control at 4.5h	No	ns	> 0.9999
WT control at 4.5h vs. Nrko SHH at 4.5h	No	ns	0.2879
WT control at 4.5h vs. Nrko control at 24h	Yes	*	0.0293
WT control at 4.5h vs. Nrko SHH at 24h	No	ns	0.0655
WT SHH at 4.5h vs. WT control at 24h	No	ns	> 0.9999
WT SHH at 4.5h vs. WT SHH at 24h	No	ns	0.5385
WT SHH at 4.5h vs. Nrko control at 4.5h	No	ns	> 0.9999
WT SHH at 4.5h vs. Nrko SHH at 4.5h	**No**	**ns**	**> 0.9999**
WT SHH at 4.5h vs. Nrko control at 24h	No	ns	> 0.9999
WT SHH at 4.5h vs. Nrko SHH at 24h	No	ns	> 0.9999
WT control at 24h vs. WT SHH at 24h	**No**	**ns**	**> 0.9999**
WT control at 24h vs. Nrko control at 4.5h	No	ns	> 0.9999
WT control at 24h vs. Nrko SHH at 4.5h	No	ns	> 0.9999
WT control at 24h vs. Nrko control at 24h	No	ns	> 0.9999
WT control at 24h vs. Nrko SHH at 24h	No	ns	> 0.9999
WT SHH at 24h vs. Nrko control at 4.5h	Yes	*	0.0428
WT SHH at 24h vs. Nrko SHH at 4.5h	No	ns	> 0.9999
WT SHH at 24h vs. Nrko control at 24h	No	ns	> 0.9999
WT SHH at 24h vs. Nrko SHH at 24h	**No**	**ns**	**> 0.9999**
Nrko control at 4.5h vs. Nrko SHH at 4.5h	**No**	**ns**	**> 0.9999**
Nrko control at 4.5h vs. Nrko control at 24h	No	ns	0.1117
Nrko control at 4.5h vs. Nrko SHH at 24h	No	ns	0.2487
Nrko SHH at 4.5h vs. Nrko control at 24h	No	ns	> 0.9999
Nrko SHH at 4.5h vs. Nrko SHH at 24h	No	ns	> 0.9999
Nrko control at 24h vs. Nrko SHH at 24h	**No**	**ns**	**> 0.9999**

Fig 5.7. Quantitative PCR measurement of *Ptch1* transcripts after addition of SHH for 4.5 and 24 hours to WT and *Nrcam*$^{-/-}$ GNPs. The WT and *Nrcam*$^{-/-}$ GNPs were cultured for 1.5 hours, then treated with either SHH or SAG for 4.5 or 24 hours. The RNA was extracted and reverse-transcribed to cDNA to perform qPCR. The graph shows as fold change of *Ptch1* expression level normalised to those of *Gapdh* from each 3 independent experiments. The data are graphed showing the Standard Error of the Mean (SEM) and tested for statistically significant differences among the control and treated samples using one-way ANOVA, followed by Bonferroni's post-test. The bar graphs show Mean±SEM. Confidence interval was set to 95%, with a *p*-value less than 0.05 taken as statistically significant. Statistical significances are indicated as asterisks; *: $p<0.05$, **: $p<0.01$, ***: $p<0.001$, ****: $p<0.0001$ and N.S.: not significant. The different data groups were analysed using 1-way ANOVA and statistic details are shown in the tables.

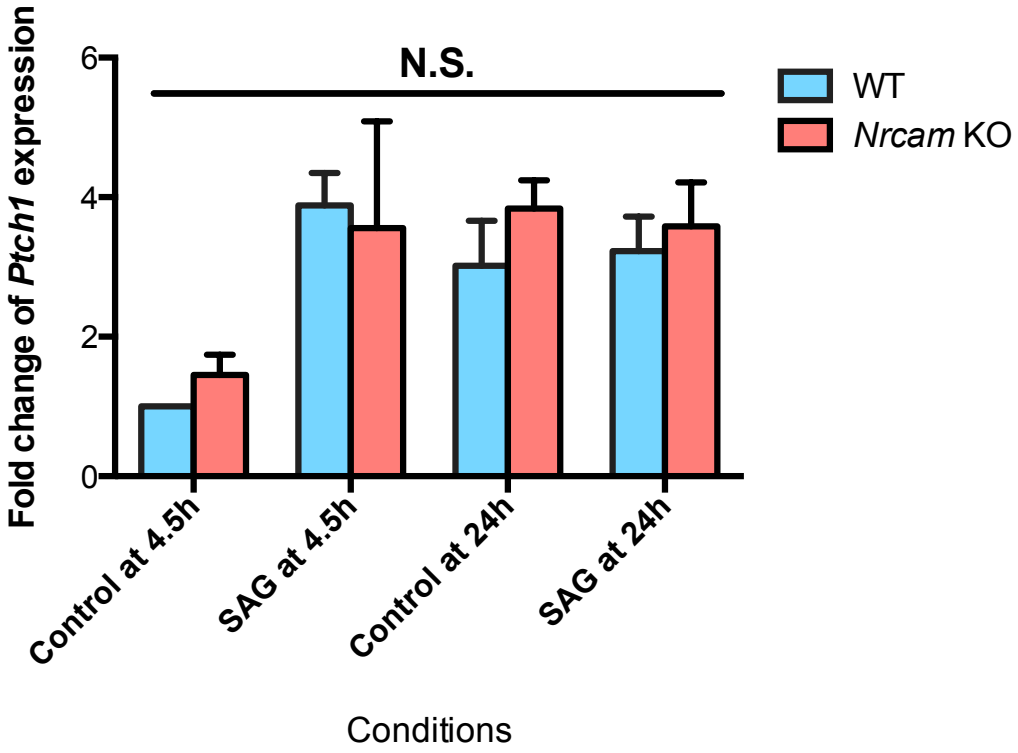
N.S.
WT
Nrcam KO
Fold change of Ptch1 expression
6
4
2
0
Control at 4.5h
SAG at 4.5h
Control at 24h
SAG at 24h
Conditions

One-way analysis of variance	
F value	2.540
P value	0.0581
P value summary	ns
Are differences among means statistically significant? (P<0.05)	No
R square	0.5263

Bonferroni's multiple comparisons test	Significant?	Summary	Adjusted P Value
WT control at 4.5h vs. WT SHH at 4.5h	No	ns	> 0.9999
WT control at 4.5h vs. WT control at 24h	No	ns	0.3321
WT control at 4.5h vs. WT SHH at 24h	Yes	*	0.0113
WT control at 4.5h vs. Nrko control at 4.5h	No	ns	> 0.9999
WT control at 4.5h vs. Nrko SHH at 4.5h	No	ns	0.2879
WT control at 4.5h vs. Nrko control at 24h	Yes	*	0.0293
WT control at 4.5h vs. Nrko SHH at 24h	No	ns	0.0655
WT SHH at 4.5h vs. WT control at 24h	No	ns	> 0.9999
WT SHH at 4.5h vs. WT SHH at 24h	No	ns	0.5385
WT SHH at 4.5h vs. Nrko control at 4.5h	No	ns	> 0.9999
WT SHH at 4.5h vs. Nrko SHH at 4.5h	**No**	**ns**	**> 0.9999**
WT SHH at 4.5h vs. Nrko control at 24h	No	ns	> 0.9999
WT SHH at 4.5h vs. Nrko SHH at 24h	No	ns	> 0.9999
WT control at 24h vs. WT SHH at 24h	No	ns	> 0.9999
WT control at 24h vs. Nrko control at 4.5h	No	ns	> 0.9999
WT control at 24h vs. Nrko SHH at 4.5h	No	ns	> 0.9999
WT control at 24h vs. Nrko control at 24h	No	ns	> 0.9999
WT control at 24h vs. Nrko SHH at 24h	No	ns	> 0.9999
WT SHH at 24h vs. Nrko control at 4.5h	Yes	*	0.0428
WT SHH at 24h vs. Nrko SHH at 4.5h	No	ns	> 0.9999
WT SHH at 24h vs. Nrko control at 24h	No	ns	> 0.9999
WT SHH at 24h vs. Nrko SHH at 24h	**No**	**ns**	**> 0.9999**
Nrko control at 4.5h vs. Nrko SHH at 4.5h	No	ns	> 0.9999
Nrko control at 4.5h vs. Nrko control at 24h	No	ns	0.1117
Nrko control at 4.5h vs. Nrko SHH at 24h	No	ns	0.2487
Nrko SHH at 4.5h vs. Nrko control at 24h	No	ns	> 0.9999
Nrko SHH at 4.5h vs. Nrko SHH at 24h	No	ns	> 0.9999
Nrko control at 24h vs. Nrko SHH at 24h	No	ns	> 0.9999

Fig 5.8. Quantitative PCR measurement of *Ptch1* transcripts after addition of SAG for 4.5 and 24 hours to WT and *Nrcam*$^{-/-}$ GNPs. (A) The WT and *Nrcam*$^{-/-}$ GNPs were cultured for 1.5 hours, and then treated with SAG for 4.5 or 24 hours. The RNA was extracted and reverse-transcribed to cDNA to perform qPCR. The graph shows as fold change of *Ptch1* expression level normalised to those of *Gapdh* from each 3 independent experiments and then the data were treated as in Fig 5.7.

Although this data clearly showed that the *Gli1* transcription levels were significantly affected by loss of NRCAM, it is not confirmed by the *Ptch1* transcription result. Although I can still see the trends in the *Ptch1* induction, which are consistent with the *Gli1* induction results – i.e. suggesting that there is more SHH signaling at 4.5 hours when NRCAM is missing compare to WT GNPs and the signal in *Nrcam*$^{-/-}$ GNPs is lower when compared with WT GNPs at 24 hours post-SHH treatment – the high levels of *Ptch1* in the control cells at 24 hours makes this difficult to interpret. In addition, I noticed that the variability among the triplicates was noticeably high (the C_t variance: SD = 0.14-0.48). Even after removing outliers in some replicates (see chapter 2, section 2.12.6 for the criteria applied in outlier removal), the Ct variance in some replicated samples was still higher than 0.3, which according to the manufacturer's guidelines, indicates that there may be a problem with the precision of the assay particularly in *Ptch1* induction results (see also Discussion).

5.2.2 Investigation of Gli1 fluorescent intensity in the staining of GNPs in response to SHH or SAG

As an alternative to looking at *Gli1 and Ptch1* gene transcriptions, I considered whether instead protein levels could be followed. However, preliminary experiments (not shown) suggested that obtaining sufficient numbers of purified GNPs to assay protein levels by Western blotting for each condition would be difficult. Therefore, instead I attempted to quantitate GLI1 protein levels in WT and *Nrcam*$^{-/-}$ GNPs after addition of SHH and SAG using GLI1 fluorescence intensity (see Methods, section 2.7).

As shown in Fig 5.9, after 4.5 hours SHH treatment, the GLI1 fluorescence intensity of WT GNPs as well as *Nrcam*$^{-/-}$ GNPs, was significantly increased when compared to the control. Interestingly, however, the GLI1 fluorescence in *Nrcam*$^{-/-}$ GNPs was significantly increased compared to the WT controls. By contrast, after 4.5 hour SAG treatment, although GLI1 protein levels were significantly increased in WT GNPs, when NRCAM is missing there was apparently no increase in GLI1 fluorescence relative to the untreated cells.

Thus, the increase in GLI1 protein level when NRCAM is missing at early time point is consistent with the qPCR result from the previous section, which suggested that *Gli1* and possibly *Ptch1* transcripts are elevated in *Nrcam*$^{-/-}$ GNPs compared to WT GNPs after SHH treatment for 4.5 hours (Figs 5.5 and 5.7). Curiously, however, the GLI1 fluorescent intensity in SAG induced *Nrcam*$^{-/-}$

GNPs hardly changed when compare with that in control *Nrcam*$^{-/-}$ GNPs, which contrasts with the results from the qPCR experiments (see Fig 5.6).

A

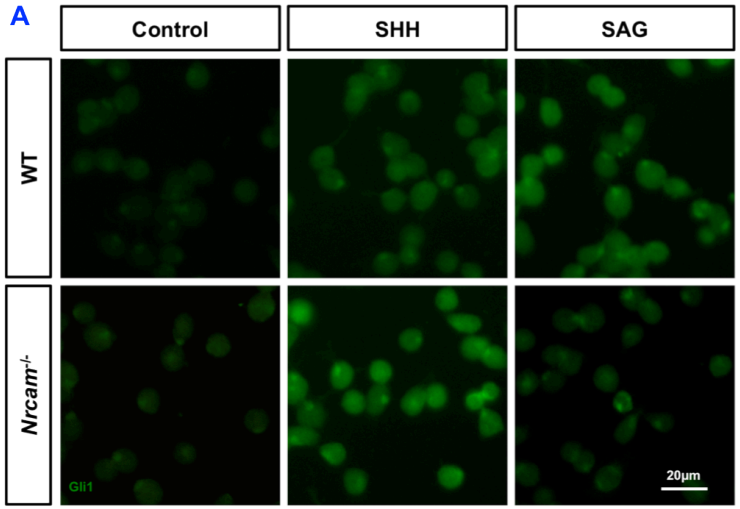

B

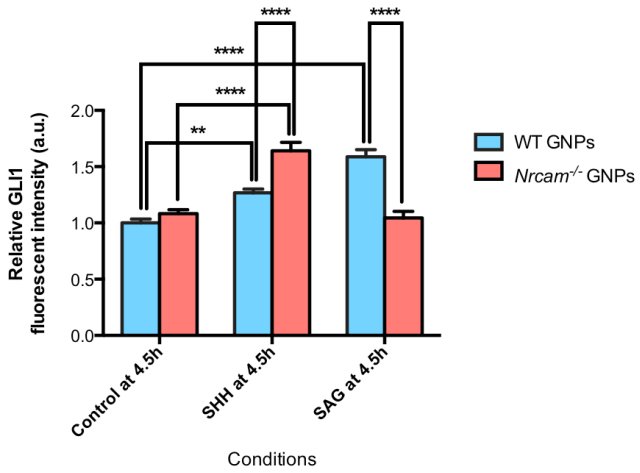

C

One-way analysis of variance	
F value	29.00
P value	<0.0001
P value summary	****
Are differences among means statistically significant? (P<0.05)	Yes
R square	0.3826

Bonferroni's multiple comparisons test	Significant?	Summary	Adjusted P Value
WT control at 4.5h vs. WT SHH at 4.5h	**Yes**	**	**0.0057**
WT control at 4.5h vs. WT SAG at 4.5h	**Yes**	****	**< 0.0001**
WT control at 4.5h vs. Nrko control at 4.5h	No	ns	> 0.9999
WT control at 4.5h vs. Nrko SHH at 4.5h	Yes	****	< 0.0001
WT control at 4.5h vs. Nrko SAG at 4.5h	No	ns	> 0.9999
WT SHH at 4.5h vs. WT SAG at 4.5h	Yes	***	0.0003
WT SHH at 4.5h vs. Nrko control at 4.5h	No	ns	0.2027
WT SHH at 4.5h vs. Nrko SHH at 4.5h	**Yes**	****	**< 0.0001**
WT SHH at 4.5h vs. Nrko SAG at 4.5h	Yes	*	0.045
WT SAG at 4.5h vs. Nrko control at 4.5h	Yes	****	< 0.0001
WT SAG at 4.5h vs. Nrko SHH at 4.5h	No	ns	> 0.9999
WT SAG at 4.5h vs. Nrko SAG at 4.5h	Yes	****	< 0.0001
Nrko control at 4.5h vs. Nrko SHH at 4.5h	**Yes**	****	**< 0.0001**
Nrko control at 4.5h vs. Nrko SAG at 4.5h	**No**	**ns**	**> 0.9999**
Nrko SHH at 4.5h vs. Nrko SAG at 4.5h	Yes	****	< 0.0001

Fig 5.9. Mean fluorescent intensity of GLI1 in WT and *Nrcam*$^{-/-}$ GNPs treated with SHH or SAG for 4.5 hours. **(A)** Immunostaining in cultured GNPs of P5 mice with anti-GLI1 antibody (green) compared between wild type and *Nrcam*$^{-/-}$ GNPs after addition of SHH and SAG (100nM) for 4.5 hours. Scale bar = 20μm **(B)** The graph shows relative mean fluorescent intensity of GLI1 (a.u.) from each of 3 independent experiments (3n). The data are graphed showing the Standard Error of the Mean (SEM) and tested for statistically significant differences among the control and treated samples using one-way ANOVA, followed by Bonferroni's post-test. The bar graphs show Mean±SEM of fluorescence from 1,200-1,600 GNPs/condition/experiment. Confidence interval was set to 95%, with a *p*-value less than 0.05 taken as statistically significant. Statistical significances are indicated as asterisks; *: $p<0.05$, **: $p<0.01$, ***: $p<0.001$, ****: $p<0.0001$ and N.S.: not significant. **(C)** The different data groups were analysed using 1-way ANOVA and statistic details are shown in the tables.

5.2.3 Investigation of GLI1 protein in NRCAM over-expressed NIH3T3-GL cells in response to SHH

To obtain corroborative evidence that NRCAM is affecting SHH signalling in GNPs, ideally an experiment should be performed to re-introduce NRCAM to the *Nrcam*$^{-/-}$ GNPs to see if this can rescue the normal dynamics of SHH signalling. However, there are a number of obstacles to doing this in GNPs: preliminary results showed that only 5-8% of GNPs can be electroporated with a GFP (Green Fluorescent Protein) construct (data not shown). Even if a higher transfection rate could be achieved, high level expression of the transfected construct cannot be achieved in the timescale required; as is typical for most transient transfections, expression can only be weakly detected, if at all, 6 hours after transfection, and the peak of expression comes 24 hours or more after transfection. Therefore because GNPs cannot be cultured as progenitors for extended periods, even with the addition of SHH (Miyazawa et al., 2000), it is not practical to attempt a rescue in GNPs.

As an alternative, I therefore attempted to overexpress NRCAM in NIH3T3 cells which normally do not express NRCAM (see previous chapter, fig 4.1 and (Conacci-Sorrell et al., 2002). NIH3T3 cells are easily transfected and this cell type is widely used to study the SHH pathway (Hillman et al., 2011, Milenkovic et al., 2009, Rohatgi et al., 2007, Humke et al., 2010), so I therefore decided to determine whether this might be a suitable system in which to test whether NRCAM affects SHH signalling. The levels of GLI1 and PTCH1 in NIH3T3 cells have been shown to rise detectably following just 4 hours of SHH induction (Humke et al., 2010, Hillman et al., 2011), suggesting that this may be a practical approach.

5.2.3.1 Choice of cell for NRCAM over-expression

Although I had previously shown that NRCAM can be overexpressed in the NIH3T3 cells provided to us by Dr Verdon Taylor (see figure 4.1), I discovered that the GLI1 response of these cells was very low, even when stimulated with SAG (Fig 5.10A), indicating that this subline has a very different response to SHH to that reported in the literature (Hillman et al., 2011). I therefore screened other NIH3T3 sublines for SHH responses and NRCAM transfectabilty. A subline provided by Prof. Hilary Powers (Sheffield), showed more GLI1 expression in response to SHH and SAG (Fig 5.10A), however, the cells did not express NRCAM when transfected with *Nrcam*-HA (Fig 5.10B).

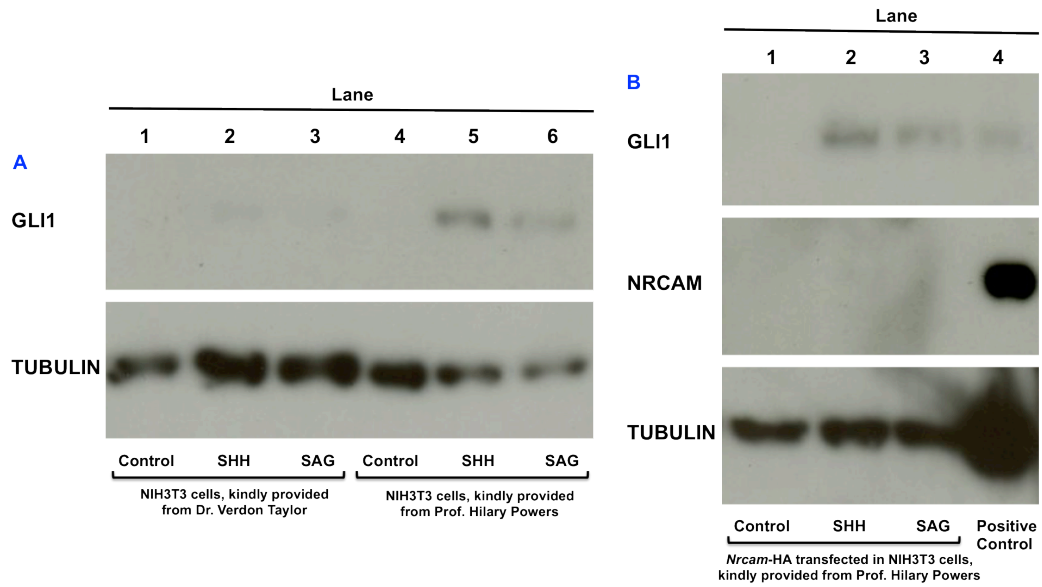

Fig. 5.10. Verification of GLI1 expression in 2 lines of NIH3T3 cells. Immunoblots with antibodies to GLI1, NRCAM and TUBULIN were used to assess amount of protein in extracts from NIH3T3 cells. Immunoblotting for TUBULIN served as a control for equal well loading **(A)** The level of GLI1 expression was observed after addition of SHH and SAG for 24 hours to 2 lines of NIH3T3 cells. The NIH3T3 cells, kindly provided from Prof. Hilary Powers showed more GLI1 expression in response to either SHH (lane 5) or SAG (lane 6) than NIH3T3 cells, kindly provided from Dr. Verdon Taylor. **(B)** Immunoblot of protein from NIH3T3 cells, kindly provided from Prof. Hilary Powers, showed GLI1 response after addition of SHH (lane 2) or SAG (lane 3), however, the cells were not able to express NRCAM when they were transfected with *Nrcam*-HA. Positive control is protein from mouse embryo at E13.5 (lane 4).

Fortunately, I received 2 further sublines of NIH3T3 cells (which I refer to as NIH3T3-FC and NIH3T3-GL), kindly provided by Dr. Frederic Charron (Montreal, Canada), originally constructed in the lab of Dr. Stephane Angers (Toronto, Canada). NIH3T3-GL cells are stably transfected with a firefly luciferase reporter construct that is driven by a concatemer of GLI1 (8x*gli*) binding sites and has been used previously to monitor SHH responses (Charron, Pers. Comm.). As shown in Fig 5.11A, the NIH3T3-FC cells were successfully transfected with *Nrcam*-HA, but there was no response to SHH or SAG even in the controls. By contrast, the NIH3T3-GL subline (Fig 5.11B) was SHH-responsive and able to express transfected *Nrcam*. For these reasons, NIH3T3-GL cells were used in subsequent studies.

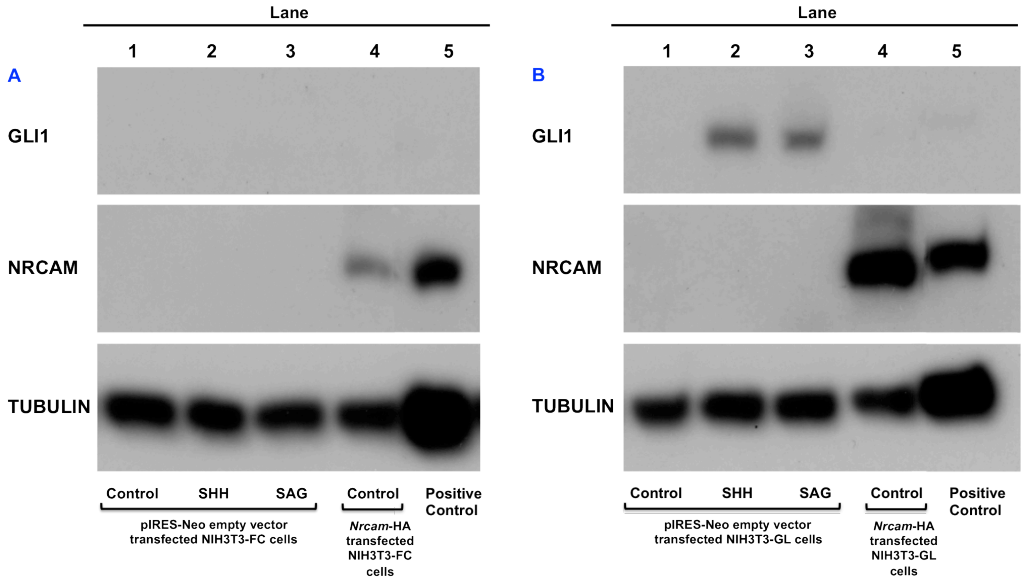

Fig. 5.11. Verification of GLI1 expression in NIH3T3-FC and NIH3T3-GL cells. Immunoblots with antibodies to GLI1, NRCAM and TUBULIN were used to access amount of protein in extracts from NIH3T3-FC and NIH3T3-GL cells, kindly provided from Dr. Frederic Charron (Montreal, Canada) and Associate Professor Stephane Angers (Toronto, Canada), transfected with *Nrcam*-HA and treated with SHH and SAG for 24 hours **(A)** Although the NIH3T3-FC cells were able to express NRCAM after *Nrcam*-HA transfection, they hardly showed GLI1 expression in response to SHH or SAG; whereas, **(B)** NIH3T3-GL cells can express more NRCAM after *Nrcam*-HA transfection and also showed more GLI1 response when SHH or SAG was added to the cells. Positive control is protein from mouse embryo at E13.5 (lane 7).

5.2.3.2 SHH signalling is not significantly affected in *Nrcam*-HA transfected NIH3T3-GL cells

To investigate whether NRCAM affects SHH signalling in NIH3T3-GL cells, I transfected *Nrcam*-HA after plating the cells for 24 hours. After 24-hour-transfection, the cells were serum-starved for 24 hours, followed by 4.5/24 hour-SHH or SAG treatment and then tested responses by evaluating GLI1 protein expression on western blots (see Methods, section 2.11). As shown in Fig 5.12, although there was not a significant induction of GLI1 protein 4.5 hours post-SHH/SAG treatment, there was a strong induction at 24 hours post-SHH/SAG treatment in both transfected and non-transfected *Nrcam*-HA NIH3T3-GL cells. The amount of GLI1 response was not significantly affected by NRCAM expression, however in both cases at 24 hours the trend was towards lowered GLI1 levels when NRCAM was present.

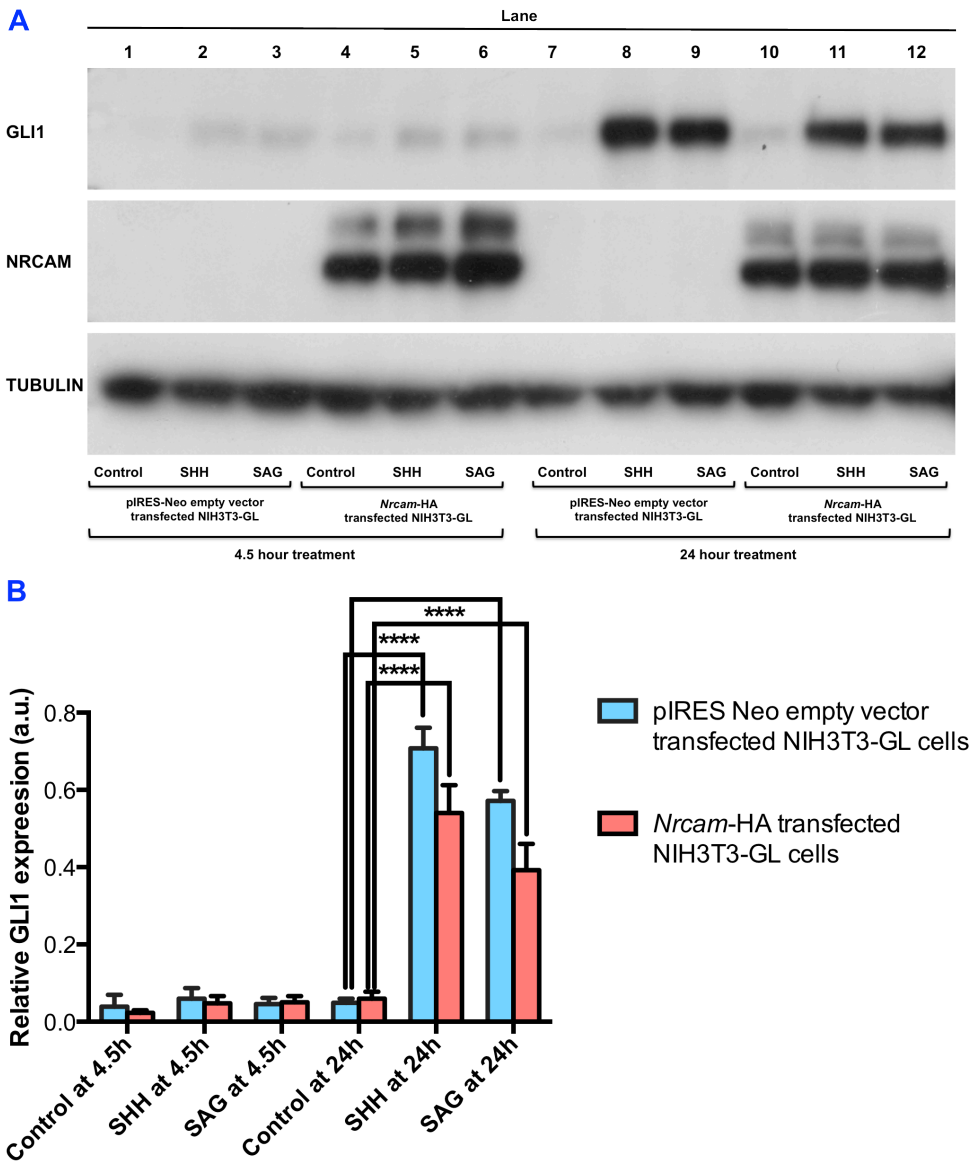

Fig 5.12. The Expression level of GLI1 in NIH3T3-GL cells after *Nrcam*-HA transfection. **(A)** Immunoblots of GLI1 protein after transfection of *Nrcam*-HA in NIH3T3-GL cells in response to SHH or SAG for 4.5 and 24 hours **(B)** Quantitation of GLI1 protein by densitometry of three independent immunoblots (3n) normalised to tubulin in the same lane. The data are graphed showing the Standard Error of the Mean (SEM) and tested for statistically significant differences among the control and treated samples using one-way ANOVA, followed by Bonferroni's post-test. The bar graphs show Mean±SEM. Confidence interval was set to 95%, with a *p*-value less than 0.05 taken as statistically significant. Statistical significances are indicated as asterisks; *: $p<0.05$, **: $p<0.01$, ***: $p<0.001$, ****: $p<0.0001$ and N.S.: not significant. **(C)** The different data groups were analysed using 1-way ANOVA and statistic details are shown in the tables.

C

One-way analysis of variance	
F value	49.34
P value	<0.0001
P value summary	****
Are differences among means statistically significant? (P<0.05)	Yes
R square	0.9577

Bonferroni's multiple comparisons test	Significant?	Summary	Adjusted P Value
pIRES Neo empty vector_ctrl at 4.5h vs. pIRES Neo empty vector_SHH at 4.5h	No	ns	> 0.9999
pIRES Neo empty vector_ctrl at 4.5h vs. pIRES Neo empty vector_SAG at 4.5h	No	ns	> 0.9999
pIRES Neo empty vector_ctrl at 4.5h vs. *Nrcam*-HA_ctrl at 4.5h	No	ns	> 0.9999
pIRES Neo empty vector_ctrl at 4.5h vs. *Nrcam*-HA_SHH at 4.5h	No	ns	> 0.9999
pIRES Neo empty vector_ctrl at 4.5h vs. *Nrcam*-HA_SAG at 4.5h	No	ns	> 0.9999
pIRES Neo empty vector_ctrl at 4.5h vs. pIRES Neo empty vector_ctrl at 24h	No	ns	> 0.9999
pIRES Neo empty vector_ctrl at 4.5h vs. pIRES Neo empty vector_SHH at 24h	Yes	****	< 0.0001
pIRES Neo empty vector_ctrl at 4.5h vs. pIRES Neo empty vector_SAG at 24h	Yes	****	< 0.0001
pIRES Neo empty vector_ctrl at 4.5h vs. *Nrcam*-HA_Ctrl at 24h	No	ns	> 0.9999
pIRES Neo empty vector_ctrl at 4.5h vs. *Nrcam*-HA_SHH at 24h	Yes	****	< 0.0001
pIRES Neo empty vector_ctrl at 4.5h vs. *Nrcam*-HA_SAG at 24h	Yes	****	< 0.0001
pIRES Neo empty vector_SHH at 4.5h vs. pIRES Neo empty vector_SAG at 4.5h	No	ns	> 0.9999
pIRES Neo empty vector_SHH at 4.5h vs. *Nrcam*-HA_ctrl at 4.5h	No	ns	> 0.9999
pIRES Neo empty vector_SHH at 4.5h vs. *Nrcam*-HA_SHH at 4.5h	No	ns	> 0.9999
pIRES Neo empty vector_SHH at 4.5h vs. *Nrcam*-HA_SAG at 4.5h	No	ns	> 0.9999
pIRES Neo empty vector_SHH at 4.5h vs. pIRES Neo empty vector_ctrl at 24h	No	ns	> 0.9999
pIRES Neo empty vector_SHH at 4.5h vs. pIRES Neo empty vector_SHH at 24h	Yes	****	< 0.0001
pIRES Neo empty vector_SHH at 4.5h vs. pIRES Neo empty vector_SAG at 24h	Yes	****	< 0.0001
pIRES Neo empty vector_SHH at 4.5h vs. *Nrcam*-HA_Ctrl at 24h	No	ns	> 0.9999
pIRES Neo empty vector_SHH at 4.5h vs. *Nrcam*-HA_SHH at 24h	Yes	****	< 0.0001
pIRES Neo empty vector_SHH at 4.5h vs. *Nrcam*-HA_SAG at 24h	Yes	****	< 0.0001
pIRES Neo empty vector_SAG at 4.5h vs. *Nrcam*-HA_ctrl at 4.5h	No	ns	> 0.9999
pIRES Neo empty vector_SAG at 4.5h vs. *Nrcam*-HA_SHH at 4.5h	No	ns	> 0.9999
pIRES Neo empty vector_SAG at 4.5h vs. *Nrcam*-HA_SAG at 4.5h	No	ns	> 0.9999
pIRES Neo empty vector_SAG at 4.5h vs. pIRES Neo empty vector_ctrl at 24h	No	ns	> 0.9999
pIRES Neo empty vector_SAG at 4.5h vs. pIRES Neo empty vector_SHH at 24h	Yes	****	< 0.0001
pIRES Neo empty vector_SAG at 4.5h vs. pIRES Neo empty vector_SAG at 24h	Yes	****	< 0.0001
pIRES Neo empty vector_SAG at 4.5h vs. *Nrcam*-HA_Ctrl at 24h	No	ns	> 0.9999
pIRES Neo empty vector_SAG at 4.5h vs. *Nrcam*-HA_SHH at 24h	Yes	****	< 0.0001
pIRES Neo empty vector_SAG at 4.5h vs. *Nrcam*-HA_SAG at 24h	Yes	****	< 0.0001
Nrcam-HA_ctrl at 4.5h vs. *Nrcam*-HA_SHH at 4.5h	No	ns	> 0.9999
Nrcam-HA_ctrl at 4.5h vs. *Nrcam*-HA_SAG at 4.5h	No	ns	> 0.9999
Nrcam-HA_ctrl at 4.5h vs. pIRES Neo empty vector_ctrl at 24h	No	ns	> 0.9999
Nrcam-HA_ctrl at 4.5h vs. pIRES Neo empty vector_SHH at 24h	Yes	****	< 0.0001
Nrcam-HA_ctrl at 4.5h vs. pIRES Neo empty vector_SAG at 24h	Yes	****	< 0.0001
Nrcam-HA_ctrl at 4.5h vs. *Nrcam*-HA_Ctrl at 24h	No	ns	> 0.9999
Nrcam-HA_ctrl at 4.5h vs. *Nrcam*-HA_SHH at 24h	Yes	****	< 0.0001
Nrcam-HA_ctrl at 4.5h vs. *Nrcam*-HA_SAG at 24h	Yes	****	< 0.0001
Nrcam-HA_SHH at 4.5h vs. *Nrcam*-HA_SAG at 4.5h	No	ns	> 0.9999
Nrcam-HA_SHH at 4.5h vs. pIRES Neo empty vector_ctrl at 24h	No	ns	> 0.9999
Nrcam-HA_SHH at 4.5h vs. pIRES Neo empty vector_SHH at 24h	Yes	****	< 0.0001
Nrcam-HA_SHH at 4.5h vs. pIRES Neo empty vector_SAG at 24h	Yes	****	< 0.0001
Nrcam-HA_SHH at 4.5h vs. *Nrcam*-HA_Ctrl at 24h	No	ns	> 0.9999
Nrcam-HA_SHH at 4.5h vs. *Nrcam*-HA_SHH at 24h	Yes	****	< 0.0001
Nrcam-HA_SHH at 4.5h vs. *Nrcam*-HA_SAG at 24h	Yes	****	< 0.0001
Nrcam-HA_SAG at 4.5h vs. pIRES Neo empty vector_ctrl at 24h	No	ns	> 0.9999
Nrcam-HA_SAG at 4.5h vs. pIRES Neo empty vector_SHH at 24h	Yes	****	< 0.0001
Nrcam-HA_SAG at 4.5h vs. pIRES Neo empty vector_SAG at 24h	Yes	****	< 0.0001
Nrcam-HA_SAG at 4.5h vs. *Nrcam*-HA_Ctrl at 24h	No	ns	> 0.9999
Nrcam-HA_SAG at 4.5h vs. *Nrcam*-HA_SHH at 24h	Yes	****	< 0.0001
Nrcam-HA_SAG at 4.5h vs. *Nrcam*-HA_SAG at 24h	Yes	****	< 0.0001
pIRES Neo empty vector_ctrl at 24h vs. pIRES Neo empty vector_SHH at 24h	**Yes**	****	**< 0.0001**
pIRES Neo empty vector_ctrl at 24h vs. pIRES Neo empty vector_SAG at 24h	**Yes**	****	**< 0.0001**
pIRES Neo empty vector_ctrl at 24h vs. *Nrcam*-HA_Ctrl at 24h	No	ns	> 0.9999
pIRES Neo empty vector_ctrl at 24h vs. *Nrcam*-HA_SHH at 24h	Yes	****	< 0.0001
pIRES Neo empty vector_ctrl at 24h vs. *Nrcam*-HA_SAG at 24h	Yes	****	< 0.0001
pIRES Neo empty vector_SHH at 24h vs. pIRES Neo empty vector_SAG at 24h	No	ns	> 0.9999
pIRES Neo empty vector_SHH at 24h vs. *Nrcam*-HA_Ctrl at 24h	Yes	****	< 0.0001
pIRES Neo empty vector_SHH at 24h vs. *Nrcam*-HA_SHH at 24h	**No**	**ns**	**0.2482**
pIRES Neo empty vector_SHH at 24h vs. *Nrcam*-HA_SAG at 24h	Yes	***	0.0002
pIRES Neo empty vector_SAG at 24h vs. *Nrcam*-HA_Ctrl at 24h	Yes	****	< 0.0001
pIRES Neo empty vector_SAG at 24h vs. *Nrcam*-HA_SHH at 24h	No	ns	> 0.9999
pIRES Neo empty vector_SAG at 24h vs. *Nrcam*-HA_SAG at 24h	**No**	**ns**	**0.1398**
***Nrcam*-HA_Ctrl at 24h vs. *Nrcam*-HA_SHH at 24h**	**Yes**	****	**< 0.0001**
***Nrcam*-HA_Ctrl at 24h vs. *Nrcam*-HA_SAG at 24h**	**Yes**	****	**< 0.0001**
Nrcam-HA_SHH at 24h vs. *Nrcam*-HA_SAG at 24h	No	ns	0.5905

5.3 Discussion

In this chapter, I attempted to investigate whether NRCAM has an effect on SHH signalling, by looking at both loss of NRCAM function in GNPs and gain of NRCAM function in NIH3T3-GL cells. The loss of function experiments in GNPs seemed to indicate that SHH signalling might be increased at 4.5 hours post-induction, but subsequently decreased at 24 hours post-induction. However, the gain of function experiment failed to demonstrate a significant effect of NRCAM overexpression on SHH signalling in NIH3T3-GL cells.

Although the results demonstrating that loss of NRCAM increased the *Gli1* transcription levels at 4.5 hours after addition of SHH are in agreement with the results from GLI fluorescent intensity at the same time point, I am still uncertain about the later time point results, in which the qPCR data showed that the *Gli1* transcription levels were decreased at 24 hours in response to SHH when NRCAM is missing, as one important data point, GLI1 fluorescent intensity after 24 hours of SHH addition to GNPs, was omitted. This clearly will need to be investigated further in the future. However, there are a few important points that I am able to discuss as follows.

5.3.1 Is SHH signalling really affected by loss of NRCAM?

Although the *Gli1* transcription levels were significantly affected when NRCAM is missing at early and late time points, my inability to demonstrate a significant induction of *Ptch1* gene expression by SHH, even when the results were also statistically post-tested by the Tukey test (data not shown), suggests that the qPCR assay may be inadequate, because *Ptch1* induction after SHH treatment has previously been reported in GNPs (Wechsler-Reya and Scott, 1999). Notably, our data showed that there was a high *Ptch1* induction even in the untreated WT control at 24 hours when compared with to that at 4.5 hours, which suggests that somehow *Ptch1* is being induced in our culture conditions. Although using Northern blotting rather than qPCR, Wechsler-Reya et al. also reported an increase in *Ptch1* expressions 24 hours after GNPs were treated with SHH at different time points, maximally at 24 hours, but interestingly they did not include a non-induced control at the later time point (Wechsler-Reya and Scott, 1999), making it unclear whether the induction of *Ptch1* was due solely to the addition of SHH. Indeed, it is known that GNPs will proliferate autonomously if plated at a sufficiently high density, most likely mediated by the Notch pathway (Solecki et al., 2001), and there is complex cross-talk between the SHH, Wnt

and Notch pathways (Behesti and Marino, 2009) that may contribute to this *Ptch1* activation. For this reason, *Ptch1* induction may not be the best readout of SHH signalling and indeed Ptch1 and Gli1 expression *in vivo* are not always exactly coincident (compare figure 2s in Corrales et al., 2004 and Lewis et al., 2004, for example). Nonetheless, although loss of NRCAM did not significantly affect *Ptch1* transcripts, it at least showed a trend towards induction of *Ptch1* at 4.5 and 24 hours SHH treatment (Fig 5.7), consistent with the *Gli1* transcription results (Figs 5.5).

Even though my results appear to show a significant effect on *Gli1* transcription levels of the loss of NRCAM, there are a number of technical caveats that should be taken into account. The first is that the experiments were set up in parallel each with its own standard curve derived from the untreated wild type GNPs control at 4.5 hour. Because there were not a sufficient number of wells to run every condition at the same time, I decided not to run the WT GNPs untreated control again, but to use the value from the standard curve. This means that the value of the WT GNPs untreated control at 4.5 hour is equal to 1 in every biological replication and there is, therefore, no variation in the control samples, which complicates comparisons to the other samples. I am aware that this was not the perfect way to perform the experiments and if I were to repeat this I would have used a separate cDNA to make the standard curve for each experiment.

The second caveat is that in light of the highly variable *Ptch1* results I obtained (see above), and similar variability in the results of other users assaying other cells and genes, the qPCR machine was re-calibrated shortly after I completed my experiments. A comparison of the reproducibility of the results across the PCR plate before and after the re-calibration demonstrated that the machine indeed showed considerable variability across the plate at the time I performed my *Ptch1* experiments (Fig. 5.13), which may also have affected the *Gli1* experiments done prior to that. As indicated above, we had had some doubts about the *Ptch1* data at the time and had tried to remove some outliers to correct for the variability, although the C_t variability remained high, even after these removals. Outliers were also removed from *Gli1* data (see methods, section 2.12.6), but to a much lesser extent than was the case for *Ptch1*. Unfortunately, lack of time has prevented me repeating these experiments. This variability may explain my inability to detect statistically significant variation

between samples despite the appearance of some suggestive trends in the results.

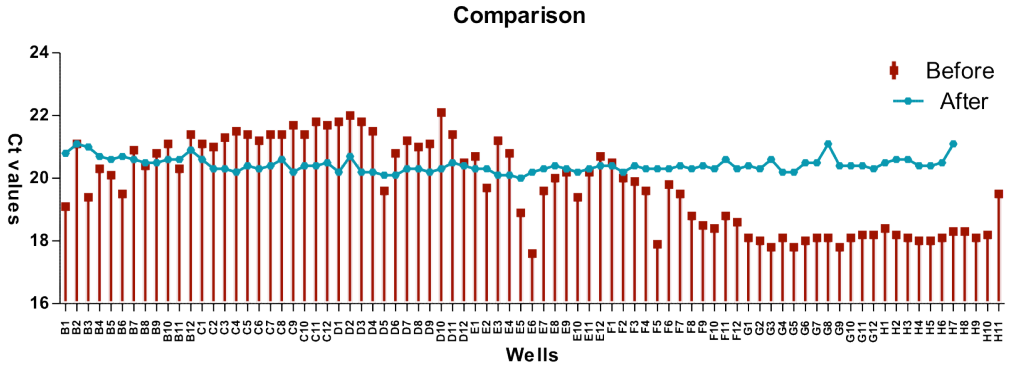

Fig 5.13. qPCR machine performances before and after standardization. The qPCR reactions were performed using the same sample in every well before and after qPCR machine servicing. Before machine standardization, the red graphs showed high variation between each sample; however, they looked more consistent after the qPCR machine was recently serviced and standardised (blue graphs). The qPCR reactions were performed by Sarah Jacob Eshtan and Milene Massucci Bissoli, PhD students in Rivolta lab, University of Sheffield.

Despite these caveats, a number of points suggest that loss of NRCAM does affect SHH signalling in GNPs: first, as shown in previous chapters, the absence of NRCAM affects the translocation of SMO and PTCH1 in cilia. Second, despite the lack of statistical proof, *Ptch1* transcription levels showed a trend in the same direction as that of *Gli1,* which was that when NRCAM is missing there appeared to be more *Gli1* and *Ptch1* transcripts at 4.5 hours, but less at 24 hours (Fig 5.5 and 5.7), suggesting that when NRCAM is missing, SHH signalling was increased at the early time point and yet decreased at 24 hours. An increase in SHH signalling at 4.5 hours with NRCAM loss is also consistent with that seen in the assay of GLI1 protein levels by anti-GLI1 fluorescence intensity of GNPs at 4.5 hours. Unfortunately, we do not know what occurs later because I ran out of time to perform the experiment at the later time point (24 hours).

In the gain of function study, I tested to see if NRCAM has any effect on SHH signalling by overexpressing it in NIH3T3-GL cells. The GLI1 induction was shown after 24 hours of SHH or SAG treatment, consistent with (Hillman et al.,

2011) in both non-transfected and NRCAM transfected NIH3T3-GL cells. However, I found that this SHH signalling was not significantly changed with NRCAM overexpression, although at 24 hour post-SHH induction, there was a trend to suggest that GLI1 expression might be decreasing.

This suggestive result from the gain function experiment might appear to contradict those from the loss of function of NRCAM experiments because in both cases SHH signalling seems to be reduced at 24 hours. However, there are a number of reasons that it is difficult to compare these results: Firstly, the experiments were performed in different cell types (GNPs and NIH3T3-GL cells). Although both of them respond to SHH (and SAG), it is not clear that they necessarily will respond in the same way. For example, it is known that different cell types express different combinations of accessory SHH-binding molecules that affect the SHH response (Tenzen et al., 2006, Izzi et al., 2011). Secondly, NIH3T3 cells not only do not express NRCAM, but they also are unlikely to express at least two ligands for NRCAM, TAG-1 and F3, which are expressed by GNPs. This may be important, as binding of these ligands appears to affect the response of GNPs to SHH (Xenaki et al., 2011). Lastly, it is also difficult to compare *Gli1* mRNA levels with GLI1 protein levels. Clearly it might have been better to have compared the same readout, whether this should have been mRNA transcription or protein expression is a good point for discussion as obviously the further downstream of the initial signalling monitors, the more opportunity there is for other regulation to occur.

Despite the difficulties discussed above, the results of this chapter seem to tentatively to suggest that *Nrcam*$^{-/-}$ GNPs, perhaps surprisingly, exhibit relatively more SHH signalling early on followed by a subsequent relative fall in signalling. Exactly, how these results are related to the results from the previous chapters and what this might mean will be discussed in the next chapter.

Chapter 6

General discussion

Despite considerable research into the area, how tissue and organ morphogenesis is regulated, particularly how growth is controlled is still not clearly understood. At an organismal level, hormones and growth factors (especially insulin-like growth factors; IGFs) in the circulation play an important role in size control, as do other extrinsic factors such as availability of nutrients. However, intrinsic mechanisms also limit growth and organs somehow 'know' when they reach the correct size (Leevers and McNeill, 2005). A central role in many tissues is played by the Hippo pathway intracellularly and, although extracellular secreted factors such as DPP/BMPs and Wnts impinge on its regulation, major regulation of the pathway appears to come from cell adhesion and cell polarity inputs (Zhao et al., 2011). Exactly how these inputs detect growth and size is not understood, but it is perhaps not surprising that cells are not simply programmed to undergo a specific number of cell divisions and then stop, but instead constantly receive inputs from their neighbors to enable them to proliferate and then differentiate in a co-ordinated manner. Understanding how this occurs is important for understanding development, cancer and tissue regeneration.

Previous work from our lab and others has strongly suggested that L1-CNTN adhesion molecules play a role in controlling the growth of the cerebellum. Sakurai et al. (2001) showed that *L1* and *Nrcam* null mice exhibit small reductions in the size of specific, yet distinct cerebellar lobules as single mutants, and that combination of these mutations results in severe cerebellar defects, including the reduction or disappearance of some fissures, a decrease of the thickness of IGL and a dramatic decrease in overall cerebellar size. This suggested the functional redundancy of L1 and NRCAM in cerebellar morphogenesis, most likely affecting granule cell development (Sakurai et al., 2001). Premature expression of F3/contactin – a ligand of L1 and NRCAM normally expressed only by post-mitotic granule neurons – on proliferating granule neuron progenitors, also suppressed cerebellar growth, albeit it transiently, and inhibited GNP proliferation *in vitro* (Bizzoca et al., 2003).

Our laboratory subsequently demonstrated that purified F3 protein can suppress SHH-induced GNP proliferation *in vitro* (Xenaki et al., 2011). Modulation of SHH can control both the shape and size of the cerebellum (Corrales et al., 2004, Corrales et al., 2006, Lewis et al., 2004). Although L1-CNTNs have been shown to modulate the proliferation of the progenitors of other cell types through Notch (F3 acting on oligodendrocytes; (Hu et al., 2003)) or Amyloid β precursor protein

(TAG-1 acting on cortical progenitors; (Ma et al., 2008), the results of Xenaki et al., strongly suggested that F3 has its effect through binding to NRCAM on the surface of GNPs. Therefore, the key question in this study is how L1-CNTNs function in regulating SHH activity.

Through the previous three chapters, several approaches were used to understand the mechanism underlying how NRCAM modulates SHH-induced proliferation of GNPs. The key findings in this study are summarised as follows: First, I showed for the first time that L1-CNTNs can be found located in the primary cilium. Second, I showed that loss of NRCAM from GNPs suppresses the translocation of PTCH1 out of the primary cilium of GNPs in response to SHH and also the subsequent translocation into the cilium of SMO. Third, my co-immunoprecipitation results indicate that NRCAM directly associates with PTCH1, but not SMO, consistent with the idea that NRCAM may be involved in the trafficking of PTCH1. Finally, my preliminary analysis of immediate early responses to SHH, notably induction of *Gli1* mRNA transcription, suggests that loss of NRCAM may affect the kinetics of the SHH response: Unexpectedly, SHH signalling in NRCAM null GNPs appeared to be increased at the early, 4.5-hour time point, at which I had previously seen an apparent failure of PTCH1 to leave, and of SMO to enter the primary cilium. However, by 24 hours, levels of *Gli1* mRNA were significantly less than in WT GNPs. The significance of these findings is discussed below.

6.1 The presence of NRCAM and TAG-1 in primary cilia of GNPs

Our immunofluorescence visualisation of NRCAM and TAG-1 in the primary cilium of GNPs is, as far as we are aware, the first direct imaging of this class of molecule in cilia. Although the specificity of antibodies is always to be treated with caution, especially when using polyclonal antibodies to molecules that belong to a closely related family, we have good reason to be confident that NRCAM is indeed present in GNP primary cilia, not least because the immunoreactivity we saw was not present in the cilia of *Nrcam*$^{-/-}$ GNPs (Fig 3.9B). Similarly, although we did not test GNPs from TAG-1 null animals, the 4D7 antibody is a monoclonal of well-characterised specificity (Furley et al., 1990) that is widely used.

There is, in fact, evidence from other sources that L1-CNTNs are present in cilia. For example, L1 can be found in the Blacque serial analysis of gene expression (SAGE) ciliome database (Blacque et al., 2005)

(http://www.sfu.ca/~leroux/ciliome_database.htm) and reviewed in (Inglis et al., 2006). That L1 might be involved in ciliary function is interesting since the L1 knockout mouse displays some of the characteristics of the ciliopathies, for example hydrocephalus and infertility (see also discussion, Chapter 3).

Perhaps surprisingly, F3 is reported to be present, among some 868 other proteins, in the primary cilia of choroid plexus epithelium cells (CPECs) (Narita et al., 2012). No role for F3 in choroid plexus (CP) function has been described and, although it is interesting to speculate whether the presence of an L1 ligand in the CP has anything to do with the hydrocephalus seen in L1 null mice. L1 also has not been reported to be expressed in the CP and indeed hydrocephalus is not associated with the F3-binding domains of L1 (Itoh et al., 2004).

The inclusion of F3 in the ciliome of CPECs but not, as I have shown, in that of cerebellar GNPs, makes the important point that the 'ciliome' is not a fixed set of proteins. However, there are clearly proteins common to most cilia (Inglis et al., 2006). Among these are a set of Rab GTPases that are involved in ciliary trafficking, including Rab5, Rab8, Rab10, Rab11 and Rab23, (Hsiao et al., 2012). Boehlke et al (2010) demonstrated that different Rabs have distinct functions. For example, trafficking of KIM1, an apical membrane receptor, but not SMO, is influenced by Rab5, whereas, Rab8 mediates ciliary protein transport of SMO, KIM1 and EB1, the microtubular tip protein. Rab23, a negative regulator of SHH signalling (Eggenschwiler et al., 2001), is known to be involved in regulating SMO levels (Boehlke et al., 2010). Babbey et al. showed that the colocalisation of Rab10 and Sec8, an exocyst protein, at the base of cilia in renal epithelial cells, together with the physical interaction of Rab10 and Sec8 suggests that Rab10 is associated with the membrane transport to the primary cilia (Babbey et al., 2010). Rab11 was originally identified as a key regulator of membrane trafficking from the trans-Golgi network and recycling endosome to the plasma membrane, but is also found enriched at the base of the primary cilium and suppression of its function affects primary ciliogenesis (Knodler et al., 2010, Das and Guo, 2011). Recent evidence also suggests that interacts genetically with *Smo* (Alvers et al., 2014). Interestingly, unpublished work from our lab (Dang and Furley, unpublished) suggests that in sensory growth cones, L1 recycles via the Rab11 recycling pathway, which is another potential link of L1-CNTNs to ciliary function.

My finding that NRCAM is present in primary cilia of purified P5 cerebellar GNPs is somewhat surprising, as these cells *in vivo* are mainly localised in the oEGL, where NRCAM immunostaining relatively weak (Xenaki et al., 2011). One possibility is that in these progenitor cells, its critical function occurs in cilia alone and therefore its overall low level of expression is not important so long as it is present in the cilia. Another possibility is that NRCAM expression in GNPs varies with the phase of the cell cycle, reflecting that the presence of the cilium on the cell is related to the cell cycle; the generation of primary cilia occurs in G1/G0 phase and the cilia is most obviously seen in S phase (Plotnikova et al., 2009). In this case, cells of the oEGL in other phases of the cell cycle may not express high levels of NRCAM explaining why the NRCAM expression is relatively weak in oEGL compared to IGL. However, arguing against this is the fact that NRCAM immunoreactivity on GNPs was present throughout the cell, not only in the primary cilia of GNPs, and there was no major variation in overall levels between cells in culture.

A more likely possibility is that NRCAM plays other roles in addition to its function in the SHH signalling pathway, after GNPs exit the cell cycle. In fact, most previous studies have focused on post-mitotic roles for NRCAM, although these were mainly based on antibody or overexpression perturbations of *in vitro* functions. Thus, for example, Sakurai et al. (2001) suggested that NRCAM and L1 are required for survival and neurite outgrowth of differentiated cells; although the survival and outgrowth of NRCAM-deficient granule cells was similar to WT cells, their survival and to a lesser extent their outgrowth was significantly diminished after addition of a function blocking anti-L1 antibody (Sakurai et al., 2001). Similarly, Davey et al (2005) demonstrated that neurite outgrowth from cerebellar granule cells in culture could be blocked by transfection of *Nrcam* constructs containing deletions of their intracellular domains, which were presumed therefore to be acting in a dominant negative manner (Davey et al., 2005). However, there is clear evidence that NRCAM has roles later in differentiation in the assembly of the Node of Ranvier (Feinberg et al., 2010).

The complexity of the interdependence between granule neurons, Bergmann glia and Purkinje cells (Vogel et al., 1989, Roussel and Hatten, 2011) and the evident redundancy between L1 and NRCAM makes dissecting which of these roles is most significant in producing the phenotype seen by Sakurai difficult. It seems unlikely that its role in Node of Ranvier formation plays a part in this.

While we cannot rule out that NRCAM may have a role either in GNP migration or axon outgrowth that in turn may affect GNP survival, my finding that NRCAM can be found in the primary cilia of proliferating GNPs is provocative and clearly suggests that NRCAM is important for progenitor responses to SHH.

6.2 NRCAM and the SHH pathway.

The presence of NRCAM in the cilium in the right time and in the right place to affect responses to SHH, led us to propose that NRCAM could play a role in either PTCH or SMO trafficking in primary cilia of GNPs. Exactly how either of these proteins is tranlocated to or from the cilium is controversial. Most is known about SMO: early studies showed its translocation to be dependent on the intraflagellar transport complex (May et al., 2005) and to be mediated by ß-arrestins, which appear to link SMO to the kinesin-2 motor complex via Kif3A (Kovacs et al., 2008). ß-arrestins are involved broadly in the internalisation of GPCRs (Lefkowitz et al., 2006) and so one model suggests SMO may be trafficked to the cilium from the membrane via Golgi or recycling derived vesicles present at the base of the cilium. However, using microscopy-based pulse-chase analysis, Melenkovic et al. (2009) showed that SMO can translocate from the NIH3T3 cell membrane to the primary cilia via the so-called lateral transport route, in which SMO in some way is passed directly from the plasma membrane to the ciliary membrane without being internalised. Interestingly, the same study demonstrates that although lateral transport appears to be immediate early route of SMO to the cilium, at later time points there is also a contribution from internalised vesicles (Milenkovic et al., 2009).

By contrast, much less is known about how PTCH translocates in the cilium. Early studies indicate that SHH gets internalised to endocytic vesicles after binding to PTCH1 (Incardona et al., 2000) and that in *Drosophila* HH internalisation is facilitated by the GPI-linked Dally-like protein (DLP), which is required for 'full-strength' HH signalling in the wing imaginal disc (Gallet et al., 2008). However, it is unclear that this is the mechanism by which PTCH is removed from the cilia in vertebrates (we speculated that there is physically no room for vesicle internalisation in the cilium because it has been shown that vesicles are not translocating into the cilium (Finetti et al., 2011)), rather than the mechanism by which accumulation of SHH is controlled, which is thought to be important in the creation of morphogen gradients (Briscoe and Therond, 2013).

My data demonstrates that NRCAM and PTCH1 can be co-immunoprecipitated when transfected into Cos-7 cells suggesting that they are closely associated in this context. That there is some specificity to this interaction was shown by the fact that SMO, also a multipass membrane receptor, does not co-IP with NRCAM. However, two other control proteins, TIE-2 and FGFR3, also co-immunoprecipitated with PTCH1, making us less confident of the significance of the interaction. On the other hand, PTCH and NRCAM are clearly both to be found co-localised in cilia, although this does not imply that they are interacting physically. Corroboration of this idea will require live cell imaging of the two molecules following SHH binding to determine whether NRCAM can be seen to segregate to the same intracellular vesicles as PTCH1.

6.3 Loss of NRCAM affects SHH signalling pathway

The results from the third and fourth chapters showed that loss of NRCAM affects the localisation of PTCH and SMO, and that NRCAM may interact with PTCH1, suggesting that NRCAM may play a role in SHH signalling. We therefore asked whether loss of NRCAM affects SHH signalling. Because loss of NRCAM led to a failure of PTCH to leave the cilium by 4.5 hours, we supposed that this would result in less signalling at the same time point. Unexpectedly, we found that in fact SHH signalling is significantly increased by loss of NRCAM at early time point, at least as judged by *Gli1* mRNA induction. However, after 24 hours of SHH treatment, SHH signalling levels were significantly lower than in WT GNPs.

In principle, PTCH translocation out of the primary cilium after SHH stimulation allows SMO to go into the cilium (Corbit et al., 2005, Rohatgi et al., 2007), leading to the generation of activator form of GLIs and stimulation of *Ptch1*, *Gli1* transcriptions (Wechsler-Reya and Scott, 1999). Here then, the question is why NRCAM null GNPs exhibit a failure of SMO ciliary localisation but show an increase in SHH signalling after addition of SHH for 4.5 hours, and then relatively lower SHH signalling after 24 hours. Corbit et al. showed that SMO localisation in primary cilia is required for SHH signalling (Corbit et al., 2005), however, in this study I demonstrated that SHH signalling is increased at 4.5 hours when the cells have low SMO ciliary localisation, but dropped at 24 hours in NRCAM knockout GNPs. Some possibilities to explain these results are as follows:

The first possible explanation could be that in these circumstances SHH is signalling via a noncanonical hedgehog signalling-type 1 (Jenkins, 2009), in which SHH can independently induce proliferation without SMO involvement and independent of transcriptional change of *Gli* transcriptional factors (Brennan et al., 2012). However, that this pathway is used seems unlikely as the *Nrcam*$^{-/-}$ GNPs definitely exhibited an initial increase in GLI1 induction at 4.5 SHH treatment.

The second possibility is that an increase in GLI1 expression at the early time point (4.5 hours after addition of SHH) could be due to the small amount of SMO that is found in the cilia of *Nrcam*$^{-/-}$ GNPs: around 12.04±3.64% of cilia are occupied by SMO irrespective of whether or not SHH is added (fig 3.9). However, this seems unlikely as the immunostaining studies showed that GLI1 protein expression is elevated in considerably more than just 12% of the GNPs from *Nrcam*$^{-/-}$ mice (Fig. 5.9).

The next possibility is that SMO does not need to be in the cilia to signal. Although the recent model of how SMO is activated in vertebrate SHH signalling suggests that this occurs inside primary cilia (Rohatgi and Scott, 2007), it remains unproven whether SMO might also be active outside the primary cilium. Indeed, recently, it has been shown that the localisation of SMO outside the primary cilium can mediate chemotaxis in response to SHH (Bijlsma et al., 2012). However, that this pathway is active in our *Nrcam*$^{-/-}$ GNP response seems unlikely, as this cilium-independent pathway does not activate GLI1 (Bijlsma et al., 2012).

Another possibility is that loss of NRCAM has affected the kinetics of PTCH1 and SMO ciliary trafficking. Previous work from our lab and others has shown that changing the complement of L1-CNTNs present in the cell can change the endocytosis and re-cycling of associated cell surface molecules (Dang et al., 2012). Thus, we might speculate that loss of NRCAM leads to a more rapid turnover of PTCH1 and that the apparent failure of PTCH1 to leave the cilium in NRCAM null GNPs after 4.5 hours actually reflects that an initial phase of signalling has been completed but instead of SMO remaining stably in the cilium it has turned over and been replaced by a new lot of PTCH1. This would be consistent with the fact that we still see SHH signalling being generated at the early time point in NRCAM knockout GNPs.

In fact, 4.5 hours is a relatively long time in terms of receptor recycling, indeed some receptors, for example the neuropilins, can return to the cell surface within minutes of ligand binding (Piper et al., 2005). Looking at SMO and PTCH1 localisation at earlier time points would help to determine whether this hypothesis is correct.

Why, in this case, SMO would be unstable in the cilium is not clear, but one possibility is that this reflects the different pools of SMO that were found to enter the cilium after SHH treatment by Milenkovic et al (2009). Interestingly, SMO entering the cilium by lateral transport from the plasma membrane peaked 1 hour after SHH treatment and was subsequently replaced by SMO derived from intracellular sources (Milenkovic et al., 2009). If NRCAM somehow affects the second wave of SMO entry, not the first, this may explain why SHH signalling is not sustained at the 24- hour time point in NRCAM null GNPs.

Another consideration is whether the level of SHH used to stimulate the cells affects the translocation behaviour of SMO. In my experiments, the level of SHH I used was determined by titrating SHH with GNPs and using the minimum concentration required to drive maximal proliferation of GNPs after 24 hours of treatment, rather than that required to drive maximal expression of *Ptch* and *Gli1*. This equated to about 30nM of recombinant SHH (R&D; see Methods). By comparison, Wechsler-Reya and Scott used 150 nM SHH to investigate SHH-induced proliferation of GNP response at 48 hours and showed maximal *Ptch* and *Gli* expressions at 24 hours upon the addition of SHH (Wechsler-Reya and Scott, 1999). Clearly, the SHH concentration that we used was relatively lower and exposure time of the GNPs to SHH shorter at the time proliferation was measured (24 hours versus 48 hours). This might affect the level of *Gli1* and *Ptch1* responses, because the exposure time of SHH and the level of SHH ligand available to the cells are key factors that influence the response of SHH (Dessaud et al., 2007).

As far as we are aware, no one has determined the minimum levels of SHH required to induce SMO translocation into the cilium and, indeed, the levels of SHH used in the key study of SMO translocation are not precisely specified (Rohatgi et al., 2007), making this hard to relate to our own work. Thus, although it is established that cilial function is required for full activation of SHH signalling (Corbit et al., 2005), it remains possible that some SHH signalling can occur without SMO translocation. An important proof of the requirement for SMO

to translocate to cilia in order for Gli1 to be activated was the failure of a ciliary localisation defective mutant of SMO (CLDSmo) to induce Gli1 expression (Corbit et al., 2005). However, we note that in this case Gli1 expression was monitored 18 hours after SHH addition. In *Nrcam*$^{-/-}$ GNPs, although we saw a sizeable induction of Gli1 4.5 hours after SHH addition, by 24 hours Gli1 expression was not significantly different to control and substantially less than WT (Fig 5.5). Further studies in these differing systems, with more precisely controlled times and levels of SHH signalling, will be required to establish whether in fact some signalling can be generated without the necessity for SMO translocation to the cilium.

A further complication is that we observed that *Ptch* and *Gli1* expression was not always exactly coincident, consistent with the observations of others (Rios et al., 2004, Bermudez et al., 2013). Thus, it is possible that the Gli1 expression we see also does not reflect the initiation of full activation of SHH signalling. The use additional targets of SHH signalling, such as *Nmyc* (Kenney et al., 2003, Oliver et al., 2003), would help to confirm the significance of these results.

Another question that arises is why the NRCAM null GNPs appear still to proliferate in response to SHH (Xenaki et al., 2011). In fact, this may reflect the early *Gli1* induction that I have described. Because the SHH signal is not sustained, we might have expected that the level of proliferation induction would have been less than in WT. In fact, we have not yet made a careful comparison with wild type, so this is still possible and my lab is currently doing experiments to determine this. An alternative possibility is that even if the level is the same, it is still possible that this reflects the involvement of NRCAM in an unknown pathway to enhance the SHH-induced proliferation of GNPs. For example, Insulin Growth Factor (IGF) has been shown that it can potentiate cell proliferation as IGF signalling synergises with SHH signalling. Moreover, IGF-1 and IGF2-induced proliferations are not dependent on the function of SMO (Fernandez et al., 2010) (see Introduction, section 1.4.5.1). Although, this can explain why the GNPs can proliferate without SMO entry to primary cilia and why NRCAM knockout mice are not lethal, there is no evidence to suggest that NRCAM is involved in the IGF signalling pathway. In addition, it is not clear how IGF signalling would result in *Gli1* mRNA induction.

Of particular interest is that two candidate proteins that have been shown to affect the strength of SHH signalling are Neuropilins 1 and 2 (NRPs) (Hillman et

al., 2011), to which L1 and NRCAM have been shown to bind respectively (Falk et al., 2005). Although Hillman et al. did not address whether the time course of SHH pathway activation was different when NRP expression was inhibited, the strength of the signal was significantly reduced after 24 hours of SHH treatment if *Nrp* mRNA translation was inhibited. Interestingly, NRP1 levels are induced by SHH but at a later time point than PTCH1, suggesting a positive feedback loop is indirectly activated. We therefore speculate that NRCAM and NRPs may together be involved in modulating SHH signalling. Interestingly, preliminary results from Matthew Scott's lab suggest that, although there is no effect on SMO translocation, there may be a subtle effect of *Nrp* knockdown in NIH3T3 cells on the movement of PTCH1 out of the cilium (Xuecai Ge, Pers. Comm.).

Therefore future experiments will aim to test whether NRCAM works together with NRP1/NRP2 in SHH pathway. In GNPs we will look for co-localisation of NRPs with NRCAM and with PTCH1 and/or SMO. PTCH1 and SMO ciliary localisation will also be determined both earlier than 4.5 hours (see above) and after 24 hour SHH treatment to see whether the response is simply delayed, or whether SMO continues to be excluded from cilia in the *Nrcam*$^{-/-}$ GNPs. These sets of future experiment might provide evidence to clearly explain why loss of NRCAM increases SHH signalling at early time point but not later and whether NRCAM works with NRPs.

Our working model of how NRCAM might be involved in SHH signalling in the primary cilium is depicted in Fig. 6.1. We are biased towards NRCAM interacting with PTCH1, partly because of my demonstration that PTCH1 can co-immunoprecipitate with NRCAM, but also because PTCH1 fails to leave the cilium in the NRCAM null GNPs; if NRCAM was regulating SMO entry it is not clear why this would affect PTCH1 exit. However, clearly there are complex feedback pathways at work in the SHH response, so it remains possible that NRCAM controls the access of one or all of the proposed pools of SMO to the cilium, either partly or completely. It is also possible that L1 is involved in ths process, since it also can bind neuropilins and F3 (Falk et al., 2005). To date our protein expression and F3-binding data do not support a role for L1 in controlling events prior to cell cycle exit (Xenaki et al., 2011), but given that NRCAM was originally said not to be on proliferating GNPs (Sakurai et al., 2001), we may need to test this more rigourously. Overall, we expect that more detailed observation of the localisation of the relevant proteins will clarify which of these possibilities is most relevant.

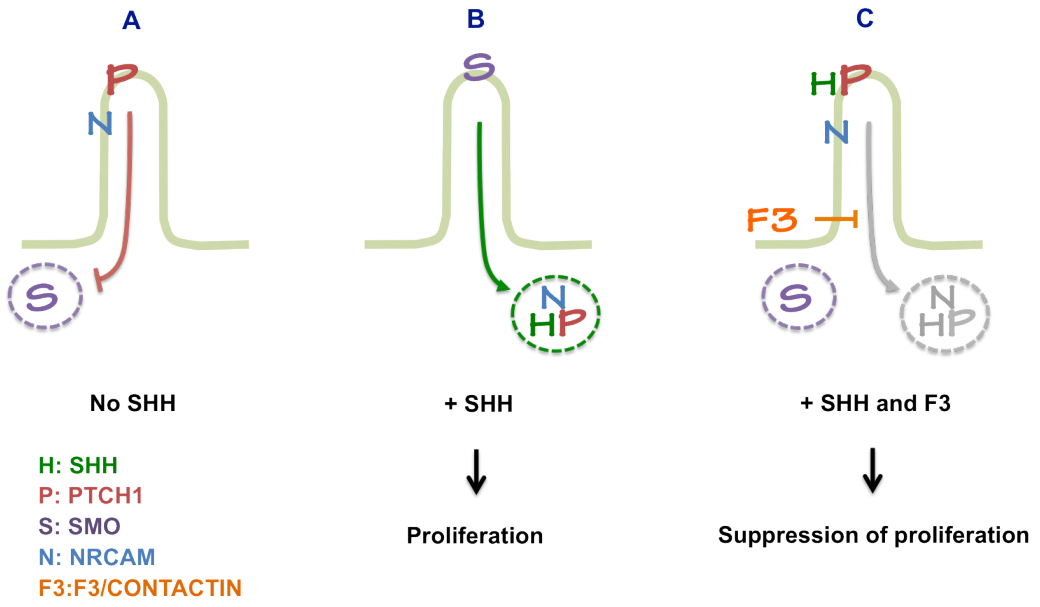

Fig 6.1. Proposed model of the interaction of NRCAM and PTCH1 mediates the translocation of PTCH1 in primary cilia. **(A)** In the absence of SHH, the ciliary localisation of PTCH1 inhibits SMO translocating to the primary cilium, resulting in no transcription of SHH target genes. **(B)** In the presence of SHH, NRCAM, interacting with PTCH1 mediates the translocation of SHH and PTCH1 complex out of the primary cilium and this allows SMO entry to the cilium, leading to the transcription of SHH target genes and proliferation. **(C)** In the presence of SHH and F3, F3 inhibits the translocation of SHH and PTCH1 complex out of the primary cilium, resulting in suppression of proliferation.

6.4 Concluding remarks and future perspectives

We showed here the novel role of NRCAM in primary cilium of GNP and the requirement of NRCAM for the ciliary localisations of SHH components, PTCH1 and SMO. An interaction of PTCH1 and NRCAM in transfected cells was also demonstrated. My preliminary results also suggest that SHH signalling is significantly increased by loss of NRCAM at the early time point but subsequently strongly diminished. We propose a model of how NRCAM is involved in PTCH1 trafficking out of the cilium and speculate that NRPs might participate in the kinetics of NRCAM-mediated SHH signalling. Future works will focus on the kinetics of translocation of SHH protein components in the primary cilia of GNPs. Live cell imaging need to be performed to determine whether NRCAM really interacts with PTCH1 in the cell and translocate PTCH1 out of cilium, how fast this occurs when the cell response to SHH and to investigate if

and how NRPs are involved in this situation. Although our results seem to suggest that NRCAM physically interacted with PTCH1 not SMO, we do not know what happens to downstream SHH signalling targets, such as SuFu, and GLIs, and whether loss of NRCAM also affects them. Given that we have evidence of NRCAM affecting SHH signalling, it will also be interesting to investigate whether there is a genetic interaction of *Nrcam* and *Shh in vivo*. We hope that the discovery of the role of L1-CNTNs in modulating SHH signaling could lead to novel potential treatments for MB in the future.

References

AGIC, A., VON WUSSOW, U., STARZINSKI-POWITZ, A., DIEDRICH, K., ALTEVOGT, P. & HORNUNG, D. 2010. Inhibition of cell proliferation, adhesion, and invasion with an anti-L1-cell adhesion molecule monoclonal antibody in an in vitro endometriosis model. *Fertility and sterility,* 94**,** 1102-4.

ALDER, J., LEE, K. J., JESSELL, T. M. & HATTEN, M. E. 1999. Generation of cerebellar granule neurons in vivo by transplantation of BMP-treated neural progenitor cells. *Nature neuroscience,* 2**,** 535-40.

ALIEVA, I. B. & VOROBJEV, I. A. 2004. Vertebrate primary cilia: a sensory part of centrosomal complex in tissue cells, but a "sleeping beauty" in cultured cells? *Cell biology international,* 28**,** 139-50.

ALTMAN, J. & BAYER, S. A. 1997. Development of the Cerebellar System: in Relation to Its Evolution, Structure and Functions.

ALVERS, A. L., RYAN, S., SCHERZ, P. J., HUISKEN, J. & BAGNAT, M. 2014. Single continuous lumen formation in the zebrafish gut is mediated by smoothened-dependent tissue remodeling. *Development,* 141**,** 1110-9.

ANNE, S. L., GOVEK, E. E., AYRAULT, O., KIM, J. H., ZHU, X., MURPHY, D. A., VAN AELST, L., ROUSSEL, M. F. & HATTEN, M. E. 2013. WNT3 Inhibits Cerebellar Granule Neuron Progenitor Proliferation and Medulloblastoma Formation via MAPK Activation. *PloS one,* 8**,** e81769.

ARLT, M. J., NOVAK-HOFER, I., GAST, D., GSCHWEND, V., MOLDENHAUER, G., GRUNBERG, J., HONER, M., SCHUBIGER, P. A., ALTEVOGT, P. & KRUGER, A. 2006. Efficient inhibition of intra-peritoneal tumor growth and dissemination of human ovarian carcinoma cells in nude mice by anti-L1-cell adhesion molecule monoclonal antibody treatment. *Cancer research,* 66**,** 936-43.

BABBEY, C. M., BACALLAO, R. L. & DUNN, K. W. 2010. Rab10 associates with primary cilia and the exocyst complex in renal epithelial cells. *American journal of physiology. Renal physiology,* 299**,** F495-506.

BALASKAS, N., RIBEIRO, A., PANOVSKA, J., DESSAUD, E., SASAI, N., PAGE, K. M., BRISCOE, J. & RIBES, V. 2012. Gene regulatory logic for reading the Sonic Hedgehog signaling gradient in the vertebrate neural tube. *Cell,* 148**,** 273-84.

BAPTISTA, C. A., HATTEN, M. E., BLAZESKI, R. & MASON, C. A. 1994. Cell-cell interactions influence survival and differentiation of purified Purkinje cells in vitro. *Neuron,* 12**,** 243-60.

BARAKAT, B., YU, L., LO, C., VU, D., DE LUCA, E., CAIN, J. E., MARTELLOTTO, L. G., DEDHAR, S., SADLER, A. J., WANG, D., WATKINS, D. N. & HANNIGAN, G. E. 2013. Interaction of smoothened with integrin-linked kinase in primary cilia mediates Hedgehog signalling. *EMBO reports*.

BEHESTI, H. & MARINO, S. 2009. Cerebellar granule cells: insights into proliferation, differentiation, and role in medulloblastoma pathogenesis. *Int J Biochem Cell Biol,* 41**,** 435-45.

BERBARI, N. F., BISHOP, G. A., ASKWITH, C. C., LEWIS, J. S. & MYKYTYN, K. 2007. Hippocampal neurons possess primary cilia in culture. *Journal of neuroscience research,* 85**,** 1095-100.

BERGLUND, E. O., MURAI, K. K., FREDETTE, B., SEKERKOVA, G., MARTURANO, B., WEBER, L., MUGNAINI, E. & RANSCHT, B. 1999. Ataxia and abnormal cerebellar microorganization in mice with ablated contactin gene expression. *Neuron,* 24**,** 739-50.

BERMUDEZ, O., HENNEN, E., KOCH, I., LINDNER, M. & EICKELBERG, O. 2013. Gli1 mediates lung cancer cell proliferation and Sonic Hedgehog-dependent mesenchymal cell activation. *PloS one,* 8**,** e63226.

BIGNAMI, A., ENG, L. F., DAHL, D. & UYEDA, C. T. 1972. Localization of the glial fibrillary acidic protein in astrocytes by immunofluorescence. *Brain research,* 43**,** 429-35.

BIJLSMA, M. F., DAMHOFER, H. & ROELINK, H. 2012. Hedgehog-stimulated chemotaxis is mediated by smoothened located outside the primary cilium. *Science signaling,* 5**,** ra60.

BITGOOD, M. J., SHEN, L. & MCMAHON, A. P. 1996. Sertoli cell signaling by Desert hedgehog regulates the male germline. *Current biology : CB,* 6**,** 298-304.

BIZZOCA, A., CORSI, P., POLIZZI, A., PINTO, M. F., XENAKI, D., FURLEY, A. J. & GENNARINI, G. 2012. F3/Contactin acts as a modulator of neurogenesis during cerebral cortex development. *Developmental biology,* 365**,** 133-51.

BIZZOCA, A., VIRGINTINO, D., LORUSSO, L., BUTTIGLIONE, M., YOSHIDA, L., POLIZZI, A., TATTOLI, M., CAGIANO, R., ROSSI, F., KOZLOV, S., FURLEY, A. & GENNARINI, G. 2003. Transgenic mice expressing F3/contactin from the TAG-1 promoter exhibit developmentally regulated changes in the differentiation of cerebellar neurons. *Development,* 130**,** 29-43.

BLACQUE, O. E., PERENS, E. A., BOROEVICH, K. A., INGLIS, P. N., LI, C., WARNER, A., KHATTRA, J., HOLT, R. A., OU, G., MAH, A. K., MCKAY, S. J., HUANG, P., SWOBODA, P., JONES, S. J., MARRA, M. A., BAILLIE, D. L., MOERMAN, D. G., SHAHAM, S. & LEROUX, M. R. 2005. Functional genomics of the cilium, a sensory organelle. *Current biology : CB,* 15**,** 935-41.

BLAESS, S., GRAUS-PORTA, D., BELVINDRAH, R., RADAKOVITS, R., PONS, S., LITTLEWOOD-EVANS, A., SENFTEN, M., GUO, H., LI, Y., MINER, J. H., REICHARDT, L. F. & MULLER, U. 2004. Beta1-integrins are critical for cerebellar granule cell precursor proliferation. *J Neurosci,* 24**,** 3402-12.

BODENANT, C., LAQUERRIERE, A., PARESY, M., HEMET, J., VAUDRY, H. & LEROUX, P. 1997. Somatostatin does not affect multiplication of granule cells in the rat cerebellum. *Peptides,* 18**,** 257-62.

BOEHLKE, C., BASHKUROV, M., BUESCHER, A., KRICK, T., JOHN, A. K., NITSCHKE, R., WALZ, G. & KUEHN, E. W. 2010. Differential role of Rab proteins in ciliary trafficking: Rab23 regulates smoothened levels. *Journal of cell science,* 123**,** 1460-7.

BOOKOUT, A. L., CUMMINS, C. L., MANGELSDORF, D. J., PESOLA, J. M. & KRAMER, M. F. 2006. High-throughput real-time quantitative reverse transcription PCR. *Current protocols in molecular biology / edited by Frederick M. Ausubel ... [et al.],* Chapter 15**,** Unit 15 8.

BOYLE, M. E., BERGLUND, E. O., MURAI, K. K., WEBER, L., PELES, E. & RANSCHT, B. 2001. Contactin orchestrates assembly of the septate-like junctions at the paranode in myelinated peripheral nerve. *Neuron,* 30**,** 385-97.

BRAILOV, I., BANCILA, M., BRISORGUEIL, M. J., MIQUEL, M. C., HAMON, M. & VERGE, D. 2000. Localization of 5-HT(6) receptors at the plasma membrane of neuronal cilia in the rat brain. *Brain research,* 872**,** 271-5.

BRENNAN, D., CHEN, X., CHENG, L., MAHONEY, M. & RIOBO, N. A. 2012. Noncanonical Hedgehog signaling. *Vitamins and hormones,* 88**,** 55-72.

BRISCOE, J. 2009. Making a grade: Sonic Hedgehog signalling and the control of neural cell fate. *The EMBO journal,* 28**,** 457-65.

BRISCOE, J. & THEROND, P. P. 2013. The mechanisms of Hedgehog signalling and its roles in development and disease. *Nature reviews. Molecular cell biology,* 14**,** 416-29.

BRUMMENDORF, T. & LEMMON, V. 2001. Immunoglobulin superfamily receptors: cis-interactions, intracellular adapters and alternative splicing regulate adhesion. *Current opinion in cell biology,* 13**,** 611-8.

BRUMMENDORF, T. & RATHJEN, F. G. 1995. Cell adhesion molecules 1: immunoglobulin superfamily. *Protein Profile,* 2**,** 963-1108.

BYRD, N., BECKER, S., MAYE, P., NARASIMHAIAH, R., ST-JACQUES, B., ZHANG, X., MCMAHON, J., MCMAHON, A. & GRABEL, L. 2002. Hedgehog is required for murine yolk sac angiogenesis. *Development,* 129**,** 361-72.

CANTAGREL, V., SILHAVY, J. L., BIELAS, S. L., SWISTUN, D., MARSH, S. E., BERTRAND, J. Y., AUDOLLENT, S., ATTIE-BITACH, T., HOLDEN, K. R., DOBYNS, W. B., TRAVER, D., AL-GAZALI, L., ALI, B. R., LINDNER, T. H., CASPARY, T., OTTO, E. A., HILDEBRANDT, F., GLASS, I. A., LOGAN, C. V., JOHNSON, C. A., BENNETT, C., BRANCATI, F., VALENTE, E. M., WOODS, C. G. & GLEESON, J. G. 2008. Mutations in the cilia gene ARL13B lead to the classical form of Joubert syndrome. *American journal of human genetics,* 83**,** 170-9.

CAPARROS-MARTIN, J. A., VALENCIA, M., REYTOR, E., PACHECO, M., FERNANDEZ, M., PEREZ-AYTES, A., GEAN, E., LAPUNZINA, P., PETERS, H., GOODSHIP, J. A. & RUIZ-PEREZ, V. L. 2013. The ciliary Evc/Evc2 complex interacts with Smo and controls Hedgehog pathway activity in chondrocytes by regulating Sufu/Gli3 dissociation and Gli3 trafficking in primary cilia. *Human molecular genetics,* 22**,** 124-39.

CARLOTTI, C. G., JR., SMITH, C. & RUTKA, J. T. 2008. The molecular genetics of medulloblastoma: an assessment of new therapeutic targets. *Neurosurgical review,* 31**,** 359-68; discussion 368-9.

CARPENTER, D., STONE, D. M., BRUSH, J., RYAN, A., ARMANINI, M., FRANTZ, G., ROSENTHAL, A. & DE SAUVAGE, F. J. 1998. Characterization of two patched receptors for the vertebrate hedgehog protein family. *Proceedings of the National Academy of Sciences of the United States of America,* 95**,** 13630-4.

CASTELLANI, V., FALK, J. & ROUGON, G. 2004. Semaphorin3A-induced receptor endocytosis during axon guidance responses is mediated by L1 CAM. *Molecular and cellular neurosciences,* 26**,** 89-100.

CHEN, J. K., TAIPALE, J., YOUNG, K. E., MAITI, T. & BEACHY, P. A. 2002. Small molecule modulation of Smoothened activity. *Proceedings of the National Academy of Sciences of the United States of America,* 99**,** 14071-6.

CHEN, W., BURGESS, S. & HOPKINS, N. 2001. Analysis of the zebrafish smoothened mutant reveals conserved and divergent functions of hedgehog activity. *Development,* 128**,** 2385-96.

CHEN, W., REN, X. R., NELSON, C. D., BARAK, L. S., CHEN, J. K., BEACHY, P. A., DE SAUVAGE, F. & LEFKOWITZ, R. J. 2004. Activity-dependent internalization of smoothened mediated by beta-arrestin 2 and GRK2. *Science,* 306**,** 2257-60.

CHEN, Y. & STRUHL, G. 1996. Dual roles for patched in sequestering and transducing Hedgehog. *Cell,* 87**,** 553-63.

CHEUNG, H. O., ZHANG, X., RIBEIRO, A., MO, R., MAKINO, S., PUVIINDRAN, V., LAW, K. K., BRISCOE, J. & HUI, C. C. 2009. The kinesin protein Kif7 is a critical regulator of Gli transcription factors in mammalian hedgehog signaling. *Science signaling,* 2**,** ra29.

CHIANG, C., LITINGTUNG, Y., LEE, E., YOUNG, K. E., CORDEN, J. L., WESTPHAL, H. & BEACHY, P. A. 1996. Cyclopia and defective axial patterning in mice lacking Sonic hedgehog gene function. *Nature,* 383**,** 407-13.

CHINTAGUMPALA, M., BERG, S. & BLANEY, S. M. 2001. Treatment controversies in medulloblastoma. *Current opinion in oncology,* 13**,** 154-9.

CHIZHIKOV, V. V., DAVENPORT, J., ZHANG, Q., SHIH, E. K., CABELLO, O. A., FUCHS, J. L., YODER, B. K. & MILLEN, K. J. 2007. Cilia proteins control cerebellar morphogenesis by promoting expansion of the granule progenitor pool. *The Journal of neuroscience : the official journal of the Society for Neuroscience,* 27**,** 9780-9.

COHEN, N. R., TAYLOR, J. S., SCOTT, L. B., GUILLERY, R. W., SORIANO, P. & FURLEY, A. J. 1998. Errors in corticospinal axon guidance in mice lacking the neural cell adhesion molecule L1. *Current biology : CB,* 8**,** 26-33.

CONACCI-SORRELL, M. E., BEN-YEDIDIA, T., SHTUTMAN, M., FEINSTEIN, E., EINAT, P. & BEN-ZE'EV, A. 2002. Nr-CAM is a target gene of the beta-catenin/LEF-1 pathway in melanoma and colon cancer and its expression enhances motility and confers tumorigenesis. *Genes & development,* 16**,** 2058-72.

CORBIT, K. C., AANSTAD, P., SINGLA, V., NORMAN, A. R., STAINIER, D. Y. & REITER, J. F. 2005. Vertebrate Smoothened functions at the primary cilium. *Nature,* 437**,** 1018-21.

CORRALES, J. D., BLAESS, S., MAHONEY, E. M. & JOYNER, A. L. 2006. The level of sonic hedgehog signaling regulates the complexity of cerebellar foliation. *Development,* 133**,** 1811-21.

CORRALES, J. D., ROCCO, G. L., BLAESS, S., GUO, Q. & JOYNER, A. L. 2004. Spatial pattern of sonic hedgehog signaling through Gli genes during cerebellum development. *Development,* 131**,** 5581-90.

DAHMANE, N. & RUIZ I ALTABA, A. 1999. Sonic hedgehog regulates the growth and patterning of the cerebellum. *Development,* 126**,** 3089-100.

DALE PURVES, G. J. A., DAVID FITZPATRICK, LAWRENCE C KATZ, ANTHONY-SAMUEL LAMANTIA, JAMES O MCNAMARA, AND S MARK WILLIAMS 2001. *Neuroscience,* Sunderland (MA), Sinauer Associates.

DANG, P., SMYTHE, E. & FURLEY, A. J. 2012. TAG1 regulates the endocytic trafficking and signaling of the semaphorin3A receptor complex. *The Journal of neuroscience : the official journal of the Society for Neuroscience,* 32**,** 10370-82.

DAS, A. & GUO, W. 2011. Rabs and the exocyst in ciliogenesis, tubulogenesis and beyond. *Trends in cell biology,* 21**,** 383-6.

DAVEY, F., HILL, M., FALK, J., SANS, N. & GUNN-MOORE, F. J. 2005. Synapse associated protein 102 is a novel binding partner to the cytoplasmic terminus of neurone-glial related cell adhesion molecule. *Journal of neurochemistry,* 94**,** 1243-53.

DECKER, L., BARON, W. & FFRENCH-CONSTANT, C. 2004. Lipid rafts: microenvironments for integrin-growth factor interactions in neural development. *Biochemical Society transactions,* 32**,** 426-30.

DEL CERRO, M. P. & SNIDER, R. S. 1972. Studies on the developing cerebellum. II. The ultrastructure of the external granular layer. *The Journal of comparative neurology,* 144**,** 131-64.

DESSAUD, E., YANG, L. L., HILL, K., COX, B., ULLOA, F., RIBEIRO, A., MYNETT, A., NOVITCH, B. G. & BRISCOE, J. 2007. Interpretation of the sonic hedgehog morphogen gradient by a temporal adaptation mechanism. *Nature,* 450**,** 717-20.

DHALL, G. 2009. Medulloblastoma. *Journal of child neurology,* 24**,** 1418-30.

DIHNE, M., BERNREUTHER, C., SIBBE, M., PAULUS, W. & SCHACHNER, M. 2003. A new role for the cell adhesion molecule L1 in neural precursor cell proliferation, differentiation, and transmitter-specific subtype generation. *The Journal of neuroscience : the official journal of the Society for Neuroscience,* 23**,** 6638-50.

DZHASHIASHVILI, Y., ZHANG, Y., GALINSKA, J., LAM, I., GRUMET, M. & SALZER, J. L. 2007. Nodes of Ranvier and axon initial segments are ankyrin G-dependent domains that assemble by distinct mechanisms. *The Journal of cell biology,* 177**,** 857-70.

EGGENSCHWILER, J. T., ESPINOZA, E. & ANDERSON, K. V. 2001. Rab23 is an essential negative regulator of the mouse Sonic hedgehog signalling pathway. *Nature,* 412**,** 194-8.

ENDOH-YAMAGAMI, S., EVANGELISTA, M., WILSON, D., WEN, X., THEUNISSEN, J. W., PHAMLUONG, K., DAVIS, M., SCALES, S. J., SOLLOWAY, M. J., DE SAUVAGE, F. J. & PETERSON, A. S. 2009. The mammalian Cos2 homolog Kif7 plays an essential role in modulating Hh signal transduction during development. *Current biology : CB,* 19**,** 1320-6.

ENGELKAMP, D., RASHBASS, P., SEAWRIGHT, A. & VAN HEYNINGEN, V. 1999. Role of Pax6 in development of the cerebellar system. *Development,* 126**,** 3585-96.

FAIVRE-SARRAILH, C., FALK, J., POLLERBERG, E., SCHACHNER, M. & ROUGON, G. 1999. NrCAM, cerebellar granule cell receptor for the neuronal adhesion molecule F3, displays an actin-dependent mobility in growth cones. *J Cell Sci,* 112 Pt 18**,** 3015-27.

FALK, J., BECHARA, A., FIORE, R., NAWABI, H., ZHOU, H., HOYO-BECERRA, C., BOZON, M., ROUGON, G., GRUMET, M., PUSCHEL, A. W., SANES, J. R. & CASTELLANI, V. 2005. Dual functional activity of semaphorin 3B is required for positioning the anterior commissure. *Neuron,* 48**,** 63-75.

FAN, X. & EBERHART, C. G. 2008. Medulloblastoma stem cells. *J Clin Oncol,* 26**,** 2821-7.

FEINBERG, K., ESHED-EISENBACH, Y., FRECHTER, S., AMOR, V., SALOMON, D., SABANAY, H., DUPREE, J. L., GRUMET, M., BROPHY, P. J., SHRAGER, P. & PELES, E. 2010. A glial signal consisting of gliomedin and NrCAM clusters axonal Na+ channels during the formation of nodes of Ranvier. *Neuron,* 65**,** 490-502.

FERNANDEZ, C., TATARD, V. M., BERTRAND, N. & DAHMANE, N. 2010. Differential modulation of Sonic-hedgehog-induced cerebellar granule cell precursor proliferation by the IGF signaling network. *Developmental neuroscience,* 32**,** 59-70.

FINETTI, F., PACCANI, S. R., ROSENBAUM, J. & BALDARI, C. T. 2011. Intraflagellar transport: a new player at the immune synapse. *Trends in immunology,* 32**,** 139-45.

FU, M., LUI, V. C., SHAM, M. H., PACHNIS, V. & TAM, P. K. 2004. Sonic hedgehog regulates the proliferation, differentiation, and migration of enteric neural crest cells in gut. *The Journal of cell biology,* 166**,** 673-84.

FURLEY, A. J., MORTON, S. B., MANALO, D., KARAGOGEOS, D., DODD, J. & JESSELL, T. M. 1990. The axonal glycoprotein TAG-1 is an immunoglobulin superfamily member with neurite outgrowth-promoting activity. *Cell,* 61**,** 157-70.

GALLAGHER, J. 2007. Messages in the matrix: proteoglycans go the distance. *Dev Cell,* 13**,** 166-7.

GALLET, A., STACCINI-LAVENANT, L. & THEROND, P. P. 2008. Cellular trafficking of the glypican Dally-like is required for full-strength Hedgehog signaling and wingless transcytosis. *Developmental cell,* 14**,** 712-25.

GAO, W. O., HEINTZ, N. & HATTEN, M. E. 1991. Cerebellar granule cell neurogenesis is regulated by cell-cell interactions in vitro. *Neuron,* 6**,** 705-15.

GIANGASPERO, F., EBERHART, C., HAAPASALO, H., PIETSCH, T., WIESTLER, O. D. & ELLISON, D. W. 2007. *WHO Classification of Tumors of the Central Nervous System. ,* Lyon, IARC Press.

GILBERT, S. F. 2000. *Developmental Biology,* Sunderland (MA), Sinauer Associates.

GILBERTSON, R. J. 2004. Medulloblastoma: signalling a change in treatment. *The lancet oncology,* 5**,** 209-18.

GLIENKE, J., SCHMITT, A. O., PILARSKY, C., HINZMANN, B., WEISS, B., ROSENTHAL, A. & THIERAUCH, K. H. 2000. Differential gene

expression by endothelial cells in distinct angiogenic states. *European journal of biochemistry / FEBS,* 267**,** 2820-30.
GLUZMAN, Y. 1981. SV40-transformed simian cells support the replication of early SV40 mutants. *Cell,* 23**,** 175-82.
GOETZ, S. C. & ANDERSON, K. V. 2010. The primary cilium: a signalling centre during vertebrate development. *Nature reviews. Genetics,* 11**,** 331-44.
GOLDOWITZ, D. & HAMRE, K. 1998. The cells and molecules that make a cerebellum. *Trends Neurosci,* 21**,** 375-82.
GOODRICH, L. V., JOHNSON, R. L., MILENKOVIC, L., MCMAHON, J. A. & SCOTT, M. P. 1996. Conservation of the hedgehog/patched signaling pathway from flies to mice: induction of a mouse patched gene by Hedgehog. *Genes & development,* 10**,** 301-12.
GOODRICH, L. V., MILENKOVIC, L., HIGGINS, K. M. & SCOTT, M. P. 1997. Altered neural cell fates and medulloblastoma in mouse patched mutants. *Science,* 277**,** 1109-13.
GRAHAM, F. L., SMILEY, J., RUSSELL, W. C. & NAIRN, R. 1977. Characteristics of a human cell line transformed by DNA from human adenovirus type 5. *The Journal of general virology,* 36**,** 59-74.
GUSTAFSSON, M. G. 2000. Surpassing the lateral resolution limit by a factor of two using structured illumination microscopy. *Journal of microscopy,* 198**,** 82-7.
HAMRE, K. M. & GOLDOWITZ, D. 1997. meander tail acts intrinsic to granule cell precursors to disrupt cerebellar development: analysis of meander tail chimeric mice. *Development,* 124**,** 4201-12.
HAN, Y. G., SPASSKY, N., ROMAGUERA-ROS, M., GARCIA-VERDUGO, J. M., AGUILAR, A., SCHNEIDER-MAUNOURY, S. & ALVAREZ-BUYLLA, A. 2008. Hedgehog signaling and primary cilia are required for the formation of adult neural stem cells. *Nature neuroscience,* 11**,** 277-84.
HANDEL, M., SCHULZ, S., STANARIUS, A., SCHREFF, M., ERDTMANN-VOURLIOTIS, M., SCHMIDT, H., WOLF, G. & HOLLT, V. 1999. Selective targeting of somatostatin receptor 3 to neuronal cilia. *Neuroscience,* 89**,** 909-26.
HATTEN, M. E. 1985. Neuronal regulation of astroglial morphology and proliferation in vitro. *The Journal of cell biology,* 100**,** 384-96.
HATTEN, M. E., ALDER, J., ZIMMERMAN, K. & HEINTZ, N. 1997. Genes involved in cerebellar cell specification and differentiation. *Current opinion in neurobiology,* 7**,** 40-7.
HATTEN, M. E. & HEINTZ, N. 1995. Mechanisms of neural patterning and specification in the developing cerebellum. *Annu Rev Neurosci,* 18**,** 385-408.
HATTON, B. A., VILLAVICENCIO, E. H., TSUCHIYA, K. D., PRITCHARD, J. I., DITZLER, S., PULLAR, B., HANSEN, S., KNOBLAUGH, S. E., LEE, D., EBERHART, C. G., HALLAHAN, A. R. & OLSON, J. M. 2008. The Smo/Smo model: hedgehog-induced medulloblastoma with 90% incidence and leptomeningeal spread. *Cancer Res,* 68**,** 1768-76.
HAYCRAFT, C. J., BANIZS, B., AYDIN-SON, Y., ZHANG, Q., MICHAUD, E. J. & YODER, B. K. 2005. Gli2 and Gli3 localize to cilia and require the

intraflagellar transport protein polaris for processing and function. *PLoS Genet,* 1**,** e53.
HEEMSKERK, J. & DINARDO, S. 1994. Drosophila hedgehog acts as a morphogen in cellular patterning. *Cell,* 76**,** 449-60.
HERRON, L. R., HILL, M., DAVEY, F. & GUNN-MOORE, F. J. 2009. The intracellular interactions of the L1 family of cell adhesion molecules. *The Biochemical journal,* 419**,** 519-31.
HEYDEN, A., ANGENSTEIN, F., SALLAZ, M., SEIDENBECHER, C. & MONTAG, D. 2008. Abnormal axonal guidance and brain anatomy in mouse mutants for the cell recognition molecules close homolog of L1 and NgCAM-related cell adhesion molecule. *Neuroscience,* 155**,** 221-33.
HILLMAN, R. T., FENG, B. Y., NI, J., WOO, W. M., MILENKOVIC, L., HAYDEN GEPHART, M. G., TERUEL, M. N., ORO, A. E., CHEN, J. K. & SCOTT, M. P. 2011. Neuropilins are positive regulators of Hedgehog signal transduction. *Genes & development,* 25**,** 2333-46.
HIRANO, S. & TAKEICHI, M. 2012. Cadherins in brain morphogenesis and wiring. *Physiological reviews,* 92**,** 597-634.
HO, K. S. & SCOTT, M. P. 2002. Sonic hedgehog in the nervous system: functions, modifications and mechanisms. *Current opinion in neurobiology,* 12**,** 57-63.
HOLM, J., HILLENBRAND, R., STEUBER, V., BARTSCH, U., MOOS, M., LUBBERT, H., MONTAG, D. & SCHACHNER, M. 1996. Structural features of a close homologue of L1 (CHL1) in the mouse: a new member of the L1 family of neural recognition molecules. *The European journal of neuroscience,* 8**,** 1613-29.
HSIAO, Y. C., TUZ, K. & FERLAND, R. J. 2012. Trafficking in and to the primary cilium. *Cilia,* 1**,** 4.
HU, Q. D., ANG, B. T., KARSAK, M., HU, W. P., CUI, X. Y., DUKA, T., TAKEDA, Y., CHIA, W., SANKAR, N., NG, Y. K., LING, E. A., MACIAG, T., SMALL, D., TRIFONOVA, R., KOPAN, R., OKANO, H., NAKAFUKU, M., CHIBA, S., HIRAI, H., ASTER, J. C., SCHACHNER, M., PALLEN, C. J., WATANABE, K. & XIAO, Z. C. 2003. F3/contactin acts as a functional ligand for Notch during oligodendrocyte maturation. *Cell,* 115**,** 163-75.
HUANGFU, D. & ANDERSON, K. V. 2005. Cilia and Hedgehog responsiveness in the mouse. *Proc Natl Acad Sci U S A,* 102**,** 11325-30.
HUANGFU, D. & ANDERSON, K. V. 2006. Signaling from Smo to Ci/Gli: conservation and divergence of Hedgehog pathways from Drosophila to vertebrates. *Development,* 133**,** 3-14.
HUANGFU, D., LIU, A., RAKEMAN, A. S., MURCIA, N. S., NISWANDER, L. & ANDERSON, K. V. 2003. Hedgehog signalling in the mouse requires intraflagellar transport proteins. *Nature,* 426**,** 83-7.
HUMKE, E. W., DORN, K. V., MILENKOVIC, L., SCOTT, M. P. & ROHATGI, R. 2010. The output of Hedgehog signaling is controlled by the dynamic association between Suppressor of Fused and the Gli proteins. *Genes & development,* 24**,** 670-82.
INCARDONA, J. P., GRUENBERG, J. & ROELINK, H. 2002. Sonic hedgehog induces the segregation of patched and smoothened in endosomes. *Current biology : CB,* 12**,** 983-95.

INCARDONA, J. P., LEE, J. H., ROBERTSON, C. P., ENGA, K., KAPUR, R. P. & ROELINK, H. 2000. Receptor-mediated endocytosis of soluble and membrane-tethered Sonic hedgehog by Patched-1. *Proceedings of the National Academy of Sciences of the United States of America,* 97**,** 12044-9.

INGHAM, P. W. 1998. Transducing Hedgehog: the story so far. *Embo J,* 17**,** 3505-11.

INGHAM, P. W. & MCMAHON, A. P. 2001. Hedgehog signaling in animal development: paradigms and principles. *Genes & development,* 15**,** 3059-87.

INGHAM, P. W. & PLACZEK, M. 2006. Orchestrating ontogenesis: variations on a theme by sonic hedgehog. *Nat Rev Genet,* 7**,** 841-50.

INGLIS, P. N., BOROEVICH, K. A. & LEROUX, M. R. 2006. Piecing together a ciliome. *Trends in genetics : TIG,* 22**,** 491-500.

ITO, M. 1998. Cerebellar learning in the vestibulo-ocular reflex. *Trends in cognitive sciences,* 2**,** 313-21.

ITO, M. 2000. Mechanisms of motor learning in the cerebellum. *Brain research,* 886**,** 237-245.

ITO, M. 2002. The molecular organization of cerebellar long-term depression. *Nature reviews. Neuroscience,* 3**,** 896-902.

ITOH, K., CHENG, L., KAMEI, Y., FUSHIKI, S., KAMIGUCHI, H., GUTWEIN, P., STOECK, A., ARNOLD, B., ALTEVOGT, P. & LEMMON, V. 2004. Brain development in mice lacking L1-L1 homophilic adhesion. *The Journal of cell biology,* 165**,** 145-54.

IZZI, L., LEVESQUE, M., MORIN, S., LANIEL, D., WILKES, B. C., MILLE, F., KRAUSS, R. S., MCMAHON, A. P., ALLEN, B. L. & CHARRON, F. 2011. Boc and Gas1 each form distinct Shh receptor complexes with Ptch1 and are required for Shh-mediated cell proliferation. *Developmental cell,* 20**,** 788-801.

JENKINS, D. 2009. Hedgehog signalling: emerging evidence for non-canonical pathways. *Cellular signalling,* 21**,** 1023-34.

JIANG, J. & HUI, C. C. 2008. Hedgehog signaling in development and cancer. *Developmental cell,* 15**,** 801-12.

KAMIGUCHI, H. 2007. The role of cell adhesion molecules in axon growth and guidance. *Adv Exp Med Biol,* 621**,** 95-103.

KATIDOU, M., VIDAKI, M., STRIGINI, M. & KARAGOGEOS, D. 2008. The immunoglobulin superfamily of neuronal cell adhesion molecules: lessons from animal models and correlation with human disease. *Biotechnology journal,* 3**,** 1564-80.

KATOH, Y. & KATOH, M. 2004. KIF27 is one of orthologs for Drosophila Costal-2. *International journal of oncology,* 25**,** 1875-80.

KEEGAN, K., JOHNSON, D. E., WILLIAMS, L. T. & HAYMAN, M. J. 1991. Isolation of an additional member of the fibroblast growth factor receptor family, FGFR-3. *Proceedings of the National Academy of Sciences of the United States of America,* 88**,** 1095-9.

KENNEY, A. M., COLE, M. D. & ROWITCH, D. H. 2003. Nmyc upregulation by sonic hedgehog signaling promotes proliferation in developing cerebellar granule neuron precursors. *Development,* 130**,** 15-28.

KIPRILOV, E. N., AWAN, A., DESPRAT, R., VELHO, M., CLEMENT, C. A., BYSKOV, A. G., ANDERSEN, C. Y., SATIR, P., BOUHASSIRA, E. E., CHRISTENSEN, S. T. & HIRSCH, R. E. 2008. Human embryonic stem cells in culture possess primary cilia with hedgehog signaling machinery. *The Journal of cell biology,* 180**,** 897-904.

KNODLER, A., FENG, S., ZHANG, J., ZHANG, X., DAS, A., PERANEN, J. & GUO, W. 2010. Coordination of Rab8 and Rab11 in primary ciliogenesis. *Proceedings of the National Academy of Sciences of the United States of America,* 107**,** 6346-51.

KOFUJI, P., HOFER, M., MILLEN, K. J., MILLONIG, J. H., DAVIDSON, N., LESTER, H. A. & HATTEN, M. E. 1996. Functional analysis of the weaver mutant GIRK2 K+ channel and rescue of weaver granule cells. *Neuron,* 16**,** 941-52.

KOMURO, H., YACUBOVA, E. & RAKIC, P. 2001. Mode and tempo of tangential cell migration in the cerebellar external granular layer. *The Journal of neuroscience : the official journal of the Society for Neuroscience,* 21**,** 527-40.

KOOL, M., KORSHUNOV, A., REMKE, M., JONES, D. T., SCHLANSTEIN, M., NORTHCOTT, P. A., CHO, Y. J., KOSTER, J., SCHOUTEN-VAN MEETEREN, A., VAN VUURDEN, D., CLIFFORD, S. C., PIETSCH, T., VON BUEREN, A. O., RUTKOWSKI, S., MCCABE, M., COLLINS, V. P., BACKLUND, M. L., HABERLER, C., BOURDEAUT, F., DELATTRE, O., DOZ, F., ELLISON, D. W., GILBERTSON, R. J., POMEROY, S. L., TAYLOR, M. D., LICHTER, P. & PFISTER, S. M. 2012. Molecular subgroups of medulloblastoma: an international meta-analysis of transcriptome, genetic aberrations, and clinical data of WNT, SHH, Group 3, and Group 4 medulloblastomas. *Acta neuropathologica,* 123**,** 473-84.

KOVACS, J. J., WHALEN, E. J., LIU, R., XIAO, K., KIM, J., CHEN, M., WANG, J., CHEN, W. & LEFKOWITZ, R. J. 2008. Beta-arrestin-mediated localization of smoothened to the primary cilium. *Science,* 320**,** 1777-81.

KUMADA, T., JIANG, Y., KAWANAMI, A., CAMERON, D. B. & KOMURO, H. 2009. Autonomous turning of cerebellar granule cells in vitro by intrinsic programs. *Developmental biology,* 326**,** 237-49.

LAW, C. O., KIRBY, R. J., AGHAMOHAMMADZADEH, S. & FURLEY, A. J. 2008. The neural adhesion molecule TAG-1 modulates responses of sensory axons to diffusible guidance signals. *Development,* 135**,** 2361-71.

LEE, H. Y., GREENE, L. A., MASON, C. A. & MANZINI, M. C. 2009. Isolation and culture of post-natal mouse cerebellar granule neuron progenitor cells and neurons. *Journal of visualized experiments : JoVE*.

LEE, J., PLATT, K. A., CENSULLO, P. & RUIZ I ALTABA, A. 1997. Gli1 is a target of Sonic hedgehog that induces ventral neural tube development. *Development,* 124**,** 2537-52.

LEE, Y., KAWAGOE, R., SASAI, K., LI, Y., RUSSELL, H. R., CURRAN, T. & MCKINNON, P. J. 2007. Loss of suppressor-of-fused function promotes tumorigenesis. *Oncogene,* 26**,** 6442-7.

LEEVERS, S. J. & MCNEILL, H. 2005. Controlling the size of organs and organisms. *Current opinion in cell biology,* 17**,** 604-9.

LEFKOWITZ, R. J., RAJAGOPAL, K. & WHALEN, E. J. 2006. New roles for beta-arrestins in cell signaling: not just for seven-transmembrane receptors. *Molecular cell,* 24**,** 643-52.

LEPPER, C., CONWAY, S. J. & FAN, C. M. 2009. Adult satellite cells and embryonic muscle progenitors have distinct genetic requirements. *Nature,* 460**,** 627-31.

LEWIS, P. M., GRITLI-LINDE, A., SMEYNE, R., KOTTMANN, A. & MCMAHON, A. P. 2004. Sonic hedgehog signaling is required for expansion of granule neuron precursors and patterning of the mouse cerebellum. *Dev Biol,* 270**,** 393-410.

LI, K. K., LAU, K. M. & NG, H. K. 2013. Signaling pathway and molecular subgroups of medulloblastoma. *International journal of clinical and experimental pathology,* 6**,** 1211-22.

LIEM, K. F., JR., HE, M., OCBINA, P. J. & ANDERSON, K. V. 2009. Mouse Kif7/Costal2 is a cilia-associated protein that regulates Sonic hedgehog signaling. *Proceedings of the National Academy of Sciences of the United States of America,* 106**,** 13377-82.

LIN, X. & BULLEIT, R. F. 1997. Insulin-like growth factor I (IGF-I) is a critical trophic factor for developing cerebellar granule cells. *Brain research. Developmental brain research,* 99**,** 234-42.

LOUVI, A. & ARTAVANIS-TSAKONAS, S. 2006. Notch signalling in vertebrate neural development. *Nat Rev Neurosci,* 7**,** 93-102.

LU, J., CHEN, M., REN, X. R., WANG, J., LYERLY, H. K., BARAK, L. & CHEN, W. 2013. Regulation of hedgehog signaling by Myc-interacting zinc finger protein 1, Miz1. *PloS one,* 8**,** e63353.

LUSTIG, M., ERSKINE, L., MASON, C. A., GRUMET, M. & SAKURAI, T. 2001. Nr-CAM expression in the developing mouse nervous system: ventral midline structures, specific fiber tracts, and neuropilar regions. *The Journal of comparative neurology,* 434**,** 13-28.

MA, Q. H., BAGNARD, D., XIAO, Z. C. & DAWE, G. S. 2008. A TAG on to the neurogenic functions of APP. *Cell adhesion & migration,* 2**,** 2-8.

MACHOLD, R. P., KITTELL, D. J. & FISHELL, G. J. 2007. Antagonism between Notch and bone morphogenetic protein receptor signaling regulates neurogenesis in the cerebellar rhombic lip. *Neural development,* 2**,** 5.

MANESS, P. F. & SCHACHNER, M. 2007. Neural recognition molecules of the immunoglobulin superfamily: signaling transducers of axon guidance and neuronal migration. *Nat Neurosci,* 10**,** 19-26.

MARINO, S. 2005. Medulloblastoma: developmental mechanisms out of control. *Trends in molecular medicine,* 11**,** 17-22.

MARQUES, G. & FAN, C. M. 2002. Growth arrest specific gene 1: a fuel for driving growth in the cerebellum. *Cerebellum,* 1**,** 259-63.

MARTI, E. & BOVOLENTA, P. 2002. Sonic hedgehog in CNS development: one signal, multiple outputs. *Trends in neurosciences,* 25**,** 89-96.

MARTIN, V., CARRILLO, G., TORROJA, C. & GUERRERO, I. 2001. The sterol-sensing domain of Patched protein seems to control Smoothened activity through Patched vesicular trafficking. *Current biology : CB,* 11**,** 601-7.

MARTINEZ, C., CORNEJO, V. H., LOIS, P., ELLIS, T., SOLIS, N. P., WAINWRIGHT, B. J. & PALMA, V. 2013. Proliferation of murine

midbrain neural stem cells depends upon an endogenous sonic hedgehog (Shh) source. *PloS one,* 8**,** e65818.

MAY, S. R., ASHIQUE, A. M., KARLEN, M., WANG, B., SHEN, Y., ZARBALIS, K., REITER, J., ERICSON, J. & PETERSON, A. S. 2005. Loss of the retrograde motor for IFT disrupts localization of Smo to cilia and prevents the expression of both activator and repressor functions of Gli. *Developmental biology,* 287**,** 378-89.

MCMAHON, A. P., INGHAM, P. W. & TABIN, C. J. 2003. Developmental roles and clinical significance of hedgehog signaling. *Current topics in developmental biology,* 53**,** 1-114.

MICHAUD, E. J. & YODER, B. K. 2006. The primary cilium in cell signaling and cancer. *Cancer research,* 66**,** 6463-7.

MILENKOVIC, L., SCOTT, M. P. & ROHATGI, R. 2009. Lateral transport of Smoothened from the plasma membrane to the membrane of the cilium. *The Journal of cell biology,* 187**,** 365-74.

MIYAZAWA, K., HIMI, T., GARCIA, V., YAMAGISHI, H., SATO, S. & ISHIZAKI, Y. 2000. A role for p27/Kip1 in the control of cerebellar granule cell precursor proliferation. *The Journal of neuroscience : the official journal of the Society for Neuroscience,* 20**,** 5756-63.

MORALES, G., HUBERT, M., BRUMMENDORF, T., TREUBERT, U., TARNOK, A., SCHWARZ, U. & RATHJEN, F. G. 1993. Induction of axonal growth by heterophilic interactions between the cell surface recognition proteins F11 and Nr-CAM/Bravo. *Neuron,* 11**,** 1113-22.

MORE, M. I., KIRSCH, F. P. & RATHJEN, F. G. 2001. Targeted ablation of NrCAM or ankyrin-B results in disorganized lens fibers leading to cataract formation. *The Journal of cell biology,* 154**,** 187-96.

MUKHOPADHYAY, A., KRISHNASWAMI, S. R., COWING-ZITRON, C., HUNG, N. J., REILLY-RHOTEN, H., BURNS, J. & YU, B. D. 2013. Negative regulation of Shh levels by Kras and Fgfr2 during hair follicle development. *Developmental biology,* 373**,** 373-82.

MULHERN, R. K., PALMER, S. L., MERCHANT, T. E., WALLACE, D., KOCAK, M., BROUWERS, P., KRULL, K., CHINTAGUMPALA, M., STARGATT, R., ASHLEY, D. M., TYC, V. L., KUN, L., BOYETT, J. & GAJJAR, A. 2005. Neurocognitive consequences of risk-adapted therapy for childhood medulloblastoma. *Journal of clinical oncology : official journal of the American Society of Clinical Oncology,* 23**,** 5511-9.

MULLEN, R. J., HAMRE, K. M. & GOLDOWITZ, D. 1997. Cerebellar mutant mice and chimeras revisited. *Perspect Dev Neurobiol,* 5**,** 43-55.

MURONE, M., ROSENTHAL, A. & DE SAUVAGE, F. J. 1999. Sonic hedgehog signaling by the patched-smoothened receptor complex. *Current biology : CB,* 9**,** 76-84.

NARITA, K., KOZUKA-HATA, H., NONAMI, Y., AO-KONDO, H., SUZUKI, T., NAKAMURA, H., YAMAKAWA, K., OYAMA, M., INOUE, T. & TAKEDA, S. 2012. Proteomic analysis of multiple primary cilia reveals a novel mode of ciliary development in mammals. *Biology open,* 1**,** 815-25.

NIEUWENHUIS, E. & HUI, C. C. 2005. Hedgehog signaling and congenital malformations. *Clinical genetics,* 67**,** 193-208.

NUSSLEIN-VOLHARD, C. & WIESCHAUS, E. 1980. Mutations affecting segment number and polarity in Drosophila. *Nature,* 287**,** 795-801.

OLIVER, T. G., GRASFEDER, L. L., CARROLL, A. L., KAISER, C., GILLINGHAM, C. L., LIN, S. M., WICKRAMASINGHE, R., SCOTT, M. P. & WECHSLER-REYA, R. J. 2003. Transcriptional profiling of the Sonic hedgehog response: a critical role for N-myc in proliferation of neuronal precursors. *Proceedings of the National Academy of Sciences of the United States of America,* 100**,** 7331-6.

ORO, A. E., HIGGINS, K. M., HU, Z., BONIFAS, J. M., EPSTEIN, E. H., JR. & SCOTT, M. P. 1997. Basal cell carcinomas in mice overexpressing sonic hedgehog. *Science,* 276**,** 817-21.

PARTANEN, J. & DUMONT, D. J. 1999. Functions of Tie1 and Tie2 receptor tyrosine kinases in vascular development. *Current topics in microbiology and immunology,* 237**,** 159-72.

PAZOUR, G. J. & BLOODGOOD, R. A. 2008. Targeting proteins to the ciliary membrane. *Current topics in developmental biology,* 85**,** 115-49.

PETRALIA, R. S., SCHWARTZ, C. M., WANG, Y. X., MATTSON, M. P. & YAO, P. J. 2011. Subcellular localization of Patched and Smoothened, the receptors for Sonic hedgehog signaling, in the hippocampal neuron. *The Journal of comparative neurology,* 519**,** 3684-99.

PETRALIA, R. S., WANG, Y. X., MATTSON, M. P. & YAO, P. J. 2012. Subcellular distribution of patched and smoothened in the cerebellar neurons. *Cerebellum,* 11**,** 972-81.

PIETSCH, T., WAHA, A., KOCH, A., KRAUS, J., ALBRECHT, S., TONN, J., SORENSEN, N., BERTHOLD, F., HENK, B., SCHMANDT, N., WOLF, H. K., VON DEIMLING, A., WAINWRIGHT, B., CHENEVIX-TRENCH, G., WIESTLER, O. D. & WICKING, C. 1997. Medulloblastomas of the desmoplastic variant carry mutations of the human homologue of Drosophila patched. *Cancer research,* 57**,** 2085-8.

PIPER, M., SALIH, S., WEINL, C., HOLT, C. E. & HARRIS, W. A. 2005. Endocytosis-dependent desensitization and protein synthesis-dependent resensitization in retinal growth cone adaptation. *Nature neuroscience,* 8**,** 179-86.

PLAISANT, M., GIORGETTI-PERALDI, S., GABRIELSON, M., LOUBAT, A., DANI, C. & PERALDI, P. 2011. Inhibition of hedgehog signaling decreases proliferation and clonogenicity of human mesenchymal stem cells. *PloS one,* 6**,** e16798.

PLOTNIKOVA, O. V., PUGACHEVA, E. N. & GOLEMIS, E. A. 2009. Primary cilia and the cell cycle. *Methods in cell biology,* 94**,** 137-60.

POLIAK, S., SALOMON, D., ELHANANY, H., SABANAY, H., KIERNAN, B., PEVNY, L., STEWART, C. L., XU, X., CHIU, S. Y., SHRAGER, P., FURLEY, A. J. & PELES, E. 2003. Juxtaparanodal clustering of Shaker-like K+ channels in myelinated axons depends on Caspr2 and TAG-1. *J Cell Biol,* 162**,** 1149-60.

PONS, S., TREJO, J. L., MARTINEZ-MORALES, J. R. & MARTI, E. 2001. Vitronectin regulates Sonic hedgehog activity during cerebellum development through CREB phosphorylation. *Development,* 128**,** 1481-92.

POOLE, C. A., JENSEN, C. G., SNYDER, J. A., GRAY, C. G., HERMANUTZ, V. L. & WHEATLEY, D. N. 1997. Confocal analysis of primary cilia structure

and colocalization with the Golgi apparatus in chondrocytes and aortic smooth muscle cells. *Cell biology international,* 21**,** 483-94.

RADONIC, A., THULKE, S., MACKAY, I. M., LANDT, O., SIEGERT, W. & NITSCHE, A. 2004. Guideline to reference gene selection for quantitative real-time PCR. *Biochemical and biophysical research communications,* 313**,** 856-62.

RIBI, K., RELLY, C., LANDOLT, M. A., ALBER, F. D., BOLTSHAUSER, E. & GROTZER, M. A. 2005. Outcome of medulloblastoma in children: long-term complications and quality of life. *Neuropediatrics,* 36**,** 357-65.

RIOS, I., ALVAREZ-RODRIGUEZ, R., MARTI, E. & PONS, S. 2004. Bmp2 antagonizes sonic hedgehog-mediated proliferation of cerebellar granule neurones through Smad5 signalling. *Development,* 131**,** 3159-68.

ROHATGI, R., MILENKOVIC, L. & SCOTT, M. P. 2007. Patched1 regulates hedgehog signaling at the primary cilium. *Science,* 317**,** 372-6.

ROHATGI, R. & SCOTT, M. P. 2007. Patching the gaps in Hedgehog signalling. *Nature cell biology,* 9**,** 1005-9.

ROMER, J. T., KIMURA, H., MAGDALENO, S., SASAI, K., FULLER, C., BAINES, H., CONNELLY, M., STEWART, C. F., GOULD, S., RUBIN, L. L. & CURRAN, T. 2004. Suppression of the Shh pathway using a small molecule inhibitor eliminates medulloblastoma in Ptc1(+/-)p53(-/-) mice. *Cancer cell,* 6**,** 229-40.

ROUSSEL, M. F. & HATTEN, M. E. 2011. Cerebellum development and medulloblastoma. *Current topics in developmental biology,* 94**,** 235-82.

RUIZ I ALTABA, A., PALMA, V. & DAHMANE, N. 2002. Hedgehog-Gli signalling and the growth of the brain. *Nat Rev Neurosci,* 3**,** 24-33.

SAKURAI, T., LUSTIG, M., BABIARZ, J., FURLEY, A. J., TAIT, S., BROPHY, P. J., BROWN, S. A., BROWN, L. Y., MASON, C. A. & GRUMET, M. 2001. Overlapping functions of the cell adhesion molecules Nr-CAM and L1 in cerebellar granule cell development. *The Journal of cell biology,* 154**,** 1259-73.

SAKURAI, T., LUSTIG, M., NATIV, M., HEMPERLY, J. J., SCHLESSINGER, J., PELES, E. & GRUMET, M. 1997. Induction of neurite outgrowth through contactin and Nr-CAM by extracellular regions of glial receptor tyrosine phosphatase beta. *The Journal of cell biology,* 136**,** 907-18.

SALZER, J. L. 2003. Polarized domains of myelinated axons. *Neuron,* 40**,** 297-318.

SCHMITTGEN, T. D. & LIVAK, K. J. 2008. Analyzing real-time PCR data by the comparative C(T) method. *Nature protocols,* 3**,** 1101-8.

SCHRAMM, M., EIMERL, S. & COSTA, E. 1990. Serum and depolarizing agents cause acute neurotoxicity in cultured cerebellar granule cells: role of the glutamate receptor responsive to N-methyl-D-aspartate. *Proceedings of the National Academy of Sciences of the United States of America,* 87**,** 1193-7.

SHENOY, S. K., MODI, A. S., SHUKLA, A. K., XIAO, K., BERTHOUZE, M., AHN, S., WILKINSON, K. D., MILLER, W. E. & LEFKOWITZ, R. J. 2009. Beta-arrestin-dependent signaling and trafficking of 7-transmembrane

receptors is reciprocally regulated by the deubiquitinase USP33 and the E3 ligase Mdm2. *Proceedings of the National Academy of Sciences of the United States of America,* 106**,** 6650-5.

SHIMODA, Y. & WATANABE, K. 2009. Contactins: emerging key roles in the development and function of the nervous system. *Cell adhesion & migration,* 3**,** 64-70.

SIMPSON, F., KERR, M. C. & WICKING, C. 2009. Trafficking, development and hedgehog. *Mechanisms of development,* 126**,** 279-88.

SMOLL, N. R. & DRUMMOND, K. J. 2012. The incidence of medulloblastomas and primitive neurectodermal tumours in adults and children. *Journal of clinical neuroscience : official journal of the Neurosurgical Society of Australasia,* 19**,** 1541-4.

SODERBERG, O., GULLBERG, M., JARVIUS, M., RIDDERSTRALE, K., LEUCHOWIUS, K. J., JARVIUS, J., WESTER, K., HYDBRING, P., BAHRAM, F., LARSSON, L. G. & LANDEGREN, U. 2006. Direct observation of individual endogenous protein complexes in situ by proximity ligation. *Nature methods,* 3**,** 995-1000.

SOLECKI, D. J., LIU, X. L., TOMODA, T., FANG, Y. & HATTEN, M. E. 2001. Activated Notch2 signaling inhibits differentiation of cerebellar granule neuron precursors by maintaining proliferation. *Neuron,* 31**,** 557-68.

SPASSKY, N., HAN, Y. G., AGUILAR, A., STREHL, L., BESSE, L., LACLEF, C., ROS, M. R., GARCIA-VERDUGO, J. M. & ALVAREZ-BUYLLA, A. 2008. Primary cilia are required for cerebellar development and Shh-dependent expansion of progenitor pool. *Developmental biology,* 317**,** 246-59.

STONE, D. M., HYNES, M., ARMANINI, M., SWANSON, T. A., GU, Q., JOHNSON, R. L., SCOTT, M. P., PENNICA, D., GODDARD, A., PHILLIPS, H., NOLL, M., HOOPER, J. E., DE SAUVAGE, F. & ROSENTHAL, A. 1996. The tumour-suppressor gene patched encodes a candidate receptor for Sonic hedgehog. *Nature,* 384**,** 129-34.

STRIGINI, M. & COHEN, S. M. 1999. Formation of morphogen gradients in the Drosophila wing. *Seminars in cell & developmental biology,* 10**,** 335-44.

TAO, Y., BLACK, I. B. & DICICCO-BLOOM, E. 1996. Neurogenesis in neonatal rat brain is regulated by peripheral injection of basic fibroblast growth factor (bFGF). *The Journal of comparative neurology,* 376**,** 653-63.

TAY, S. Y., INGHAM, P. W. & ROY, S. 2005. A homologue of the Drosophila kinesin-like protein Costal2 regulates Hedgehog signal transduction in the vertebrate embryo. *Development,* 132**,** 625-34.

TAYLOR, M. D., NORTHCOTT, P. A., KORSHUNOV, A., REMKE, M., CHO, Y. J., CLIFFORD, S. C., EBERHART, C. G., PARSONS, D. W., RUTKOWSKI, S., GAJJAR, A., ELLISON, D. W., LICHTER, P., GILBERTSON, R. J., POMEROY, S. L., KOOL, M. & PFISTER, S. M. 2012. Molecular subgroups of medulloblastoma: the current consensus. *Acta neuropathologica,* 123**,** 465-72.

TENZEN, T., ALLEN, B. L., COLE, F., KANG, J. S., KRAUSS, R. S. & MCMAHON, A. P. 2006. The cell surface membrane proteins Cdo and Boc are

components and targets of the Hedgehog signaling pathway and feedback network in mice. *Developmental cell,* 10**,** 647-56.

THELEN, K., KEDAR, V., PANICKER, A. K., SCHMID, R. S., MIDKIFF, B. R. & MANESS, P. F. 2002. The neural cell adhesion molecule L1 potentiates integrin-dependent cell migration to extracellular matrix proteins. *The Journal of neuroscience : the official journal of the Society for Neuroscience,* 22**,** 4918-31.

TORROJA, C., GORFINKIEL, N. & GUERRERO, I. 2004. Patched controls the Hedgehog gradient by endocytosis in a dynamin-dependent manner, but this internalization does not play a major role in signal transduction. *Development,* 131**,** 2395-408.

TRUETT, G. E., HEEGER, P., MYNATT, R. L., TRUETT, A. A., WALKER, J. A. & WARMAN, M. L. 2000. Preparation of PCR-quality mouse genomic DNA with hot sodium hydroxide and tris (HotSHOT). *BioTechniques,* 29**,** 52, 54.

TUKACHINSKY, H., LOPEZ, L. V. & SALIC, A. 2010. A mechanism for vertebrate Hedgehog signaling: recruitment to cilia and dissociation of SuFu-Gli protein complexes. *The Journal of cell biology,* 191**,** 415-28.

VARJOSALO, M. & TAIPALE, J. 2008. Hedgehog: functions and mechanisms. *Genes & development,* 22**,** 2454-72.

VEENING, J. W., SMITS, W. K., HAMOEN, L. W., JONGBLOED, J. D. & KUIPERS, O. P. 2004. Visualization of differential gene expression by improved cyan fluorescent protein and yellow fluorescent protein production in Bacillus subtilis. *Applied and environmental microbiology,* 70**,** 6809-15.

VOGEL, M. W., SUNTER, K. & HERRUP, K. 1989. Numerical matching between granule and Purkinje cells in lurcher chimeric mice: a hypothesis for the trophic rescue of granule cells from target-related cell death. *The Journal of neuroscience : the official journal of the Society for Neuroscience,* 9**,** 3454-62.

VORTKAMP, A., LEE, K., LANSKE, B., SEGRE, G. V., KRONENBERG, H. M. & TABIN, C. J. 1996. Regulation of rate of cartilage differentiation by Indian hedgehog and PTH-related protein. *Science,* 273**,** 613-22.

WALLACE, V. A. 1999. Purkinje-cell-derived Sonic hedgehog regulates granule neuron precursor cell proliferation in the developing mouse cerebellum. *Current biology : CB,* 9**,** 445-8.

WANG, V. Y. & ZOGHBI, H. Y. 2001. Genetic regulation of cerebellar development. *Nature reviews. Neuroscience,* 2**,** 484-91.

WECHSLER-REYA, R. J. & SCOTT, M. P. 1999. Control of neuronal precursor proliferation in the cerebellum by Sonic Hedgehog. *Neuron,* 22**,** 103-14.

WILLIAMS, S. E., GRUMET, M., COLMAN, D. R., HENKEMEYER, M., MASON, C. A. & SAKURAI, T. 2006. A role for Nr-CAM in the patterning of binocular visual pathways. *Neuron,* 50**,** 535-47.

WILSON, C. W., CHEN, M. H. & CHUANG, P. T. 2009. Smoothened adopts multiple active and inactive conformations capable of trafficking to the primary cilium. *PloS one,* 4**,** e5182.

WINGATE, R. J. 2001. The rhombic lip and early cerebellar development. *Current opinion in neurobiology,* 11**,** 82-8.

WOLPERT, L. 1969. Positional information and the spatial pattern of cellular differentiation. *Journal of theoretical biology,* 25**,** 1-47.

WOLPERT, L. 1996. One hundred years of positional information. *Trends in genetics : TIG,* 12**,** 359-64.

WOLTER, M., REIFENBERGER, J., SOMMER, C., RUZICKA, T. & REIFENBERGER, G. 1997. Mutations in the human homologue of the Drosophila segment polarity gene patched (PTCH) in sporadic basal cell carcinomas of the skin and primitive neuroectodermal tumors of the central nervous system. *Cancer research,* 57**,** 2581-5.

WOOST, P. G., KOLB, R. J., FINESILVER, M., MACKRAJ, I., IMBODEN, H., COFFMAN, T. M. & HOPFER, U. 2006. Strategy for the development of a matched set of transport-competent, angiotensin receptor-deficient proximal tubule cell lines. *In vitro cellular & developmental biology. Animal,* 42**,** 189-200.

XENAKI, D., MARTIN, I. B., YOSHIDA, L., OHYAMA, K., GENNARINI, G., GRUMET, M., SAKURAI, T. & FURLEY, A. J. 2011. F3/contactin and TAG1 play antagonistic roles in the regulation of sonic hedgehog-induced cerebellar granule neuron progenitor proliferation. *Development,* 138**,** 519-29.

XIE, J., MURONE, M., LUOH, S. M., RYAN, A., GU, Q., ZHANG, C., BONIFAS, J. M., LAM, C. W., HYNES, M., GODDARD, A., ROSENTHAL, A., EPSTEIN, E. H., JR. & DE SAUVAGE, F. J. 1998. Activating Smoothened mutations in sporadic basal-cell carcinoma. *Nature,* 391**,** 90-2.

YACUBOVA, E. & KOMURO, H. 2003. Cellular and molecular mechanisms of cerebellar granule cell migration. *Cell biochemistry and biophysics,* 37**,** 213-34.

YAMASAKI, M., THOMPSON, P. & LEMMON, V. 1997. CRASH syndrome: mutations in L1CAM correlate with severity of the disease. *Neuropediatrics,* 28**,** 175-8.

YE, P., XING, Y., DAI, Z. & D'ERCOLE, A. J. 1996. In vivo actions of insulin-like growth factor-I (IGF-I) on cerebellum development in transgenic mice: evidence that IGF-I increases proliferation of granule cell progenitors. *Brain research. Developmental brain research,* 95**,** 44-54.

YEO, C. H. & HESSLOW, G. 1998. Cerebellum and conditioned reflexes. *Trends in cognitive sciences,* 2**,** 322-30.

YOO, J. W., WANG, Y. & MCMAHON, A. P. 2012. Temporal and spatial analysis of Smoothened at the primary cilium. *The harvard undergraduate research journal,* 5**,** 18-24.

ZHANG, J., SHEMEZIS, J. R., MCQUINN, E. R., WANG, J., SVERDLOV, M. & CHENN, A. 2013. AKT activation by N-cadherin regulates beta-catenin signaling and neuronal differentiation during cortical development. *Neural development,* 8**,** 7.

ZHANG, X. M., RAMALHO-SANTOS, M. & MCMAHON, A. P. 2001. Smoothened mutants reveal redundant roles for Shh and Ihh signaling including regulation of L/R symmetry by the mouse node. *Cell,* 106**,** 781-92.

ZHAO, B., TUMANENG, K. & GUAN, K. L. 2011. The Hippo pathway in organ size control, tissue regeneration and stem cell self-renewal. *Nature cell biology,* 13**,** 877-83.

ZHENG, X., SAUNDERS, T. L., CAMPER, S. A., SAMUELSON, L. C. & GINSBURG, D. 1995. Vitronectin is not essential for normal mammalian development and fertility. *Proc Natl Acad Sci U S A,* 92**,** 12426-30.

ZHU, A. J., ZHENG, L., SUYAMA, K. & SCOTT, M. P. 2003. Altered localization of Drosophila Smoothened protein activates Hedgehog signal transduction. *Genes & development,* 17**,** 1240-52.

ZONTA, B., DESMAZIERES, A., RINALDI, A., TAIT, S., SHERMAN, D. L., NOLAN, M. F. & BROPHY, P. J. 2011. A critical role for Neurofascin in regulating action potential initiation through maintenance of the axon initial segment. *Neuron,* 69**,** 945-56.

ZURAWEL, R. H., ALLEN, C., CHIAPPA, S., CATO, W., BIEGEL, J., COGEN, P., DE SAUVAGE, F. & RAFFEL, C. 2000. Analysis of PTCH/SMO/SHH pathway genes in medulloblastoma. *Genes, chromosomes & cancer,* 27**,** 44-51.